

**UNIVERSITÉ DE  
STRASBOURG**



**ÉCOLE DOCTORALE 222**

**Laboratoire de Catalyse Chimique**

**Institut de Science et d'Ingénierie Supramoléculaires (ISIS)**

# **THÈSE de DOCTORAT**

Présentée par :

**Harpreet KAUR**

Soutenue le : **06 Décembre 2022**

Pour obtenir le grade de : **Docteur de l'université de Strasbourg**

Discipline/ Spécialité : Chimie

## **Non-enzymatic synthesis and oligomerization of amino acids under primitive Earth conditions**

**THÈSE dirigée par :**

**Prof. Joseph MORAN**

Directeur de thèse, Université de Strasbourg

**RAPPORTEURS :**

**Prof. Yannick VALLEE**

Rapporteur, Université de Grenoble Alpes

**Prof. Jeremy WULFF**

Rapporteur, Université de Victoria

---

**AUTRES MEMBRES DU JURY :**

**Dr. Claudia BONFIO**

Examineur, Université de Strasbourg

**Dedicated to**

My Waheguru,

beloved grandparents, specially to S. Mukhtiar Singh

Mumma ਕੁਲਬੀਰ ਕੌਰ and Papa ਅਰਵਿੰਦਰ ਸਿੰਘ

Veer ਕਿਰਪਾਲ ਸਿੰਘ

other Pariwaar, dost and well-wishers

## Table of Contents

<b>LIST OF ABBREVIATIONS.....</b>	<b>7</b>
<b>ACKNOWLEDGEMENTS.....</b>	<b>8</b>
<b>RESUME.....</b>	<b>9</b>

### PART I

<b>Introduction.....</b>	<b>18</b>
1. The origin of Life.....	19
2. Planetary perspective and early earth conditions .....	19
3. Life's essentials .....	23
4. Energy sources for the first Life .....	25
5. Phylometabolic analysis of biochemical pathways .....	26
6. Life's origins are subject to different theories and hypothesis.....	30
7. Metabolism under abiotic conditions: a plausible model .....	34
8. Core metabolic pathways biochemistry .....	38
8.1. The acetyl-CoA pathway .....	39
8.2. rTCA cycle and its analogue: glyoxylate/pyruvate reaction network.....	40
8.3. Amino acids.....	44
8.3.1. Structure of amino acids .....	45
8.3.2. Amino acid biosynthesis.....	46
8.4. Peptides .....	47
8.5. Carbohydrates (sugars).....	48
8.6. Fatty acids (lipids) .....	49
8.7. Nucleic acids .....	50
<b>Thesis perspective .....</b>	<b>53</b>

## PART II

<b>Results and discussion.....</b>	<b>54</b>
<b>9. Amino acids .....</b>	<b>55</b>
9.1. Prebiotic attempts to explain amino acids synthesis via reductive amination ..	56
9.2. Prebiotic attempts to explain amino acids synthesis via transamination .....	57
<b>10. Research objective: non-enzymatic transamination reactions .....</b>	<b>59</b>
10.1. Results and discussion.....	59
10.2. Isotope effects .....	66
10.2.1. Transamination reactions of glyoxylate .....	67
10.2.2. Transamination reactions of pyruvate .....	68
10.3. Proposed reaction mechanism for catalytic transamination .....	72
10.4. Acidities of imines and roles of different metals.....	73
10.5. Conclusions.....	76
<b>11. Rare metal catalysis at the origin of protometabolism? .....</b>	<b>77</b>
11.1. Prebiotic attempts towards protometabolic reaction networks.....	79
11.2. Research objective: H <sub>2</sub> driven reductive amination and protometabolic reaction networks.....	82
11.3. Results and discussion.....	84
11.3.1. Reductive amination.....	84
11.3.2. Oxaloacetate/glyoxylate reaction network, an analogue of rTCA cycle...	89
11.3.3. Reaction network driven by H <sub>2</sub> under Pd catalysis, connecting rTCA analogue to amino acids .....	92
11.3.4. Control experiments of the reaction network .....	96
11.3.5. Pd catalysts analysis in our reactions .....	98
11.4. Conclusions.....	99
<b>12. Diamidophosphate (DAP) as a potential prebiotic source of amino acids and their oligomers.....</b>	<b>100</b>
12.1. Prebiotic attempts to explain amino acids oligomerization .....	100
12.2. Research objective: peptide synthesis in water mediated by DAP .....	101
12.3. Results and discussion.....	102
12.4. Conclusions.....	113



## PART III

<b>Supporting information.....</b>	<b>114</b>
<b>13. Transamination.....</b>	<b>115</b>
13.1. Materials and methods .....	115
13.2. Product analysis by NMR spectroscopy .....	116
13.3. Procedures and experimental data.....	119
13.4. Transamination reaction of glyoxylate with glutamic acid .....	119
13.5. Transamination reaction of pyruvate with glutamic acid .....	123
13.6. Transamination reaction of different ketoacids with amino acids.....	127
<b>14. Reductive amination and oxaloacetate/glyoxylate reaction networks .....</b>	<b>140</b>
14.1. Materials and methods .....	140
14.2. Product identification by NMR and GC-MS .....	141
14.3. Reductive amination under hydrogen gas using ammonium bicarbonate ..	142
14.4. Reductive amination with ammonium formate .....	142
14.5. Reductive amination under H <sub>2</sub> (5 bar) without HCO <sub>3</sub> <sup>-</sup> source with ammonium chloride.....	143
14.6. Reductive amination at 5 °C with ammonium formate .....	144
14.7. Reductive amination with different concentrations of ammonium .....	145
14.8. General procedure for oxaloacetate/glyoxylate reaction networks in the presence of formate .....	145
14.9. General procedure for oxaloacetate/glyoxylate reaction networks in the presence of bicarbonate and H <sub>2</sub> .....	146
14.10. General procedure for oxaloacetate/glyoxylate reaction networks control experiments .....	147
14.11. Reductive amination with different Pd catalysts on different supports and with meteorite .....	148
14.12. Preparation of the Pd catalysts .....	149
14.13. Characterization of the catalysts .....	150
14.14. Experimental data .....	150
<b>15. DAP: amino acids synthesis and oligomerization .....</b>	<b>190</b>
15.1. Materials and methods .....	190
15.2. Product analysis .....	190

15.2.1. NMR spectroscopy .....	190
15.2.2. U-HPLC-QTOF-MS .....	191
15.2.3. Derivatization method for amino acids and peptides analysis .....	192
15.3. Diamidophosphate synthesis procedure .....	192
15.4. Reductive amination reaction of pyruvate with DAP .....	193
15.5. Reductive amination reaction of different ketoacids with DAP .....	194
15.6. Oligomerization reaction of different amino acids with DAP .....	195
15.7. Experimental data .....	196
<b>General conclusions .....</b>	<b>216</b>
<b>References .....</b>	<b>217</b>

## List of Abbreviations

<b>Actyl CoA</b>	Acetyl conenzyme A	<b>MS</b>	Mass spectrometer
<b>Ala</b>	Alanine	<b>m/z</b>	Mass to charge ratio
<b>AMP</b>	Adenosine monophosphate	<b>NMR</b>	Nuclear magnetic resonance
<b>ATP</b>	Adenosine triphosphate	<b>NO<sub>3</sub><sup>-</sup></b>	Nitrate
<b>atm</b>	Atmosphere	<b>N<sub>2</sub></b>	Nitrogen
<b>CAPA</b>	Cyclic and phosphoryl-activated amino acids	<b>NH<sub>3</sub></b>	Ammonia
<b>CDI</b>	1,1'-Carbonyldiimidazole	<b>NADP</b>	Nicotinamide adenine dinucleotide phosphate
<b>CH<sub>4</sub></b>	Methane	<b>°C</b>	Degree celsius
<b>CMP</b>	Cytosine monophosphate	<b>OMP</b>	Orotidine monophosphate
<b>CO</b>	Carbon monoxide	<b>OPA</b>	o-phthalaldehyde
<b>CO<sub>2</sub></b>	Carbon dioxide	<b>O<sub>3</sub></b>	Ozone
<b>CODH/ACS</b>	Carbon monoxide dehydrogenase/acetyl-CoA synthase	<b>PEP</b>	Phosphoenolpyruvate
<b>DAP</b>	Diamido phosphate	<b>ppm</b>	Part per million
<b>DFT</b>	Density functional theory	<b>PRPP</b>	5-Phospho-D-ribose 1-diphosphate
<b>DNA</b>	Deoxyribonucleic acid	<b>PLP</b>	Pyridoxal phosphate
<b>equiv.</b>	Equivalent	<b>QTOF</b>	Quadrupole time of flight
<b>EtOAc</b>	Ethyl acetate	<b>R5P</b>	Ribose 5-phosphate
<b>Gly</b>	Gycine	<b>RNA</b>	Ribonucleic acid
<b>h</b>	Hour	<b>r.t.</b>	Room temperature
<b>HSCoA</b>	Coenzyme A	<b>rTCA</b>	Reductive tricarboxylic acid
	Phosphoric acid	<b>SO<sub>2</sub></b>	Sulfur dioxide
<b>H<sub>2</sub></b>	Hydrogen	<b>t</b>	Time
<b>HCO<sub>3</sub><sup>-</sup></b>	Bicarbonate	<b>temp.</b>	Temperature
<b>HCO<sub>2</sub><sup>-</sup></b>	Formate	<b>TMP</b>	Trimetaphosphate
<b>HCN</b>	Hydrogen cyanide	<b>UMP</b>	Uridine monophosphate
<b>H<sub>2</sub>S</b>	Hydrogen sulfide	<b>UV</b>	Ultra-violet
<b>H<sub>2</sub>O</b>	Water	<b>w/w</b>	Weight by weight
<b>KIE</b>	Kinetic isotope effect	<b>W-L pathway</b>	Wood-Ljungdahl pathway
<b>LUCA</b>	Last Universal Common Ancestor	<b>μL</b>	Microliter
<b>LHB</b>	Late heavy bombardment		
<b>M</b>	Molar		
<b>mg</b>	Milligram		
<b>mL</b>	Milliliter		
<b>mM</b>	Millimolar		

## Acknowledgement

It has been an honor and a pleasure working in the lab of Prof. Joseph Moran. I am extremely grateful for the opportunity. My sincere thanks go out to him for his continuous guidance and patience during my PhD studies. Having his support, knowledge, and experience allowed me to grow as a scientist. He provided me a platform which helped to shape my career towards a better future.

I would like to express my deepest appreciation to the rest of my thesis committee: Prof Jeremy Wulff; Prof Yannick Vallee and Dr. Claudia Bonfio, for their valuable time and interest in the research.

I'd like to acknowledge the ERC and Volkswagen grant for their financial support to this thesis.

I would like to thank Dr. David Leboeuf, for his insightful comments and encouragement. I would like to express my gratitude to Dr. Kamila for the correction of my thesis and her invaluable support throughout my PhD and professional career. My sincere thanks goes to Dr. Mayer for his time to do my thesis corrections, stimulating discussions, immense support, encouragement and fun times during my studies.

Additionally, I appreciate Cyril, Jean-Louis, Maurice and Bruno's technical support. Especially, I am grateful to Wahnyalo for his analytical support.

Thanks to Quentin, Weiqiang, Abhijit, Nik, Florent, Robin, Valentyn, Corinna, Cappucine, Andrei, Florent, Elodie, Louis and Sergio for their valuable discussions to the research and for spending time together in the lab, as well as in social settings. Special thanks to Sophia, Joris, Cyprien, Marie, Paul, Jan, Maciek, Wahnyalo, Edouard, Silvana, Lucas and Michel, for their kind help, support and happy times in all the ways that have made my study and life wonderful in Strasbourg. Additionally, I'm grateful to ISIS and all the people i know, for giving me wonderful experiences.

I would like to thank Jing, for always being there for me, being my support in all the ways and providing me so much care. Emilie, for her kindness, help, encouragement and listening ear in all the ups and downs. Ankita for her advice, care and encouragement. I would like to thank my friend Paola and Snigdha for always being supportive in Life. All of them's support is worth than I can express on a paper.

I wish to express my sincerest gratitude to Annia and Nathalie for their love and care, as well as their assistance in all administrative matters.

Last but not least, I wish to extend my gratitude to my family, grandparents, parents, and little brother. This journey would not have been possible without their tremendous support, understanding, and sacrifices. Thank you for always loving me and inspiring me.

## **RESUME DE LA THESE DE DOCTORAT**

### **Synthèse et oligomérisation non enzymatique d'acides aminés en conditions terrestres primitives**

#### **1. Introduction**

L'apparition des voies métaboliques de base sur Terre constitue l'un des défis majeurs dans l'étude de l'origine de la vie. L'analyse des réseaux métaboliques et la phylogénétique suggèrent que la biochimie primitive était pilotée par la réduction avec de l'hydrogène gazeux, construite à partir de bicarbonate/ $\text{CO}_2$ , et utilisait des réactions similaires à celles que l'on trouve dans les organismes modernes. Conformément à ces prédictions, des analogues de voies métaboliques entières, ou de fragments de celles-ci, ont été trouvés par catalyse métallique ou ionique, incluant notamment le cycle de Krebs ou le cycle de Krebs inversé, la voie de l'acétyl CoA, la glycolyse, la voie des pentoses phosphates ainsi que la gluconéogenèse au cours des huit dernières années, réduisant ainsi l'écart entre la chimie prébiotique et le métabolisme ancien. Ces observations appuient les propositions selon lesquelles les précurseurs de certaines voies métaboliques fondamentales sont apparues sous catalyse inorganique, puis ont été affinés par organocatalyse à partir de cofacteurs et, finalement, par des enzymes.

Les protéines constituent l'un des piliers chimiques de la vie et les acides aminés sont leurs éléments constitutifs. Dans tous les organismes vivants, les acides aminés sont synthétisés par amination réductrice et transamination. On a longtemps émis l'hypothèse que les acides aminés étaient déjà impliqués dans l'évolution chimique qui a précédé la vie. Ici, nous décrivons la synthèse d'acides aminés par amination réductrice et transamination et leurs oligomérisations sous une grande variété de métaux/ions métalliques comme catalyseurs dans des conditions douces similaires à la biologie et plausibles d'un point de vue prébiotique.

## 2. Résultats et discussion

### 2.1. Amination réductrice

Les quatre principaux acides aminés les plus anciens que l'on retrouve dans le métabolisme de base sont la glycine, l'aspartate, l'alanine et l'acide glutamique. Ils sont précurseurs d'autres acides aminés et de métabolites biologiques plus complexes tels que les protéines, les ribonucléotides et les acides gras. La synthèse d'acides aminés a été décrite auparavant dans un contexte prébiotique, mais dans chaque cas, elle nécessitait des conditions difficiles incompatibles avec d'autres chimies ou en désaccord avec la géochimie primitive utilisant par exemple un excès conséquent d'ammoniac (150 équiv.), des températures élevées (50-75 °C) ou un pH largement inférieur ou supérieur à 7. De plus, ces conditions n'étaient pas compatibles avec l'oxaloacétate, dont l'acide aminé correspondant, l'aspartate, est le précurseur biosynthétique essentiel du ribonucléotide pyrimidine. Dans le cas de l'oxaloacétate, l'un des principaux défis est que son amination réductrice doit l'emporter sur sa décarboxylation en pyruvate qui est très rapide à température élevée. De nombreux processus chimiques ont été découverts pour la première fois avec des métaux rares à l'activité catalytique innée, mais dont leur rareté incite désormais à les remplacer par des catalyseurs basés sur des métaux abondants. Cependant, comme les métaux abondants sont de mauvais catalyseurs en l'absence de ligands, leur utilisation ne devient possible que lorsque des ligands organiques sophistiqués capables d'améliorer les propriétés catalytiques des métaux abondants deviennent accessibles. Nous avons donc décidé que les métaux précieux connus pour catalyser efficacement les réactions d'hydrogénation et de transfert d'hydrogène dans l'eau à faible charge et sans ligands exogènes (par exemple Pd, Pt, Rh, Ir) devaient être évalués expérimentalement dans le contexte de la chimie prébiotique. En utilisant le Pd/C comme catalyseur (1 mol%, 32 ppm dans le mélange réactionnel par rapport au Pd) avec soit de l'hydrogène gazeux, soit du formate (5 équiv.) comme agent réducteur à pH 7-8 et 22 °C pendant 72 h, nous avons constaté que l'amination réductrice était compatible avec sept  $\alpha$ -cétoacides biologiques différents (glyoxylate, pyruvate,  $\alpha$ -cétoglutarate, oxaloacétate,  $\alpha$ -cétoisocaproate,  $\alpha$ -cétisovalérate et  $\alpha$ -cétob- $\beta$ -méthylvalérate) malgré l'utilisation de seulement 5 équiv. d'ammonium. Les acides aminés biologiques correspondants (glycine, alanine, glutamate, aspartate, leucine,

valine et isoleucine) ont été obtenus comme produit principal avec un rendement de 20-78% et une sélectivité supérieure à 6:1 pour l'acide  $\alpha$ -aminé par rapport à l'acide  $\alpha$ -hydroxy dans presque tous les cas (Schéma 1). Il est intéressant de noter que la réaction est lente et qu'elle perd presque toute sa sélectivité si de l'hydrogène gazeux (5 bar) est utilisé au lieu du formiate ou d'un mélange  $\text{H}_2/\text{HCO}_3^-$ , ce qui suggère que l'amination réductrice sous  $\text{H}_2/\text{HCO}_3^-$  n'est pas une hydrogénation directe mais une hydrogénation de transfert via le formiate généré in situ.

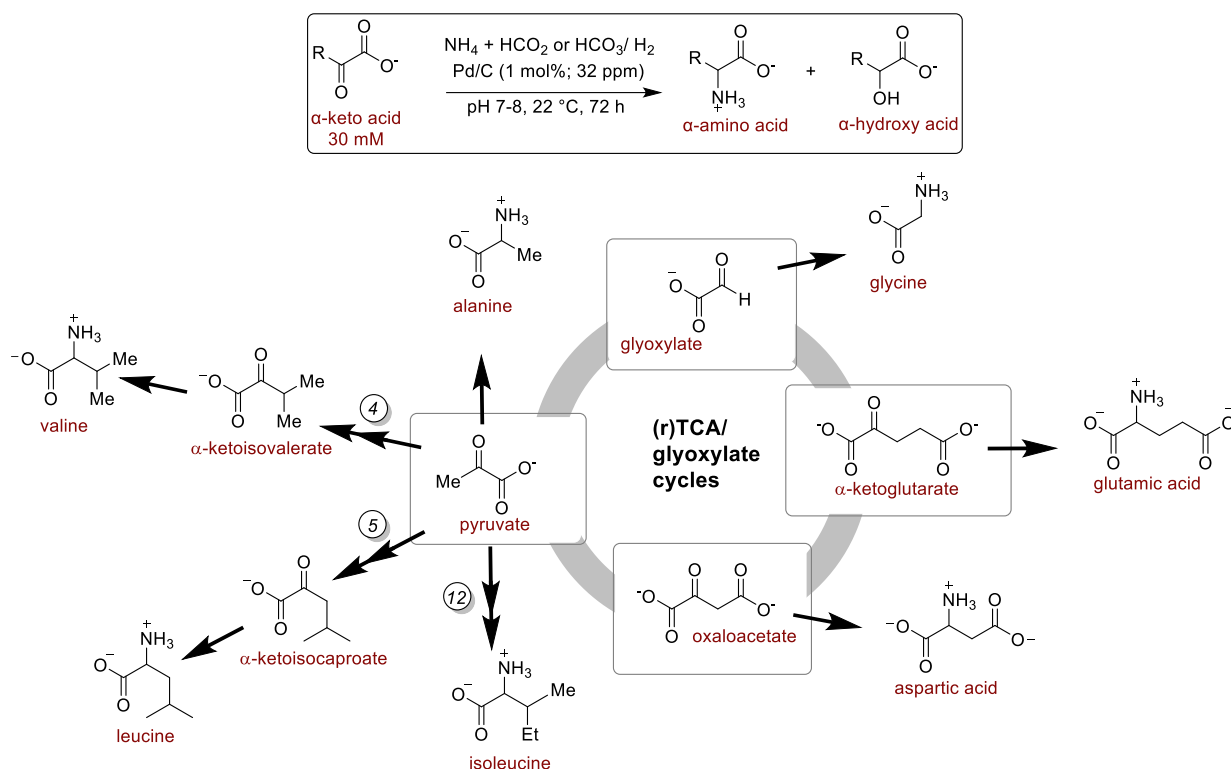


**Schéma.1** Amination réductrice catalysée par des ppm de Pd/C à température ambiante.

*N.B. Les nombres sur les flèches indiquent la formation de cétoacides correspondant à l'acide aminé à partir des cétoacides métaboliques centraux.*

## 2.2. Réseau de réactions piloté par le dihydrogène sous catalyse au palladium, reliant un analogue du cycle rTCA aux acides aminés.

Fascinés par l'activité catalytique exceptionnelle du palladium dans notre amination réductrice, nous avons étendu notre étude à la synthèse monotope comprenant un analogue du cycle rTCA et l'amination réductrice des cétoacides formés, obtenant ainsi

un réseau de réactions métaboliques mutuellement compatibles et une chimie autoorganisée (Schéma 2). Lorsque l'oxaloacétate (60 mM) et le glyoxylate (120 mM) sont mélangés en présence de 10 équivalents de formiate d'ammonium ou d'un mélange bicarbonate d'ammonium/dihydrogène et de traces de Pd/C (1 mol% de Pd par rapport à l'oxaloacétate) à température ambiante et dans l'eau à pH 7-8, on obtient après 72 h le mélange réactionnel complexe représenté Schéma 2. Dans ce mélange réactionnel des intermédiaires du cycle rTCA/TCA ( $\alpha$ -cétoglutarate et pyruvate), cinq  $\alpha$ -cétoacides supplémentaires qui sont des homologues à un carbone de ceux du cycle rTCA/TCA (formiate de maloylé, formiate de fumaroylé, formiate d'isocitroylé, formiate d'aconitoylé et formiate de citroylé), quatre acides aminés (glycine, alanine, aspartate et glutamate) et trois hydroxyacides (glycolate, lactate et malate) ont été identifiés. Le réseau réactionnel global est composé de quatre sous-systèmes interconnectés, comme décrit dans la Schéma 2, de l'intérieur vers l'extérieur: 1) hydrogénation du bicarbonate en formiate en présence de dihydrogène; 2) synthèse de cétoacides analogue au cycle de Krebs inverse par aldolisation et hydrogénation par transfert; 3) synthèse d'acides aminés par amination réductrice de cétoacides en présence d'ammoniac; et 4) réduction des cétoacides en hydroxyacides. Ces résultats sont prometteurs dans un contexte prébiotique, car ce type de réseau complexe n'a jamais été réalisé auparavant dans des conditions monotopiques et sans intervention humaine.

En résumé, la clé de la réactivité est l'utilisation de Pd à l'état de traces, qui catalyse l'hydrogénation ou transfère hydrogénative réactions dans l'eau. Les métaux précieux comme le Pd sont de puissants catalyseurs, mais ils n'ont pas été pris en compte dans la chimie prébiotique, probablement en raison de leur faible abondance globale dans la croûte terrestre, généralement au niveau du ppb. Cependant, le Pd et d'autres métaux précieux se trouvent souvent à des concentrations élevées dans des environnements localisés et peuvent donc avoir joué un rôle dans l'auto-organisation chimique à l'origine de la vie. Par exemple, certains échantillons de pentlandite trouvés en Russie contiennent jusqu'à 11 % en poids de Pd. L'hydrogène gazeux soutient de nombreux écosystèmes sur Terre et est produit en continu par des processus géochimiques, notamment la serpentinisation dans les systèmes hydrothermaux et la radiolyse de l'eau dans la croûte profonde. H<sub>2</sub> peut également avoir été produit en quantités énormes (jusqu'à 90 bar) par des événements d'impact au début de l'histoire de la Terre et avoir mis jusqu'à 200 Myr pour se dissiper. Ainsi, des éléments



catalytiques rares auraient pu avoir de nombreuses occasions d'interagir avec le  $\text{CO}_2/\text{HCO}_3^-$ , le  $\text{H}_2$  et l'ammoniac et auraient pu contribuer à initier et à modeler une chimie prébiotique auto-organisée sur la Terre primitive.

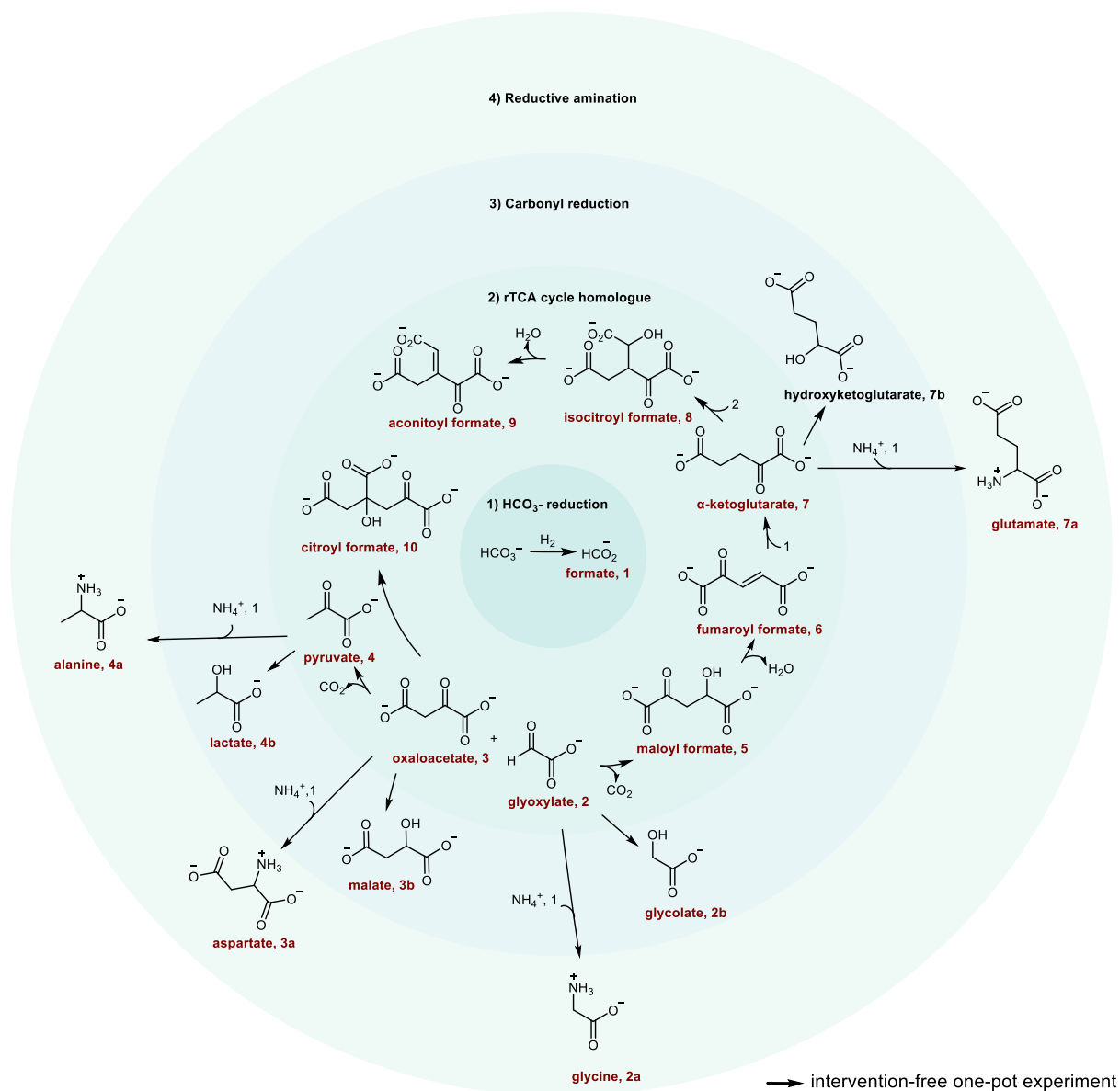


**Schéma 2.** Réseau de réactions piloté par le dihydrogène sous catalyse au palladium.

### 2.3. Transamination

La transamination est le processus biologique par lequel l'ammoniac est transféré entre les acides aminés et les cétoacides. En biologie, les réactions de transamination sont catalysées par la combinaison d'un cofacteur, le phosphate de pyridoxal (PLP), et d'une enzyme, une transaminase. Cependant, il n'existe aucun exemple de réaction métabolique dans lequel les trois niveaux de complexité catalytique (par exemple, 1. ion métallique, 2. cofacteur avec ou sans ions métalliques, et 3. cofacteur + enzyme) sont démontrés et compris mécaniquement dans des conditions biologiques, ce qui rend difficile d'apprécier comment une telle progression évolutive a pu se produire en biochimie. Ici, nous avons identifié les ions métalliques capables de catalyser la transamination dans des conditions pertinentes pour la biologie (pH 7, 20-50 °C) et avons étudié le mécanisme en détail. Le  $\text{Cu}^{2+}$ ,  $\text{Ni}^{2+}$ ,  $\text{Co}^{2+}$ , et  $\text{V}^{5+}$  ont été identifiés comme les catalyseurs les plus viables.

Les réactions de transamination sont connues depuis des décennies pour se produire en l'absence d'enzymes, mais on ne savait pas dans quelle mesure les métaux seuls pouvaient agir comme catalyseurs dans des conditions biologiques, ni même s'ils pouvaient présenter une rotation catalytique. Dans ce travail, nous avons montré que les ions  $\text{Co}^{2+}$ ,  $\text{Ni}^{2+}$ ,  $\text{Cu}^{2+}$  et  $\text{V}^{5+}$  peuvent, non seulement favoriser, mais aussi catalyser efficacement les réactions de transamination, même sans PLP (Schéma 3.) Une combinaison d'expériences cinétiques et mécanistiques et de calculs DFT a permis de comprendre les étapes clés de la réaction et de justifier les deux principales façons dont les métaux peuvent catalyser les réactions de transamination.  $\text{Co}^{2+}$  et  $\text{Cu}^{2+}$  augmentent principalement la vitesse de transamination en augmentant la concentration disponible des intermédiaires chélate réactifs métal-imine.  $\text{V}^{5+}$  accélère principalement la vitesse en augmentant l'acidité des protons CH du chélate d'imine, ce qui à son tour augmente la constante de vitesse pour l'étape clé de déprotonation.  $\text{Ni}^{2+}$  fonctionne par ces deux mécanismes dans une certaine mesure.

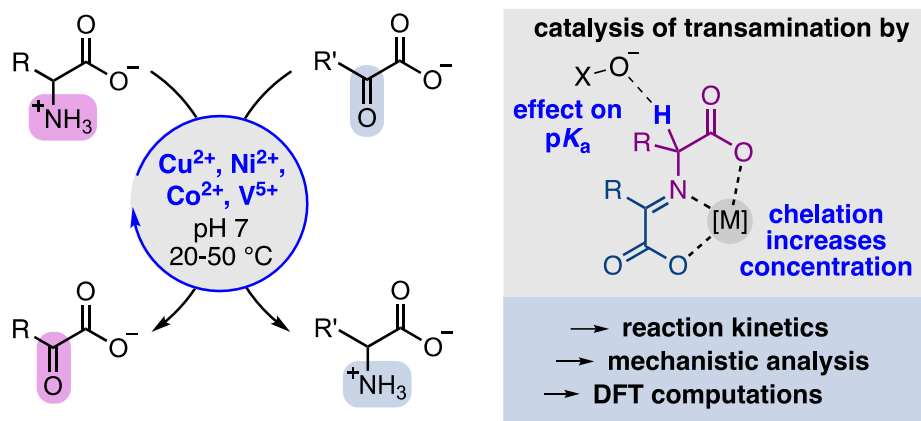


**Schéma 3.** Transamination par des ions métalliques.

### Mécanisme de la réaction

Sur la base de nos études cinétiques, qui montrent la nature catalytique de la réaction, et des structures établies des chélates de métal-imine, nous avons proposé le mécanisme de réaction décrit dans le schéma 4. La réaction s'initie en formant de petites quantités d'un ion iminium I-1. L'échange de  $H^+$  contre le métal de transition donne un complexe métal-imine I-2. La déprotonation de I-2 donne l'ylure d'azométhine entièrement conjugué I-3, qui, lors de la re-protonation, forme soit l'adduit d'imine d'origine I-2, soit l'isomère I-2'. L'hydrolyse de I-2' libère finalement les produits de la réaction. En présence de quantités catalytiques de métal, toute la séquence est réversible et se traduira par des concentrations d'acides aminés et céto en fonction des énergies relatives des réactifs et des produits. En formant les chélates métal-imine I-2, les ions métalliques peuvent influencer la vitesse de la séquence de transamination par deux mécanismes prédominants, qui ne sont pas mutuellement exclusifs. Soit ils peuvent augmenter la concentration de l'intermédiaire imine réactif, en imposant une constante de liaison plus élevée, soit ils peuvent augmenter l'acidité du fragment CH dans I-2 et donc le taux de déprotonation en I-3. En variante, la réaction de transamination peut également se dérouler via une voie sans métal nettement plus lente par déprotonation directe de l'espèce iminium I-1 en ylure d'azométhine I-4.

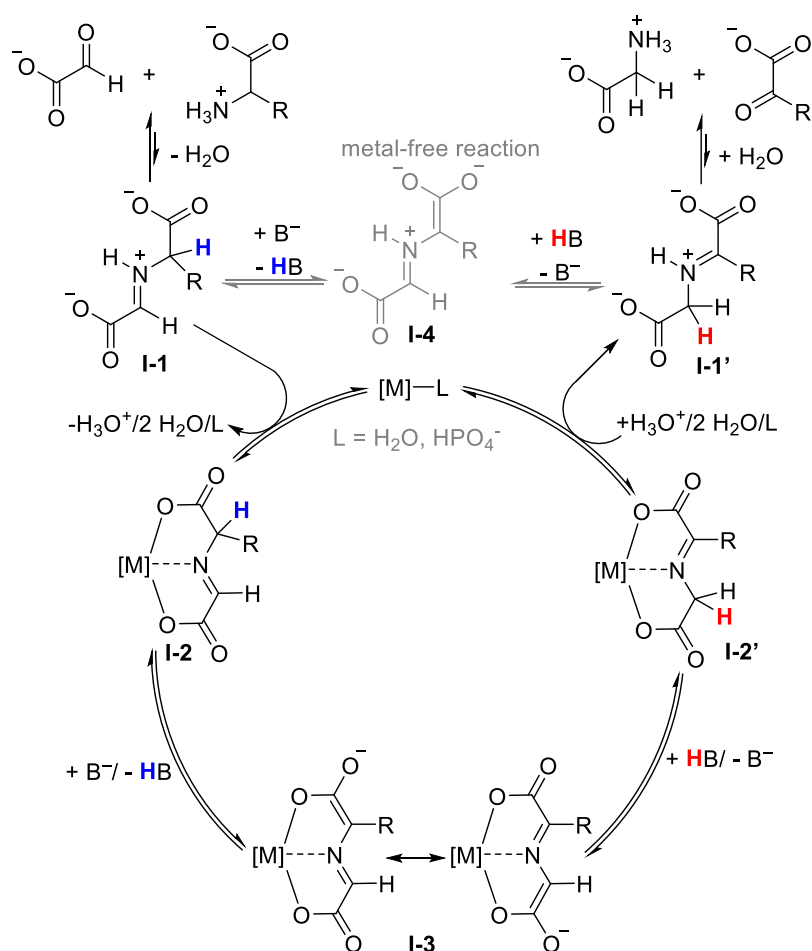


**Schéma 4.** Mécanisme de réaction proposé pour la transamination catalytique.

## 2.4. Diamidophosphate (DAP) comme source prébiotique potentielle d'acides aminés et leurs oligomères

La synthèse des acides aminés et leur oligomérisation ultérieure pour former des peptides dans l'eau sont des étapes cruciales pour l'origine de la vie. En biochimie, plusieurs acides aminés sont biosynthétisés par amination réductrice formelle d'un α-cétoacide, soit par amination réductrice directe avec l'ammoniac, soit par transamination. Cependant, les rapports précédents sur la synthèse d'acides aminés prébiotiques par amination réductrice ne sont pas toujours réalistes (pH extrême, ammoniac hautement concentré, etc.) ou nécessitent des environnements incompatibles avec la génération conséquente des oligomères correspondants. Nous démontrons ici que le DAP (diamidophosphate), un réactif prébiotique plausible obtenu

à partir de la réaction de phosphates inorganiques et d'ammoniac, sert de donneur d'ammoniac pour l'amination réductrice catalysée par un métal de transition employant  $H_2$  comme agent réducteur dans un environnement prébiotique plausible. De plus, le DAP agit comme un agent de phosphorylation pour permettre l'oligomérisation des acides aminés dans les mêmes conditions de réaction. Ainsi, dans une expérience monotopique, des oligopeptides peuvent être obtenus à partir d'acides  $\alpha$ -cétoniques en rendements faibles à modérés. (Schéma 5.)

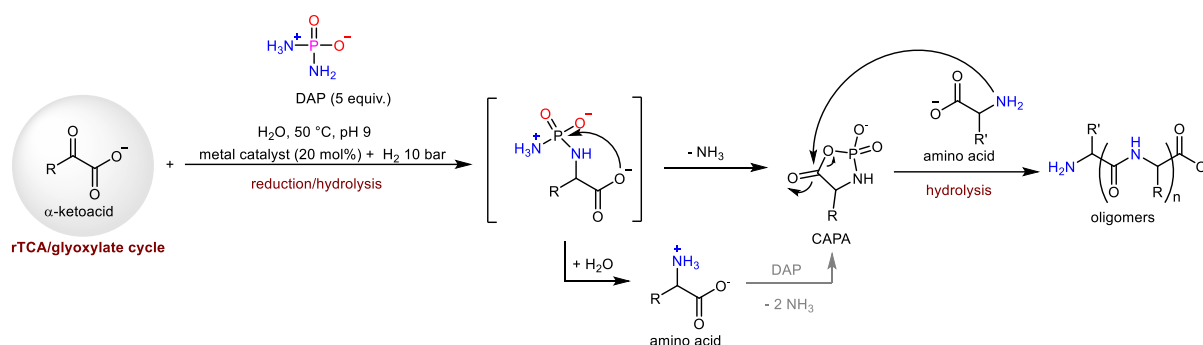


**Schéma 5.** Synthèse et oligomérisation non enzymatique d'acides aminés en présence de catalyseur métallique et de  $H_2$  comme agent réducteur à 50 °C.

### 3. Conclusion générale

Ces études ont permis de découvrir avec succès l'influence de divers métaux sur des réactions non enzymatiques dans des conditions biologiques, expliquant ainsi les premiers temps de l'évolution des voies métaboliques. Certains catalyseurs analysés dans ce contexte étaient traditionnellement des métaux ou des minéraux géochimiquement abondants, en particulier ceux que l'on retrouve dans les sites actifs de métalloenzymes. Cependant, comme la chimie auto-organisée pouvait débiter à des échelles microscopiques, une abondance locale élevée d'un catalyseur, plutôt qu'une abondance générale élevée, peut être nécessaire pour amorcer cette chimie. Nous avons donc souligné que les métaux rares, grâce à leurs propriétés catalytiques exceptionnelles, ont possiblement contribué à initier la chimie auto-organisée qui a par la suite conduit à la vie avec des métaux de terres abondantes.

## **PART I. INTRODUCTION**

## **1. The origin of life**

For centuries, philosophers and thinkers have wondered about the origin of life on Earth and its possible presence on other planets. As a result of recent advances in several scientific disciplines, the origin of life has become a fundamental scientific question that can be addressed using experimental methods. Additionally, space exploration focused on the habitability of planetary bodies has sparked a great interest in the origins of life research. Once it has begun, life's development and proliferation are well known to us.<sup>1</sup> Despite this, the answer to “how did life originate from inorganic matter?” – one of science’s most exciting questions – remains a mystery.

It is estimated that the Earth is 4.54 billion years old.<sup>2</sup> The earliest undisputed evidence of life on Earth dates back at least 3.5 billion years.<sup>3</sup> Origin of life is a very complex subject that requires the collaboration of many disciplines, including chemistry, biology, biochemistry, geology, physics, planetology, and palaeontology. Although the questions they attempt to answer differ, they all have a common theme: Why did Earth develop life, and how did Earth's geological evolution affect the origin and evolution of life? How did life as we know it begin? How do energy, entropy, and complexity play a role in this process? How do we define life when conducting research on it?<sup>4</sup> There are several theories regarding how life came into existence, which will be discussed later.

## **2. Planetary perspective and early Earth conditions**

What makes the Earth a habitable planet? In this subchapter, I will recap how our planet came into existence and became habitable to life. The Solar System emerged about 4.6 billion years ago from a nebula – a cloud made of dust and gas, mostly hydrogen and helium, with traces of other atoms. The Sun was formed when the nebula contracted into a disc shape, collapsing on itself, as the heavier matter was in the centre. The rest of the matter gathered in smaller clumps in the outer parts of what is known as an accretion disc.<sup>2</sup> This led to proto-planets, which became larger as more matter accumulated. With increasing contraction, pressures increased, resulting in the solar nebula getting warmer and the protoplanets getting even hotter with the heat generated by the growing proto-Sun.<sup>2</sup> Small rocky, icy, and metallic bodies left over from the formation of the Solar System fill an area between the inner and outer planets

known as the asteroid belt. No planet formed in this area because Jupiter's gravity likely played a significant role in preventing the formation of any large planets in this zone. Furthermore, comets and asteroids that may otherwise strike Earth are deflected by the tremendous gravitational field of Jupiter, protecting our planet.<sup>5</sup>

Scientists describe a habitable environment on Earth as "Goldilocks Conditions." This is an area in space in which a planet is just at the proper distance from its star so that its surface is neither too hot nor too cold, thus making it an appropriate host for life.<sup>6</sup> Specific characteristics of our planet that allowed for life's development are:<sup>7</sup>

- rocky in composition and size, with enough gravity to maintain an atmosphere;
- a thick atmosphere that protects the planet from solar radiation and creates a greenhouse effect, which prevents temperatures from fluctuating drastically;
- a mean temperature and pressure that is close to the triple point of water (0.01 °C and 0.06 atm: the temperature and pressure at which the three phases of a substance (solid, liquid, gas) coexist in thermodynamic equilibrium);
- geodynamics that enables weathering and CO<sub>2</sub> recycling;
- a magnetic field generated by the iron-rich core dynamo that protects the planet from stellar winds;
- the presence of a relatively large satellite (the Moon) in order to prevent drastic temperature changes over short periods – it allows for four seasons on Earth;
- the ozone layer (O<sub>3</sub>), produced from molecular oxygen, acts as a shield against excessive ultraviolet radiation.

Earth's conditions were not always like what they are today. To understand how life began, we must also understand how the early Earth looked. Scientists divide the 4.57 billion years of the Earth's existence into smaller periods called eons. For the origins of life, two important eons must be considered: the Hadean (since the Earth was still being formed until 4 billion years ago) and the Archean (between 4 and 2.5 billion years ago).

The Hadean period was marked by hot volcanic environments and heavy bombardment by extraterrestrial bodies, such as asteroids. As a result, the surface would have remained molten and extremely hot for a long time. A notable event occurred 4.4 billion years ago: another planet called Theia, about the size of Mars, hit



the Earth, tilting its rotational axis. As Earth and Theia coalesced, parts of the crust and mantle were ejected into space, generating a ring of debris that eventually formed the Moon.<sup>8</sup> However, geological records do not provide a precise timeline for this impact. Lunar data indicate a relatively quiescent period from 4.4 to 4.0 Ga followed by a 'late heavy bombardment' (LHB) between 3.8 and 4.0 Ga (the later Hadean to early Archean ).<sup>9,10</sup> LHB is essential as it helped to add more elements (iron, nickel, zinc, cobalt, palladium, platinum, etc.) into the upper mantle/crust, as most of the Earth's original elements had been sequestered in the core. At the beginning of Earth's formation, different kinds of matter were more or less homogeneously mixed. Gravity eventually pulled denser elements like iron and nickel (siderophilic elements) into the core of the planet. Silicon, copper, calcium, aluminum, iron, and other lighter materials like sodium and magnesium remained closer to the surface.<sup>11</sup> As the Earth evolved/grew, it accumulated hundreds of different types of minerals.<sup>12,13</sup> The Earth had higher radioactive isotope concentrations during the Hadean when it had a much hotter interior, and volcanism occurred frequently, especially early in the period. There is no clear indication of when the first crust formed, but evidence from Jack Hills zircon suggests that some solid crust existed around 4.4 billion years ago.<sup>14</sup> Acasta gneiss, found in Canada, is the oldest crust known (4.2 billion years old),<sup>15</sup> which probably partially melted due to LHB. The early crust must have solidified directly from the magma ocean and would have been unstable due to mantle upwelling and downwelling. This resulted in chaotic tectonics (plate tectonics are caused by convection in the mantle, leading to consistent outgassing of volatiles in the continental crust). The Earth's surface had stabilized by the transition period between Hadean and Archean to a degree that allowed a solid and continuous crust to form.<sup>16</sup> A significant event of the Archean was the formation of large continents. Archaean Earth had proper plate tectonics and extensive hydrothermal activity, resulting in three times as much heat flow as today.<sup>17</sup> Stromatolites, which are the remains of microbial mats formed by cyanobacteria, are the oldest fossils of living organisms recognized by scientists. They indicate that single-celled life was already thriving on Earth at that time (3.48 billion years ago).<sup>18</sup>

The early atmosphere of planet Earth was mainly rich in hydrogen since most of the matter in the solar system is hydrogen. Other elements (such as carbon, oxygen, nitrogen, and sulfur) were therefore bound to hydrogen in reduced forms, such as CH<sub>4</sub>

(methane),  $\text{NH}_3$  (ammonia),  $\text{H}_2\text{S}$  (hydrogen sulfide), and  $\text{H}_2\text{O}$  (water).<sup>19</sup> However, such an atmosphere would have been blasted away by meteor impacts. Gases released from volcanoes and other vents through the crust were more likely the source of the Earth's atmosphere 3.8 billion years ago. It was mainly composed of water vapor ( $\text{H}_2\text{O}$ ), carbon dioxide ( $\text{CO}_2$ ), nitrogen gas ( $\text{N}_2$ ), and other gases such as hydrogen ( $\text{H}_2$ ), methane ( $\text{CH}_4$ ), hydrogen sulfide ( $\text{H}_2\text{S}$ ), sulfur dioxide ( $\text{SO}_2$ ), and carbon monoxide ( $\text{CO}$ ). There was nearly no oxygen ( $\text{O}_2$ ) present in its free form.<sup>20</sup> Lightning, volcanic activity, and ultraviolet radiation were much more intense as no ozone layer existed yet. Water vapor and greenhouse gases kept the Earth warm during those times, despite the Sun being about 25% less bright.<sup>21</sup> It is important to note that today the majority of carbon exists bound in minerals rather than in the form of  $\text{CO}_2$  (the atmospheric  $\text{CO}_2$  concentrations are currently about 0.03%.)

There is a lively scientific debate over the origins of Earth's water. Deuterium (a heavier isotope of hydrogen) was created in the Big Bang. Its distribution throughout the proto-solar nebula from which other bodies formed, including planet Earth, was locked in early during the formation of the Solar System.<sup>22</sup> There is no known process that can decrease the D/H ratio on Earth over time.<sup>23</sup> Thus, the D/H ratio may be a valuable tool for explaining the origin of water, whether it came from Earth's interior (from the solar nebula as it was locked in) or via asteroids. To our knowledge, the ocean water D/H ratio is  $(1.5576 \pm 0.0005) \times 10^{-4}$ , and it represents a mixture of all the sources (water locked in since Earth's formation or from asteroid sources) contributing to Earth's reservoirs and is used as a tool to understand the origins of the planet's water.<sup>24</sup>

Two prevailing theories typically explain water accumulation on Earth's surface in sufficient quantities to form oceans. One hypothesis states that Earth got its water from extraplanetary sources. Asteroids, called carbonaceous chondrites, which are usually rich in water and other elements like carbon and nitrogen, have the same deuterium-to-hydrogen ratio as Earth's oceans.<sup>25</sup> According to this hypothesis, the Earth was too hot to hold the water that it got from the solar nebula early on, and it would have been lost during early impacts and collisions. Thus water stored in its rocks would not have been enough to form oceans. Another hypothesis says that the Earth held on to water during planetary accretion because there would have been ice in the solar nebula. Some of that water might have remained inside the Earth, trapped in minerals,

and therefore was not lost to the early atmosphere during large impacts. Eventually, volcanic eruptions and plate tectonics could bring trapped water to the surface via hot volatiles from the planet's mantle. Water would have quickly condensed into aqueous oceans as the magma ocean cooled down. It has been found that ratios of hydrogen isotopes in some of the oldest rocks on Earth are similar to those of the solar nebula, making this hypothesis more credible.<sup>26,27</sup> The fact that neither of these hypotheses is mutually exclusive further complicates the picture. It is possible that some of the water could be delivered by asteroids while some could originate from the Earth's interior. The Earth is actually a dry rock planet with only 0.022% of its mass being water, and though there is very little water stored in rocks, the mantle contains two-thirds of the Earth's mass, so the total amount of water that can be contained in it is quite large.<sup>28</sup> From both hypotheses, we can conclude that most of the water on Earth was already present during its early evolution.

Early waters were slightly acidic (modern oceans are slightly alkaline) due to the high levels of CO<sub>2</sub> in the atmosphere, which could have led to the formation of compounds acidic in nature, such as carbonic acid.<sup>29</sup> Now, being familiar with early Earth's conditions, let's look at what is essential to life. This information will help us understand why life uses the chemistry we see in biology and how it came into being.

### 3. Life's essentials

Earth is the only known inhabited planet, and all its life depends on liquid water. **Water** covers approximately 70 % of the Earth's surface.<sup>30</sup> But why is water so essential to life? Several unique properties of water make it indispensable to life. Life depends on chemical reactions for energy, growth, and waste elimination, and water is a suitable candidate to facilitate these functions. On the molecular level, water is a polar molecule with partial positive charges on the hydrogen atoms and a partial negative charge on the oxygen atom. The high electronegativity of oxygen results in strong hydrogen bonds, which allows water to be a liquid in a wide temperature range (0-100°C). Comparatively, most other common solvents, such as ammonia and methane, are liquid at a limited temperature range (-33 and -82 ° C, respectively), which is too extreme for known life's chemistry.<sup>31,32</sup> Furthermore, thanks to its molecular properties, water is an excellent solvent for most biological compounds and, therefore, facilitates

chemical reactions that occur in living organisms. Even though some organic molecules cannot be dissolved in water, boundary surfaces may form, such as vesicles, creating a protected microenvironment with different physico-chemical conditions. Additionally, as a result of the ability to form hydrogen bonds, water molecules maintain their integrity through strong cohesive forces and a high surface tension. Cohesive and adhesive properties are essential for fluid transport and encourage compounds to react with each other. For example, they make it possible to transport nutrients in trees against gravity. It is unusual for a solvent to be denser as a liquid than as a solid, but water holds this property,<sup>33</sup> which prevents ponds, lakes, and oceans from freezing and allows life to flourish. In addition, the high polarity of water makes it possible to contain salts that are essential for life. Additional physical properties of water, such as its ability to retain heat, make it useful for various purposes. Water possesses a high specific heat capacity ( $4.184 \text{ J kg}^{-1} \text{ }^{\circ}\text{C}^{-1}$ ), which means that a lot of energy is required to raise the temperature of a certain amount of water. Accordingly, due to its high specific heat capacity, water helps to regulate extremes in the environment, which is imperative to life's existence.<sup>34</sup> Finally, water exists in all three phases on Earth, allowing for a diversity of microclimates.

Other essential ingredients to life are the six elements: carbon, hydrogen, nitrogen, oxygen, phosphorus, and sulfur (**CHNOPS**). Why are these six elements important? Their abundance in nature is what makes them good in the first place. Moreover, their physico-chemical properties make them able to facilitate life's chemistry. The carbon atom easily forms bonds with other carbon atoms. This allows them to form huge chains that act as skeletons for other atoms. Acid-base effects allow nitrogen, hydrogen, and oxygen to bond with carbon, forming amino acids, lipids, DNA, and RNA nucleobases. The surplus of electrons in sulfur drives electron shuttle, so sulfides and sulfates help catalyze reactions. Lastly, phosphorus is important to metabolism because polyphosphate molecules like ATP (adenosine triphosphate) can store a lot of energy in their chemical bonds ( $\Delta G = -7.3 \text{ kcal/mol}$ ).<sup>35</sup> When the bond is broken, its energy is released, enabling life to function.<sup>36</sup>

#### 4. Energy sources for the first life

All life forms require energy to function. In order to have a good conceptual baseline for origin of life studies, we need to understand how organisms acquire and use the energy they need to grow and reproduce. To this end, it is helpful to establish a classification of the nutritional processes of ancient and modern life. A myriad of interconnected reactions enable modern organisms to accomplish their energy needs, and nutrition is the process by which they obtain them. Nutrition comes in two forms: autotrophic and heterotrophic (Figure 1). Autotrophs make their own organic molecules, harnessing energy from the environment via inorganic inputs. In contrast, heterotrophs obtain their metabolic energy through the breakdown of organic molecules found in the environment. Did the first lifeforms belong to the heterotrophic or the autotrophic group? In the autotrophic scenario, inorganic molecules such as  $H_2$  and  $CO_2$  (which, as mentioned earlier, are two of the most common molecules widely available on the early Earth) provide a constant flux of matter necessary to kick-start the emergence of life by fixing  $CO_2$  into biomass. From a nutritional point of view, the earliest forms of life were probably autotrophs in accordance with early Earth geochemical conditions.<sup>37,38</sup> Furthermore, organic molecules required for heterotrophy would have been in short supply on early Earth. Therefore, heterotrophs eventually evolved once a primary ecology based on autotrophy had evolved to support them.<sup>39</sup>

Autotrophs use two different methods to generate energy (Figure 1). Several organisms extract chemical energy from inorganic molecules (a process called lithotrophy) and others by capturing solar radiation (photosynthesis). Lithotrophy was likely the first autotrophic metabolism.<sup>39</sup> For example, the most ancient Archean microorganisms, called methanogens, gain energy via lithotrophy by reducing carbon dioxide to methane ( $CH_4$ ) with electrons from  $H_2$ .<sup>39</sup> Such processes fall under the category of reductive metabolism, where organisms obtain energy by reducing or reductively forming C-C bonds (for example Acetyl CoA pathway), using dihydrogen,  $H_2S$  or another source of electrons. Due to the highly reducing environment found on the early Earth, it is believed that the first lifeforms relied upon reductive metabolism in the origin's scenario.<sup>20</sup> This idea is further supported by phylogenetic data discussed in the following paragraph.

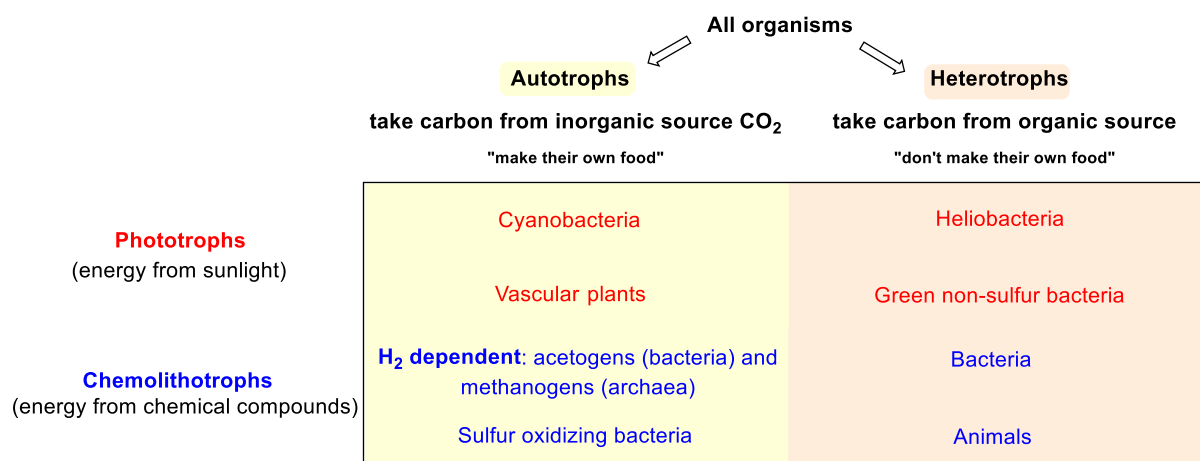


**Figure 1.** Two forms of nutrition: autotrophic and heterotrophic.

## 5. Phylometabolic analysis of biochemical pathways

Phylogenetics is the study of evolutionary relationships within biology. When applied to the biochemical organisation of metabolism, such (phylometabolic) analyses can reveal which pathways may have operated in ancient life. With advances in genetics and bacterial taxonomy, Woese discovered in the 1970s that different species share surprisingly few basic features and processes (genetic code, similar biochemical pathways). As part of an update to Darwin's hypothesis (postulated in 1859), he proposed an ancient group of organisms that would predate the three domains, Bacteria, Archaea, and Eukarya but would also have strong genetic – and consequently biochemical – similarities.<sup>40</sup>

Many metabolic reactions are found in the biosphere, but the most conserved and probably also the oldest ones are the acetyl coenzyme A pathway and the reductive tricarboxylic acid cycle (rTCA), that occur in some deep-branching organisms (earliest life forms).<sup>41</sup> This suggests that life has always built its biomass from  $\text{CO}_2$ . The acetyl CoA pathway, often referred to as the Wood-Ljungdahl pathway (the W-L pathway), is considered the oldest metabolic pathway shared between archaea and bacteria (Figure 2).<sup>42,43</sup> This pathway is short, linear, anaerobic, and reliant on transition metals. As for the outcome,  $\text{CO}_2$  is fixed/reduced to acetate and methane in methanogens and to acetate in acetogens.<sup>44</sup> The W-L-type pathways are characterized by the fact that, rather than consuming free energy for biomass production, they participate in the chemiosmotic potential generation and thus are also free-energy-harvesting

processes. In aceto- and methanogens, the W-L-type metabolism is thus a bioenergetic and a carbon-fixing system at the same time. In contrast, in almost all other species, carbon fixation and free energy harvesting occur in distinct pathways, and the coupling is ensured by ATP and NAD(P)H.<sup>45,46</sup> For the reasons described above, the W-L pathway is hypothesized to have initially arisen from prebiotic chemistry.<sup>47,48,49</sup> The reductive tricarboxylic acid cycle, also known as the reverse Krebs cycle (rTCA cycle), the reverse citric acid cycle, or the Arnon cycle, was discovered for the first time by Arnon and co-workers in 1966 in deep-branching organisms, such as *Chlorobium thiosulfatophilum* bacterium, which use CO<sub>2</sub> as a building block.<sup>49</sup> The rTCA cycle operates anti-clockwise compared to the classical Krebs cycle and uses a reducing source of electrons directly from the environment, such as H<sub>2</sub>, H<sub>2</sub>S, or Fe<sup>2+</sup>. Later in 1980, Hoffman and co-workers recognized this pathway as a plausible candidate for the earliest CO<sub>2</sub>-fixation pathway.<sup>50</sup> It contains what is known as the five universal precursors to all pathways in biochemistry: (1) Acetate is the biosynthetic precursor to lipids, (2) pyruvate is the precursor to sugars and various amino acids, (3) oxaloacetate is the precursor to various amino acids and pyrimidines, (4) succinate is the precursor to various cofactors, and (5) α-ketoglutarate is the precursor to various amino acids. The (r)TCA cycle can therefore be viewed as the gearbox of the metabolic reaction network. Besides its role in biosynthesis, the (r)TCA cycle has autocatalytic properties.<sup>51</sup> Starting from acetate, a complete turn of the cycle would generate one molecule of oxaloacetate and one of acetate, thus regenerating the molecule that began the cycle. To maintain the cycle without enzymes, which would have been the case when life formed on early Earth, any such cycle with yields < 50% would have failed to survive due to parasitic reactions.<sup>52</sup> However, this problem could be overcome in the presence of a “feeder” pathway, such as the W-L pathway, capable of continuously supplying acetate, one of the rTCA cycle intermediates. In addition to the generation of acetate, the W-L chemistry is moderately exergonic, allowing an early organism to extract energy from the process.<sup>45</sup> Thus, a hypothetical network combining the W-L pathway and the rTCA cycle has been proposed as an ancient metabolic network.<sup>39</sup> In the prebiotic context, while the W-L pathway would provide a constant supply of acetate from geochemical inputs, the reverse citric acid cycle chemistry would subsequently build up the biochemical reaction network, resulting in *stabilized network autocatalysis*. This could allow an organism to obtain both the energy and the carbon for it to flourish (Figure 2).<sup>53</sup> The

oxidative version of this cycle (operating in the opposite, i.e., clockwise direction), also known as the TCA or the citric acid cycle, was discovered in 1937.<sup>54</sup> In heterotrophic organisms, the TCA cycle is used to break down complex molecules like sugars and lipids to produce smaller building blocks and energy, which can be utilized for further growth. The phylogenetic data on the earliest known organisms is not conclusive about whether the first citric acid cycle was oxidative, reductive, or perhaps ran in parallel in both directions at its origins.<sup>55</sup> We may argue, based on various studies and Earth's geochemical conditions, that the rTCA cycle predated the oxidative version, and both cycles would have coexisted when appropriate mechanisms were met. As a result, prebiotic chemists have focused on both oxidative and reductive cycles, but with a special emphasis on the rTCA cycle. Furthermore, a simpler version of the rTCA cycle also has been proposed, called the linear “horseshoe” part (Figure 2).<sup>56</sup> This shorter truncated version, though not autocatalytic, still contains all five universal metabolic precursors as the rTCA cycle and might have predated the complete rTCA cycle. This model, however, remains unproven. Details of rTCA cycle biochemistry are discussed in section 8.2.

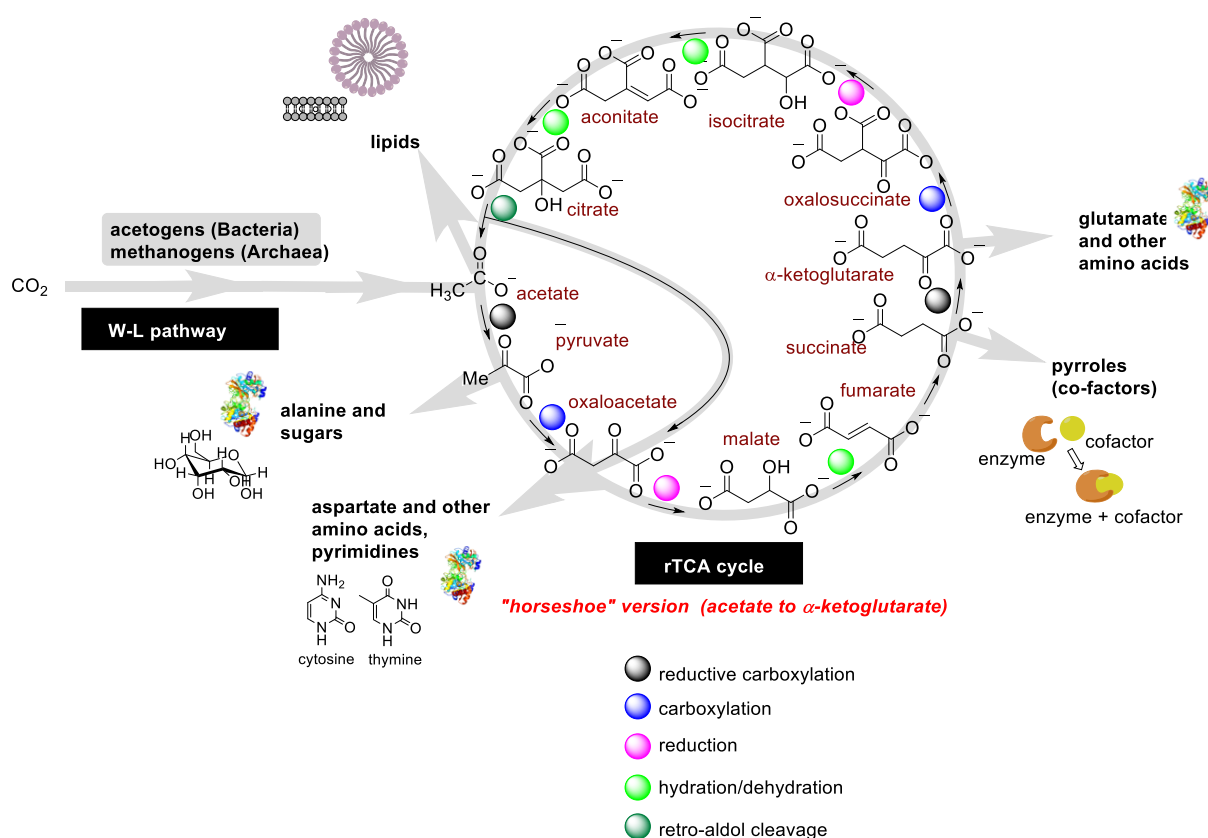


**Figure 2.** A W-L pathway and rTCA cycle (figure adapted from reference 89).



It is commonly accepted in evolutionary biology that the two phyla Archaea and Bacteria stem from a common precursor known as the Last Universal Common Ancestry (LUCA) (Figure 3).<sup>57,58,59</sup> This implies that one kind of organism is at the base of the phylogenetic tree of all organisms on Earth – a phenomenon called monophyly.<sup>60</sup> In 2016, Martin and co-workers described LUCA's plausible physiology and habitat using phylogenetic approaches. Their findings were in agreement with the hypothesis of autotrophic origins of life involving the Wood-Ljungdahl pathway in an environment rich in H<sub>2</sub>, CO<sub>2</sub>, and iron.<sup>61</sup> The data provided evidence that LUCA may have possessed a small number of genes common to all kingdoms. Therefore, the features currently found in deep-branching organisms could have been the features of LUCA as well, for instance, Fe-Ni-S clusters. These clusters are involved in the autotrophic generation of acetate using CO<sub>2</sub> and an electron source through the Wood-Ljungdahl (W-L) pathway. It has to be accepted that nothing about LUCA can be proven beyond any doubt today. However, based on the universally conserved biochemistry across currently known organisms, it seems reasonable to assume that the earliest living entities conserved energy and maintained a carbon metabolism not remarkably different from the one present in deep-branching organisms.

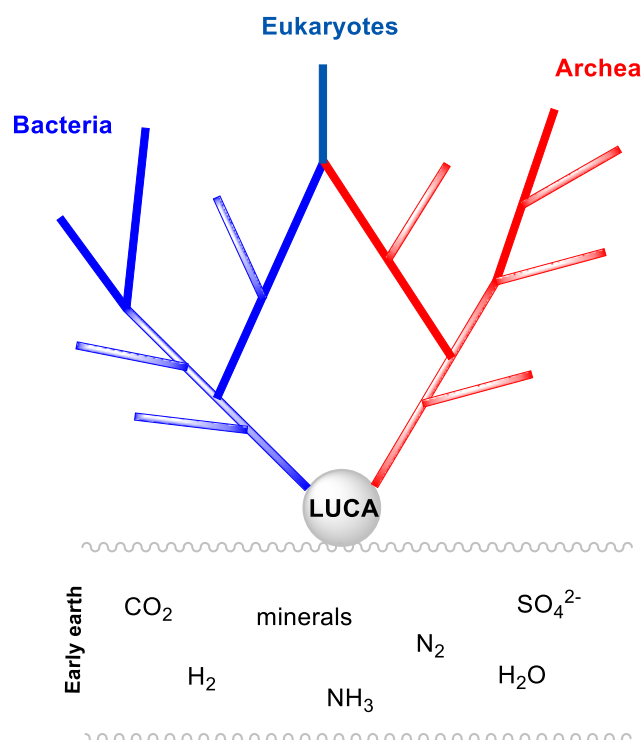


**Figure 3.** The tree of life. A conceptual interpretation of the phylogenetic tree: archaea, bacteria, and eukaryotes make the three domains, the latter deriving from the ‘fusion’ of the other two (figure adapted from reference 61).

## 6. Life's origins are subject to different theories and hypothesis

The origin of life has been studied for several centuries. Below, I will outline and briefly discuss several of the historically most prominent – and often very contrasting – theories of how life may have emerged.

In 300 BC, Aristotle proposed **the spontaneous generation hypothesis**, which states that life regularly arises from decaying organic substances (bees from flowers, mice from dirty hay).<sup>62</sup> It was not until the 17<sup>th</sup> century that this hypothesis was disproved. In 1668, **Francesco Redi** tested the spontaneous creation of maggots by placing fresh meat in three different jars. The maggots were found in the open jar but not in the sealed jar. As a result, Redi disproved the hypothesis of spontaneous generation by demonstrating that the maggots came from fly eggs.<sup>63</sup> In the 1860s, **Pasteur** performed his famous fermentation experiments: he kept dead yeast cells in a pre-sterilised flask and in another flask open to the air. Life did not appear in the former, but living organisms were found in the latter flask, demonstrating that bacteria and fungi cannot spontaneously develop in sterile and nutrient-rich media, but only from other bacteria and fungi. These results put the spontaneous generation concept to rest.<sup>64</sup> The first experimental proof that led to the assumption that **life could have been formed from inorganic molecules** was provided by **Friedrich Wöhler's** urea synthesis in 1828, which showed that biological molecules could also be produced abiotically by purely chemical means.<sup>65</sup> In 1871, **Darwin** suggested that simple chemicals in *warm bodies of water* might spontaneously produce organic compounds from inorganic material when they are exposed to heat, light, or electricity. Eventually, these organic compounds could have accumulated, replicated, and evolved into more complex forms, giving rise to primitive life.<sup>66</sup> In addition, **the Oparin-Haldane hypothesis** developed in the early 1920s further supported Darwin's "warm little pond" hypothesis by suggesting that life emerged gradually as a result of the evolution of inorganic molecules. According to their hypothesis, the early Earth had an oxygen-poor, reducing atmosphere, where molecules tend to donate electrons. Under these conditions, simple inorganic molecules could have reacted (with energy from lightning or the Sun) to form building blocks like amino acids and nucleotides, which could have accumulated in the oceans, making up a "primordial soup." Eventually, these building blocks could have combined in further reactions, forming larger and more complex molecules (polymers), such as proteins, which then assembled into structures or units

capable of sustaining and replicating themselves.<sup>67</sup> This hypothesis remained experimentally untested until 1953, when **Stanley L. Miller**, a graduate student at the University of Chicago, experimentally demonstrated in an artificial system simulating the probable conditions of primitive Earth (a highly reducing mixture of gases and electrical sparks) that organic molecules could form from inorganic components.<sup>68</sup> As a result of these findings, **Sidney Fox** developed the **proteinoid world hypothesis** in 1958, based on his observations that peptide structures are formed from amino acids in high-temperature reactions, suggesting that life might have originated from self-replicating peptides with lifelike properties.<sup>69</sup> In the contemporary prebiotic chemistry community, it is widely accepted that it was common for **meteorites and comets** to deliver certain organics to the early Earth. Murchison and other meteorites have been found to contain a wide variety of organic chemicals, e.g., amino acids, nucleobases, or other simple sugars.<sup>70,71</sup> Still, it must be noted that although these biologically-relevant molecules were delivered from space, they do not represent life. As stated by **Andreas Wagner**, life is *the combination of metabolism (a metabolic network connecting, in terms of reactions, simple building blocks into something more complex, along with the opposite process of breaking larger objects into simpler ones) and replication (the process of making more of itself)*.<sup>72</sup> This led the scientific community to face the fundamental chicken-and-egg problem in the origin of life research: which came first, replication or metabolism?

In the early 60s, following the 1953 discovery of the structure of DNA,<sup>73</sup> the “genetics first hypothesis” came into being, proposing that the first life forms were self-replicating nucleic acids, such as RNA or DNA, and other elements like metabolic networks were a later add-on to this basic system. The foundation for the “genetics first” concept was established by **John Oro's** experiment in the 1960s, where simple molecules such as HCN were shown to condense to make adenine, one of the nucleobases.<sup>74</sup> This was followed and further supported by the **Cairns-Smith's clay life hypothesis**.<sup>75</sup> It suggests that clay surfaces harbouring mineral crystals might have not only concentrated organic compounds but could have also helped arrange organic molecules into an organized pattern, much like our genes. Thus, minerals and organic molecules in clay layers would have facilitated the formation and replication of biological molecules (e.g., enzymes, polynucleotides), contributing to life's origin. This hypothesis is certainly very interesting and inspiring. In the 1960s, researchers

discovered that RNA could serve as both a genetic repository and an enzyme. These findings led **Alex Rich and Leslie Orgel** to suggest a **genetically-driven origin of life** (1960s), with biochemistry being catalyzed by RNA-like polymers.<sup>76</sup> The idea was soon endorsed by Nobel laureate **Walter Gilbert**, who in 1986 coined the term “**RNA world**”, which describes an imaginary stage of life on Earth where proteins did not yet participate in biochemical reactions, and these reactions instead relied on the catalytic activity of RNA, in a primitive self-replicating system.<sup>77</sup> In the following years, the genetics-RNA first world hypothesis got further support from the works of James Ferris’s clay-catalyzed RNA polymerizations (1988),<sup>78</sup> Eschenmoser’s nucleoside synthesis (1991),<sup>79</sup> and Peter Nielsen’s peptide nucleic acid synthesis (1991).<sup>80</sup>

At the same time, in the 1970s, various pieces of evidence pointed towards “metabolism-like chemistry” at life’s origins. For example, **Ilya Prigogine’s** work on dissipative structures and complex systems demonstrated that complex patterns emerge when energy flows through a system containing interacting particles, suggesting that life is an emergent property of complex chemical systems under a specific energetic stress.<sup>81</sup> In addition, the advancements in genetics and taxonomy allowed **Carl Woese** to revise the tree of life in the 1970s to include three domains: Bacteria, Archaea and Eukarya.<sup>82</sup> One consequence of this was the emergence of the concept of a Last Universal Common Ancestor (LUCA), which probably possessed an autotrophic anabolic metabolism, as mentioned earlier. In this way, a new origin of life hypothesis emerged – the “**metabolism-first hypothesis**” – challenging the hitherto prevalent RNA World. This hypothesis received compelling support from deep-sea explorations in the late 1970s that revealed the presence of **hydrothermal vents** (the Lost City) at the bottom of the ocean.<sup>83</sup> A hydrothermal vent releases volatile gases such as CO<sub>2</sub>, H<sub>2</sub>S, CH<sub>4</sub>, and H<sub>2</sub>, as well as hot fluid containing high concentrations of transition metals, e.g., Fe (II) and Mn (II). Once these hot fluids and gases, ejected from the vent at alkaline pH, diffuse in the cold ocean water, they form porous deposits of carbonates that look like rocky chimneys. These pores allow the hydrothermal effluent components to react in a microenvironment (allowing for a sufficient concentration of organic molecules needed for life) with large temperature, pressure, and pH gradients.<sup>83</sup> Nowadays, these microenvironments harbour rich microbial communities, representing the deepest branch of the tree of life, pointing towards the probability of these sites being one of the first settings for pre-metabolic

reactions.<sup>83,84,85</sup> Following the above discoveries, in the 1980s Nobel laureate **Christian de Duve** proposed a **thioester world** scenario for the origin of life, in which abiotically formed thioesters would act as activated intermediates for early biochemistry.<sup>86</sup> Based on the chemistry of the recently then discovered hydrothermal vents, **Günter Wächtershäuser** proposed the **iron-sulfur world scenario** in 1988.<sup>87</sup> In this model, an autocatalytic precursor to biological metabolism could have been powered by harnessing the energy gradients that are created by a redox process between sulphide rich hydrothermal fluid at alkaline pH and ferrous-iron-containing waters at acidic pH (carbon dioxide was thought to have been more abundant in the early oceans than today; therefore, the pH of early oceans is thought to be acidic).<sup>29</sup> The Wächtershäuser hypothesis is radically different from the “RNA world” hypothesis for the origin of life because it is based on *biochemical retrodiction*. The concept of biochemical retrodiction implies that primitive metabolism-like chemistry can be understood from the organization of known biochemical networks. In the subsequent years, scientists like **Wächtershäuser, Russel, Ralser, Martin, William, Moran and co-workers and others** (2000s – present) provided increasingly compelling experimental evidence supporting the metabolism-first concept, for example, in hydrothermal vent environments for some parts of protometabolism.<sup>88,89</sup>

The timeline containing various hypotheses and major research milestones in prebiotic chemistry is summarised in Figure 4. Currently, the two prevalent theories in the field are “**genetics/RNA-first**” and “**metabolism first**”. In the next section, we will discuss these theories' shortcomings and controversies. A plausible model for the emergence of life rooted in the “metabolism-first” approach will also be described.

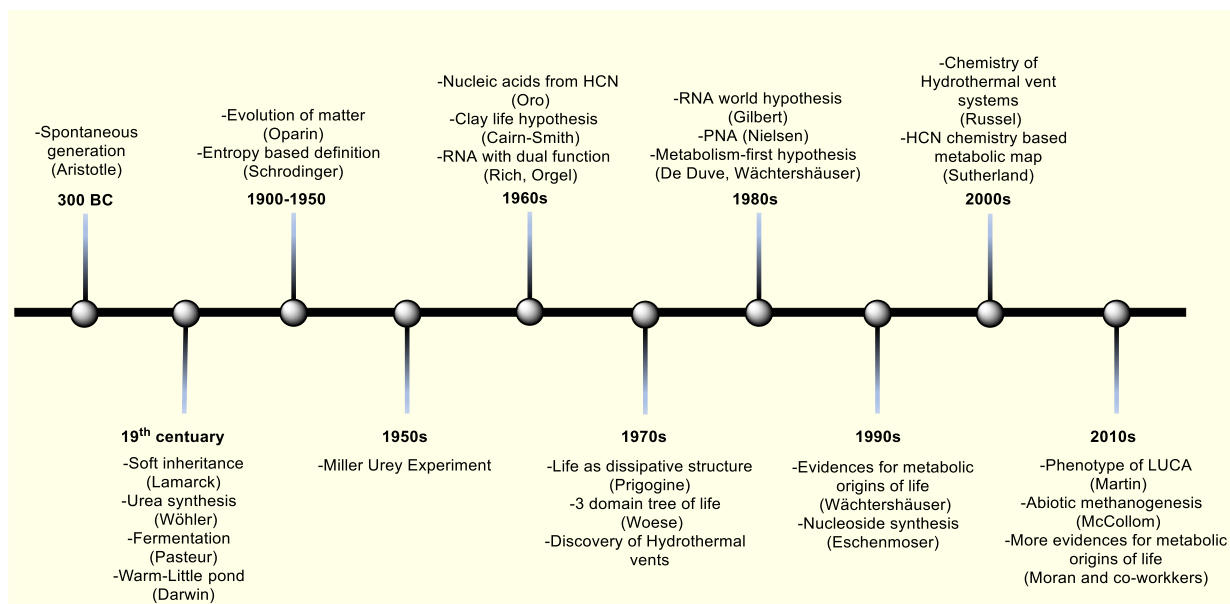


**Figure 4.** Timeline showcasing major developments in the Origin of Life research (figure adapted from reference 126).

## 7. Metabolism under abiotic conditions: a plausible model

If prebiotic chemistry aims to solve the origin of life puzzle, it must explain at least some of the overall organization of biochemistry and the types of reactions it uses under early Earth conditions and in a way that recapitulates biochemistry.<sup>1</sup> The metabolism-first hypothesis emphasizes the need for continuity in chemistry from prebiotic to primitive life,<sup>90</sup> much unlike the RNA-world scenario where many scenarios for nucleotide synthesis have no parallels with biosynthetic pathways and therefore offer little explanatory power.<sup>91</sup> The RNA world hypothesis assumes that all life's biochemistry was kick-started by RNA self-replication that itself was a result of chemistry very different from the one we know today. Therefore, this model assumes no continuity between prebiotic chemistry and biochemistry. However, if chemistry leading to life differs radically from the biochemistry we know today, we should be able to demonstrate experimentally how the transition occurred. So far, no evidence has been found to explain it. The alternative is that core metabolic pathways may not have changed much over the course of their evolution from prebiotic chemistry (in terms of its substrates, reaction pathways, catalysts, or energy coupling). The "metabolism-first" approach involves searching for naturally occurring catalysts and environmental conditions that allow chemistry-resembling core metabolic pathways to occur without

enzymes. This approach attempts to be in accordance with early Earth conditions when trying to reconstruct a non-enzymatic fundamental proto-metabolism that produces the main subsystems of biology in parallel with modern biology.<sup>92</sup> Furthermore, attempts to extract LUCA's genes using big data, although still in debate, suggest that LUCA's metabolism was not unfamiliar in the sense that it used cofactors and reactions commonly used by biology today.<sup>61</sup> Furthermore, in support of the “metabolism-first” hypothesis, the non-enzymatic formation of some of the core metabolic precursors, such as  $\alpha$ -keto acids, amino acids, and fatty acids, has recently been demonstrated under prebiotically plausible conditions, following reaction sequences that resemble core metabolic pathways.<sup>89,93,94</sup> Despite the vast chemical space of possible reaction products, these experiments displayed considerable specificity, suggesting that the core metabolism of metabolic reactions similar to those used in modern cells was not necessarily the result of the evolution of complex catalysts.<sup>95</sup> They were similarly possible under prebiotic Earth conditions with the help of inorganic catalysts (including abundant and rare metal catalysts), and their chemistries are not radically different from today's biochemistry. With time, the shift from non-enzymatic catalysis to enzyme-dominated catalysis can be explained by the following reasons: (1) limited non-enzymatic catalyst availability, (2) improved substrate specificity of enzyme-catalyzed reactions, (3) the prevention of side reactions in enzymatic catalysis, and (4) the greater possibilities of metabolic regulation offered by enzymatic catalysis.<sup>96</sup> While the RNA world hypothesis postulates ribozyme-catalyzed reactions, Markus Ralser argues that many ribozymes indirectly obtain their catalytic activity via their binding of metal ions such as zinc.<sup>95</sup> Hence, the origin of metabolism as an RNA-based metabolic reaction system seems highly unlikely without metal catalysts already in place. Nonetheless, we cannot deny the central function of RNA since it plays a dominant role both as a carrier of genetic information and as a catalyst. Therefore, once core metabolic reactions had become robust in the prebiotic scenario, genetic polymers would have emerged and contributed to the evolution of protometabolic reactions. They would have started to carry out specific reactions that otherwise would not have been possible without synergy between metabolism and genetics. Furthermore, based on the vast body of literature, most genetics-first experiments require multiple mutually incompatible steps, which require different conditions or settings, and are therefore intrinsically unlikely to have occurred on primitive Earth.<sup>97</sup> Aside from that, RNA world proposals often require continuous

delivery of substantial quantities of compounds such as cyanoacetylene, whose geochemical plausibility remains questionable.<sup>98</sup> In contrast, metabolism-first proposals utilize geochemically plausible and relatively simple inputs such as CO<sub>2</sub> and H<sub>2</sub>.<sup>88,89,90,99</sup> Another argument that disproves the plausibility of the RNA world is that the genetics-first hypothesis requires long polymers of structurally complex nucleotides (mass > 5000 D) with multiple chiral centers. At the same time, modern core metabolic cycles (such as rTCA cycle) which are at the base of rest of the biochemistry comprise small molecules (mass < 500 Da) that are often achiral.

A model that has been developed in our lab argue that life is more than just a collection of compounds. It is also a collection of processes known as metabolism.<sup>100</sup> This includes synthesis (anabolism), breakdown (catabolism), and the capture and transmission of energy (energy conservation). Thus, some fundamental questions must be asked in order to find the answer to life's origins.<sup>101</sup> These questions are: why does life ultimately build itself and decompose itself with only simple metabolic intermediates made of carbon, hydrogen, and oxygen? Why do some enzymes depend almost entirely on transition metals to catalyze their reactions? Why does nitrogen enter metabolism through reductive amination and transamination rather than Strecker's reaction? Why are sugars built through gluconeogenesis? Rather than oligomerizing HCN, why are nucleobases built from amino acids? By explaining how prebiotic chemistry is connected to modern metabolism, these questions can be answered. In order to demonstrate this continuity, one could envision a primitive version of metabolism that could build and break down keto acids, sugars, amino acids, and ribonucleotides in much the same way as today's pathways do.

Life's chemical processes form complex networks whose subsystems are kinetically linked, even when the different chemistries occur at different locations in the organism. To maintain its highly ordered state, life harnesses the dissipation of energy (out of equilibrium system).<sup>102</sup> For this reason, many researchers are looking for prebiotic chemistry with systems/subsystems that can form networks and interact in a similar way as in biochemistry, where components of networks or pathways are kinetically coupled. In attempts to build chemical systems that imitate features of life, the focus is on creating dissipative systems and maintaining non-equilibrium states. In order for this to occur, the environment would need to provide, for example, gradients of redox



potential, pH, temperature, or pressure, where, aided by naturally occurring metals or minerals, a complex reaction network could emerge and dissipate free energy.<sup>103</sup> A chemical network like this would have provided a foundation for the later development of polymer-based self-replicators, more complex organic catalysts, and organic compartments. Such a protometabolism could explain why life's biochemistry works in the way it does.<sup>101</sup>

Following the above arguments, theories of the origins of life based on metabolism-like prebiotic chemistry seem to be a viable model and may explain the complexity we observe today. In order to further elaborate the context of this thesis, I will introduce the biochemistry of core metabolic pathways, mainly focusing on amino acid synthesis, which is the focal point of this dissertation.

## 8. Core metabolic pathways biochemistry

Modern biochemistry, which consists of several interconnected subsystems of metabolic pathways, is constrained by the laws of chemistry and physics. Biochemical pathways cooperate simultaneously to enable life to generate its necessary metabolites and to obtain the energy that sustains it. Figure 5 shows a simplified overview of the core metabolic map, highlighting those pathways that are universal to the whole of biochemistry and of relevance to origin of life research. As a result, the primitive life on Earth could be organized as a proto-metabolic network built upon the combination of two known ancient carbon fixation pathways mentioned earlier, the W-L pathway and the rTCA cycle. The formation of amino acids from the rTCA cycle further expands the core carbon, hydrogen, and oxygen-based network to more complex molecules such as peptides and precursors to ribonucleotides. Because these "metabolic pillars" form the foundation of all life's chemistry, they may have also played a role in prebiotic chemistry.<sup>39,104</sup>

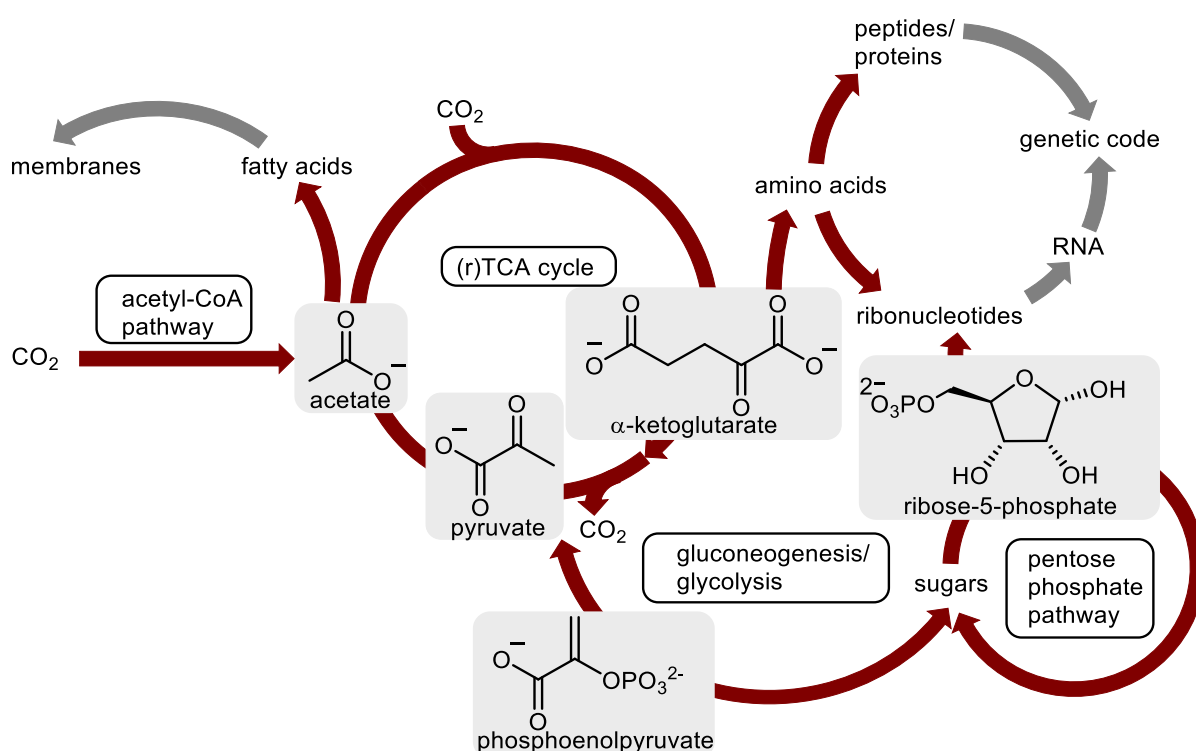


**Figure 5.** Map of core metabolism (figure adapted from reference 101).

### 8.1. The acetyl-CoA pathway (The Wood-Ljungdahl pathway)

This ancient pathway has two segments shown in Figure 6: (1) methyl synthesis from  $\text{CO}_2$  and  $\text{H}_2$ . The methyl synthesis branch is not conserved and uses different cofactors/enzymes in acetogens and methanogens (most ancient forms of life);<sup>105</sup> (2) CO-dependent acetyl CoA synthesis by carbon monoxide dehydrogenase/acetyl CoA synthase (CODH/ACS)<sup>42</sup> and this step is conserved in both archaea and bacteria (methanogens and acetogens). In acetogens, the pathway is essential for biosynthesis and energy metabolism (ATP synthesis). In methanogens, acetyl Co-A synthesis is only used for carbon metabolism, and energy metabolism is dependent on methane production (called methanogenesis).

In the first step of this pathway,  $\text{CO}_2$  is reduced using electrons from  $\text{H}_2$  to form a cofactor-bound formyl group, which undergoes further reductions to become a cofactor-bound methyl group. In the second step, one active site of a bifunctional metalloenzyme called carbon monoxide dehydrogenase/acetyl-CoA synthase (CODH/ACS) based on the Fe(Ni)S cluster catalyzes the reduction of  $\text{CO}_2$  to CO, and simultaneously, the cofactor bound methyl group is transferred at a different active site to this enzyme. Here, CO and a methyl group combine to form an acetyl-Ni species, which is then trapped by coenzyme A (HSCoA), a thiol, to produce acetyl CoA ( $\text{CH}_3\text{COSCoA}$ ), a thioester. Then, either acetyl-CoA can be converted to acetate via acetyl phosphate (energy metabolism), producing ATP,<sup>42,56</sup> or it can enter carbon metabolism in the rTCA cycle where it is converted to pyruvate. In methanogens, the cofactor-bound methyl group formed in the first step can go two ways: one is an acetyl-CoA synthesis for carbon metabolism, as recently mentioned, and the other one is ATP synthesis for energy metabolism, where it forms methane as an end-product.

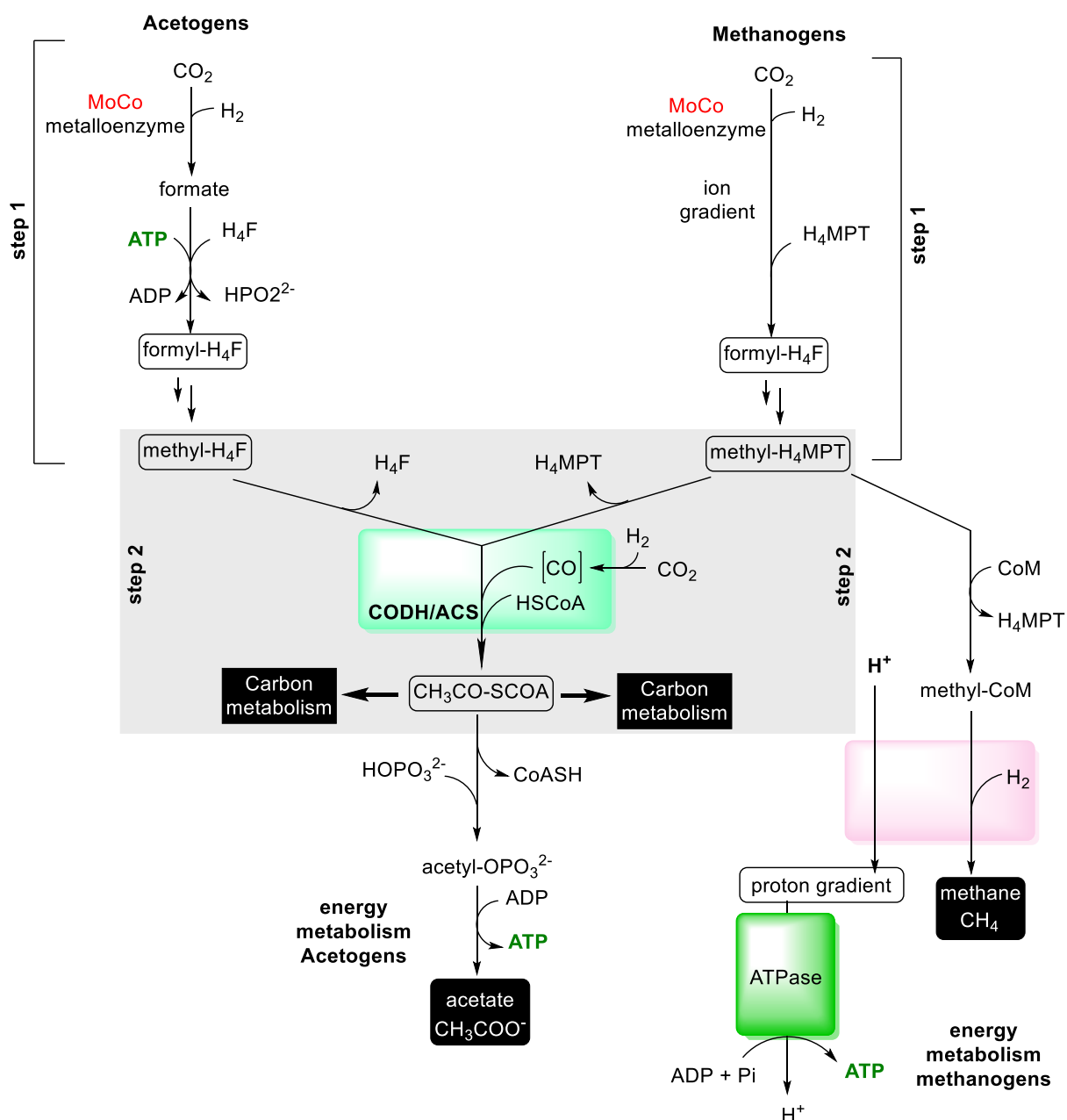


**Figure 6.** The Wood-Ljungdahl pathway in acetogens and methanogens. (**H<sub>4</sub>F**: tetrahydrofolate; **H<sub>4</sub>MPT**: tetrahydromethanopterin; **CODH/ACS**: carbon monoxide dehydrogenase/acetyl-CoA synthase; **CoASH**: coenzyme A; **CoM**: coenzyme; **MoCo**: molybdenum cofactor; **ADP** or **ATP**: adenosine di or triphosphate (Figure adapted from reference 56).

## 8.2. rTCA cycle and its analogue: glyoxylate/pyruvate reaction network

A total of ten enzymes regulate the biological rTCA cycle today, but similar steps were once catalyzed by a smaller, more promiscuous group of enzymes.<sup>106</sup> Many of the enzymes of the rTCA cycle rely on metal-based cofactors in their active sites, which may provide a clue as to how a prebiotic precursor to the cycle, catalyzed exclusively

by metal catalysts, could have originated on the early Earth.<sup>53,107,108</sup> In nature, this cycle is autocatalytic and includes ten carboxylic acids and three thioesters. These intermediates undergo six different types of reactions (Figure 7), which are (1) two reductive carboxylation reactions that form a C-C bond through two-electron reduction of CO<sub>2</sub> (step a, in Figure 7), (2) two carboxylations where C-C bond formation is ATP dependent (steps b, h), (3) three reductions (steps c, e, i), (4) three reversible hydrations and dehydrations (steps d, j, k), (5) two thioesterifications which are also ATP dependent (steps f, l), and (6) one ATP-dependent retro-aldol reaction that cleaves the C-C bond of citryl-CoA (step m). The specific mechanisms and enzymes involved in the rTCA cycle are not discussed in detail here, but a summary of the various steps in the rTCA cycle (Figure 7) will be given below:<sup>106</sup>

**I. Reductive Carboxylations (steps a, g):** catalyzed by a ferredoxin-dependent enzyme that contains a Fe-S cluster.

**II. Carboxylation (steps b, h):** pyruvate is converted into oxaloacetate in a two-step process via phosphoenolpyruvate (PEP) in step B. These steps are ATP dependent, and enzymes catalysing these steps contain divalent metals such as Mg<sup>2+</sup> or Mn<sup>2+</sup> in their active sites.

**III.  $\alpha$ -Ketoacid reduction (steps c, i):** Dehydrogenase enzymes catalyze the reversible reduction of oxaloacetate (R=H) or oxalosuccinate (R=CH<sub>2</sub>COOH) to the corresponding 2-hydroxy acids malate and isocitrate, respectively, using NADPH as the two-electron donor.

**IV. Dehydration-Hydration (steps d, j, and k):** This chemistry is reversible and is carried out by iron-sulfur cluster-containing enzymes.

**V. Alkene reduction (step e):** This reaction is catalyzed by fumarate reductase using a reductant with a low reduction potential. While many organisms use quinone (menaquinone, a vitamin K<sub>2</sub> analogue) as a reductant, certain autotrophs that operate the rTCA cycle use NADH as an electron donor.

**VI. Thioester synthesis (steps f and l):** The ATP-consuming conversion of a carboxylic acid to a thioester by succinyl CoA ligase is a critical step that, besides its important role in the rTCA cycle, controls other metabolic pathways like propanoate acid metabolism, porphyrin, and heme biosynthesis. Analogously, citryl CoA synthase

produces activated citrate thioester that undergoes retro-aldol cleavage to generate acetyl CoA, the precursor to lipid synthesis.

**VII. Retro-aldol cleavage (step m):** The redox-neutral cleavage of citryl CoA to oxaloacetate and acetyl CoA completes the rTCA cycle. The ATP-dependent enzyme citrate lyase completes this step. This reaction is critical because it imparts the rTCA cycle with an autocatalytic topology.

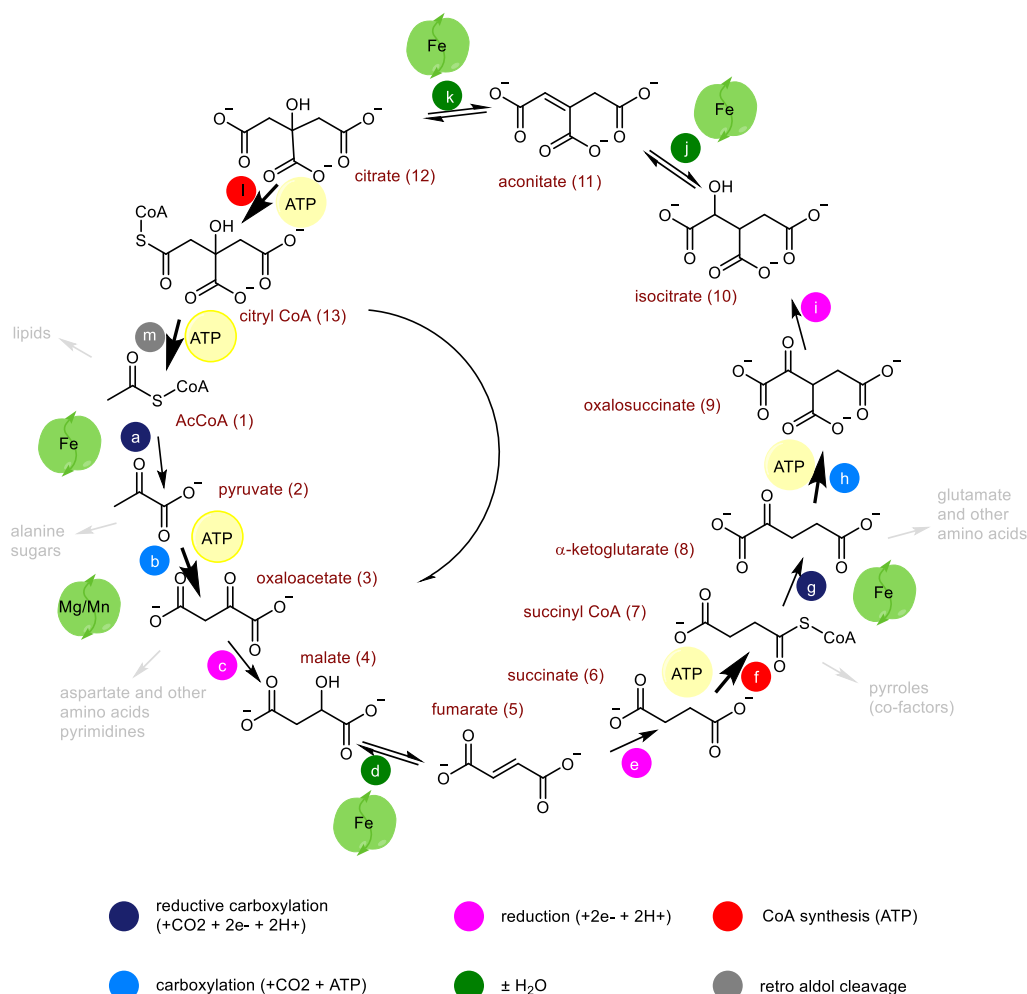


**Figure 7.** The reverse tricarboxylic acid (rTCA) cycle (figure reproduced from reference 101).

As far as prebiotic chemistry is concerned, no experimental studies have successfully completed the whole rTCA cycle using non-enzymatic chemistry since the ATP-dependent steps are missing (see section 8.2 on the rTCA cycle). Origins theories based on prebiotic analogues of biochemistry face a significant challenge in explaining

how C-C bonds can form without requiring energetically uphill ATP-consuming reactions.<sup>109</sup> Theoretical analysis of all known metabolic reactions revealed a hypothetical metabolic network that does not rely on phosphorus-containing cofactors, such as ATP, and contains all five universal metabolic precursors.<sup>110</sup> Pyruvate and glyoxylate are the two molecules that represent the biggest branching points of this hypothetical network, suggesting that primitive pre-ATP metabolisms, if they existed, would have been reliant on these two compounds (Figure 8). Pyruvate and glyoxylate as starting materials for prebiotic chemistry can be accessed through abiotic CO<sub>2</sub> fixation.<sup>111,112,113</sup> An rTCA cycle and a glyoxylate/pyruvate network studied in a prebiotic context are reported in section 11.

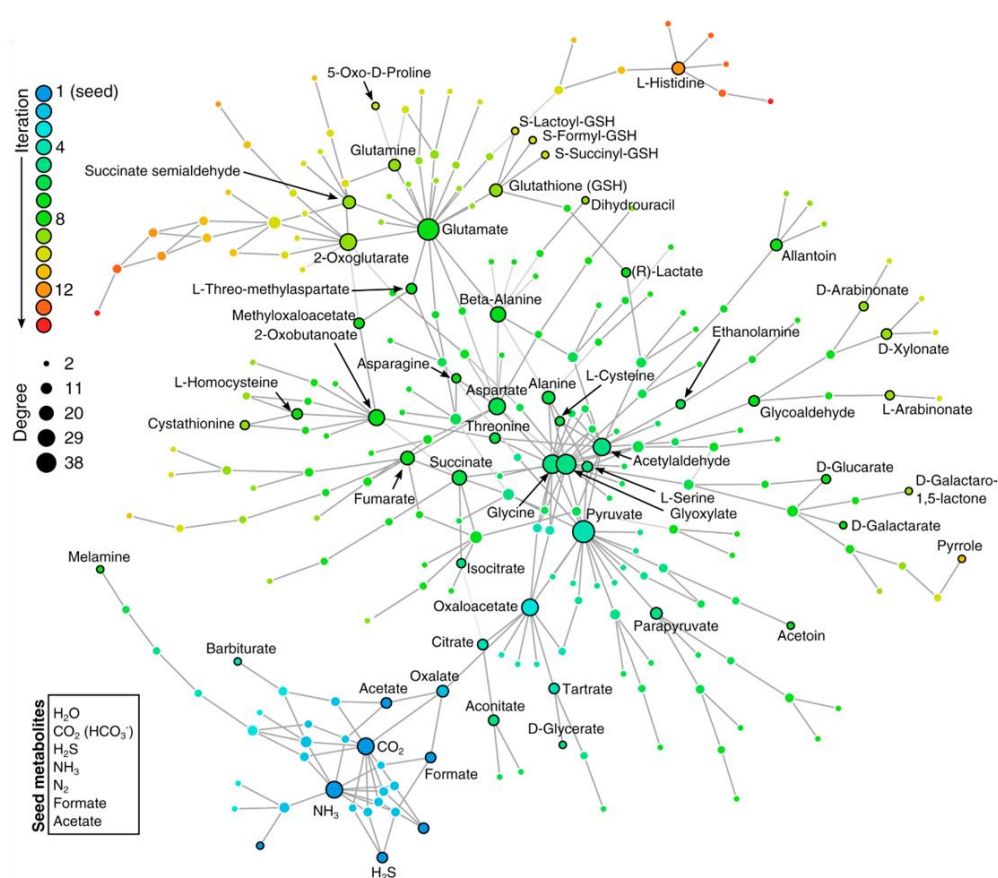


**Figure 8.** Phosphate-independent core network. The seed compounds are listed in the box at the bottom left of the figure. In the figure, reactions are not depicted, and metabolites are linked if they are interconverted through reactions responsible for expanding the network. During the network expansion, node color indicates the time (iteration) at which the metabolite appears, while node size indicates its degree, also indicative of the number of reactions added in subsequent iterations. In a few iterations from the seed, major hub metabolites (pyruvate, glutamate, and glycine) become available (blue nodes) (figure reproduced from reference 110).

### **8.3. Amino acids**

In biochemistry, amino acids are essential molecules, and twenty of them are privileged because they are the building blocks of proteins. Various cellular functions depend on amino acids, including nerve transmission and the biosynthesis of porphyrins, purines, and pyrimidines. The reason why life uses exactly twenty amino acids remains a mystery. Close observation tells us that the specific choice of the twenty amino acids by nature may be closely related to the evolution of the genetic code.<sup>114</sup> The organisation of biochemistry reveals that amino acid metabolism is closely linked to the (r)TCA cycle, which is accepted as the central hub for prebiotic chemistry (Figure 9).<sup>115</sup> In light of all this, the evolutionary origins of the chemistry of these 20 amino acids must be very ancient. When the first self-sufficient complex molecular system emerged on Earth, nucleic acids, amino acids, and peptides were probably present simultaneously. However, to unequivocally prove that amino acid biosynthesis and the genetic code share a common evolutionary history, it is necessary to gather experimental evidence.



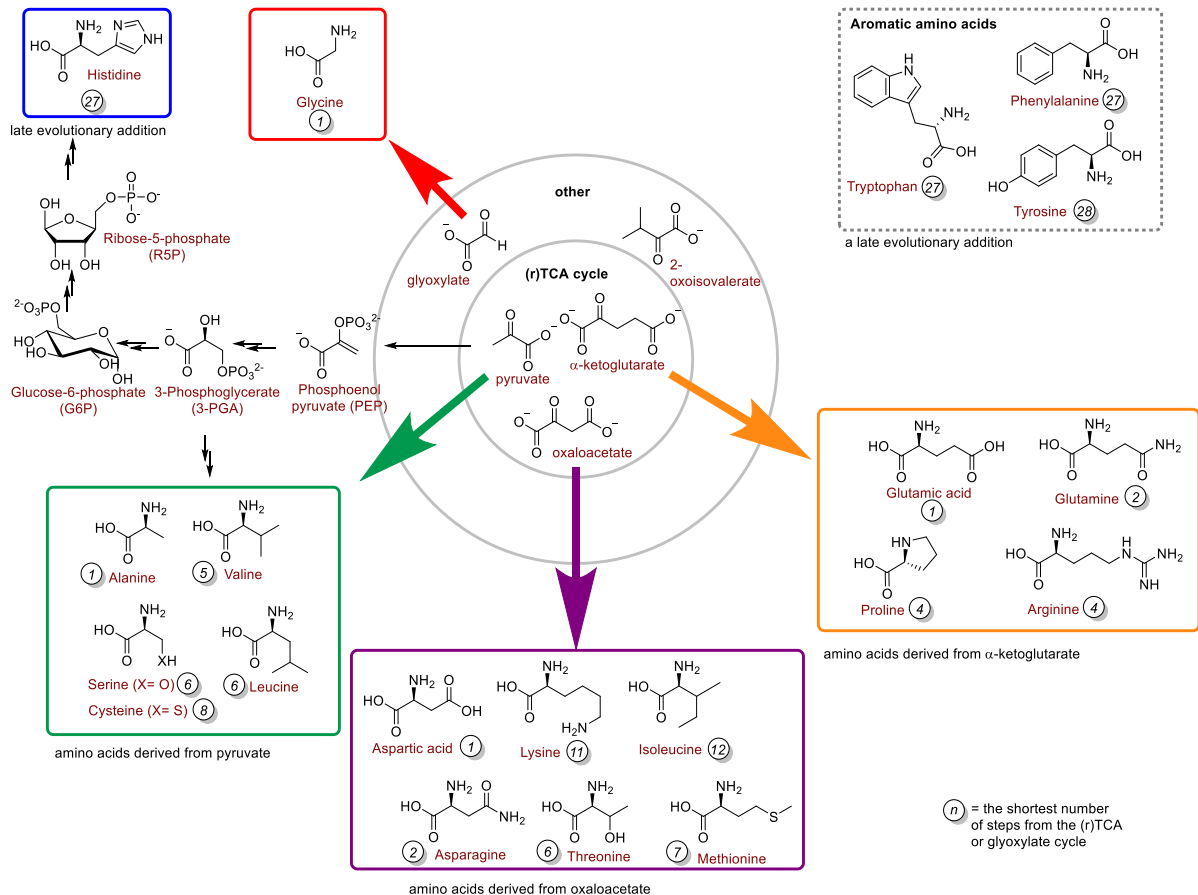


**Figure 9.** Twenty proteogenic amino acids were grouped by their biosynthetic origin (figure adapted from reference 101).

### 8.3.1. Structure of amino acids

An amino acid contains four different substituents attached to a central carbon atom (the α-C atom): the acid group (carboxylic acid group = COOH), a basic group (NH<sub>2</sub> amino group), the variable side chain called R, and a hydrogen atom (H).<sup>116</sup>

The side chain R can

- be a hydrogen atom: glycine, the simplest α-amino acid
- carry an additional acid group (COOH): aspartic acid, glutamic acid, or a modified acid group (an amide, CONH<sub>2</sub>, e.g., asparagine, glutamine)
- carry an additional basic group: arginine (a strong base), lysine, histidine (a weak base)
- carry a polar group: serine, threonine

- be a hydrocarbon (non-polar): alanine (R = methyl), phenylalanine (R = benzyl), valine (R = isopropyl)
- contain sulfur: cysteine, methionine

Accordingly, the  $\alpha$ -C atom carrying four groups with different chemical properties gives an amino acid a chiral character (apart from glycine, which is non-chiral). All proteinogenic amino acids (apart from Gly) are L-enantiomers. In a biological medium where the pH is usually buffered around 7.4 (physiological pH), amino acids have both a negative and a positive charge. The  $\text{COO}^-$  group has a  $\text{p}K_a \sim 3$ , while the  $\text{NH}_3^+$  has a  $\text{p}K_a \sim 9$ .<sup>116</sup>

### 8.3.2. Amino acid biosynthesis

A closer look at the 20 proteinogenic amino acids reveals that 16 of them are derived from the rTCA cycle intermediates pyruvate, oxaloacetate, and  $\alpha$ -ketoglutarate (Figure 9). Similarly, the other four are also derived from the rTCA cycle; however, they result from much longer biosynthetic pathways (over 20 steps). It is thus possible that the 16 amino acids synthesized in 1-12 steps may be the oldest, while those synthesized in more than 20 steps represent a later development (Figure 9).<sup>101</sup>

In living organisms, nitrogen incorporation into metabolism occurs when  $\text{N}_2$  or nitrate ( $\text{NO}_3^-$ ) is reduced to ammonia, which then undergoes reductive amination and transamination reactions via glutamate/glutamine couple (Figure 10).<sup>117</sup> First,  $\alpha$ -ketoglutarate undergoes reductive amination to glutamate, catalyzed by glutamate dehydrogenase, and then, glutamate transfers nitrogen to other  $\alpha$ -keto acids via transamination reactions. This process is mediated by enzymes called aminotransferases or transaminases that require pyridoxal phosphate as a cofactor. The mechanism proceeds in two steps. In the first step, an amine group is transferred from glutamate to pyridoxal phosphate. In the second step, the amino group from pyridoxal phosphate is transferred to the target  $\alpha$ -keto acids to generate its corresponding amino acids (Figure 10).<sup>118</sup>

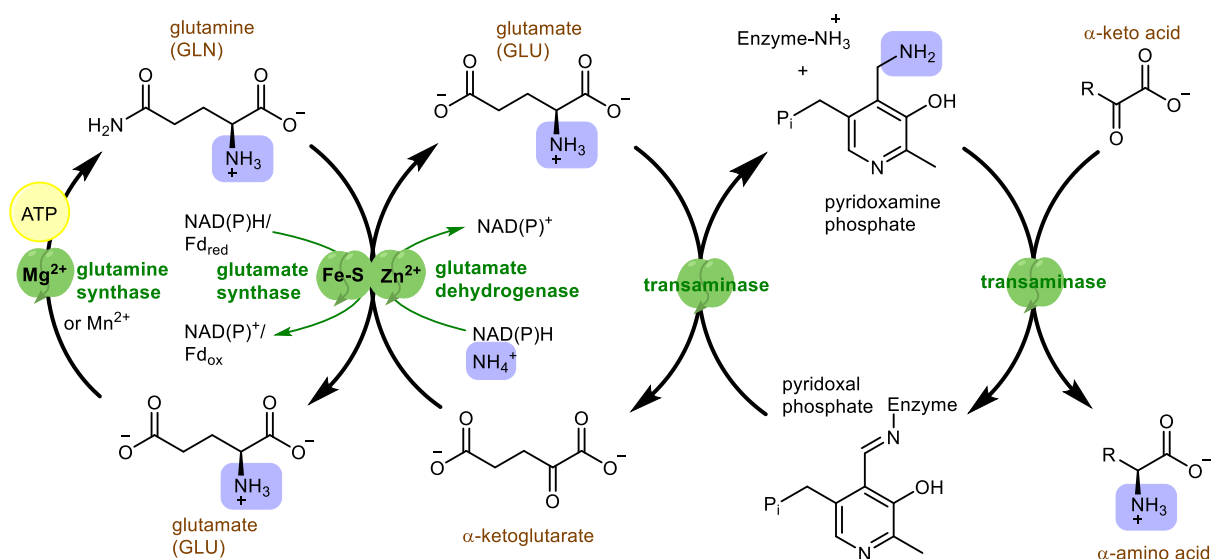


**Figure 10.** Biosynthesis of amino acids: reductive amination and transamination (Figure adapted from reference 127).

#### 8.4. Peptides

Approximately 45 % (w/w dry) of the cellular biomass consists of amino acids in the form of peptides. Amino acids are linked to one another via amide groups which are also called peptide bonds. A peptide is a short string of 2 to 50 amino acids. Sequential covalent bonds with additional amino acids yield a polypeptide chain, the building block of proteins, which feature a complete three-dimensional structure. A multitude of biological functions is provided by proteins/peptides, such as gene regulation, cell structure, catalysis of biological processes, and being the fundamental biological component for skin, hair, muscles, etc.

In the cells, proteins/peptides are synthesised by transcription and translation of the genetic code. Like proteins, DNA is a macromolecule, but in this case, the building blocks are nucleotides (Adenine, Thymine, Cytosine, Guanine). During peptide synthesis, DNA is first transcribed to RNA. RNA is another macromolecule made up of nucleotides slightly different from the ones in DNA (Adenosine, Uracil, Cytosine, Guanine). Next, in a biological process called translation, carried out by ribosomes, RNA sequences are translated into an amino acid sequence (Figure 11). During the translation process, a set of three nucleic acids, known as a “codon” is read by the ribosome; the amino acid corresponding to this codon is picked up in the surrounding

medium, using a transfer RNA possessing a sequence complementary to the codon. Then, the amino acid is added to the chain of amino acids by forming a peptide bond. The ribosome then reads the next codon, and the cycle of elongation of the  $\alpha$ -amino acid chain continues until termination (Figure 11).<sup>119</sup>

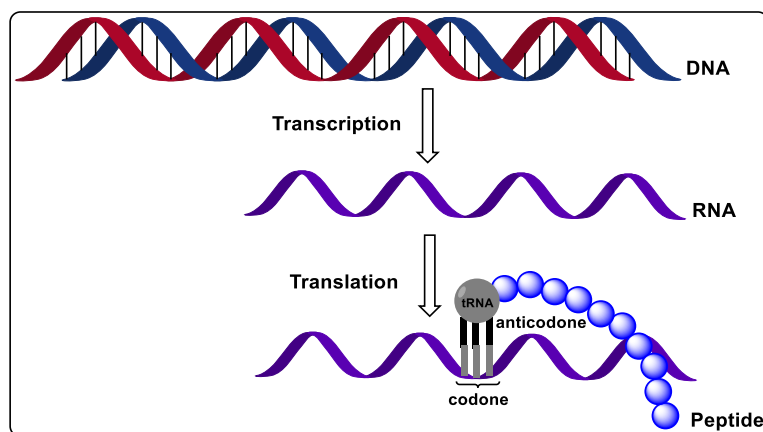


**Figure 11.** Biosynthesis of peptides: transcription and translation.

### 8.5. Carbohydrates (sugars)

Carbohydrates (sugars) are energy-providing nutrients. Additionally, two of them, ribose and deoxyribose, are present in the backbone of RNA and DNA, respectively. Carbohydrates are organic compounds consisting of carbon (C), hydrogen (H), and oxygen (O) atoms. They contain a carbonyl group (aldehyde or ketone) and at least two hydroxyl groups (-OH). In biochemistry, sugar biosynthesis starts from pyruvate and follows a pathway known as gluconeogenesis (anabolic pathway). Gluconeogenesis is conserved across all life, including archaea and bacteria.<sup>120</sup> Biological pathways, known as glycolysis and the pentose phosphate pathway, break sugars down back to pyruvate. The types of chemical mechanisms involved in all of the above-mentioned pathways, whether anabolic or catabolic, are quite similar and based on various metalloenzymes. They include phosphorylations and dephosphorylations, isomerizations, hydrations and dehydrations, and aldol and retro-aldol reactions. In these pathways, most intermediates are phosphorylated and used as synthetic precursors for other metabolic pathways. For example, glycerol-3-phosphate is involved in lipid metabolism, phosphoenolpyruvate (PEP) in aromatic

amino acids synthesis, and ribose 5-phosphate (R5P) or phosphoribosyl pyrophosphate (PRPP) – in ribonucleotides synthesis. (Figure 12)<sup>101</sup>

Prebiotic chemistry attempts to recreate sugar metabolism are discussed in a recent review by our lab, where prebiotic syntheses similar to biosynthesis are highlighted.<sup>101</sup> The pentose phosphate pathway and much of glycolysis can be enabled without enzymes by  $\text{Fe}^{2+}$ .<sup>121,122</sup> However, there has been very little research on non-enzymatic analogues of gluconeogenesis. Non-enzymatic gluconeogenesis requires the discovery of activated phosphate donors, for example, polyphosphates, and the identification of suitable mineral catalysts. Even though these goals are challenging, they are worthwhile to investigate because they would provide a fundamental understanding of why sugar metabolism works the way it does.

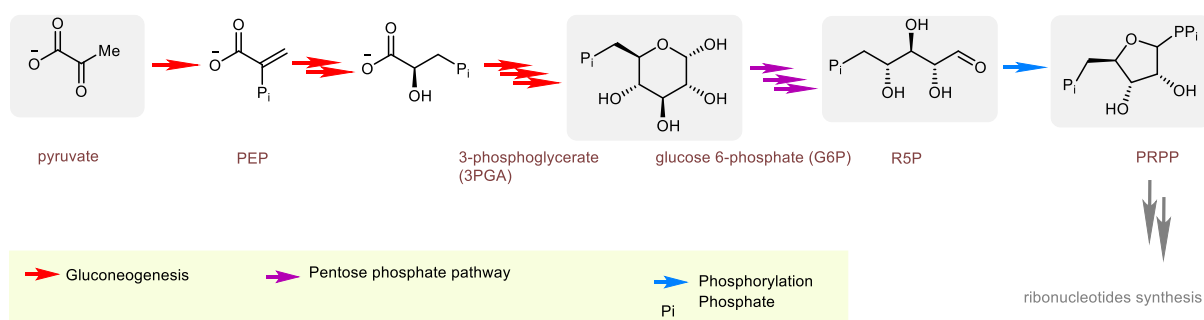


**Figure 12.** Overview of reactions from pyruvate to PRPP (Figure adapted from reference 101).

## 8.6. Fatty acids (lipids)

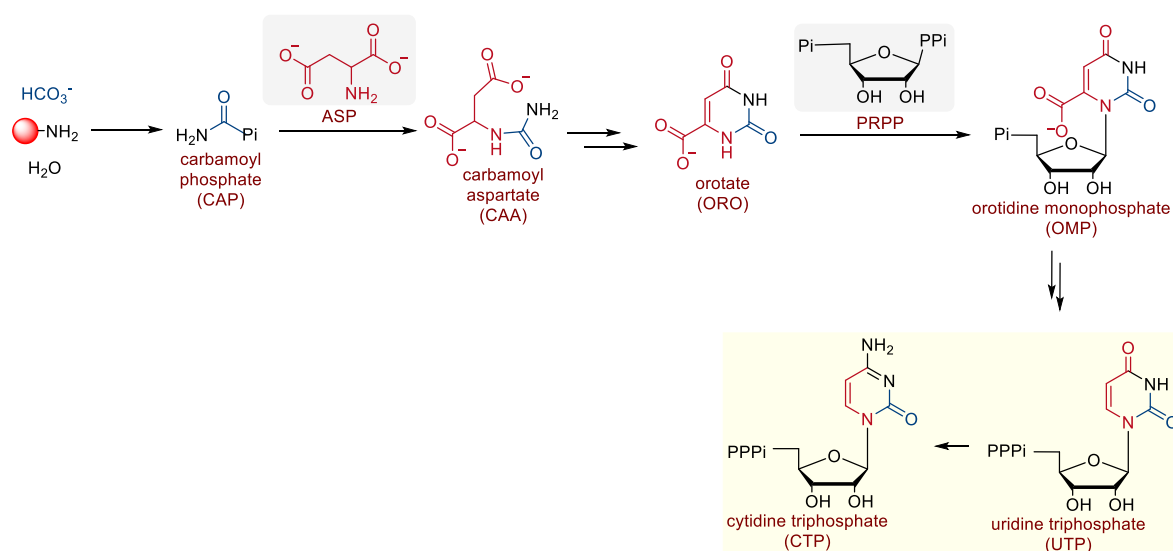
In chemistry, a fatty acid is a carboxylic acid with either a saturated or unsaturated aliphatic chain. Due to their role in forming biological cell membranes, they play an important role in compartmentalization and other functions within the organism. There has been little experimental work that recapitulates non-enzymatic fatty acid biosynthesis.<sup>101</sup> The role of fatty acids in the compartmentalization of cells is undeniable. However, it is also possible that compartmentalization during the early times of prebiotic chemistry could have been achieved by other means, such as inorganic compartments in rocks or minerals or by other types of organics present in a protometabolism. Thus, I won't discuss their biosynthesis/synthesis in detail.<sup>123,124</sup>

## 8.7. Nucleic Acids

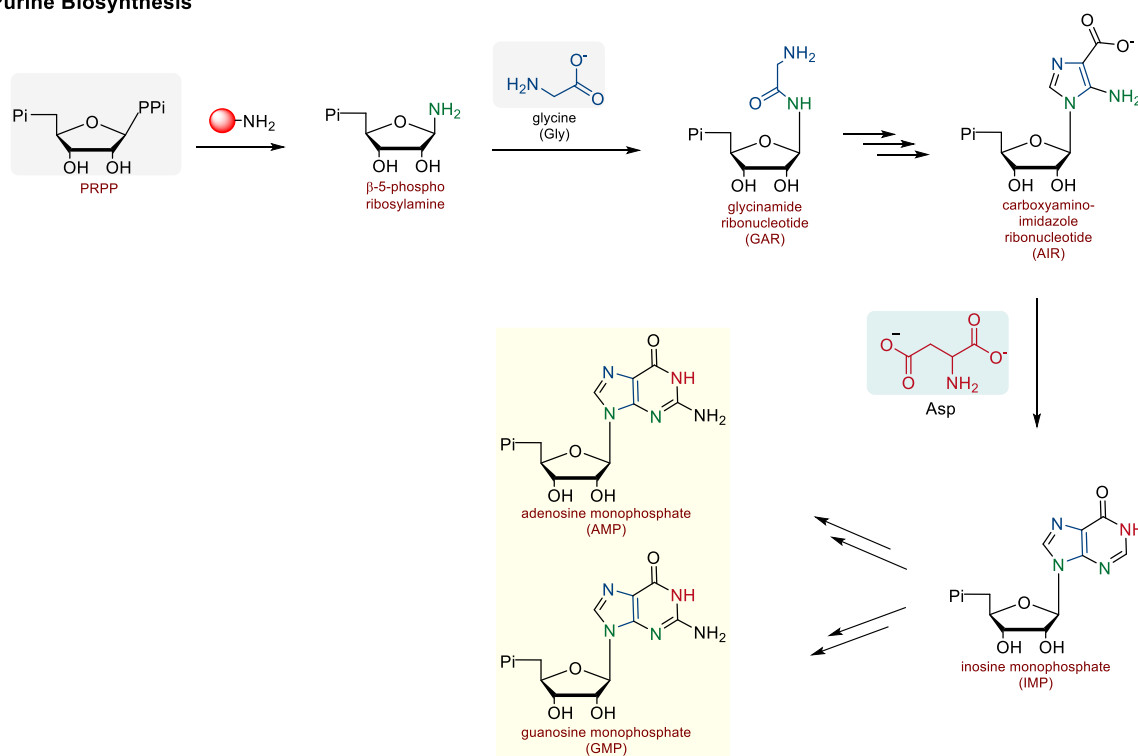
The continuity of life depends on nucleic acids, which make up the universal genetic code that governs the replication and heredity processes of all life on Earth. Additionally, nucleic acids play a key role in directing protein synthesis. The two main classes of nucleic acids are deoxyribonucleic acid (DNA) and ribonucleic acid (RNA). A ribonucleotide comprises a nitrogenous base - adenine or guanine (purines), cytosine or uracil (pyrimidines) - the pentose sugar ribose, and one or more phosphate groups (one to three). During ribonucleotide biosynthesis, ribose is always supplied as phosphoribosyl pyrophosphate (PRPP, sourced from the pentose phosphate pathway, previously discussed in carbohydrate metabolism).

Pyrimidine ribonucleotides are constructed from the coupling of PRPP and orotate, the latter of which is built from aspartate and carbamoyl phosphate via carbamoyl aspartate (Figure 13).<sup>101</sup> The coupling between PRPP and orotate gives orotidine monophosphate (OMP), followed by the synthesis of uridine monophosphate (UMP) and cytidine monophosphate (CMP). The purine ribonucleotides are produced by coupling PRPP and glycine, followed by successive reactions towards inosine monophosphate (IMP) and adenosine monophosphate (AMP). A few general observations can be made regarding the biosynthesis of ribonucleotides. Firstly, metals are present in the active sites of enzymes. Secondly, all three amino acid building blocks of nucleobases can be obtained from the rTCA cycle intermediates (aspartate from oxaloacetate and glutamine from  $\alpha$ -ketoglutarate via glutamate) or from closely related pathways (glycine from, for example, glyoxylate). PRPP is provided by sugar metabolism. These observations suggest that ribonucleotide biosynthesis probably evolved along with a metabolism that provided all these building blocks. Integrating undirected abiotic ribonucleotide synthesis with non-enzymatic pathways would be a milestone to produce its building blocks, as the “metabolism first” and “RNA world” scenarios would cease to be mutually exclusive.<sup>101</sup> In a recent work by our lab, orotate synthesis is successfully uncovered by mimicking the biological pathway.<sup>125</sup>

## Pyrimidine Biosynthesis



## Purine Biosynthesis



Pi = phosphate

PPi = pyrophosphate

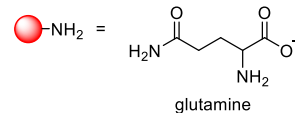


**Figure 13.** An outline of purine and pyrimidine ribonucleotide biosynthesis, highlighting the key intermediates involved in these pathways (Figure adapted from reference 101).

The laws of chemistry and physics constrain biology regardless of how life emerged. Keeping this fact in mind, prebiotic chemists have begun to focus on the chemistry that deals not only with individual syntheses or classes of biomolecules but with complex reaction networks, resembling life's metabolic pathways in some ways. As a conclusion to the introduction part, after highlighting the major components of core metabolism which form a scaffold for the whole of biochemistry, we will now discuss the experimental investigations conducted during my doctoral studies.



## **Thesis perspective**

My dissertation investigates the idea that amino acids could have been synthesised by prebiotic chemistry in the same way that life does it now. Thereby, the work carried out during my thesis sheds a light on viable prebiotic amino acid synthesis, through transamination and reductive amination reactions from  $\alpha$ -ketoacids, which are intermediates of the rTCA cycle/glyoxylate cycle.

Since amino acids are the key bridges between  $\text{CO}_2$  fixation pathways (rTCA cycle/glyoxylate cycle) and more complex systems, such as genetics, self-organised reaction networks linking amino acids and  $\alpha$ -ketoacids synthesis are also uncovered. Moreover, amino acids are precursors to peptides, thus we also explored peptide synthesis in one-pot experiments, from  $\alpha$ -ketoacids to amino acids to oligomers.

## **Part II. Results and discussion**

## 9. Amino acids

Since amino acids play a central role in life, amino acid abiogenesis is one of the most thoroughly explored areas of prebiotic chemistry. The famous Miller-Urey spark discharge experiment demonstrated the significance of amino acid synthesis in abiogenesis. It has also been discovered that amino acids are present in meteorites, within comet tails, and in space itself.<sup>128,129,130</sup> Prebiotic amino acid synthesis can also be achieved by chemistries such as the Strecker reaction with  $\alpha$ -aminonitrile intermediates) or the Bücherer–Bergs synthesis with hydantoin intermediates (Figure 14).<sup>131,132,133</sup> However, these syntheses differ strongly from how biology makes amino acids, which is from  $\alpha$ -ketoacids via transamination and reductive amination.

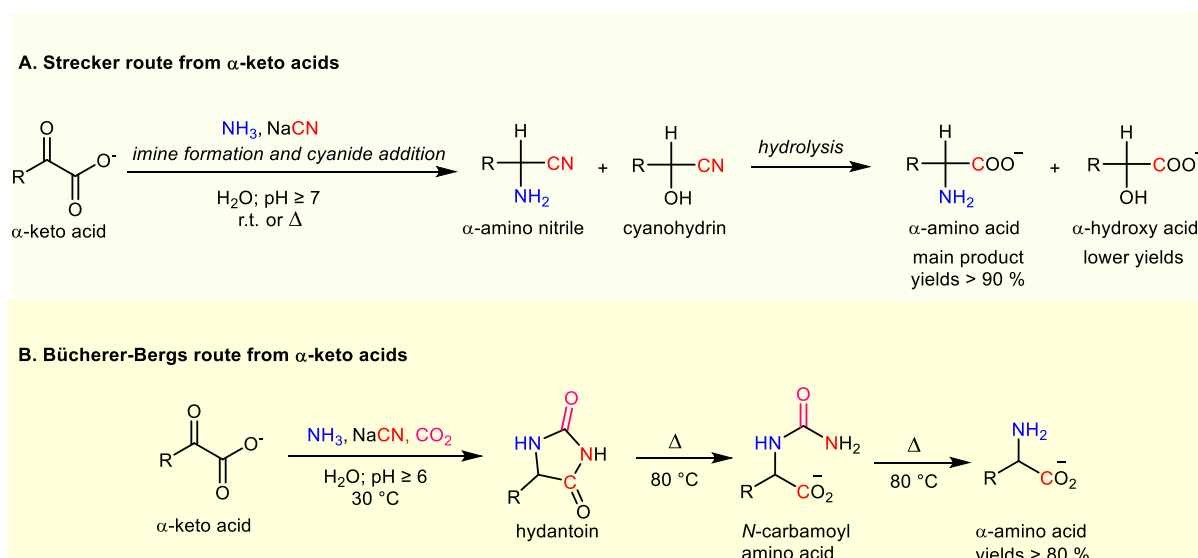


**Figure 14.** Prebiotic amino acid synthesis different from biology.

### 9.1. Prebiotic attempts to explain amino acids synthesis via reductive amination

Due to the abundance of iron minerals on planet earth and their presence in active sites of metallo enzymes, most prebiotic reductive aminations are studied using iron minerals.<sup>134</sup> Huber and Wächtershäuser; barge and co-workers have reported reductive amination with  $\text{NH}_3$  to obtain alanine, glutamate, phenyl alanine and tyrosine using Iron based minerals such as  $\text{FeS}$ ;  $\text{Fe}(\text{OH})_2$  or mixed-valence iron oxyhydroxide minerals (Figure 15A).<sup>136,137</sup> A study by Kitadai and co-workers demonstrated reductive amination of several  $\alpha$ -ketoacids (glyoxylic, pyruvic, oxaloacetic, and  $\alpha$ -ketoglutaric) promoted by partially electroreduced  $\text{FeS}$  ( $\text{FeS-Fe}^0$ ) at r.t. (Figure 15 A)<sup>135</sup> In all these reports, experiments are conducted using large excess of ammonia (typically 100 equiv. of ammonia) to push the equilibrium towards the formation of an NH-imine in water. A highly concentrated ammonia environment raises questions about its geochemical plausibility. Our lab has also reported the reduction of all four-core metabolic ketoacids (glyoxylate, pyruvate, oxaloacetate and ketoglutarate) with bifunctional amines such as hydroxylamine as nitrogen donors using metallic iron as a reductant (Figure 15B).<sup>138,139</sup> While bifunctional amines such as hydroxylamine and hydrazine may be useful, their relevance to a broader protometabolism is doubtful, due to their incompatibility with electrophilic functional groups such as thioesters and acyl phosphates.

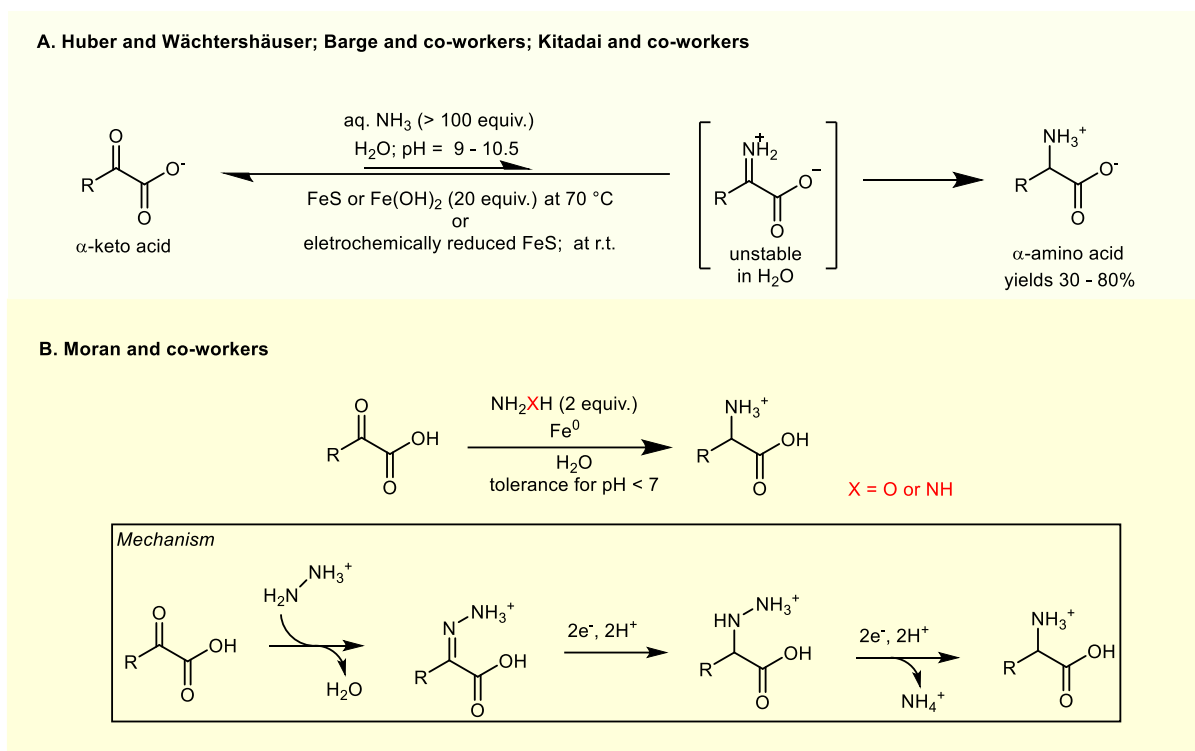


**Figure 15:** Previous examples of prebiotic reductive amination reactions.

## 9.2. Prebiotic attempts to explain amino acids synthesis via transamination

One of the first reports of non-enzymatic ketoacid transamination is from Nakada and Weinhouse in 1953 who synthesized glycine from glyoxylic acid at ambient temperature using glutamine in aqueous phosphate buffer as the amine donor (Figure 16A).<sup>140</sup> In 1959 Mix reported that different metal ions could be used between pH 4 and pH 11 and at temperatures between 37 and 70° C for the transamination of pyruvate to alanine.<sup>141</sup> In his studies, he found that ornithine and arginine were the best amine group donors, histidine was the least reactive one and  $\text{Cu}^{2+}$  was the best catalyst among several tested (Figure 16B). A few years later, Oró demonstrated the transamination of  $\alpha$ -ketoglutarate at 85°C using  $\text{Al}^{3+}$ ,  $\text{Fe}^{2+}$ ,  $\text{Fe}^{3+}$ , and  $\text{Cu}^{2+}$  as catalysts, and identifying histidine as an effective amine donor among others (Figure 16C). The best activity was observed at pH 4, whereas at neutral pH only little reactivity was observed.<sup>142</sup> Moreover, similar transamination reactions have later been reported using metal ions such as  $\text{Al}^{3+}$  and  $\text{Fe}^{2+}$ , at higher temperatures (above 70 °) and often at acidic or basic pH levels.<sup>143,144</sup>

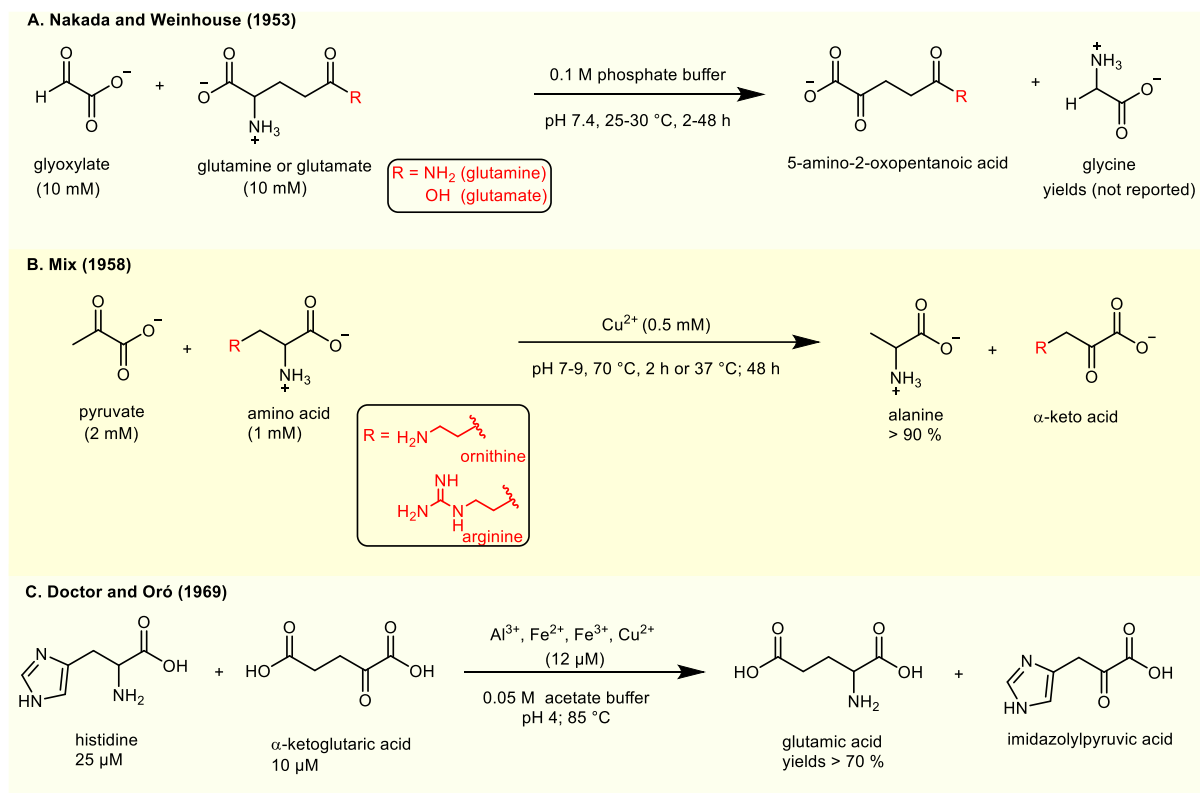


**Figure 16:** Previous examples of prebiotic transamination reactions.

## 10. Chapter's objective: non-enzymatic transamination reactions

Recently, analogues of entire metabolic pathways, or fragments thereof, have been found to occur under metal or metal ion catalysis, including the Krebs or reverse Krebs cycles, the acetyl CoA pathway, glycolysis, etc.<sup>111,121,145,146,147</sup> These observations support proposals that precursors to some core metabolic pathways emerged under inorganic catalysis and were later refined by organic catalysis from co-factors and eventually, by enzymes. Therefore, we wanted to explore amino acids synthesis via non-enzymatic transamination under biological conditions to understand whether an abiotic version of transamination catalyzed by metal ions ubiquitous on early earth might have played a role in the pre-enzymatic origins of biological amino acid metabolism. It is well established that transamination reactions still happen without enzymes under catalysis by metal ions. However, these studies are often contradicting, and the precise role of metal ions in the context of transamination including all 4-core metabolic ketoacids is limited. Mostly studies are done at higher temperatures (70-100 °C), and little work has been done on the overall mechanism of transamination. Therefore, we wanted to re-evaluate non-enzymatic transamination reactions under a wide variety of metal ions as catalysts and under plausible biological conditions (pH 7, 20-50 °C). Further, to elucidate the mechanism, kinetic, stereochemical, and computational studies were also performed. In our recent publication, my colleague Dr. Mayer describes in great detail the mechanical and computational studies that he performed, so they are not discussed into every details here.<sup>127</sup>

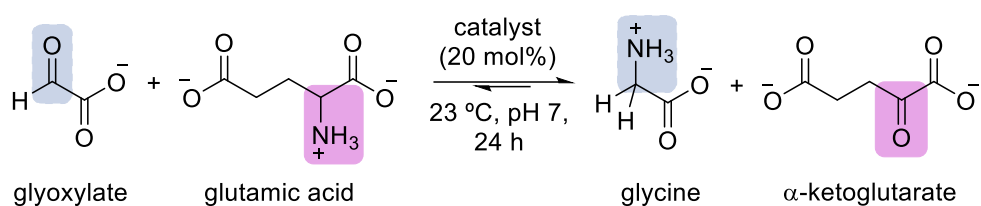
### 10.1. Results and discussion

Initially, we studied the effects of 20 mol% of chloride and sulfate salts of various transition metals on the transamination reaction between glyoxylate and glutamic acid to yield glycine and  $\alpha$ -ketoglutarate at 23 °C and pH 7 (Table 1). To avoid necessary pH adjustments for screening experiments, 1 M phosphate buffer at pH 7 was used as solvent. We found that the transamination reaction of 30 mM glyoxylate with 1.5 equiv. glutamic acid yields glycine in 0.3–91% yield as determined by quantitative <sup>1</sup>H NMR spectroscopy after removal of the metals with the ion-exchange resin Chelex (Table 1). The Gibbs free energy of the reaction was estimated to be  $\Delta G^0 = -14.9 \text{ kJ mol}^{-1}$

based on reported enzyme kinetics (see supporting information for details).<sup>148,149</sup> Thus, 29.8 mM glycine should form if the equilibrium establishes without any side reactions. In our reactions, the lower yields of glycine compared to the thermochemical prediction were attributed to the competing decomposition of glyoxylate in the presence of some metals as well as side reactions, e.g., the aldol reaction of glyoxylate with in situ formed  $\alpha$ -ketoglutarate to form isocitroyl formate and further dehydration of latter to aconitoyl formate (see Figures S1 and S2 for representative NMR spectra).<sup>144</sup> The most efficient catalysts for the transamination reaction at 23 °C and pH 7 were found to be  $\text{Ni}^{2+}$ ,  $\text{Cu}^{2+}$ ,  $\text{V}^{5+}$ , and  $\text{Co}^{2+}$  (entries 1–4).<sup>141</sup> However, many other transition metals still show a significant catalytic activity (entries 5–12), surpassing the uncatalyzed background reaction (entry 21).



**Table 1.** Reaction of glyoxylate (30 mM) and glutamic acid (45 mM) in the presence of 20 mol% of different metal salts at 23 °C (1 M phosphate buffer, pH 7, 24 h).<sup>a</sup>

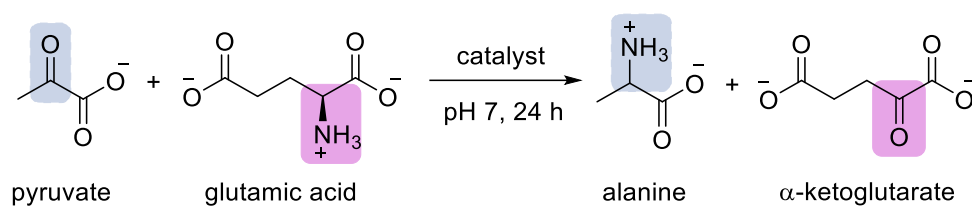


entry	catalyst	yield (%)	entry	catalyst	yield (%)
1	NiCl <sub>2</sub>	90.5 ± 1.2	12	VOSO <sub>4</sub>	1.2
2	CuCl <sub>2</sub>	86.6 ± 1.3	13	CrCl <sub>2</sub>	0.7
3	CoCl <sub>2</sub>	60.9 ± 6.9	14	MgCl <sub>2</sub>	0.5
4	NaVO <sub>3</sub>	49.0 ± 4.0	15	WCl <sub>6</sub>	0.5
5	FeCl <sub>3</sub>	25.5 ± 2.9	16	MoCl <sub>3</sub>	0.4
6	FeCl <sub>2</sub>	20.2	17	MnCl <sub>2</sub>	0.3
7	AlCl <sub>3</sub>	8.3	18	CrCl <sub>3</sub>	0.3
8	ZnCl <sub>2</sub>	7.2	19	CeCl <sub>3</sub>	0.3
9	KAl(SO <sub>4</sub> ) <sub>2</sub>	6.7	20	CaCl <sub>2</sub>	0.3
10	PdCl <sub>2</sub>	5.8	21	none	0.4 ± 0.1
11	HgCl <sub>2</sub>	5.6	22	enzyme	99.3 <sup>b</sup>

<sup>a</sup>Yields were determined by quantitative <sup>1</sup>H NMR spectroscopy with dimethyl sulfone as an internal standard after removing metal ions with Chelex. Errors correspond to standard deviations (see supporting information for details). <sup>b</sup>Maximum possible yield considering the Gibbs free energy of the reaction, the concentrations of the reactants, and the temperature.<sup>148,149</sup>

Next, we studied whether the reaction conditions identified for the transamination of glyoxylate to glycine are suitable for the transamination of pyruvate with glutamic acid to yield alanine and  $\alpha$ -ketoglutarate (Table 2). Transamination with glutamic acid to pyruvate is thermodynamically far less favoured than to glyoxylate, as evident from the only slightly exergonic Gibbs free energy of the reaction with  $\Delta G^0 = -1.04 \text{ kJ mol}^{-1}$ .<sup>148</sup> Accordingly, from 30 mM pyruvate and 45 mM glutamic acid, a maximum of 19.7 mM alanine (66% yield) should form if the equilibrium can establish without side reactions. However, the reaction with 20 mol%  $\text{Cu}^{2+}$ ,  $\text{Co}^{2+}$ ,  $\text{Ni}^{2+}$ , or  $\text{V}^{5+}$  as catalyst yielded only small amounts of alanine (less than 2 %) after 24 h at room temperature. Increasing the amount of catalyst and the reaction time resulted in higher conversion: with 50 mol%  $\text{Cu}^{2+}$ , 67% alanine formed after 72 h at 50 °C.  $\text{V}^{5+}$  and  $\text{Ni}^{2+}$  yielded less alanine (30% and 11% at 50 °C and 72 h, respectively), and  $\text{Co}^{2+}$  showed little conversion. The results in Table 2 generally parallel those of Mix, who found that  $\text{Cu}^{2+}$  was the most efficient catalyst in the transamination of pyruvate with various amine donors at 70 °C (based on the yield after 2 h, pH 7).<sup>141</sup>

**Table 2.** Transamination reaction of pyruvate (30 mM) with glutamic Acid (45 mM) at 23 °C and 50 °C (1 M phosphate buffer, pH 7).<sup>a</sup>

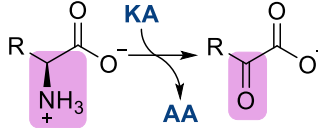
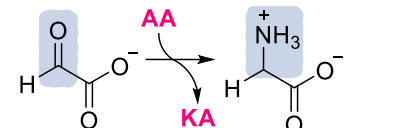
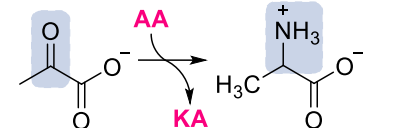
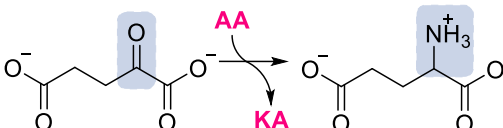
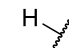
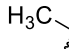
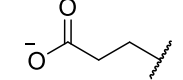
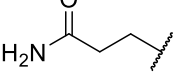
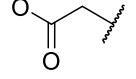
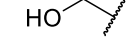


catalyst	yield (%)		yield (%)		yield (%)	
	with 20 mol%		with 50 mol%		with 100 mol%	
	23 °C	50 °C	23 °C	50 °C	23 °C	50 °C
after 24 h						
Cu <sup>2+</sup>	2.0	28	4.9	25	9.4	50
Co <sup>2+</sup>	nd	nd	nd	0.4	nd	0.7
Ni <sup>2+</sup>	nd	2.8	0.3	4.1	0.7	4.8
V <sup>5+</sup>	0.9	8.6	1.3	17	1.9	22
none	nd					
after 72 h						
Cu <sup>2+</sup>	6.6	48	19	67	21	55
Co <sup>2+</sup>	nd	0.5	nd	2.0	nd	0.9
Ni <sup>2+</sup>	0.5	7.8	0.7	11	1.8	14
V <sup>5+</sup>	3.0	15	4.2	30	4.9	39
none	nd					

<sup>a</sup>Yields were determined by quantitative <sup>1</sup>H NMR spectroscopy with dimethyl sulfone as an internal standard after removing metal ions with Chelex (see supporting information for details). nd = not detected (detection limit ≈ 0.3% alanine).

We next investigated the reactions between other amine donors and  $\alpha$ -ketoacids.  $\text{Cu}^{2+}$  was used as catalyst due to its strong performance in the reactions of glutamic acid with both glyoxylate and pyruvate. Thus, glyoxylate, pyruvate, and  $\alpha$ -ketoglutarate (30 mM) were reacted with different amino acids (45 mM) in the presence of 20 mol%  $\text{Cu}^{2+}$  at 50 °C for 72 h (Table 3). Again, thermochemistry is the factor deciding the feasibility of a specific transformation, and enzymatic data can be used to gauge the extent to which a specific combination will react. However, it must be acknowledged that the position of the equilibria will also be affected by the 20 mol% of catalyst present due to formation of metal chelates. Compared to enzyme-catalyzed transaminations, the metal-catalyzed reactions were found in most cases to reach lower yields of products compared to the enzymatic reaction. Table 3 summarizes reported Gibbs free energies for some combinations of substrates and the observed yield of the transamination product under metal catalysis. While oxaloacetate could be a possible substrate for transamination reactions to yield aspartic acid, we found that it readily undergoes decomposition to pyruvate in the presence of metal ions under the reaction conditions.<sup>166</sup> Pyruvate, in turn, undergoes transamination to yield alanine. Accordingly, we did not detect the formation of aspartic acid and, thus, did not further investigate this reaction. In line with the reported thermochemistry, transamination reactions with glyoxylate generally yield significant amounts of glycine with glutamic acid, glutamine, alanine or aspartic acid. Slightly lower concentrations of glycine were observed when serine was used as amine donor. With pyruvate as substrate, only small amounts of alanine (5.7 mM) were formed when using glycine as amine donor, in line with the unfavourable thermochemistry of the reaction. With glutamic acid, glutamine, or aspartic acid as amine donors, 5.6–29.8 mM of alanine were obtained which were highest for aspartic acid due to the formation of oxaloacetate and the subsequent side reaction mentioned above. Similar to the transamination of pyruvate with glycine, only small amounts of glutamic acid form in the reaction of  $\alpha$ -ketoglutarate with glycine. The formation of significant amounts of glutamic acid in the reactions of  $\alpha$ -ketoglutarate with alanine, glutamine, and aspartic acid highlights the similar thermochemistry of these reactions. Serine, however, only transaminates to a minor extent to both  $\alpha$ -ketoglutarate and pyruvate.

**Table 3.** Comparison of theoretical and experimentally obtained concentrations for the Cu<sup>2+</sup>-catalyzed (20 mol%) transamination of keto acids (KA, 30 mM) and amino acids (AA, 45 mM) at 50 °C (1 M phosphate buffer, pH 7, 72 h).

									
R of amino acid (AA)	$\Delta G^{0,a}$ / kJ mol <sup>-1</sup>	[glycine] <sub>enzym.</sub> <sup>b</sup> / mM	[glycine] <sub>exp.</sub> <sup>c</sup> / mM	$\Delta G^{0,a}$ / kJ mol <sup>-1</sup>	[alanine] <sub>enzym.</sub> <sup>b</sup> / mM	[alanine] <sub>exp.</sub> <sup>c</sup> / mM	$\Delta G^{0,a}$ / kJ mol <sup>-1</sup>	[glutamate] <sub>enzym.</sub> <sup>b</sup> / mM	[glutamate] <sub>exp.</sub> <sup>b</sup> / mM
	0	ident.	ident.	+13.9	2.6	4.6	+14.9	2.2	4.3
	-13.9	29.7	19.9	0	ident.	ident.	+1.04	16.3	11.6
	-14.9	29.8	24.5	-1.04	19.7	14.4	0	ident.	ident.
	d	d	24.2	d	d	11.1	d	d	6.1
	-10.2	28.8	18.2 14.7 (alanine) <sup>e</sup>	+3.66	12.2	33.0 <sup>e</sup>	+4.73	10.7	8.9 6.8 (alanine) <sup>e</sup>
	-10.8	29.1	10.2	+3.06	13.1	0.8	+4.13	11.5	≈0.5

Experimental thermochemistry from refs 22 and 23 or derived from thermodynamic cycles as shown in the Supporting Information of reference 114. **b** Calculated based on the mass action law, the reactant concentrations, and the equilibrium constants (at 298 K) obtained via the relation  $\Delta G^0 = -RT \ln K$  using  $T = 323$  K (values of  $K$  were not temperature corrected), see supporting information of reference 114. **c** Concentrations were determined by quantitative <sup>1</sup>H NMR spectroscopy with dimethyl sulfone as an internal standard after removing metal ions with Chelex. **d** Experimental thermochemistry not available. **e** Alanine is formed due to transamination to in situ formed pyruvate.

In line with our initial screening results, the relative rate enhancement observed for the transamination reaction of glyoxylate with glutamic acid was found to be  $\text{Cu}^{2+} > \text{Ni}^{2+} > \text{Co}^{2+} > \text{V}^{5+}$ . Compared to the uncatalyzed reaction, 50 mol% of  $\text{Cu}^{2+}$  increases the rate constant for the transamination reaction of glyoxylate with glutamic acid by a factor of 2700, while  $\text{Ni}^{2+}$  increases the rate by approximately a factor of 740 (Figure 17). The effect of different metals is discussed in following paragraphs. In accordance with the results from Table 1, the  $\text{Ni}^{2+}$ -catalyzed reaction is found to be slower than the  $\text{Cu}^{2+}$ -catalyzed one but yields a higher concentration of glycine. The  $\text{Cu}^{2+}$ -catalyzed reaction does not reach complete conversion due to the apparent unavailability of glyoxylate at the end of the reaction. This is attributed to the competing formation of  $\text{Cu}^{2+}$ -glyoxylate complexes.<sup>127</sup> Furthermore, the reaction kinetics at pH 7 are not affected by the effect of the buffer type and concentration.<sup>127</sup>

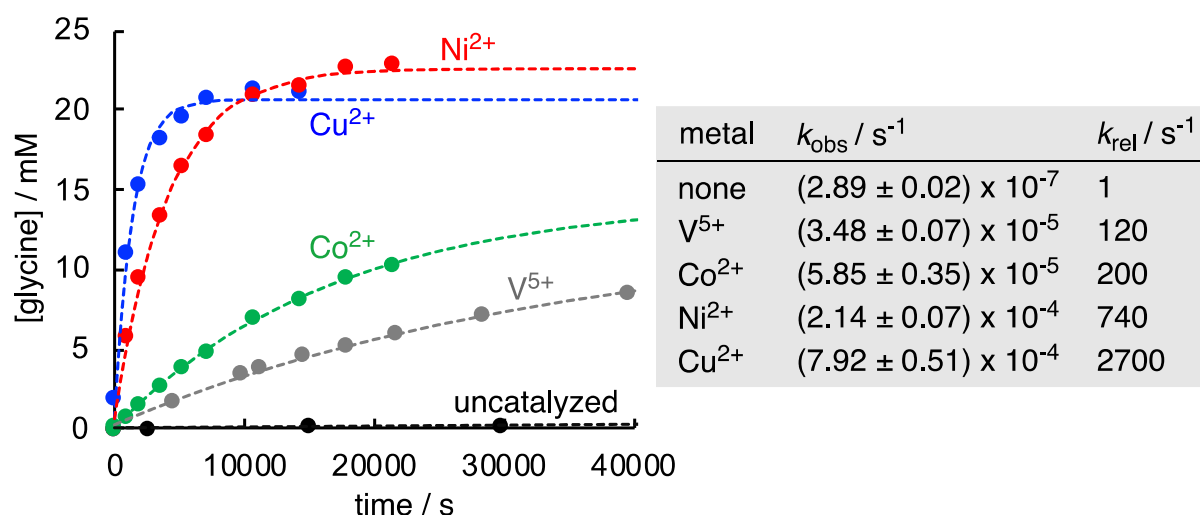


**Figure 17.** Kinetics of the reaction of glyoxylate (30 mM) with glutamic acid (30 mM) in the presence of catalyst (15 mM) in phosphate buffer at pH 7 at 23 °C. (see supporting information for more details)

## 10.2. Isotope effects

To get further insight into the mechanism and the nature of the rate-determining step of the transamination with glyoxylate and pyruvate, the kinetics of the  $\text{Cu}^{2+}$  and  $\text{V}^{5+}$  catalyzed reactions were studied in detail (Figure 18, 19). These studies were carried out by Dr. Mayer.

### 10.2.1. Transamination reactions of glyoxylate

When the reaction of glyoxylate with deuterated glutamic acid was performed in non-deuterated buffer, only the formation of unlabeled glycine was observed, suggesting the mechanism involving deprotonation and subsequent re-protonation by the solvent (Figure 18A). These results are in line with the work of Richard et al., who studied the mechanism of the deprotonation of iminium ions formed from the condensation of glycine with carbonyl compounds (e.g., acetone, phenyl glyoxylate, PLP) in buffered D<sub>2</sub>O.<sup>150,151</sup> Kinetic isotope effects (KIE) were next investigated. Compared to the reaction with non-deuterated glutamic acid, the use of *d*<sub>3</sub>-glutamic acid resulted in a decreased reaction rate and a reduction in conversion (Figure 18B/C). A comparison of the initial rates suggests a KIE of 4.8 for the Cu<sup>2+</sup>-catalyzed process. (The reason for the reduced conversion with the deuterated substrates is presently unclear, but it prevents us from comparing the first-order rate constants *k*<sub>obs</sub> directly. Therefore, we decided to compare the initial rates of the reaction instead of the first-order rates). Analogously, the KIE was determined by <sup>1</sup>H NMR kinetics for the V<sup>5+</sup>-catalyzed reaction as 6.1 (with 100 mol% NaVO<sub>3</sub>; see supporting Information reference 127). Such primary substrate KIEs are in line with a rate-determining deprotonation from **I** to **I**<sup>-</sup> (*k*<sub>B-,1</sub>, Figure 18D), followed by a fast reprotonation of **I**<sup>-</sup> to **I**' via *k*<sub>BH,2</sub>. In the case of the Cu<sup>2+</sup>- complex, the assumption of a fast re-protonation via *k*<sub>BH,2</sub> (as opposed to *k*<sub>BH,1</sub> to yield **I** again) can be justified based on the acidities *pK*<sub>a</sub> which were estimated from DFT calculations (Figure 18D), and the known relationship between basicities and rate constants for the protonation of an enolate carbon site. For details, please see computational section of reference 127. Accordingly, once **I**<sup>-</sup> is formed, protonation will predominantly occur at the glyoxylate/glycine site.<sup>152,153</sup>

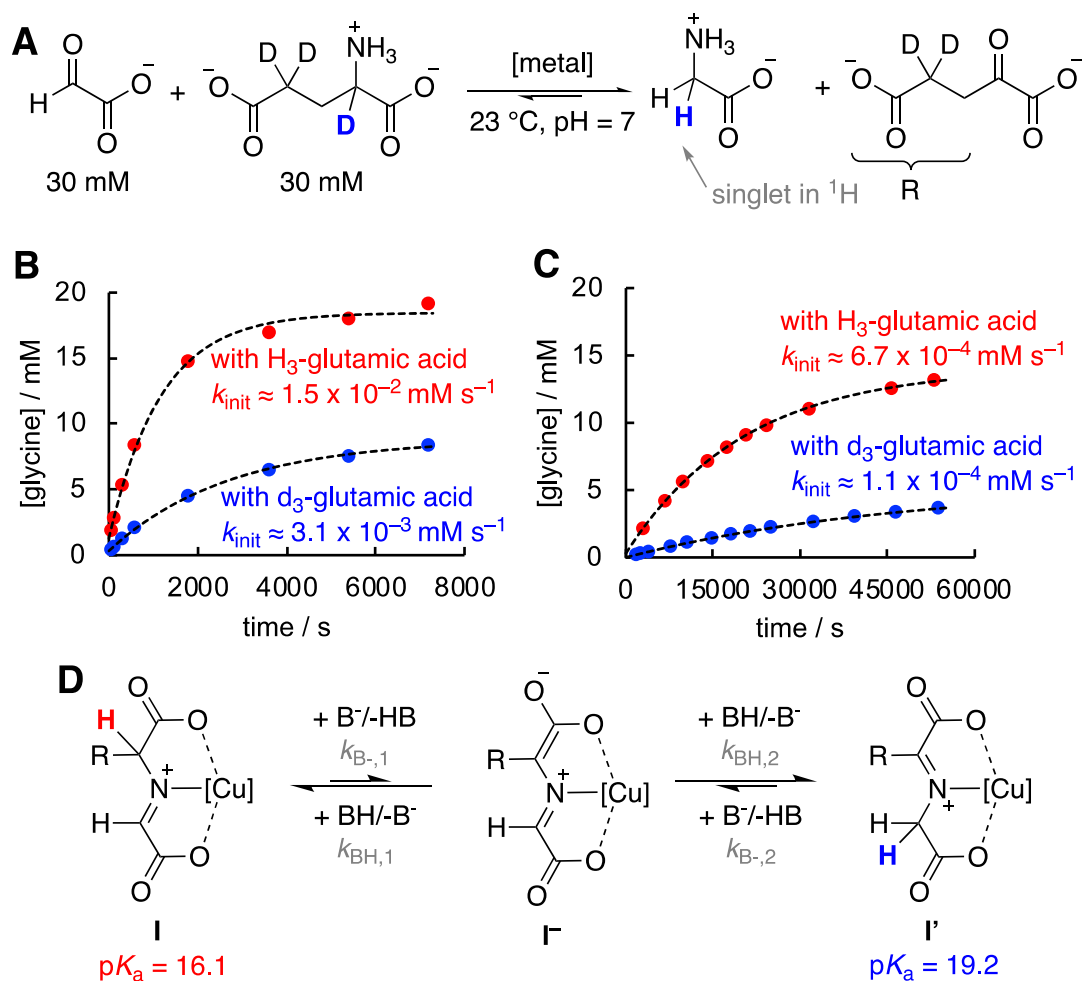


**Figure 18.** (A) Reaction of glyoxylate (30 mM) with d<sub>3</sub>-glutamic acid (30 mM). (B) Kinetics in the presence of 15 mM Cu<sup>2+</sup> in 1 M phosphate buffer and (C) 30 mM NaVO<sub>3</sub> in 0.92 M phosphate buffer at pH 7 at 23 °C. (D) Central intermediates and computed acidities pK<sub>a</sub> estimated from DFT computations (see reference 127).

### 10.2.2. Transamination reactions of pyruvate

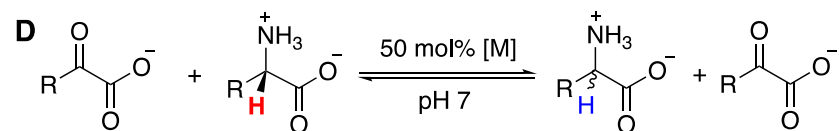
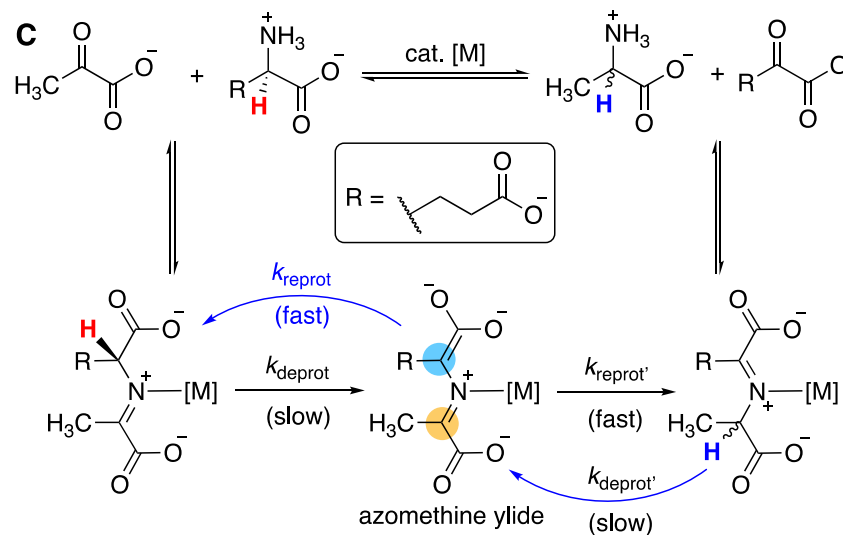
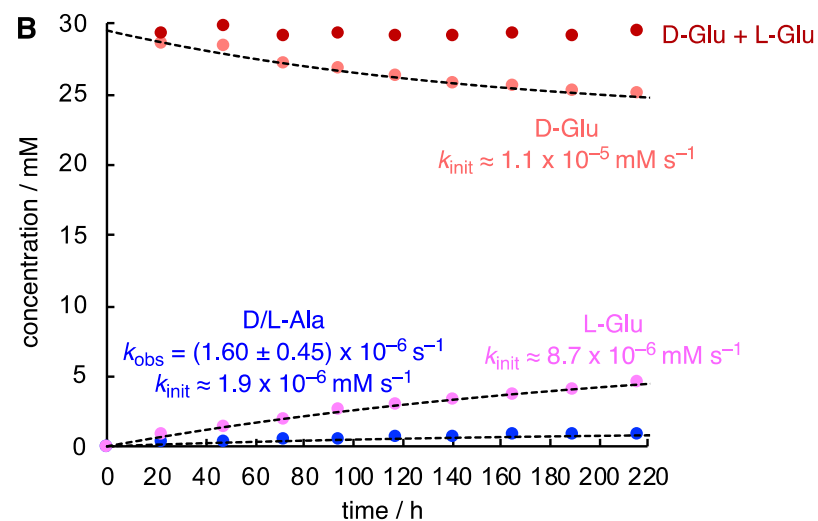
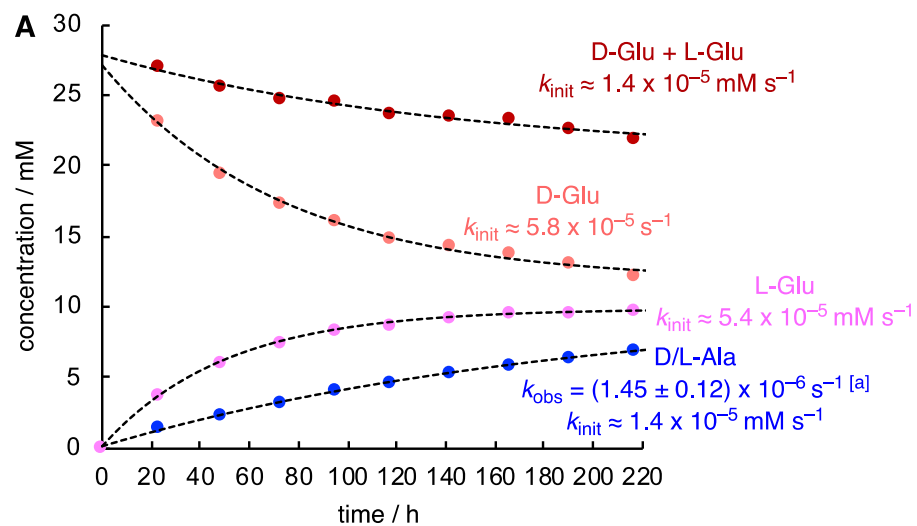
Compared to the transamination reaction of glyoxylate to glycine, that of pyruvate to alanine was generally found to require longer reaction times, higher temperatures or increased catalyst concentrations (Table 2). The kinetics of the reaction of pyruvate and glutamic acid in the presence of 50 mol% of Cu<sup>2+</sup> or V<sup>5+</sup> showed that both metals enhance the rate of transamination. In line with our initial results (Table 2), Cu<sup>2+</sup> was found to be a more efficient catalyst than vanadate (Figure 19A, B). However, when fitting the time-dependent alanine concentrations to a single-exponential, similar first



order rate constants were obtained for both the  $V^{5+}$ - and  $Cu^{2+}$ - catalyzed reactions. This can be explained by the slow competing decomposition of the vanadate, most likely to a  $V^{4+}$  species, as evidenced by the characteristic pale blue color observed after 2 weeks.<sup>167</sup> However, since the  $V^{5+}$ -catalyzed reaction reached a significantly higher conversion to alanine at 50 °C (Table 2), we conclude that the longer reaction times at ambient temperature are problematic for the determination of reaction rates. Therefore, initial rates were used to estimate the relative effects of metal salts, which indicated that the reaction catalyzed by  $Cu^{2+}$  is approximately 1 order of magnitude faster than that catalyzed by  $V^{5+}$  (Figure 19A, B). Increasing the concentration of glutamic acid had almost no effect on the rate of alanine formation with  $Cu^{2+}$  (for supporting information see reference 127).<sup>141</sup> This suggests that the  $Cu^{2+}$ -catalyzed transamination proceeds via an almost saturated catalyst. To understand the rate-determining step in reactions with pyruvate it was important to study racemization vs transamination reactions. Therefore, we used enantiomerically pure amine donor, glutamic acid. By using enantiomerically pure L- or D-glutamic acid as reactants, the concentration of all chiral species involved during the transamination process can be tracked over time (Figure 19A, B, see supporting Information of reference 127 for details).<sup>168</sup> In this way, both the forward (transamination) and backward (racemization) reaction can be followed simultaneously. Re-protonation can either occur at the same site as deprotonation (Figure 19C, blue label), resulting in racemization, or, alternatively, on the other side, resulting in transamination (orange label). As shown in Figure 19A, we found that in the  $Cu^{2+}$ -catalyzed reaction of pyruvate with L- or D-glutamic acid, racemization of glutamic acid proceeds approximately 3.9 times faster than the transamination to alanine. Analogously, analysis of the initial rates in the  $V^{5+}$ -catalyzed reaction suggested an approximately 4.6 times faster racemization compared to the transamination (Figure 19B). In the pathway in Figure 19C, racemization might occur either due to the re-protonation of the azomethine-ylide intermediate, or due to a secondary reaction, such as the direct racemization of the amino acid by the metal or through a “transamination” with the reaction product ( $\alpha$ -ketoglutarate). To differentiate between a direct racemization and these two secondary processes, we initially studied whether glutamic acid (or analogously, alanine) racemizes in the presence of  $Cu^{2+}$  or  $V^{5+}$  in the absence of keto acids. As expected, both amino acids did not show any detectable racemization within 9 days. Next, we determined the rates of the racemization of a mixture of glutamic acid and  $\alpha$ -

ketoglutarate and, analogously, of alanine and pyruvate (Figure 19D). A comparison of the initial rate of formation of L-glutamic acid from Figure 19A ( $k_{\text{init}} \approx 5.4 \times 10^{-5} \text{ mM s}^{-1}$ ) with the rate of racemization in the presence of  $\alpha$ -ketoglutarate under otherwise identical reaction conditions ( $k_{\text{init}} \approx 7.3 \times 10^{-6} \text{ mM s}^{-1}$ ) demonstrates that racemization predominantly occurs during re-protonation of the azomethine ylide and not as a subsequent step. As expected from the loss of the deuterium label during the related transamination with glyoxylate (Figure 18), the reaction of pyruvate with enantiomerically pure glutamic acid yields alanine as a mixture of the D- and L-enantiomers, as chiral information is lost in the planar azomethine ylide intermediate (Figure 19C). However, even if the initial transamination reaction would proceed with a slight preference for D- or L-alanine, the racemization of alanine with pyruvate with both  $\text{Cu}^{2+}$  and  $\text{V}^{5+}$  catalysts is faster than formation of alanine (Figure 19D). How can the relative rates of racemization ( $k_{\text{reprot}}$ ) and transamination ( $k_{\text{reprot}'}$ ) of the azomethine ylide be rationalized? As discussed above, the  $\text{Cu}^{2+}$ -catalyzed reaction seems to proceed via an almost saturated catalyst. Accordingly, in the presence of 50 mol% catalyst the reaction kinetics will predominantly reflect the interconversion of the two copperimine chelates, and the reaction rates for their formation can be neglected (We assume that also for the vanadate-catalyzed reaction with pyruvate as substrate formation/hydrolysis of the metal-chelate complexes is fast relative to the proton-transfer steps. This was validated for the analogous reaction with glyoxylate by the presence of a primary substrate KIE (Figure 18). It has been shown that the rate constants for protonation of an enolate carbon site are linearly correlated with the basicities of the respective enolates.<sup>154,155</sup> The higher the basicity of an enolate carbon atom, the faster is its protonation by an acid, e.g.,  $\text{H}_3\text{O}^+$ ,  $\text{H}_2\text{O}$ , or  $\text{H}_2\text{PO}_4^-$  from the buffer. Therefore, the observation that glutamate racemizes faster than alanine forms, suggests that the basicity of the blue carbon atom of the azomethine ylide in Figure 19C is higher than that of the orange carbon atom.

The validity of these mechanistic interpretations is confirmed by means of DFT computations as well (by Dr. Mayer, see reference 127).



amino acid/keto acid	metal	$k_{\text{obs}} / \text{s}^{-1}$	$k_{\text{init}} / \text{mM s}^{-1}$
glutamic acid/ $\alpha$ -ketoglutarate	$\text{CuCl}_2$	$(4.86 \pm 0.04) \times 10^{-7}$	$7.3 \times 10^{-6}$
glutamic acid/ $\alpha$ -ketoglutarate	$\text{NaVO}_3$	$\approx 10^{-8}$	$\approx 5 \times 10^{-7}$
alanine/pyruvate	$\text{CuCl}_2$	$(3.10 \pm 0.10) \times 10^{-6}$	$4.6 \times 10^{-5}$
alanine/pyruvate	$\text{NaVO}_3$	$(2.95 \pm 0.04) \times 10^{-7}$	$4.4 \times 10^{-6}$

**Figure 19.** Kinetics of the reaction of pyruvate (30 mM) with D-glutamic acid (30 mM) in the presence of 15 mM CuCl<sub>2</sub> **(A)** or NaVO<sub>3</sub> **(B)** at pH 7 (1 M phosphate buffer) at 23 °C (For the analogous analysis with L-glutamic acid, see supporting information of reference 127; dashed lines indicate the fitted kinetic curves). Concentrations were determined by manual sampling/quantitative <sup>1</sup>H NMR spectroscopy, and enantiomeric ratios were determined by chiral SFC analysis (see supporting information of reference 127). **(C)** Mechanistic model for racemization/transamination illustrated starting from D-amino acids. **(D)** Rate constants for the racemization of L-amino acids (30 mM) in the presence of equimolar amounts of the corresponding α-keto acids and 15 mM CuCl<sub>2</sub> or NaVO<sub>3</sub> at pH 7 (1 M phosphate buffer) at 23 °C as determined from manual sampling/chiral SFC analysis. [a] Due to the small equilibrium constant of the reaction ( $K = 1.52$ ),<sup>132</sup> the rate constants  $k_{\text{obs}}$  shows a significant contribution of the reverse reaction with  $k_{\text{forward}} = 8.75 \times 10^{-7} \text{ s}^{-1}$  and  $k_{\text{reverse}} = 5.75 \times 10^{-7} \text{ s}^{-1}$  (see reference 127).

### 10.3. Proposed reaction mechanism for catalytic transamination

Based on studies from literature and further kinetic studies,<sup>127</sup> which show the catalytic nature of the reaction, as well as the established structures of metal-imine chelates, we proposed the reaction mechanism depicted in Figure 20.<sup>141,159,160,161,169,170</sup> The reaction initiates by forming small amounts of an iminium ion **I-1**. Exchange of H<sup>+</sup> for the transition metal results in a metal-imine complex **I-2**. Deprotonation of **I-2** yields the fully conjugated azomethine ylide **I-3**, which upon re-protonation forms either the original imine adduct **I-2** or the isomeric **I-2'**. Hydrolysis of **I-2'** finally liberates the reaction products. In the presence of catalytic amounts of metal, the whole sequence is reversible and will result in concentrations of amino and keto acids depending on the relative energies of reactants and products.<sup>148,149</sup> By forming the metal-imine chelates **I-2**, metal ions can influence the rate of the transamination sequence through two predominant mechanisms, which are not mutually exclusive. Either they can increase the concentration of the reactive imine intermediate **I-2**, by enforcing a higher binding constant, or they can increase the acidity of the CH moiety in **I-2** and therefore the rate of deprotonation to **I-3**. Alternatively, the transamination reaction can also proceed via a significantly slower metal-free pathway through direct deprotonation of the iminium species **I-1** to azomethine ylide **I-4**.

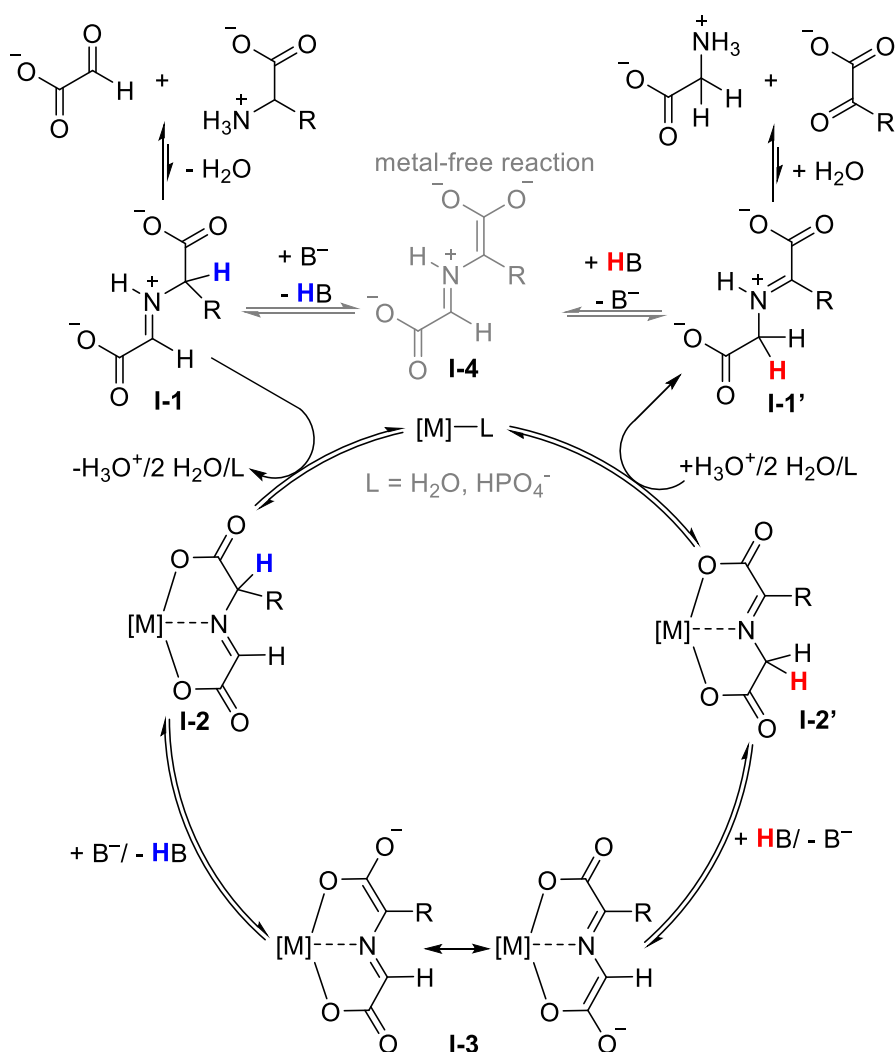


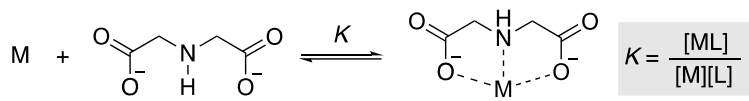
**Figure 20.** Proposed reaction mechanism for catalytic transamination.

#### 10.4. Acidities of imines and roles of different metals

Stability constants with the imine ligand for the keto/amino acid systems with metals can guide us how different metals affect the rate of transamination reactions. So far, stability constants of imine ligands like I-1 were only reported with Ni<sup>2+</sup> and Zn<sup>2+</sup>. However, Leussing found that the stability constants with the imine ligand are of similar magnitude of those with iminodiacetic acid, which are reported for many metal ions (Table 4).<sup>154,155</sup> With iminodiacetic acid the highest stability constants were observed

with Cu<sup>2+</sup>, followed by Ni<sup>2+</sup> and Co<sup>2+</sup>, a ranking agreeing with the reactivity order of the metals identified in our kinetic studies.

**Table 4.** Stability constants lg *K* for complexes of iminodiacetic acid with different divalent metals at 20 °C

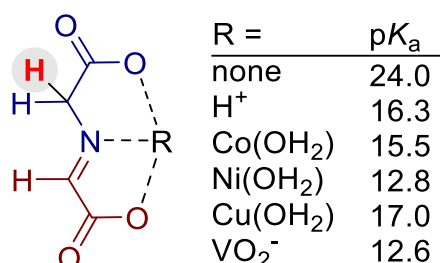


Metal	H <sup>+</sup>	Fe <sup>2+</sup>	Co <sup>2+</sup>	Ni <sup>2+</sup>	Cu <sup>2+</sup>
lg <i>b</i>	9.45	5.8	6.97	8.19	10.6

Additionally, we mentioned that metals can influence the imine C-H acidity (*pK*<sub>a</sub>) which can predict in part, the reaction rate and whether de- or re-protonation is rate determining step for the transamination reaction. The relationship between *pK*<sub>a</sub> and the rate constants for the deprotonation of amino acids and iminium ions has been extensively studied by Richard and co-workers by measuring the rate constants of deuterium exchange of the amino acids' CH protons.<sup>150,156,157</sup> To connect the systems investigated in the present study to Richard's experimental acidities, we again used DFT computations.<sup>127</sup> The computed acidities of the CH protons of the iminium ions range from 13.9 to 20.6, thus being within the range of experimental values reported by Richard.<sup>151</sup> In line with experimental findings, our computations predict that iminium ions (where H<sup>+</sup> is coordinated, not metal) are 6–10 *pK*<sub>a</sub> units more acidic than the respective imines (Figure 21).<sup>151</sup> and the imine-metal complexes are even more acidic, though to different extents compare to iminium ions and their respective imines. (Figure 21).

Overall, the coordination of Cu<sup>2+</sup> and Co<sup>2+</sup> generally results in an identical or even slightly weaker activation of the CH acidity compared to the iminium ions.<sup>158</sup> Accordingly, the catalytic activity of Co<sup>2+</sup> and Cu<sup>2+</sup> can be predominantly assigned to the high stability of the metal-imine complexes and not to activation of the substrate. With Ni<sup>2+</sup> and V<sup>5+</sup>, however, the acidity of the imine ligand is generally enhanced compared to the protonated imines. Accordingly, the catalytic activity of V<sup>5+</sup> in transamination reactions can be mostly attributed to the increase of acidity of the

substrates. With  $\text{Ni}^{2+}$ , however, the stability constants determined by Leussing for the pyruvate/  $\text{Ni}^{2+}$  system suggest that also high amounts of the imine- $\text{Ni}^{2+}$  chelates are formed, therefore, the catalytic activity of  $\text{Ni}^{2+}$  can be attributed both to strong chelation and to activation of the CH acidity.<sup>159,160,161,162</sup>



acidity of the metal-imine complexes,  
shown for glyoxylate/glycine pair as an example

**Figure 21:** Quantum-chemically calculated  $\text{pK}_{a,\text{corrDFT}}$  values of the imine species (keto acid moiety: red; amino acid: blue) calculated at the SMD( $\text{H}_2\text{O}$ )/MN15/Def2-TZVP level of theory, corrected with the experimental  $\text{pK}_a$  values ( $\text{H}_2\text{O}$ , 25 °C) from reference 151. For details, please see reference 127.

## 10.5. Conclusions

Transamination reactions have been known for decades to occur in the absence of enzymes. However, it was not known to what extent metals alone can act as catalysts under biological conditions, or even whether they can display catalytic turnover. In this work, we have shown that  $\text{Co}^{2+}$ ,  $\text{Ni}^{2+}$ ,  $\text{Cu}^{2+}$  and  $\text{V}^{5+}$  ions can, not just promote, but efficiently catalyze transamination reactions. This work provided insights into the key steps of the reaction and a rationale for the two major ways in which metals can catalyze transamination reactions.

Insights gained in the current study raises the possibility that biological transamination might have undergone an evolutionary progression from metal catalysis to PLP catalysis to PLP/transaminase catalysis without a fundamental change to the mechanism.

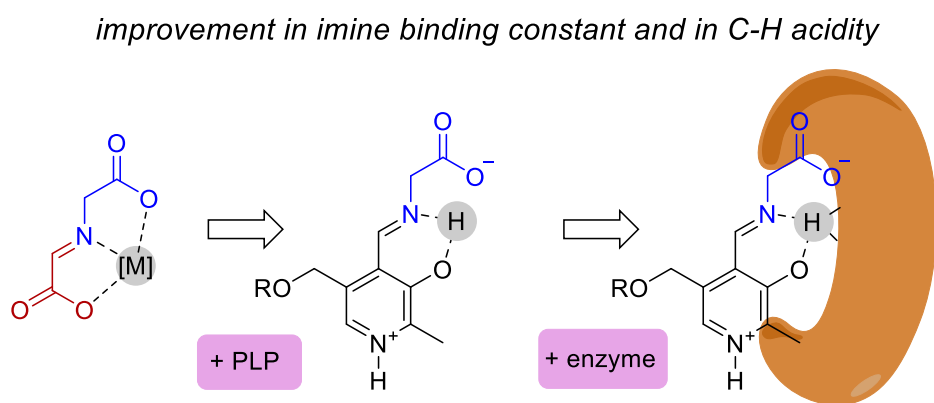


**Figure 22.** Transition from metal catalyzed transamination to cofactor and to cofactor-enzyme catalyzed reaction based on similar mechanism.

Obtaining mechanistic insight into how both biological and non-biological catalysts enable metabolic processes under biological conditions should continue to illuminate how they emerged from the earliest stages. Furthermore, beside studies on transamination within a biochemical context, non-enzymatic transamination reactions have found application in the asymmetric synthesis of amino acids using tailored organocatalysts, or the combination of organocatalysts and metal ions.<sup>163,164</sup> Recently,  $\text{Cu}^{2+}$  or  $\text{Ni}^{2+}$ -catalyzed transamination of the N-terminal sites of proteins with glyoxylate was also proposed as a method for the formation of protein bioconjugates.<sup>165</sup>



## 11. Rare metal catalysis at the origin of protometabolism?

Rare elements like Pd, Rh, Pt, and Ir are powerful catalysts. Still, they have not been considered in prebiotic chemistry due to their low overall abundance in the Earth's crust, typically on the ppb-ppm level.<sup>171</sup> However, they are often found in high concentrations in localized environments. For example, in Russia Pd has been found in pentlandite samples up to 11 wt.%.<sup>172</sup> Even if minerals with high concentrations of rare elements were completely absent on the early Earth, common rock-forming minerals with modest concentrations of rare elements might still have been critical to prebiotic chemistry.<sup>173</sup> We can support this claim by two main factors: Firstly, ppb and ppm levels would be sufficient since they are exceptionally catalytically active.<sup>174</sup> Secondly, prebiotic chemistry does not necessarily have to take place at a global scale, at least not at the beginning. This implies that rare metals might have been used earlier as catalysts to induce chemistries in niches. Afterwards, rare metals chemistry, coupled with organic molecules and other catalysts like Fe and Ni (the d orbitals of which are readily coordinated by proteins or other organics produced by the reaction network), would have strengthened the already existing chemistry and allowed it to evolve further towards more complexity. Then, these complex molecules would have helped spread self-organised chemistries across the globe with help from globally abundant metals. This may also explain why metalloenzymes in modern biochemistry are made up of earth-abundant metals and are functional when combined with complex organic molecules. A similar form of evolution occurs in industrial chemistry, where the challenge is to emulate the outstanding catalytic properties afforded by rare metals by their substitution with common metals bound by complex ligands. It is, therefore, prudent to investigate rare metals in the context of metabolic origin.

The basis of biochemistry lies in five universal metabolic precursors (acetate, pyruvate, oxaloacetate, succinate, and  $\alpha$ -ketoglutarate) built from C, O, and H. These five compounds are found directly on life's core anabolic and catabolic pathways, thereby providing them with an organizing role within metabolism.<sup>175</sup> Because molecules must be made before they can be broken down, the question of how C–C bonds could form without relying on ATP-consuming reactions is a major challenge to theories of the origin of life.<sup>109</sup> It has recently been demonstrated that nonenzymatic analogues of the reductive acetyl coenzyme A (Acetyl CoA) pathway can be achieved, in which CO<sub>2</sub> is fixed to produce acetate and pyruvate, forming C–C bonds.<sup>111,176</sup> To build compounds with more than three carbon atoms, life relies on complex enzymes and a chemical energy carrier, ATP. However, neither enzymes nor ATP could have existed on the lifeless planet Earth. If enzymes and ATP didn't exist, how did life create biochemistry? Parts of the nonenzymatic analogues of the core anabolic pathway: the reductive tricarboxylic acid cycle (rTCA or reverse Krebs cycle) have been reported.<sup>145,177,178</sup> One of the major challenges to replicating the rTCA cycle in an abiotic environment is the chemical complexity of the rTCA cycle, requiring multiple carboxylic acid intermediates that are inherently unreactive unless highly competent enzymes and specialized cofactors are present (see Introduction part on rTCA cycle). Theoretical analysis of all known metabolic reactions has revealed a robust hypothetical metabolic network that does not require any phosphorus or any cofactors such as ATP.<sup>110</sup> Within this hypothetical phosphorus-free network, only carbon, hydrogen, and oxygen make up the molecules and pyruvate (present in (r)TCA cycle) and glyoxylate (present in the glyoxylate cycle, a variation of the tricarboxylic acid cycle, which centres on the conversion of acetyl-CoA to succinate bypassing some steps of rTCA cycle) represent the biggest branching points, suggesting that a primitive pre-ATP metabolism would have relied on these two compounds (Figure 23). An evolutionary relationship between the glyoxylate cycle and the TCA/rTCA cycle (the TCA cycle is an oxidative version of the rTCA cycle) has been suggested before.<sup>180,181</sup> Pyruvate and glyoxylate are attractive as prebiotic starting materials because they can be obtained through abiotic CO<sub>2</sub> fixation<sup>111,176,182</sup> as well as by other plausible means.<sup>183,184,185</sup>

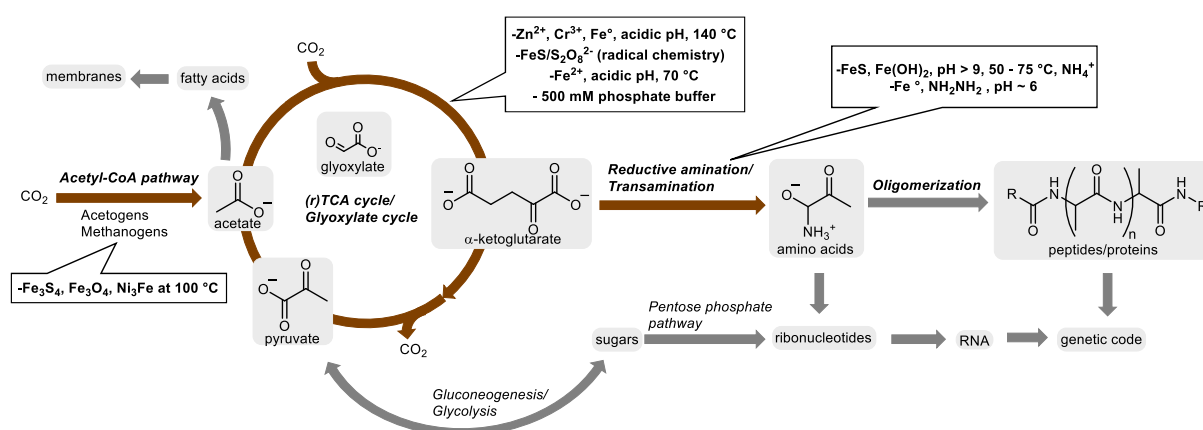


**Figure 23:** Core metabolic map showing previous prebiotic studies often relying on incompatible chemistries (figure adapted from reference 97).

### 11.1. Prebiotic attempts towards protometabolic reaction networks

Glaring differences can be noted between life's biochemical pathways and the experimentally demonstrated reaction networks that have been proposed to explain life's origins. Life's chemical networks are continuous. The products of one reaction immediately go on to react with another without externally induced changes to the conditions. Existing synthetic reaction networks that are proposed to have played a role in the origin of life and that selectively produce multiple classes of biological molecules are highly discontinuous. They require numerous sequential and well-timed changes in conditions for the products of one reaction to go on to the next reaction. They are typically driven by UV photochemistry and are built from HCN using reactions distinct from those found in metabolism.<sup>186</sup> In line with the idea that metabolites supporting multiple pathways, key classes of chemical transformations, and energetic aspects of the primordial self-organized chemistry are expected to remain preserved in biological metabolism, nonenzymatic reaction networks bearing similarities to metabolic pathways have been uncovered, narrowing the gap between prebiotic chemistry and ancient microbial metabolism.<sup>144,146</sup> Inspired by the central role of a two-carbon metabolite, glyoxylate, in a model published by theoretical biologist Daniel Segrè, our lab and that of Krishnamurthy recently described a nonenzymatic reaction network involving glyoxylate and pyruvate (Figure 24).<sup>144,146</sup> This subsystem functions as a one-carbon homologue of the rTCA cycle, all composed of  $\alpha$ -keto acids. A decarboxylative aldol reaction between pyruvate and glyoxylate occurs to give maloyl

formate, followed by dehydration to give fumaroyl formate, then an alkene reduction to give  $\alpha$ -ketoglutarate. This is followed by a second aldol reaction to give isocitroyl formate and a second dehydration to give aconitoyl formate.

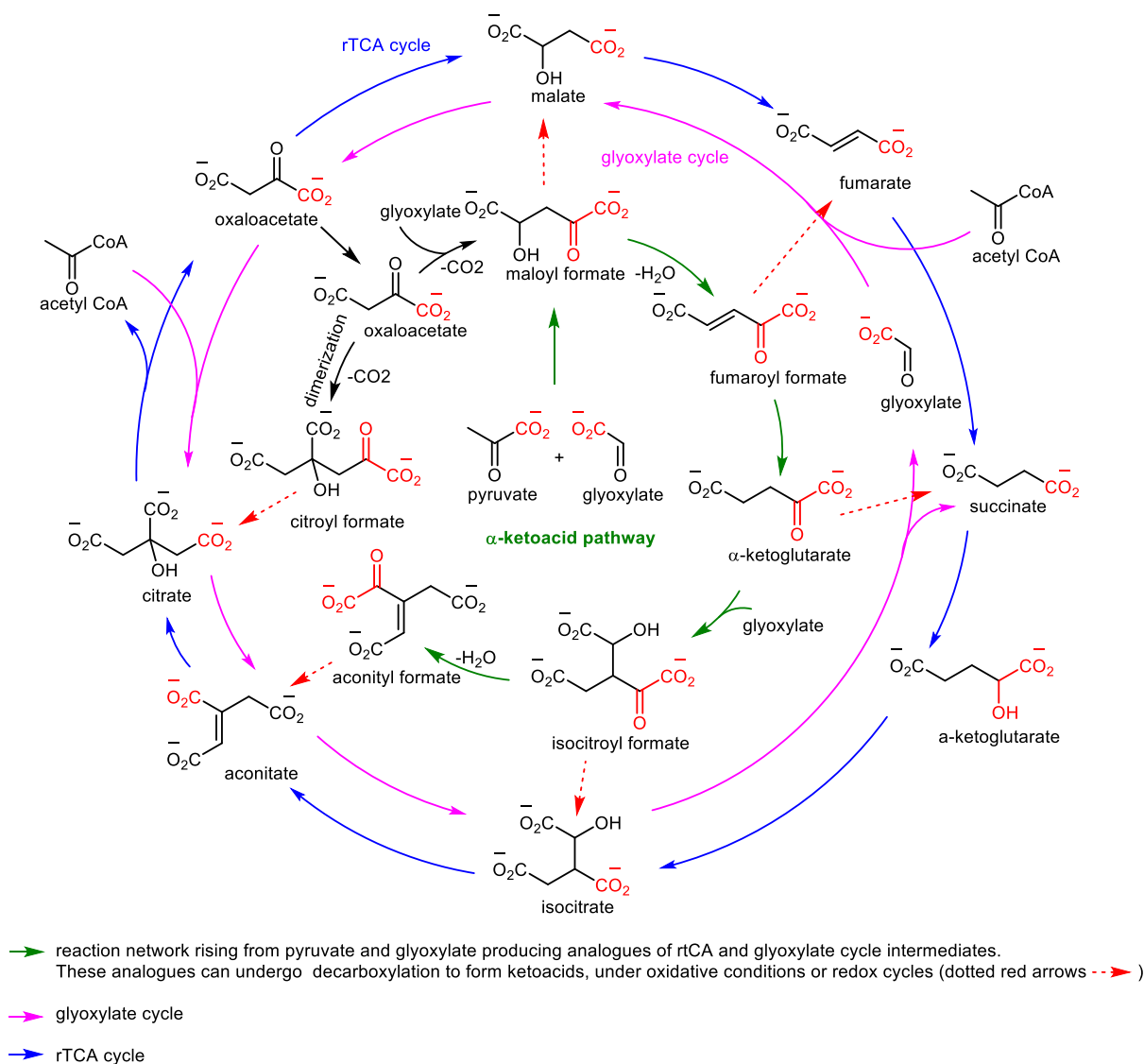


**Figure 24.** Glyoxylate and rTCA cycle and their proposed analogue from pyruvate and glyoxylate (Figure adapted from reference 144).

Our lab has described this network in  $\text{Fe}^{2+}$ -rich acidic water, pH 5, at  $70^\circ\text{C}$ .<sup>146</sup> This reaction network successfully produces all the intermediates shown in Figure 25, except oxalosuccinate and citrate. Oxaloacetate in the network is generated from malate oxidation thanks to the  $\text{Fe}^{2+}/\text{Fe}^{3+}$  redox couple; thus, in this work, the network has reductive and oxidative properties. Additionally, at the 1 h time point of the reaction,

the addition of metallic iron and the bifunctional amine hydroxylamine ( $\text{NH}_2\text{OH}$ ) to the reaction mixture converts glyoxylate, pyruvate, oxaloacetate, and  $\alpha$ -ketoglutarate to four biological amino acids: glycine, alanine, aspartate, and glutamate, respectively. However, synthesizing amino acids in this way has some drawbacks: First, bifunctional amines are not prebiotically plausible, and biology doesn't use hydrazine or hydroxylamine to synthesise amino acids. Also, the reaction requires intervention from the experimenter at a certain time point to achieve amino acid formation, as hydroxylamine is not compatible with the network if directly added at the very beginning. Overall, this network is plausible as a prebiotic analogue of the rTCA/glyoxylate cycle but not for amino acid synthesis. Krishnamurthy and co-workers also showed that the reaction of glyoxylate with pyruvate at 50 °C, in the presence of concentrated phosphate buffer (0.5 M, pH 7), produces a series of  $\alpha$ -keto acid analogues of the rTCA cycle without the need for a metal catalyst, where glyoxylate is acting as both the carbon source and reducing agent, while phosphate serves as an acid-base catalyst.<sup>144</sup> Similar to our lab's work, oxalosuccinate and citrate were also not detected in their reaction network. Additionally, oxaloacetate was absent because, in Krishnamurthy's work, the reported pathway is only anabolic (reductive). The drawback of this network is amino acid synthesis within the network is missing, stopping the network from evolving towards more complex chemistries essential for the origin of life.

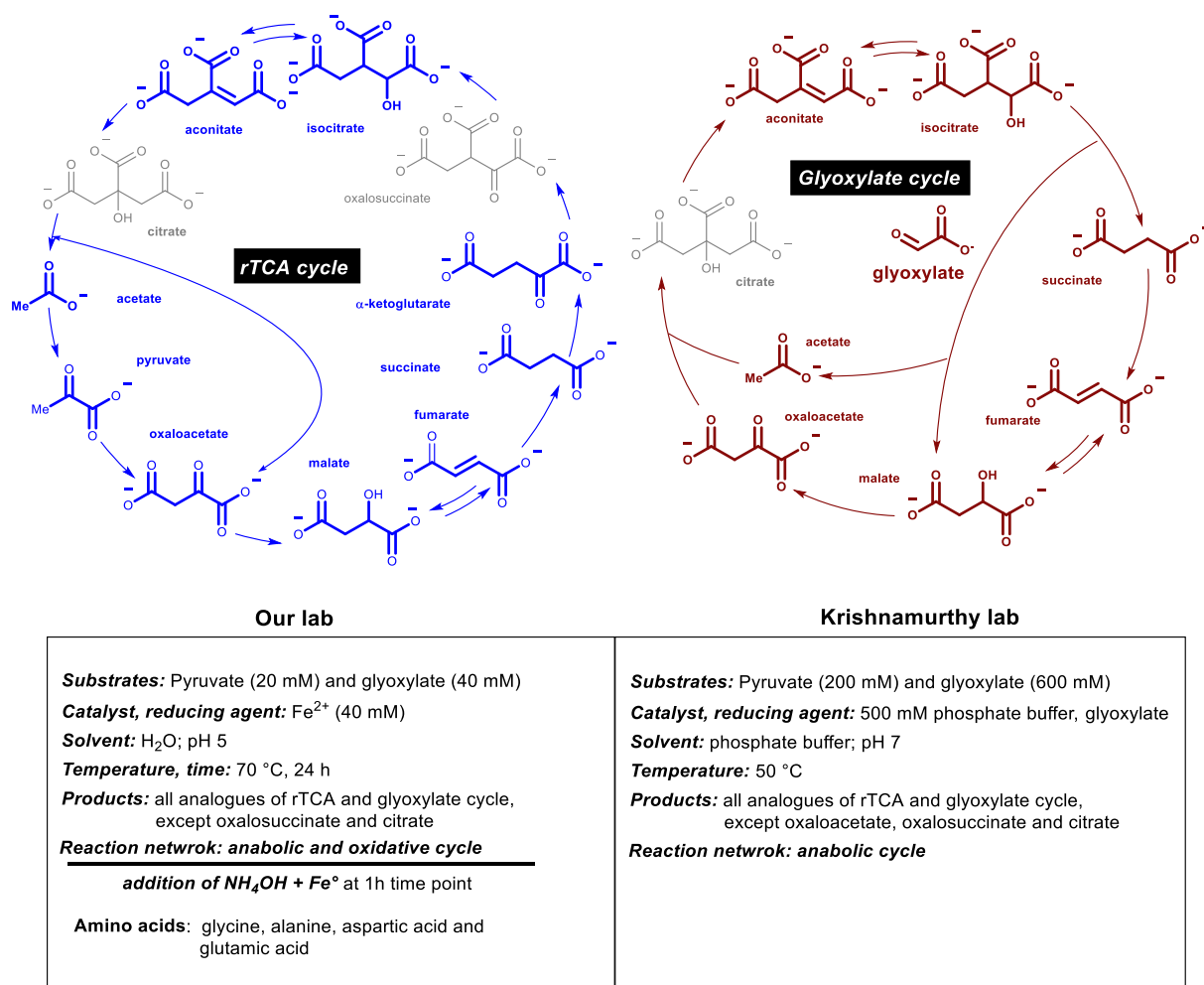


**Figure 25.** Previous studies on rTCA cycle analogue (figure adapted from reference 146).

## 11.2. Chapter's objective: $\text{H}_2$ driven reductive amination and protometabolic reaction networks

As discussed earlier in the introduction section, evidence suggests that early life-like chemistry was driven by  $\text{H}_2$  gas and built from bicarbonate/ $\text{CO}_2$ ,  $\text{NH}_3$ ,  $\text{H}_2\text{S}$ , and phosphate using reactions still found in modern microbial cells. Therefore, we aimed to investigate reaction networks driven by  $\text{H}_2$  and where chemistry could be built under plausible geochemical conditions of  $\text{NH}_3$  and  $\text{CO}_2$  (early earth geochemical conditions are discussed earlier in the introduction section). Although the reported prebiotic core metabolic pathways, or segments thereof, are continuous in isolation, chemical incompatibilities have thus far prevented the combination of multiple anabolic functions into larger continuous reaction networks, including amino acid synthesis. Furthermore,

of the reported nonenzymatic pathways, only one has been shown to be driven by  $H_2$ , the acetyl CoA pathway,<sup>147,184</sup> but further continuity towards higher order C-C bonds and incorporation of nitrogen,  $N_2$ , in its natural metabolic form,  $NH_3$ , has proven difficult, often require harsh conditions and chemistries non-compatible with each other (Figure 23).<sup>97</sup> Therefore, an experimental demonstration of a continuous prebiotic synthetic reaction network that embodies multiple metabolic functions, especially one congruent with early biochemistry and early geochemical conditions, is critical to advancing our understanding of the origin of life. Past studies in prebiotic chemistry assayed catalysts which have traditionally been geochemically abundant metals or minerals, especially those resembling the metal clusters in the active sites of enzymes. However, in the context of prebiotic chemistry, little if any attention has been given to rare metals which have outstanding catalytic properties.<sup>187</sup> Self-organizing chemistry based on ubiquitous gases like  $CO_2$  and  $H_2$  could have operated on microscopic scales wherever the needed catalysts were present. Hydrogen gas supports many ecosystems on Earth and is continuously produced by geochemical processes, including serpentinization in hydrothermal systems and water radiolysis in the deep crust.<sup>185,188</sup> Thus, rare catalytic elements could have had many opportunities to interact with  $CO_2/HCO_3^-$ ,  $H_2$ , and  $NH_4^+$  and could have contributed to initiating and templating self-organized prebiotic chemistry on the early Earth. Herein, considering the geochemical plausibility of reactants, in parallel to today's biochemistry, we describe a reaction network arising from oxaloacetate and glyoxylate containing different interlinked nonenzymatic metabolism-like subsystems that operates autonomously under mild uniform conditions and that depends on  $NH_3$  and on  $H_2$  gas. Our studies aimed to explore the reaction network, which includes the rTCA and glyoxylate cycle keto acids, of which four are precursors to all other biological amino acids. Four of these amino acids, such as glycine, alanine, aspartate, and glutamic acid, are known as being very ancient and are directly found in close proximity to core metabolism (rTCA cycle, Figure 23). In biology, they are directly synthesised from rTCA cycle intermediates (except glycine) via reductive amination and transamination. Therefore, our goal was not just to explore the rTCA and glyoxylate cycle analogue under more plausible conditions but also to incorporate amino acid synthesis. In contrast to previous studies, we chose to study a network starting from oxaloacetate, not from pyruvate, because oxaloacetate is a precursor to the amino acid aspartate, which is

involved in ribonucleotide synthesis, an important step towards functional polymers such as RNA.<sup>125</sup>

### 11.3. Results and discussion

The goal of our studies was challenging for several reasons. First, it was necessary to study reactions at room temperature since many life-sustaining compounds (such as oxaloacetate) are unstable at higher temperatures. Therefore, finding reactions at milder temperatures was critical if we wanted to further develop self-organised reaction networks from prebiotic chemistry. Secondly, we wanted to examine the incorporation of ammonia into keto acids in the same way that life produces amino acids through reductive amination. Often, amino acid synthesis is shown to occur under extreme conditions incompatible with oxaloacetate, and their prebiotic plausibility is also questionable (see section 9.1). The challenge was synthesizing amino acids at room temperature, including aspartate, using ammonium in low concentrations that are more prebiotically realistic and using hydrogen as a driving force. The third bottleneck was the use of neutral pH resembling biochemistry. Finally, we anticipated these chemistries in one pot without any intervention to achieve a self-organised core metabolic network. Considering the complexity of the reactions, we first decided to examine each subsystem individually.

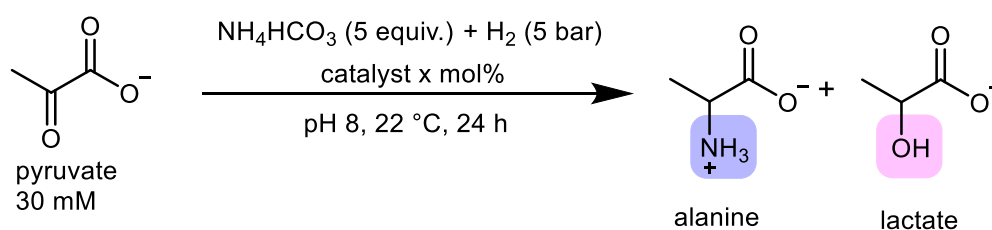
#### 11.3.1. Reductive amination

Transition metals such as cobalt, iron, and nickel, as well as rare metals like Pd and Rh, are known to efficiently catalyse hydrogenation reactions in water.<sup>174,187,189,190</sup> Thus, we wanted to investigate them to catalyze biologically relevant  $\alpha$ -keto acids reductive amination reactions at low loadings at 22 °C and near neutral pH. First, we screened various metals with the  $\alpha$ -keto acid pyruvate as a model substrate, using ammonium bicarbonate as an ammonium source under H<sub>2</sub> 5 (bar) at room temperature for 24 h in pH 8 water (Table 5). As shown in Table 5, iron, cobalt, platinum, and ruthenium did not show any reactivity while nickel, rhodium, iridium, and palladium gave alanine in yields of up to 20 %. However, iridium and rhodium yielded mostly hydroxy acid (up to 75 %), while palladium showed very good selectivity towards reductive amination compared to hydroxy acid product (yield 5%). Additionally, we



observed that Pd efficiently reduced  $\text{HCO}_3^-$  present in the system to formate.<sup>191</sup> This is another important reaction step used by  $\text{H}_2$ -dependent autotrophic organisms in  $\text{CO}_2$  assimilation, where formate is used to form C-C bonds in the WL pathway.

**Table 5.** Reaction of pyruvate (30 mM) in the presence of catalytic amounts of different metal catalysts and  $\text{NH}_4\text{HCO}_3$  under  $\text{H}_2$  (5 bar) at 22 °C,  $\text{H}_2\text{O}$  pH 7, 24 h).



entry	catalyst	mol (%)	alanine yield (%)	lactate yield (%)	formate <sup>a</sup> yield (%)	pyruvate yield (%)
1	Fe	20	-	-	-	nd <sup>b</sup>
2	Ni	20	2.2	2.0	-	41
3	Co	20	-	-	-	< 5
4	Pt/C 5 wt. %	1	-	-	-	97
5	Rh/C 5 wt. %	1	16	76	0.08	< 3
6	Pd/C 10 wt. %	1	23	4.6	27	74
7	Ru/C 5 wt. %	1	-	-	-	90
8	Ir/C 1 wt. %	1	17	78	0.03	< 1
9	-	-	-	-	-	93

<sup>a</sup> Formate yields are relative to bicarbonate concentration: 150 mM.

<sup>b</sup> In the reaction catalysed by iron starting material, pyruvate yields are not determined due to the presence of broad signal.

Thus, intrigued by the catalytic activity of Pd, we wanted to explore the impact of trace quantities of this metal on the reductive amination of seven biologically relevant  $\alpha$ -keto acids with ammonia (Figure 26). Using Pd/C as catalyst (1 mol% of Pd, 32 ppm in the reaction mixture with respect to substrate) with either  $\text{H}_2/\text{HCO}_3^-$  (5 bar/5 equiv.) or formate (5 equiv.) as the reducing agent at pH 7-8 and 22 °C for 72 h, we found the reaction to be compatible with seven different biological  $\alpha$ -keto acids (glyoxylate, pyruvate,  $\alpha$ -ketoglutarate, oxaloacetate,  $\alpha$ -ketoisocaproate,  $\alpha$ -ketoisovalerate, and  $\alpha$ -keto- $\beta$ -methylvalerate) despite using only 5 equivalents of ammonium salt (Figure 26). The corresponding biological amino acids (glycine, alanine, glutamate, aspartate, leucine, valine, and isoleucine) were obtained as the major products in 20-78% yield, with >6:1 selectivity for the  $\alpha$ -amino acid vs.  $\alpha$ -hydroxy acid in almost all cases. Interestingly, the reaction was found to be sluggish and to lose nearly all selectivity if  $\text{H}_2$  gas (5 bar) was used instead of an  $\text{H}_2/\text{HCO}_3^-$  mixture, underlying the role of  $\text{CO}_2$  in achieving selectivity of the reactions towards amino acids (Figure 26, yields in green). In the absence of the Pd/C catalyst, no products of reductive amination were observed (see supporting information). Reductive amination could even be carried out at 5 °C; pyruvate was converted to alanine with 18% yield using formate as the reducing agent and 55% yield using  $\text{H}_2/\text{HCO}_3^-$  under otherwise identical conditions (see supporting information).

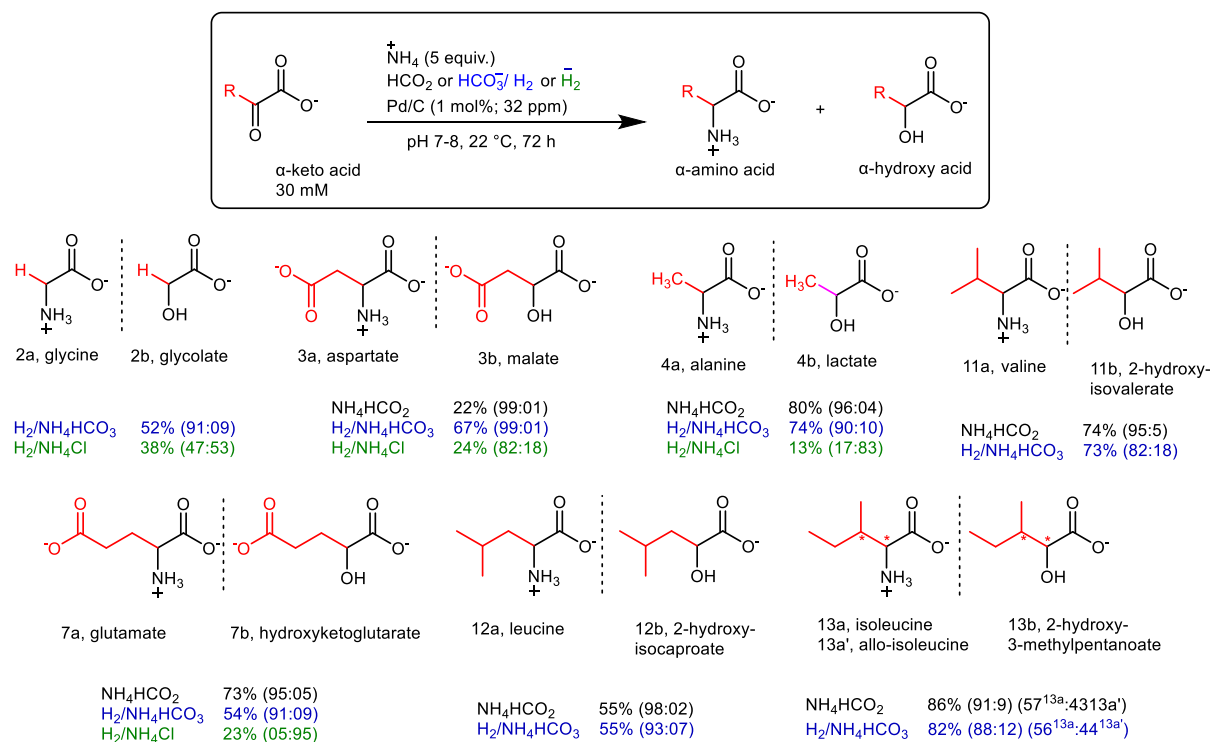
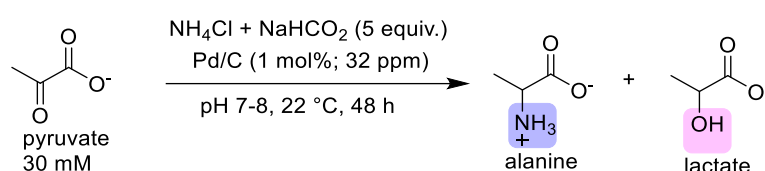


**Figure 26:** Nonenzymatic reductive amination at room temperature. Glyoxylate or the various  $\alpha$ -keto acids (30 mM) are converted to a mixture of  $\alpha$ -amino acids and  $\alpha$ -hydroxy acids upon exposure to  $\text{H}_2/\text{NH}_4\text{HCO}_3$  (in blue) or  $\text{H}_2/\text{NH}_4\text{Cl}$  (in green) (5 bar/5 equiv.) or  $\text{NH}_4\text{CHO}_2$  (in black, 5 equiv.) under catalysis from Pd/C (1 mol% of Pd, 32 ppm relative to oxaloacetate) in pH 7-8 water at 22  $^\circ\text{C}$  for 72 h. Percent yields refer to the combined yields of both products, with the amino acid/hydroxy acid product ratios given in parentheses. Yields determined by quantitative  $^1\text{H}$  NMR.

Traditionally, reductive aminations explored in a prebiotic context relies on using excess amounts of ammonia ( $\geq 100$  equivalents), which is geochemically questionable.<sup>192</sup> The reductive amination reactions reported in this work are done at much lower ammonia concentrations, thus being prebiotically more plausible. Furthermore, we carried out some experiments using various concentrations of ammonia from 0.2 equivalents to 5 equivalents to see the effect on our reaction (Figure 28). We found that the reaction still works when only 6 mM of ammonia is present in the system against 30 mM of the substrate, yielding 3% alanine. A higher concentration of ammonia with respect to pyruvate yielded more product. However, quantities of ammonia higher than 5 equivalents (150 mM) did not further influence the reaction. Overall, these results indicate the plausibility of our reaction conditions to synthesize amino acids in the presence of low ammonia concentrations present on early Earth.



Reductive amination of pyruvate (30 mM) with various concentration of  $\text{NH}_4^+$  in the presence of 5 equivalents of  $\text{NaHCO}_2$  under  $\text{Pd/C}$  catalysis (1 mol%).

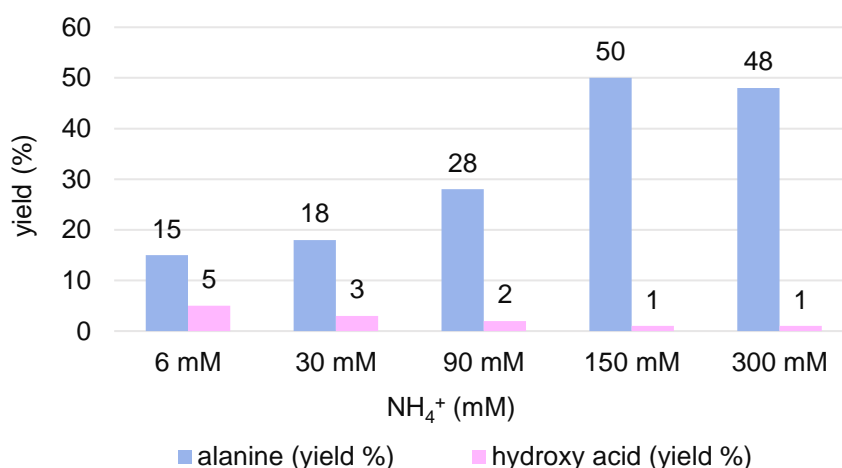


**Figure 27.** Reductive amination of pyruvate with different concentrations of  $\text{NH}_4\text{Cl}$  under catalysis from  $\text{Pd/C}$  (1 mol% of  $\text{Pd}$ , 32 ppm relative to substrate) in the presence of  $\text{Na}_2\text{HCO}_2$  as hydrogen source in pH 7-8 water at 22 °C for 48 h. Percent yields refer to the yields of products: alanine (in blue) and hydroxy acid (in pink). Yields determined by quantitative  $^1\text{H}$  NMR.

### 11.3.2. Oxaloacetate/glyoxylate reaction network, an analogue of rTCA cycle

It's known that mixing oxaloacetate and glyoxylate at pH 7-8 and room temperature proceeds towards the formation of maloyl formate and fumaroyl formate (Figure 28).<sup>144</sup> In prior reports, high temperatures and catalyst loadings were needed to overcome the reaction sequence's slowest step, which is reducing fumaroyl formate to  $\alpha$ -ketoglutarate.<sup>144,146</sup> We anticipated enhancing the rate of the reduction step at room temperature using rare metal catalysis.<sup>187,193</sup> When we mixed oxaloacetate/glyoxylate in a 1:2 ratio (60 mM/120 mM) in the presence of ppm amounts of Pd (64 ppm) and 10 equivalents of sodium formate as hydrogen source, the alkene reduction, and the entire reaction sequence, occurred at 22 °C in neutral water without any additional catalysts (Figure 28). A  $^1\text{H}$  NMR of a representative crude reaction mixture in the presence of sodium formate after 72 h is shown in Figure 29A.

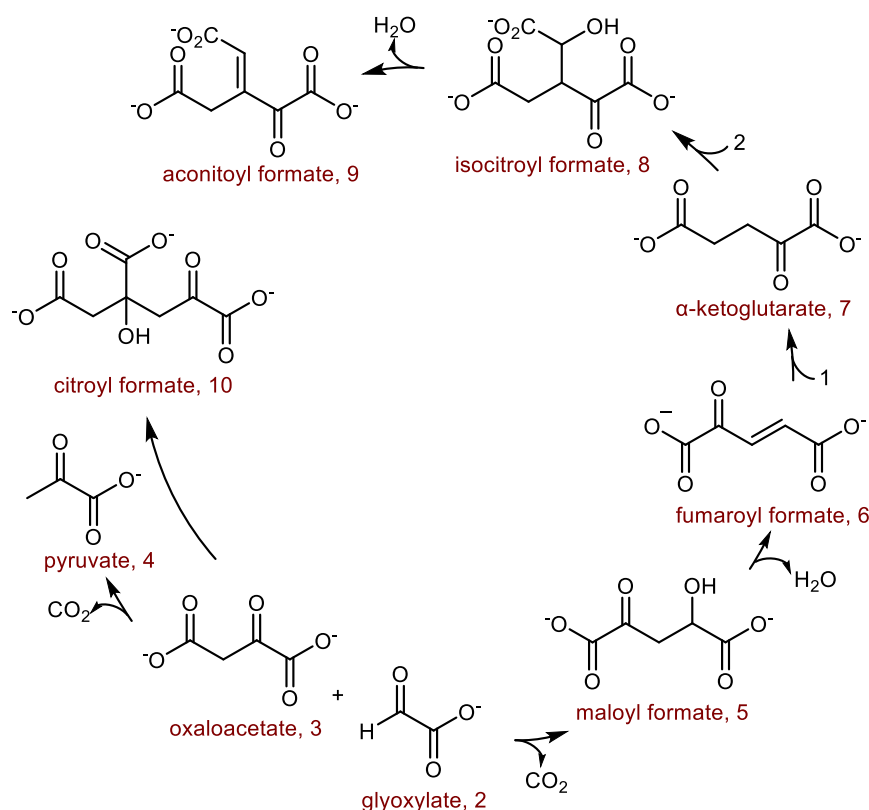


**Figure 28:** Carbon homologue of the rTCA cycle.

The reaction mixture yielded 80% maloyl formate, 0.20% fumaroyl formate, 1.2%  $\alpha$ -ketoglutarate ( $\alpha$ -KG), 0.23% of erythro-isocitroyl formate and 0.1% of aconitoyl formate. The threo diastereoisomer of isocitroyl formate was also formed, as indicated by control experiments (see Figure 34) but could not be quantified in the reaction network due to overlapping NMR signals. Pyruvate was present in 1.9% yield due to the decarboxylation of oxaloacetate. Oxaloacetate is known to dimerize to form citroyl formate,<sup>144</sup> which was not observed in our reaction. Additionally,  $\alpha$ -hydroxy acids, products stemming from the reduction of glyoxylate, pyruvate, and oxaloacetate were observed, including glycolate (0.57%), lactate (0.13%), and malate (1.8%).  $\alpha$ -Hydroxy acids are crucial in various biochemical processes regarding energy storage and conversion.<sup>194</sup> The conditions described here account for a collective 90% yield based on oxaloacetate across the various intermediates and end-products of the subsystem. The same reaction network also works under  $H_2$  pressure (5 bar), where  $H_2$  is used as hydrogen source instead of formate (Figure 29B). As in the reductive amination reactions, under  $H_2$ , we observed that  $CO_2$  present in our reactions, either coming directly from bicarbonate or from decarboxylation of glyoxylate and oxaloacetate, underwent reduction to formate via palladium catalysis (Figure 29b).<sup>191</sup> The same reaction carried out without the Pd/C catalyst still produced the initial products of aldol condensation, maloyl formate, and fumaroyl formate, but none of the products downstream of the reduction of fumaroyl formate (see control experiments Figure 33).

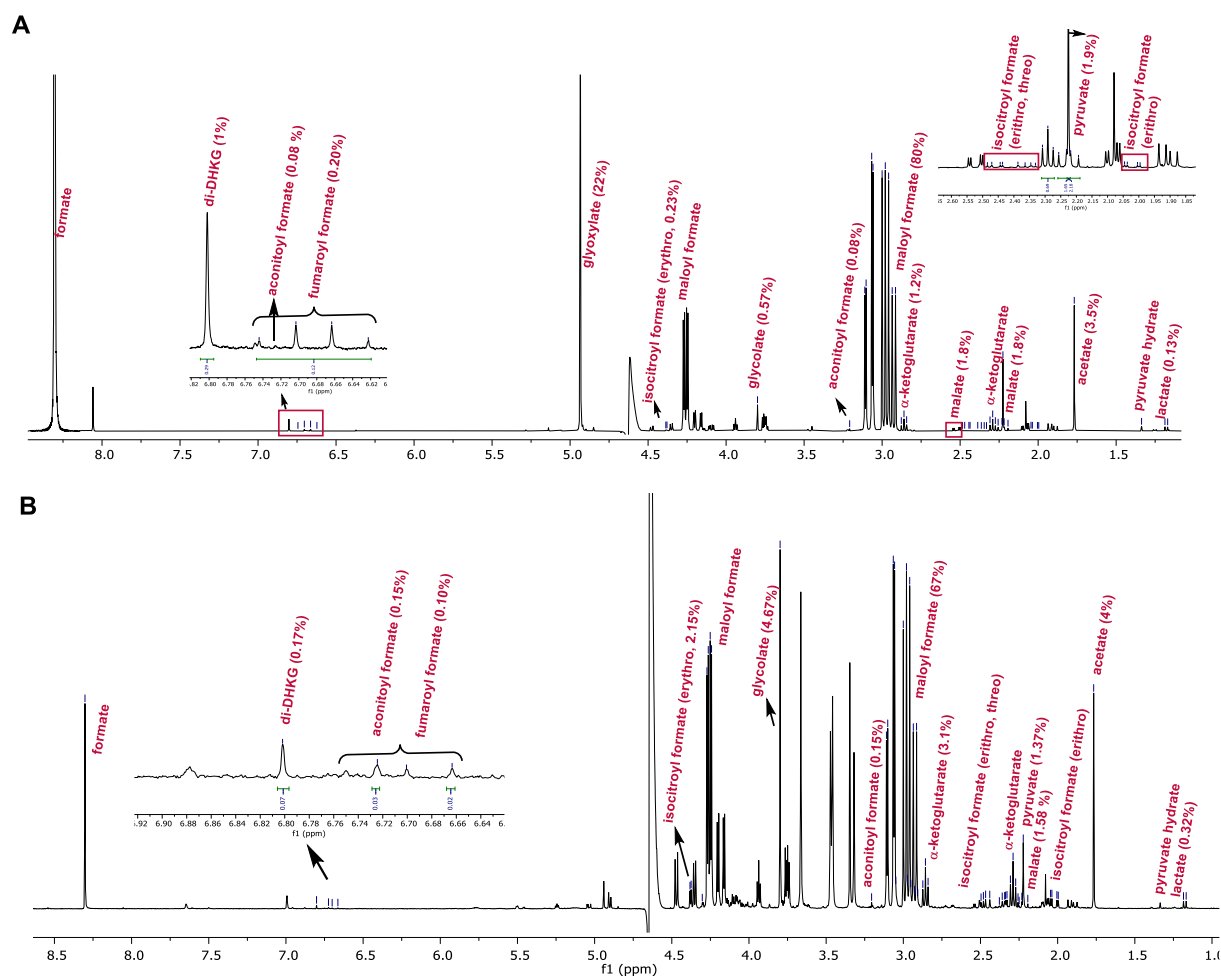


**Figure 29. Nonenzymatic one-pot experiments in pH 7-8 water at 22 °C starting from oxaloacetate (0.06 M) and glyoxylate (0.12 M).** (A)  $^1\text{H}$  NMR of the crude mixture resulting from the reaction of oxaloacetate and glyoxylate with sodium formate (10 equiv.), under catalysis by Pd/C (1 mol%, 64 ppm of Pd relative to oxaloacetate). Reported yields were determined by quantitative  $^1\text{H}$  NMR (see supporting information). Products of interest account for 90% yield based on oxaloacetate with another 1 compound (glycolate) accounting for 0.57% yield based on glyoxylate. (B)  $^1\text{H}$  NMR of the same one-pot experiment in the presence of sodium bicarbonate/ $\text{H}_2$  (10 equiv./5 bar), under catalysis by Pd/C.

*Note:* Several other compounds were observable in the  $^1\text{H}$  NMR but could not be identified.

### 11.3.3. Reaction network driven by H<sub>2</sub> under Pd catalysis, connecting rTCA analogue to amino acids.

Fascinated by the exceptional catalytic activity of palladium in our reductive amination and rTCA analogue reactions, we finally wanted to explore whether the hydrogenation of bicarbonate to formate, the rTCA cycle analogue, and reductive amination could occur in a one-pot experiment to achieve mutually compatible metabolism-like processes, thus, self-organised chemistry (Figure 30). The overall reaction network is made up of four interconnected subsystems, as described in Figure 30, from the inside out: 1) bicarbonate hydrogenation to yield formate; 2) keto acid synthesis analogous to the reverse Krebs cycle through aldol condensations and (transfer) hydrogenation; 3) amino acid synthesis via reductive amination of keto acids with ammonia; and 4) keto acid reduction to hydroxy acids.

When oxaloacetate (60 mM) and glyoxylate (120 mM) were mixed in the presence of 10 equivalents of ammonium formate with trace amounts of Pd/C (1 mol% of Pd with respect to oxaloacetate) at room temperature in pH 7-8 water over 72 h, we achieved a complex reaction mixture of which representative <sup>1</sup>H NMR is shown in Figure 31A. The reaction mixture contained intermediates of the rTCA/TCA cycle ( $\alpha$ -ketoglutarate and pyruvate), five additional  $\alpha$ -keto acids that are one-carbon homologues of those in the rTCA/TCA cycle (maloyl formate, fumaroyl formate, isocitroyl formate, aconitoyl formate, and citroyl formate), four amino acids (glycine, alanine, aspartate and glutamate (alanine and glutamate presence was detected by GC-MS, representative example Figure 32), and three hydroxy acids (glycolate, lactate, and malate). Interestingly, when ammonium ions are present in the reaction mixture, we are able to observe citroyl formate due to the decarboxylative homo-aldol condensation of oxaloacetate (Figure 31A). Thus, we can achieve the self-organised reactivity shown in Figure 30. These results are promising in a prebiotic context, as this kind of complex network has never been achieved before under one-pot conditions without human intervention. Further, when ammonium formate is present in the reaction in place of sodium formate, the alkene reduction of fumaroyl formate to  $\alpha$ -ketoglutarate was found to be improved, which indicates that inorganic salts or counter ions can influence the reactivity to various extent, an important consideration to be taken into account for scientists working in the origins of life field. Experiments in which H<sub>2</sub>/HCO<sub>3</sub><sup>-</sup> was used



as a source of H<sub>2</sub> instead of formate in the presence of ammonium ions also led to the same products (Figure 31B).

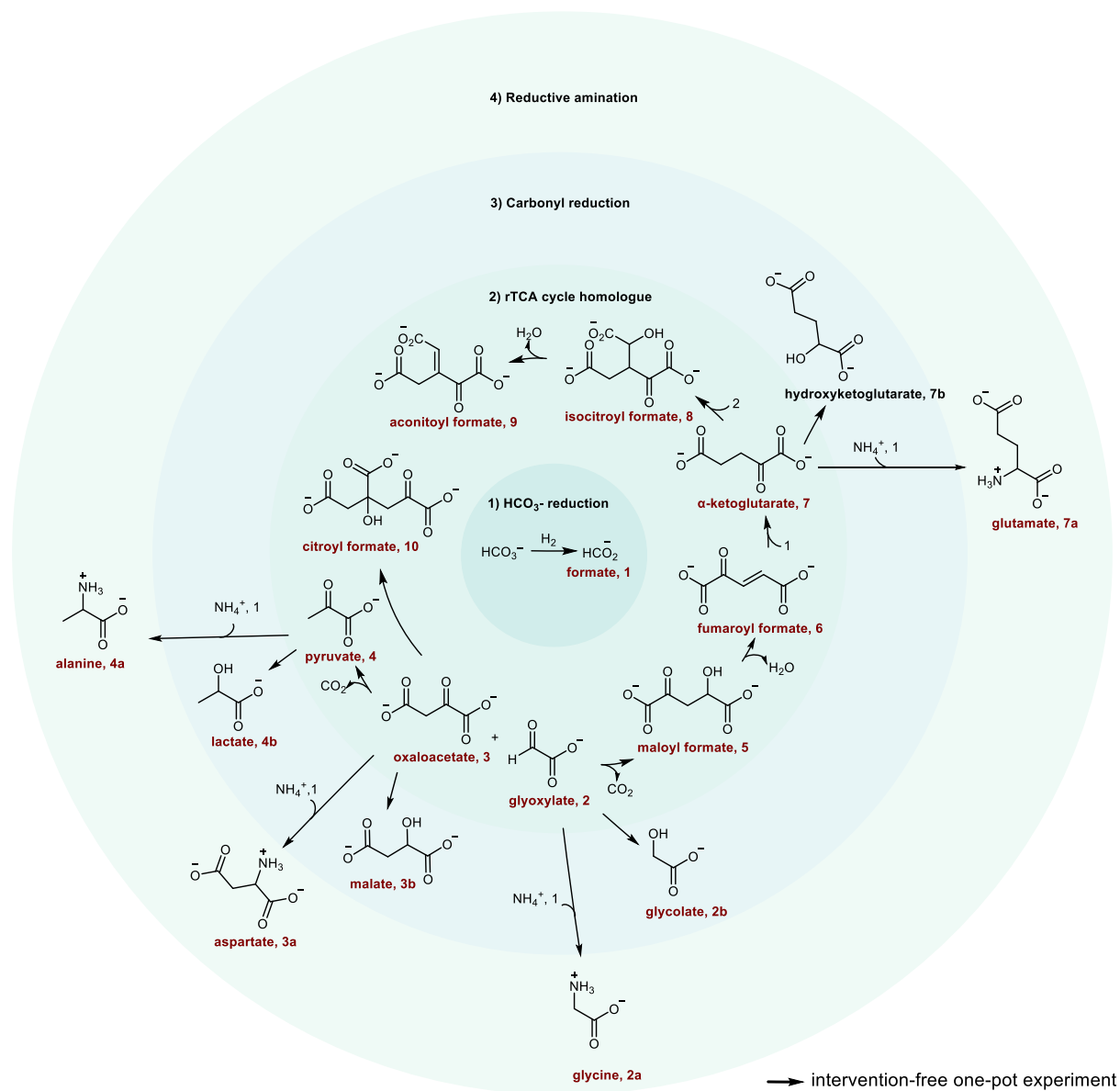


**Figure 30:** Abiotic H<sub>2</sub>-driven network connecting different subsystems from CO<sub>2</sub> to amino acids.

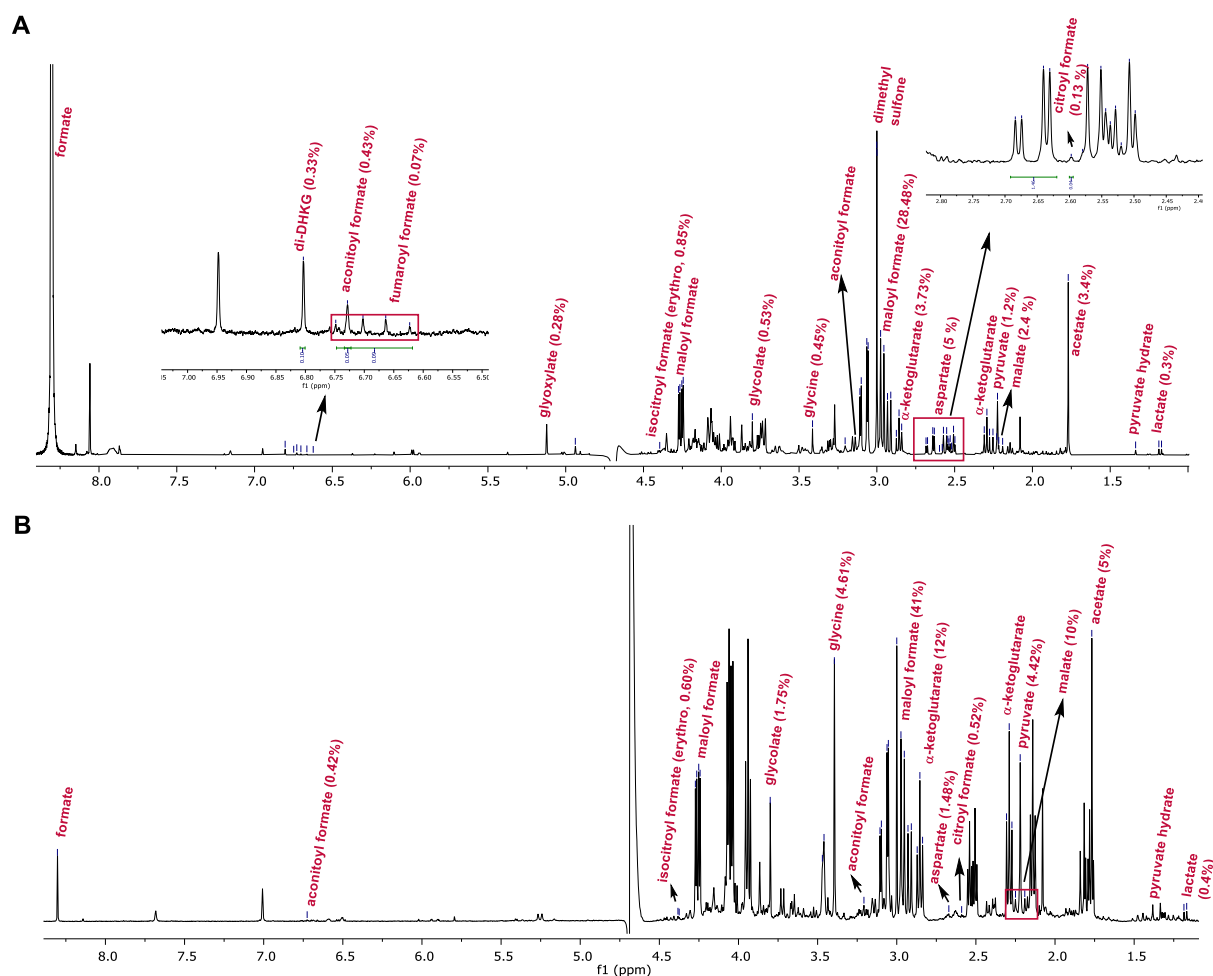


**Figure 31. Nonenzymatic one-pot experiments in pH 7-8 water at 22 °C starting from oxaloacetate (0.06 M) and glyoxylate (0.12 M) in the presence of ammonia. (A)**  $^1\text{H}$  NMR of the crude mixture resulting from the reaction of oxaloacetate and glyoxylate with ammonium formate (10 equiv.), under catalysis by Pd/C (1 mol% of Pd, 64 ppm relative to oxaloacetate). Reported yields were determined by quantitative  $^1\text{H}$  NMR (see supporting information). Products of interest account for 46% yield based on oxaloacetate with another 1 compound (glycolate) accounting for 0.53% yield based on glyoxylate. **(B)**  $^1\text{H}$  NMR of the same one-pot experiment in the presence of ammonium bicarbonate/ $\text{H}_2$  (10 equiv./5 bar), under catalysis by Pd/C.

*Note:* Several other compounds were observable in the  $^1\text{H}$  NMR but could not be identified.

Representative example of **GC-MS** analysis (qualitative results) for glycine, alanine, aspartate and glutamate is shown in Figure 32, where the reaction mixture was derivatized with ethyl chloroformate to have ester products identifiable by GC-MS analysis. Reaction products derivatized to ethyl esters were identified by comparing the mass spectra and retention times to those of analogously derivatized authentic samples

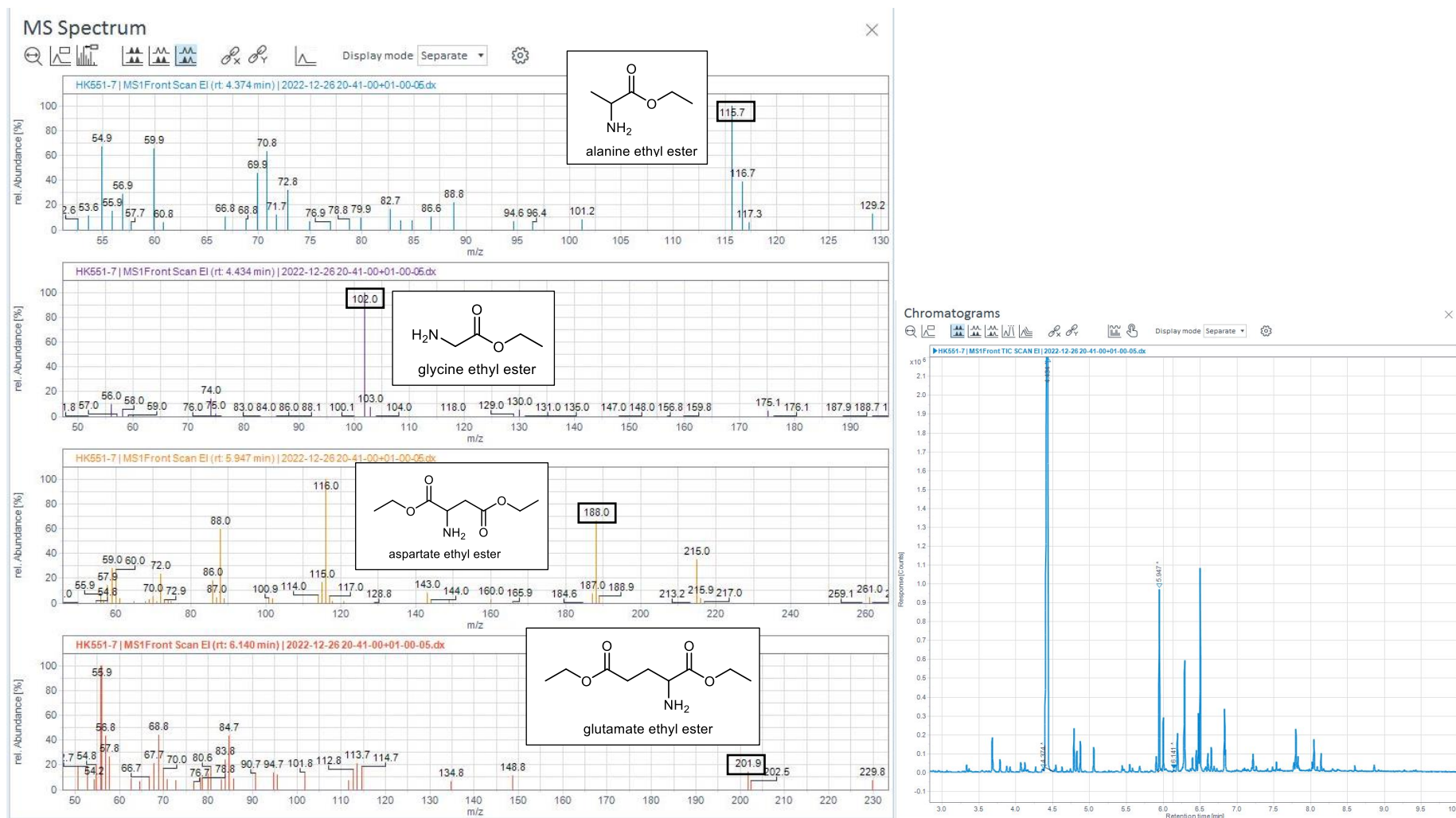


**Figure 32.** GC-MS analysis (negative mode) of nonenzymatic one-pot experiments in pH 7-8 water at 22 °C starting from oxaloacetate (0.06 M) and glyoxylate (0.12 M) in the presence of ammonium bicarbonate/H<sub>2</sub> (10 equiv./5 bar), under catalysis by Pd/C.

### 11.3.4. Network reaction control experiments

The presence of a Pd catalyst is crucial for the alkene reduction (fumaroyl formate to  $\alpha$ -ketoglutarate) and reductive amination (Figure 30). Control experiments shown in (Figure 33 and 34) shows that aldol hydration/dehydration reactions occur smoothly at room temperature, in near neutral pH waters without any catalyst. At the same time,  $\alpha$ -ketoglutarate formation (coming from fumaroyl C=C bond reduction) and amino acids are absent.

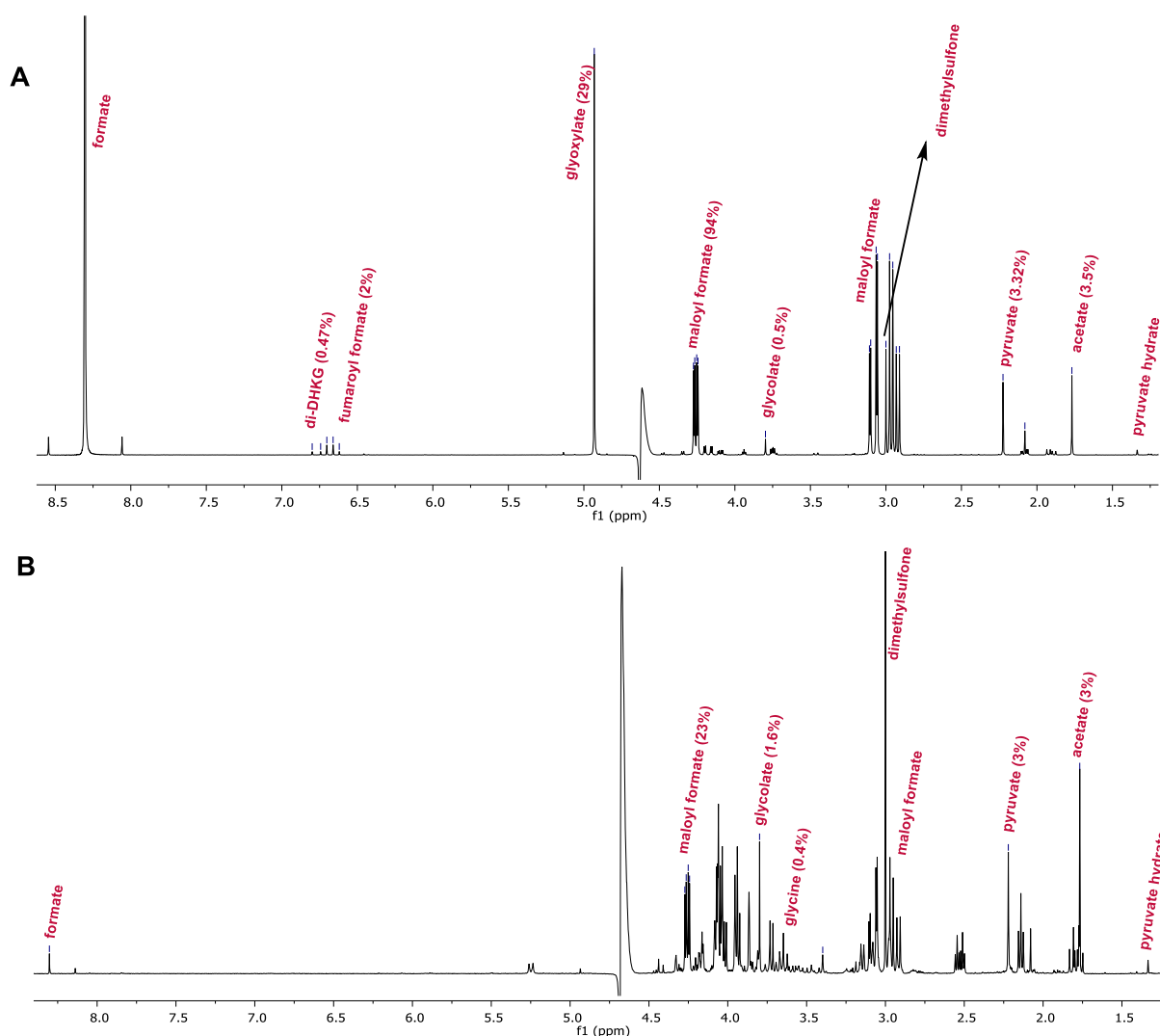


**Figure 33. Nonenzymatic one-pot experiments in pH 7-8 water at 22 °C starting from oxaloacetate (0.06 M) and glyoxylate (0.12 M) in the absence of Pd/C. (A)**  $^1\text{H}$  NMR of the crude mixture resulting from the reaction of oxaloacetate and glyoxylate in the presence of ammonium formate (10 equiv.). Reported yields were determined by quantitative  $^1\text{H}$  NMR (see supporting information). **(B)**  $^1\text{H}$  NMR of the same one-pot experiment in the presence of ammonium bicarbonate/ $\text{H}_2$  (10 equiv./5 bar).

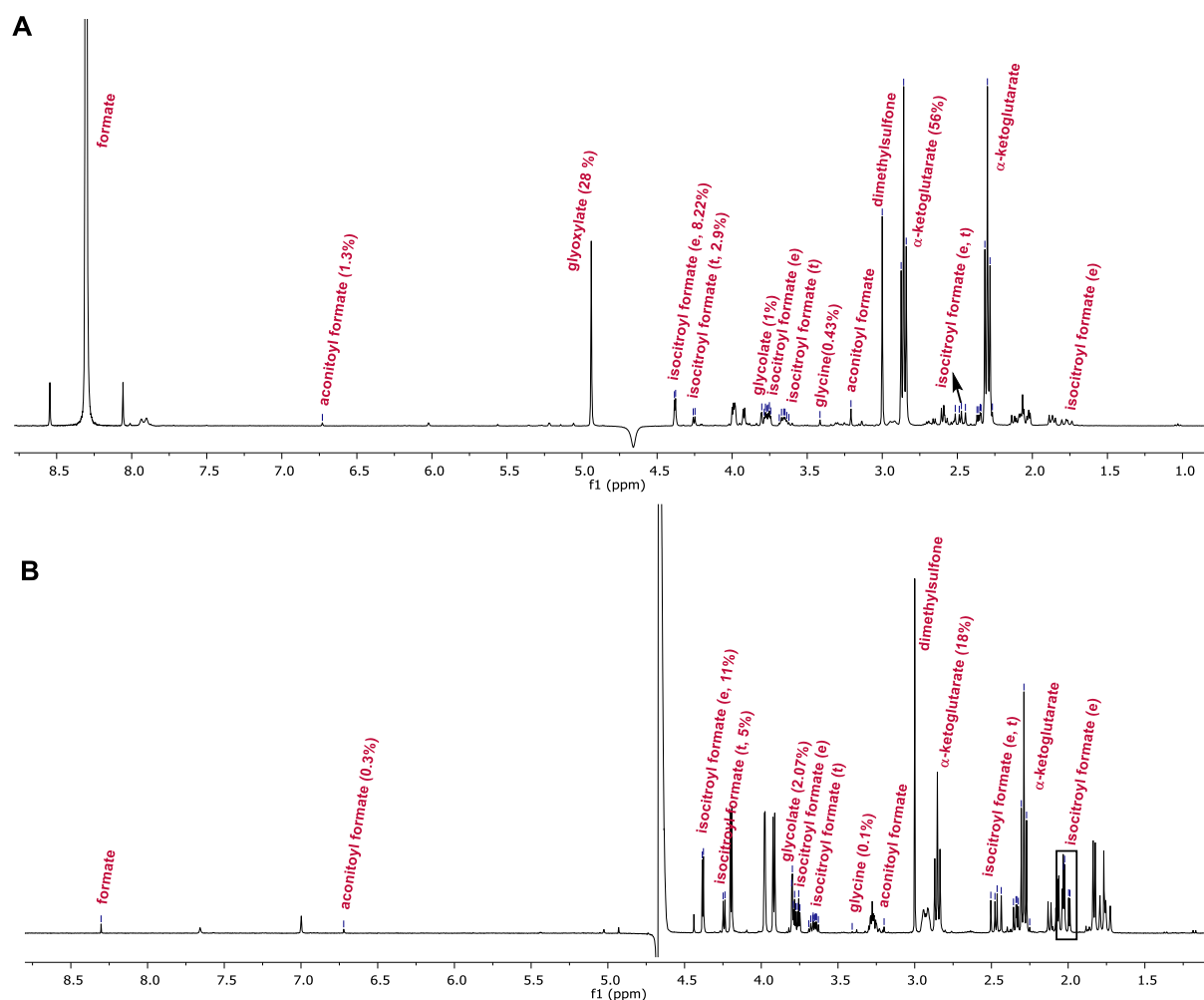


**Figure 34. Nonenzymatic one-pot experiments in pH 7-8 water at 22 °C starting from  $\alpha$ -ketoglutarate (0.06 M) and glyoxylate (0.06 M) in the absence of Pd/C. (A)**  $^1\text{H}$  NMR of the crude mixture resulting from the reaction of  $\alpha$ -ketoglutarate and glyoxylate in the presence of ammonium formate (10 equiv.). Reported yields were determined by quantitative  $^1\text{H}$  NMR (see supporting information). **(B)**  $^1\text{H}$  NMR of the same one-pot experiment in the presence of ammonium bicarbonate/ $\text{H}_2$  (10 equiv./5 bar).

### 11.3.5. Pd/C catalysts analysis

The commercial Pd/C catalyst analysis (see supporting information) showed the average particle size of Pd to be around 3 nm and confirmed previous studies showing that commercial “Pd/C” is mostly PdO rather than metallic Pd.<sup>179</sup> Thus, to get insight into the catalyst, Pd/C and PdO/C catalysts (particle sizes  $\approx 5$  nm) were synthesized by our collaborators by Dr. Harun Tüysüz and Dr. Youngdong Song (see supporting information section for details) and were tested in a representative reductive amination reaction using ammonium formate (Figure 35). We also tested Pd supported on different support (Pd/Al<sub>2</sub>O<sub>3</sub>) and Pd/C from two different suppliers (TCI and Sigma). Catalysts placed on different supports showed similar catalytic activity, but changes in particle size had a large influence. Particles of 3 nm (commercial Pd/C and Pd/ Al<sub>2</sub>O<sub>3</sub>) were substantially more active than 5 nm particles (synthesised Pd/C, PdO/C) or unsupported (commercial PdO) (Figure 35).

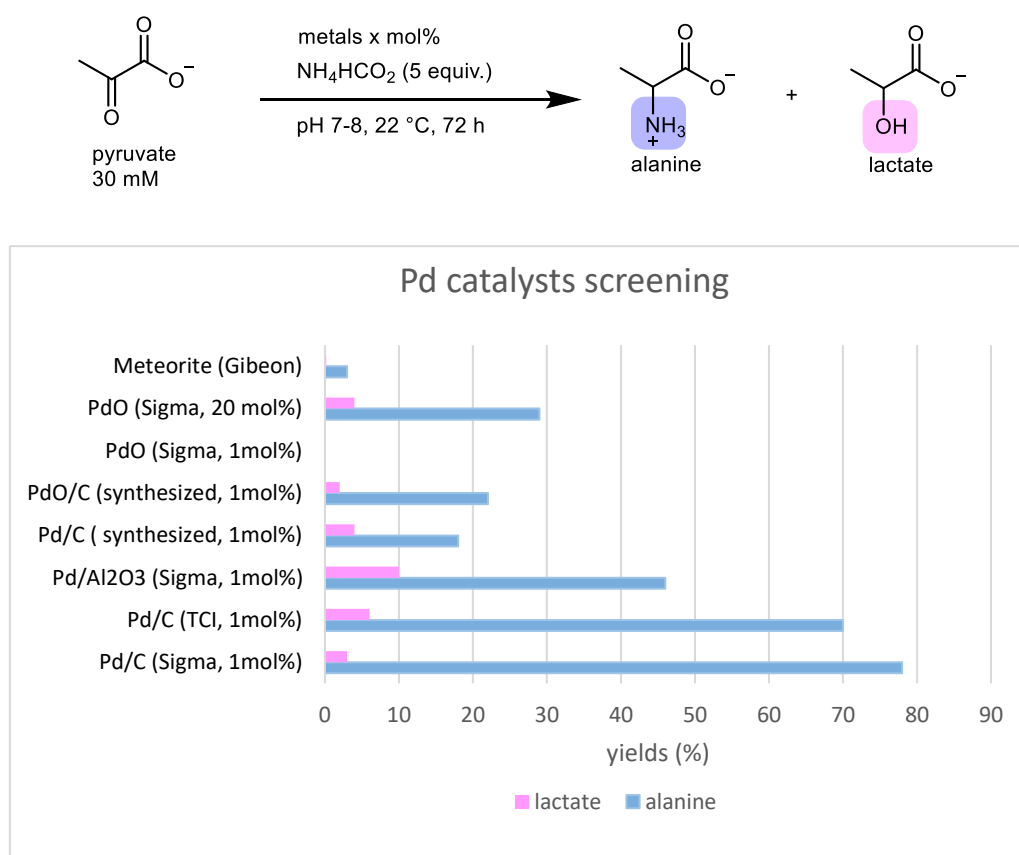


**Figure 35:** Reductive amination of pyruvate (30 mM) with ammonium formate (5 equiv.) in the presence of various Pd catalysts. The reaction with meteorite was carried under H<sub>2</sub> (5 bar) in the presence of ammonium bicarbonate (5 equiv.) as catalysis without H<sub>2</sub> in the presence of formate was not observed.

#### 11.4. Conclusions

In summary, we have described a hydrogen-driven complex reaction network that emulates the function of several interconnected biological pathways without intervention, including bicarbonate reduction,  $\alpha$ -keto acid synthesis by reductive aldol chemistry, amino acid synthesis by reductive amination and hydroxy acids synthesis via carbonyl reduction. The key to the reactivity is using rare metal catalysts such as Pd. All reactions occur independently and concurrently in water under the same conditions, at room temperature, around neutral pH, with Pd in ppm levels replacing the catalytic function of a dozen enzymes and cofactors. The network bears a strong resemblance to the metabolic core of ancient microbes, relying on  $H_2$  gas or formate to drive reductive reactions and on ammonium as nitrogen source. The unequivocal and specific correspondence of the reactions and products reported herein to the reactions comprising central microbial metabolism supports the idea that core metabolism could arise from interactions of aqueous compounds with solid-state transition metal catalysts. Rare elements may have catalyzed life's initial chemical self-organization on a local scale before being replaced by more complex but elementally abundant catalysts of its own making, thereafter, allowing it to spread to a new environment.

## **12. Diamidophosphate (DAP) as a potential prebiotic source of amino acids and their oligomers**

A peptide's fundamental role in biology makes it almost impossible to dispute that they were a major player in the emergence of life. It is now important to ask whether primordial polypeptides were based on the same set of amino acids as modern proteins or on a smaller subset, such as early amino acids: glycine, alanine, aspartate, glutamate, valine, etc.? Recent studies indicate that proteins containing only the "early" amino acids would still have been functional.<sup>196</sup> We were interested into prebiotic plausible means by which early amino acids could have been produced and subsequently elaborated into proto peptides. As there are a number of studies in the prebiotic context that explain how early peptides could have formed on early earth, why were we interested in this work? Let's review previous prebiotic attempts at amino acid oligomerization to answer this question.

### **12.1. Prebiotic attempts to explain amino acid oligomerization**

The conversion of amino acids into peptides present a considerable challenge, because the condensation reactions are thermodynamically disfavored in water.<sup>197,198</sup> Wet-dry cycling is commonly viewed as a feasible mean to overcome this barrier (Figure 36A).<sup>199,200</sup> Some clay and minerals such as zinc clays, magnetite (Fe<sub>3</sub>O<sub>4</sub>) or condensing agents such as CDI or TMP have been shown to catalyze the formation of proto polymers mediated by wet-dry cycling approach.<sup>201,202,203,204,205,206</sup> But this approach cannot give us a clue of how pre-metabolism could evolve from an abiotic to the biotic world, as it does not resemble life. Furthermore, wet-dry cycling often relies on high temperatures (> 80° C) which are not suitable for many life sustaining molecules such as ribose.  $\alpha$ -Amino nitriles formed via HCN chemistry is also widely accepted as a way to create oligopeptides (Figure 36B).<sup>207</sup> Although peptides can be achieved via HCN chemistry, amino nitriles are not used by life to form oligomers. As a result, alternative approaches are needed.



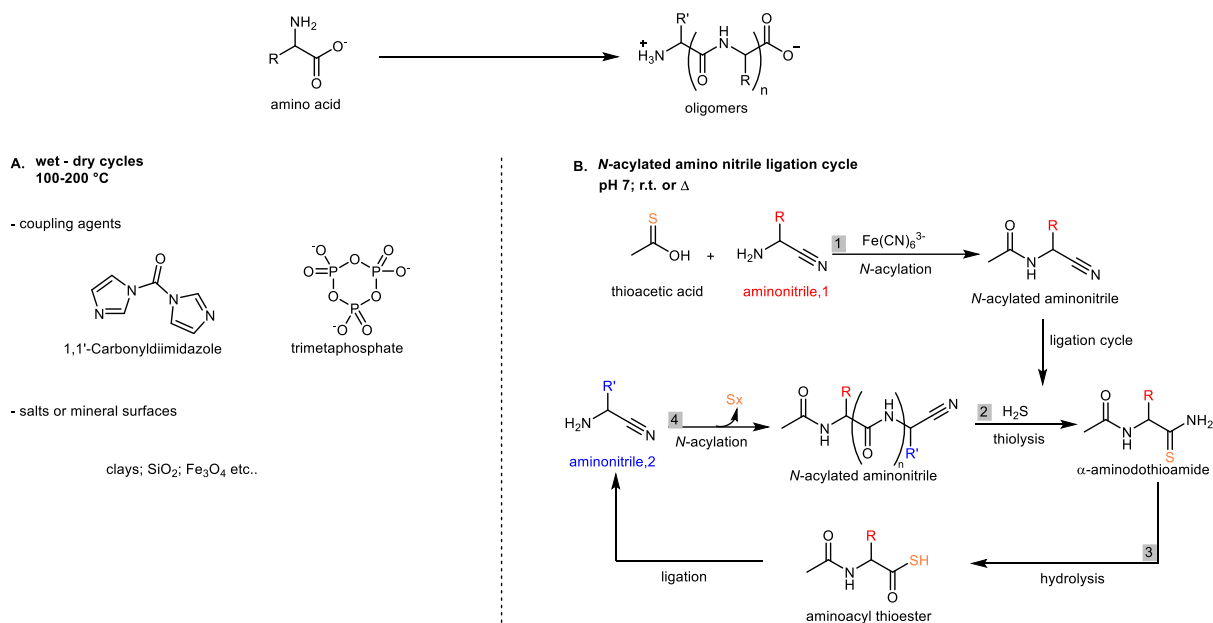


**Figure 36.** Previous studies on amino acid oligomerization.<sup>207</sup>

## 12.2. Chapter objectives: peptide synthesis in water mediated by DAP

The aim of this chapter is to explore amino acid synthesis starting from corresponding  $\alpha$ -keto acids and their subsequent oligomerization under the one-pot and prebiotically more plausible conditions mimicking biological mechanisms in water at lower temperatures. In order to achieve thermodynamically non favoured condensation in a water-rich environment, the activation of amino acid is crucial. Therefore we envisioned to activate amino acids using inorganic polyphosphates (trimetaphosphate) or amidophosphates (DAP).<sup>204,206</sup> Typically, this type of activation occurs at the amino termini, where *N*-phosphorylation releases more energy than *O*-phosphorylation.<sup>204,208</sup> Since DAP has one less negative charge than polyphosphates (Figure 37), it is less susceptible to precipitation under conditions where phosphate/polyphosphates are precipitated out by divalent metals.<sup>209</sup> Thus, the presence of DAP in the solution makes it a more plausible candidate increasing its potential for abiotic phosphorylation reactions.<sup>209</sup> In an early Earth scenario, DAP could be generated from ammonia and condensed phosphates such as trimetaphosphate (TMP), where the latter could have been available on early earth from an acidic phosphate by volcanic processing (Figure 37).<sup>210,211</sup>

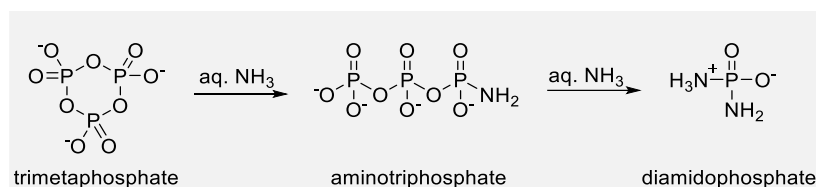


**Figure 37.** DAP synthesis from polyphosphates on early earth (figure adapted from reference 209).

DAP attracted our attention not only as a source of potential prebiotic activating agent for amino acids condensation, but also as an amine donor. DAP is monoanionic in nature. It has two  $pK_a$  values:  $pK_{a1} \sim 1.2$  and  $pK_{a2} \sim 5$ .<sup>212</sup> The first protonation  $pK_{a2}$  is assigned to the protonation of one of the  $\text{NH}_2$  group and the second protonation,  $pK_{a1}$ , probably mainly involves the oxygen atom.<sup>212</sup> As one of the  $\text{NH}_2$  is not protonated, therefore, we hypothesized that it can act as a good nucleophile to attack the carbonyl group of an  $\alpha$ -keto acid, giving amino acid as a product in the presence of a reductant, which subsequently could get activated by DAP to undergo condensation reaction to generate peptides. In Figure 38 proposed reaction scheme is shown.

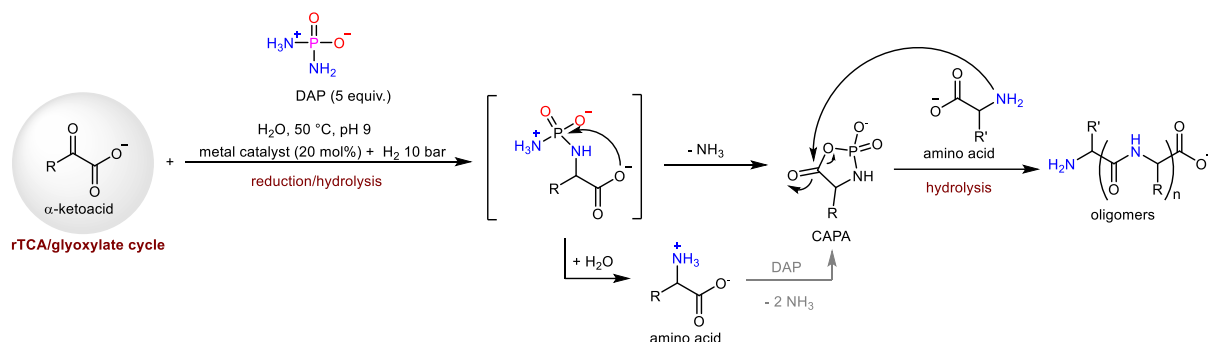


**Figure 38:** Proposed reaction scheme (CAPA, cyclic and phosphoryl-activated amino acid intermediate).

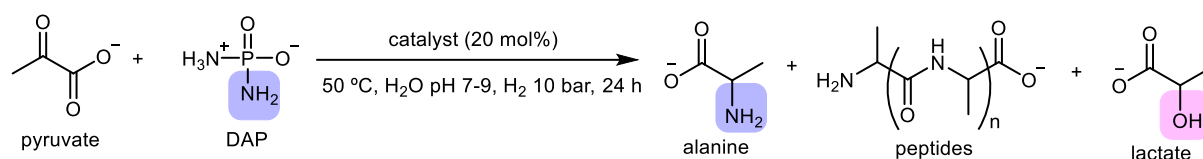
### 12.3. Results and discussions

Initially, we studied the effects of 20 mol% of various transition metals on the reductive amination reaction between pyruvate and DAP to yield alanine at 50 °C, under  $\text{H}_2$  10 bar, for 24 h in unbuffered water (Table 6). The initial reaction pH was adjusted to pH  $\sim 7$  which turns to pH  $\sim 9$  within one/two hours, due to the hydrolysis of DAP to aqueous  $\text{NH}_3$ .

We found that the reductive amination reaction of 100 mM pyruvate with 5 equiv. of DAP in the presence of Ni-Al alloy as a catalyst yielded alanine and dipeptide of alanine in 40 and 10% yield respectively, as determined by quantitative  $^1\text{H}$  NMR spectroscopy after removal of the metals with the ion-exchange resin Chelex (Table 6). The presence of ala-ala was confirmed by comparing it to the authentic sample's  $^1\text{H}$  NMR (see supporting information). In our reactions, nickel and cobalt were found to be the best catalysts, while other transition metals showed zero to very low activity. These two metals along with copper and vanadium were also found to show the catalytic activity in transamination reactions (uncovered in section 10), further strengthening the link between reductive amination and transamination reactions under plausible prebiotic environments.

The representative  $^1\text{H}$  NMR and  $^{31}\text{P}$  NMR of the reaction mixture (entry 1) are shown in supplementary Figure S22.  $^{31}\text{P}$  NMR shows that DAP undergoes loss of ammonia to form a spectrum of condensed products (P-O-P and/or P-N-P bonds), with orthophosphate as the stable end-product (Figure S22).<sup>209</sup>

**Table 6.** Reaction of pyruvate (100 mM) and DAP (5 equiv.) in the presence of 20 mol% of different metal/metal salts at 50 °C (H<sub>2</sub>O, pH 9, 24 h).<sup>a</sup>



entry	catalyst	alanine yield (%)	ala-ala yield (%)	lactate yield (%)
1	Ni-Al alloy	39.43	10.21	8.49
2	Ni-Fe alloy	32.08	5.22	5.76
3	Ni	18.12	0.91	1.71
4	Co	10.45	1.39	3.27
5	Zn	1.22	0.16	14.04
6	No metal	-	-	-

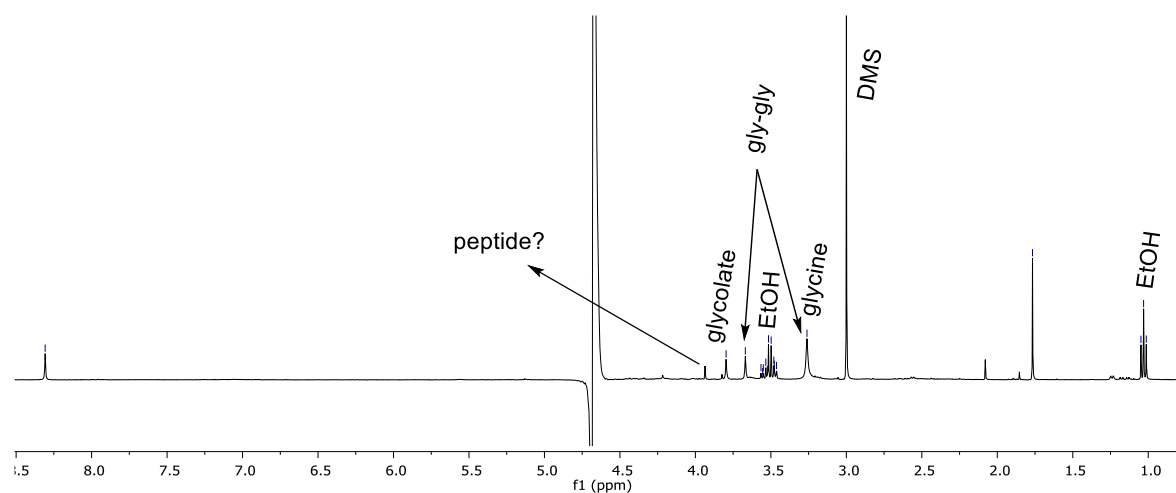
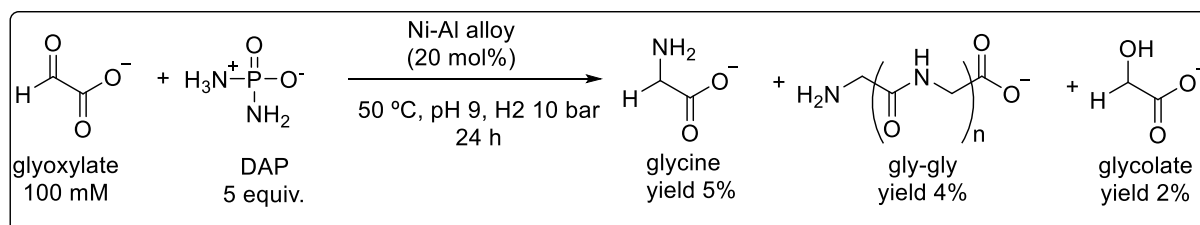
---

AlCl<sub>3</sub>; CeCl<sub>3</sub>; CO<sub>2</sub>Al<sub>2</sub>O<sub>5</sub>; CoCl<sub>2</sub>; CrCl<sub>3</sub>; Cu; CuCl<sub>2</sub>; Fe; FeS; FeO; FeCl<sub>2</sub>; Fe<sub>3</sub>O<sub>4</sub>; FeSO<sub>4</sub>; Mg; MgCl<sub>2</sub>; Mn; MnCl<sub>2</sub>; NiCl<sub>2</sub> < 1 % of products.

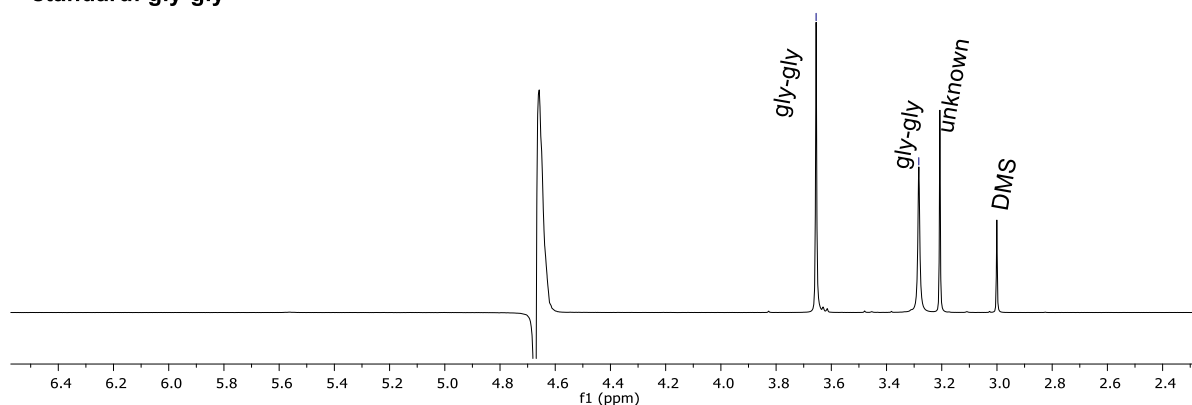
Next, we studied whether the reaction conditions identified for the reductive amination of pyruvate, are suitable for the reductive amination of glyoxylate, oxaloacetate and  $\alpha$ -ketoglutarate to glycine, aspartate, and glutamate, respectively. We have found that glyoxylate and  $\alpha$ -ketoglutarate are successfully aminated to the corresponding amino acids glycine and glutamate more selectively in comparison to hydroxy acid products (scheme 1, 2 and 3). Glycine and the dipeptide gly-gly were obtained in 5 and 4 % yields, and the presence of triglycine is also speculated (scheme 1). Pyruvate and  $\alpha$ -ketoglutarate gave relatively high yields of aminated products: alanine and the dipeptide ala-ala were obtained in 40 and 8% yields, respectively (scheme 2), while from  $\alpha$ -Ketoglutarate 24 % of glutamate, 14% of pyroglutamate (cyclized glutamate) and 2% of glutamine were obtained (scheme 3). Pyroglutamate and glutamine are two other important compounds in biochemistry, e.g. glutamine served as ammonia donor in pyrimidine nucleotide biosynthesis.<sup>97</sup> However, oxaloacetate reductive amination to

aspartate was not achieved and further oligomerization of the latter, because under these conditions oxaloacetate was decarboxylated to pyruvate under our reaction conditions.

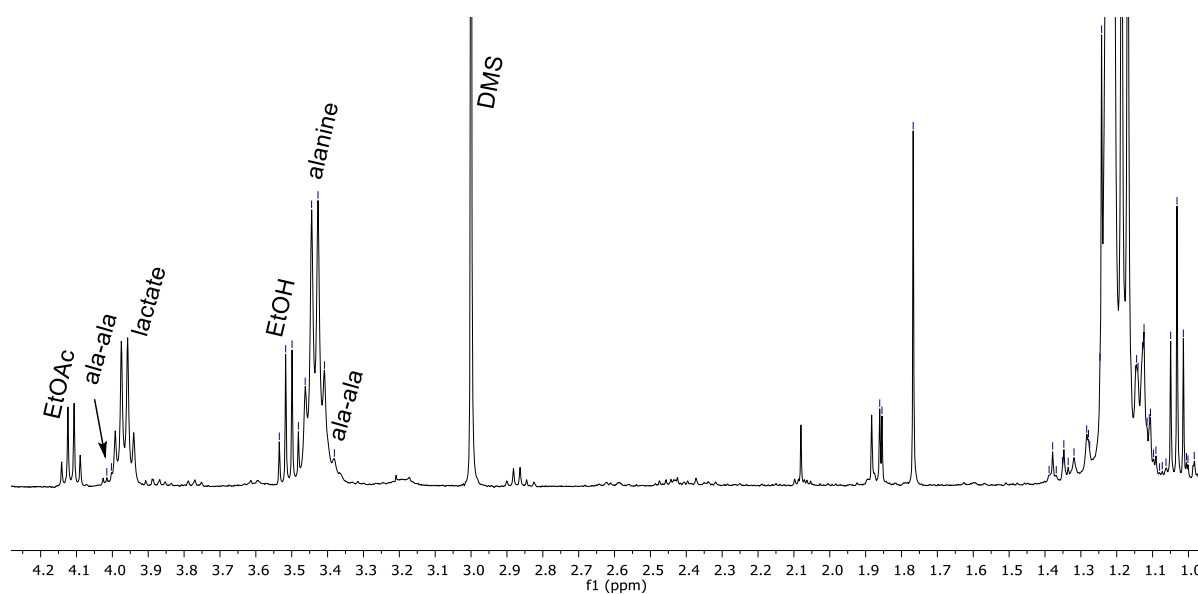
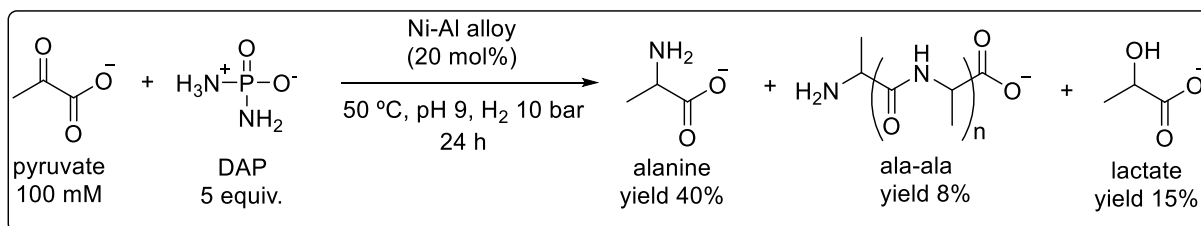
### Scheme 1. Reaction of glyoxylate with DAP under H<sub>2</sub> (10 bar) using Ni-Al catalyst



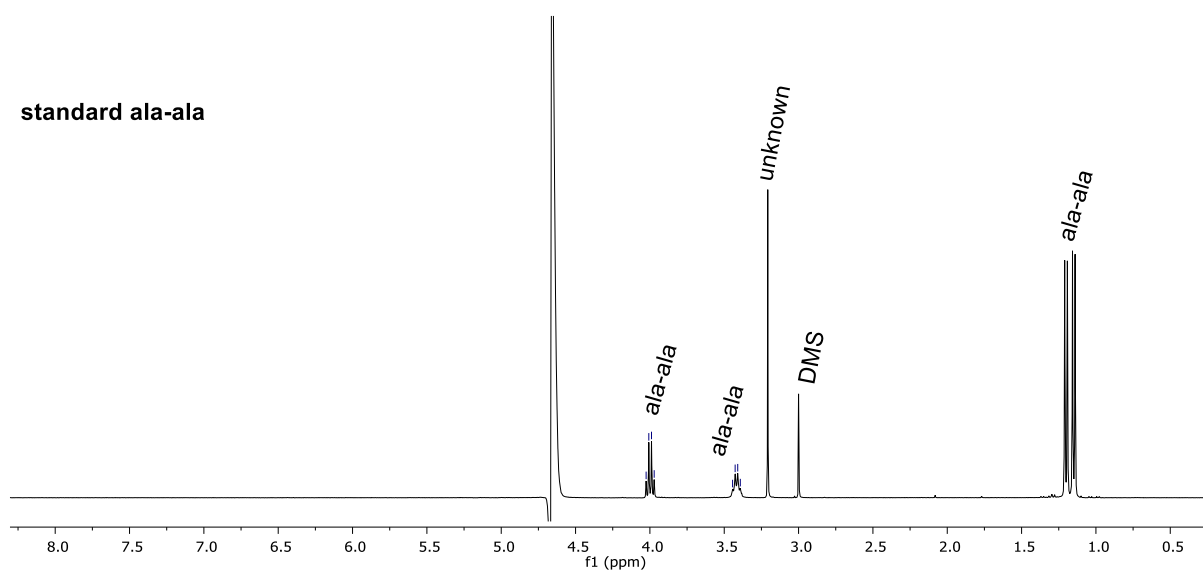
standard: gly-gly



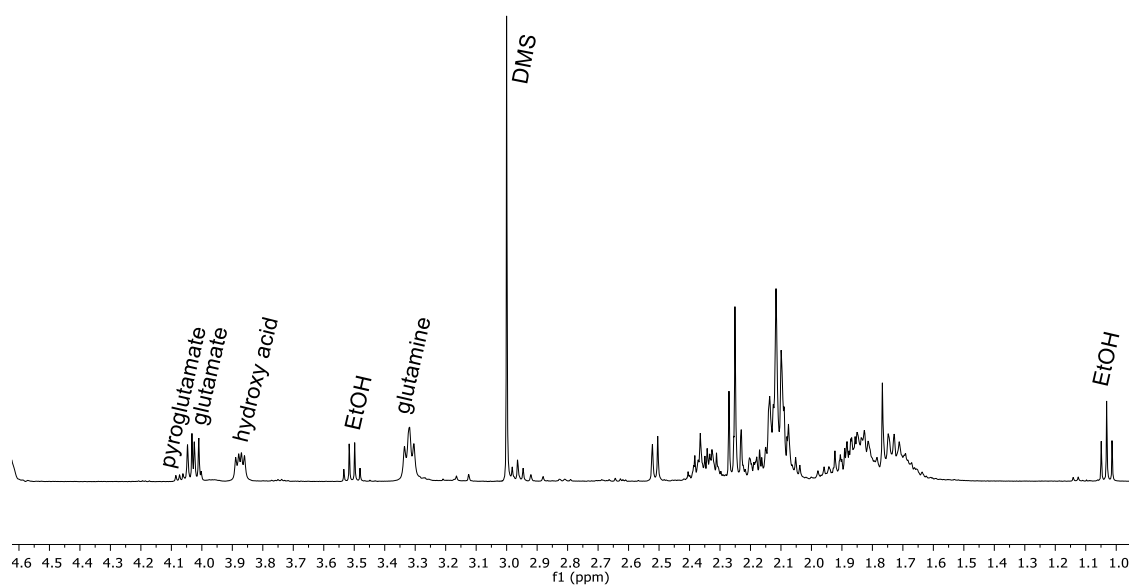
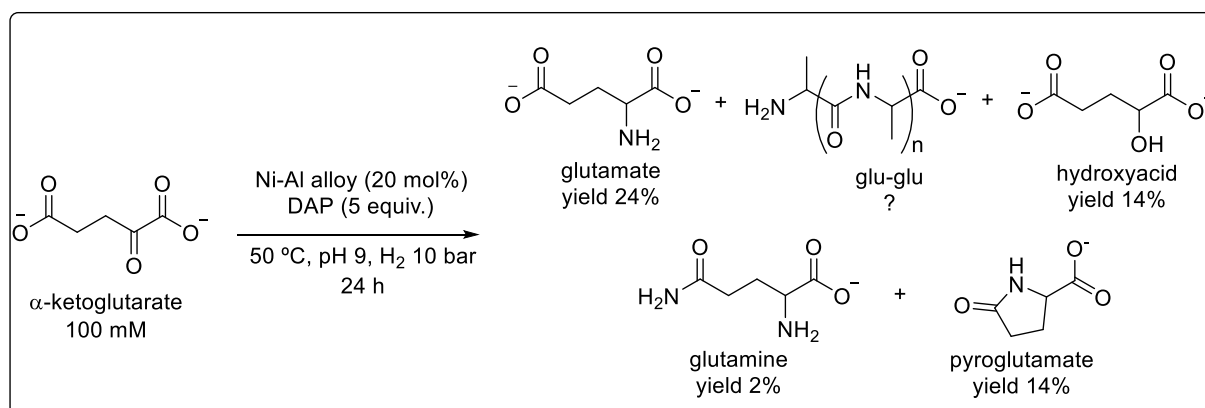
## Scheme 2. Reaction of pyruvate with DAP under H<sub>2</sub> (10 bar) using Ni-Al catalyst



standard ala-ala



**Scheme 3. Reaction of  $\alpha$ -ketoglutarate with DAP under H<sub>2</sub> (10 bar) using Ni-Al catalyst**



*Note: see supporting information for authentic standards of glutamine and pyroglutamate.*

These results showed to be promising, as in one-pot reaction we were able to get not only amino acids but also their condensation products in water rich environment at mild temperatures. Encouraged by our initial findings, next we wanted to explore amino acids condensation reactions, and then apply them to an one-pot reaction. Thus, we took all four “early amino acids” (glycine, alanine, aspartate and glutamate) and exposed them to DAP (5 equivalents) in water for 72 h at 50 °C without the Ni-Al catalyst, as the latter is only needed in the reductive amination. We choose to run reactions for 72 h instead of 24 h, as DAP is still present in the reactions after 24 h, it is not fully hydrolysed. Therefore, the idea was that by increasing reaction time, more activated species would be formed, thus the reaction could proceed further until DAP is not fully hydrolysed.

As showed in figure 39, glycine was condensed to gly-gly into 36 % yield. By NMR alone identification of longer peptides was found to be difficult, therefore, along with NMR analysis we opted for OPA (o-phthalaldehyde) derivatization method (see supporting information for more details). With this method, primary amines are easily reacted to OPA forming UV active compound, which can be easily analysed by UV-HPLC (see supporting information). Thus, we derivatized the authentics and our reactions and analysed them also with UV. Analytical methos are still underway, therefore UV chromatogram for glycine and peptides is not shown here, but the presence of dipeptides and tripeptides of glycine are confirmed by ESI-QTOF-MS analysis.



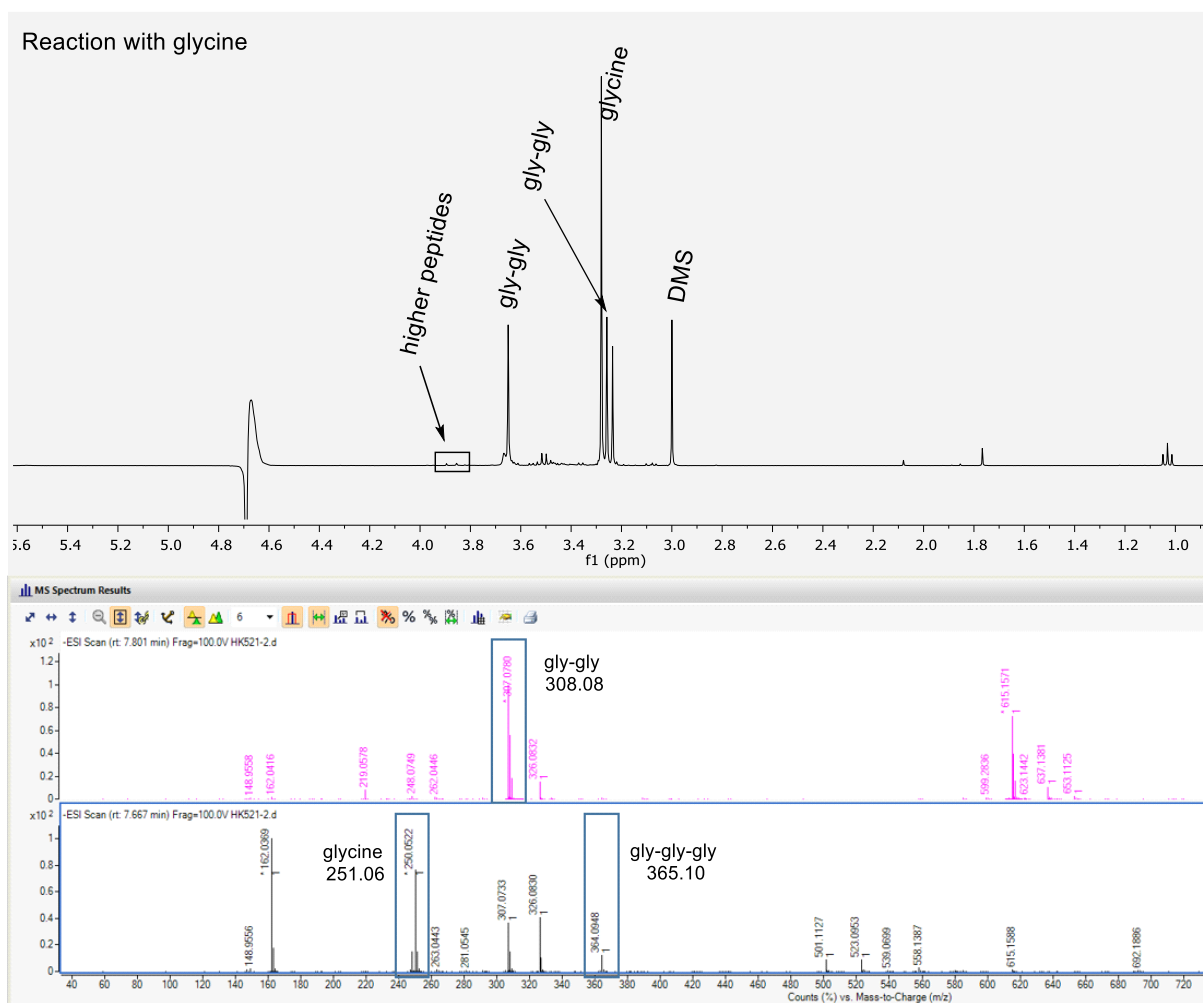


**Figure 39.** Reaction of glycine with DAP under H<sub>2</sub> (10 bar): <sup>1</sup>H NMR and ESI-QTOF-MS analysis. (for more information see supporting information). Mass shown here corresponds to OPA derivatized products.

Alanine also successfully formed ala-ala into 18% yield, confirmed also by UV analysis (Figure 40). We speculate the presence of higher peptides as well, which is difficult to say by NMR analysis and UV methods is also not yet optimised. As you can see around the time where the products came out, the baseline is not appropriate thus can generate false negative results if the product is presence in trace amounts.

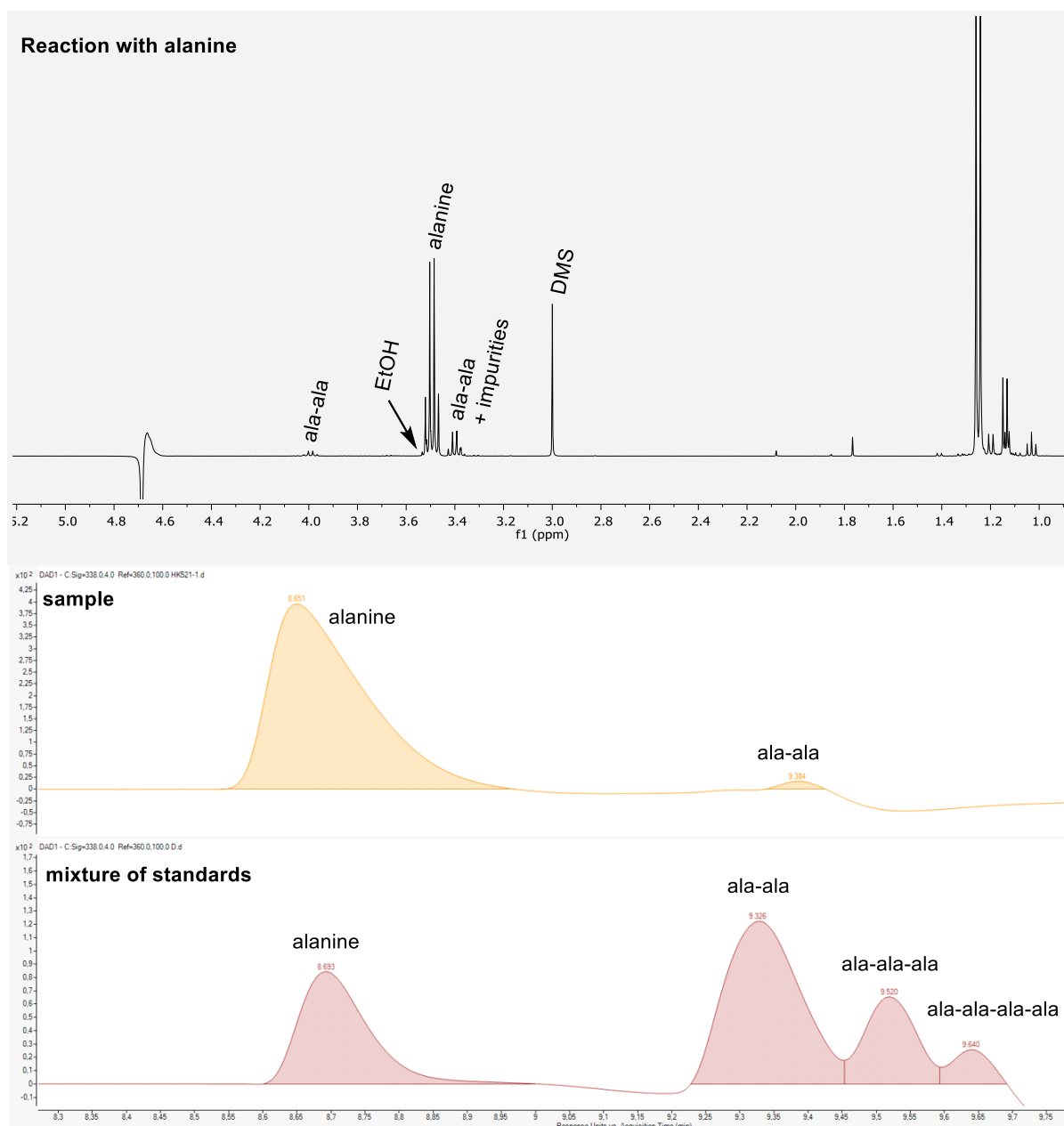


**Figure 40.** Reaction of alanine with DAP under  $\text{H}_2$  (10 bar).  $^1\text{H}$  NMR and ESI-QTOF-MS analysis. (see authentic sample of asp-asp in supporting information).

When aspartate and glutamate were placed under our reaction conditions, they also generated dipeptides and tripeptides. Aspartate yielded 13% of dipeptide asp-asp and trace amounts by tripeptide asp-asp-asp, confirmed by UV (Figure 41). The reaction of glutamate generated dipeptide glu-glu confirmed by UV analysis (Figure 42). Furthermore, glutamate was cyclised to pyroglutamate in 23% yields, which then further got aminated to glutamine producing 4% of yield.

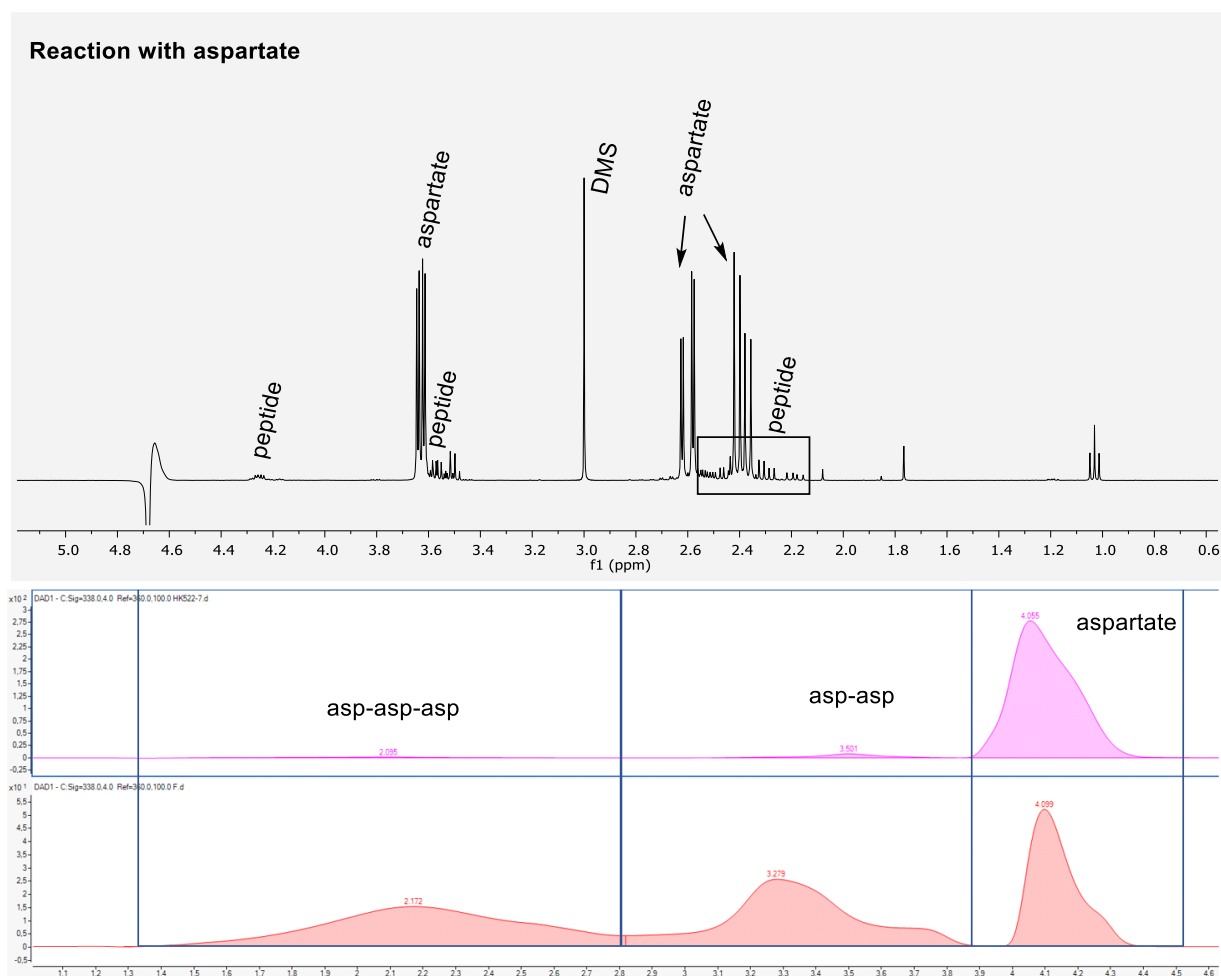


**Figure 41.** Reaction of aspartate with DAP under H<sub>2</sub> (10 bar). <sup>1</sup>HNMR and ESI-QTOF-MS analysis.

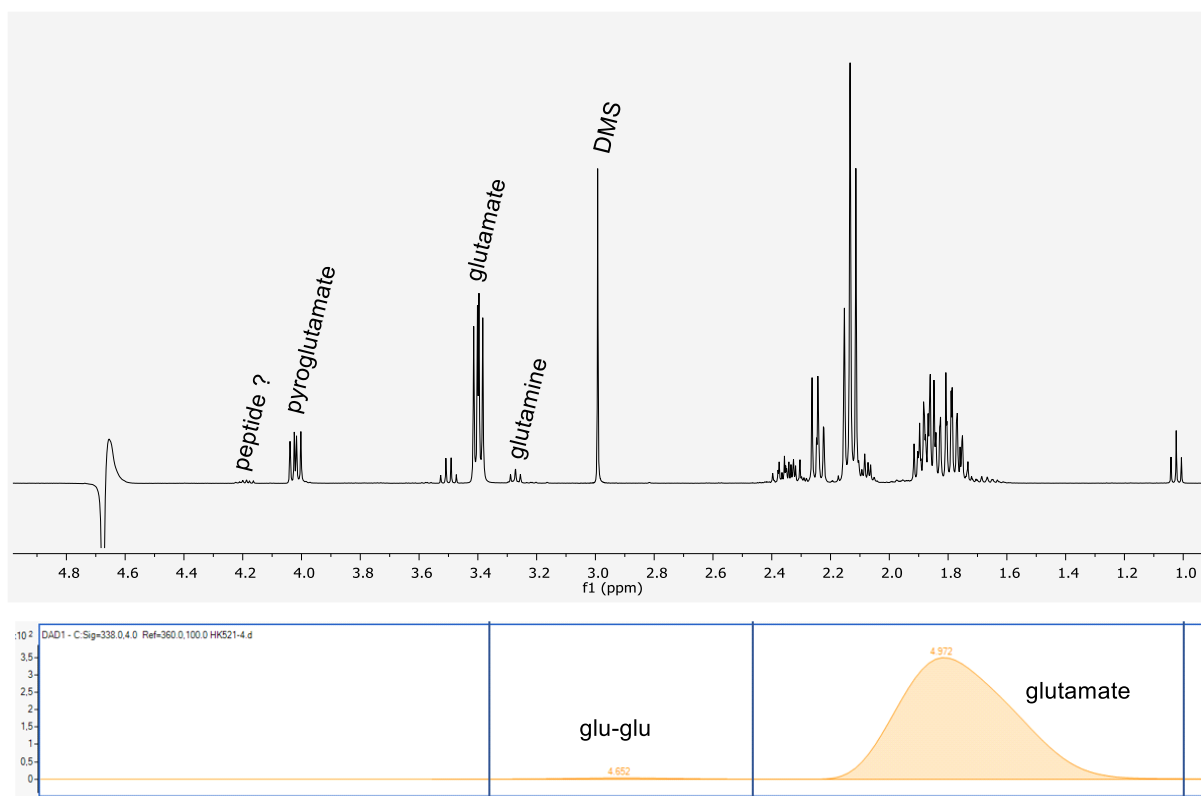


**Figure 42.** Reaction of glutamate with DAP under  $\text{H}_2$  (10 bar).  $^1\text{H}$  NMR and ESI-QTOF-MS analysis.

These are promising preliminary results, which needs to be further explored and optimised. Our findings shows that it is possible to achieve life like chemistry under early Earth conditions mimicking biological pathways when appropriate conditions are met.

## 12.4. Conclusions

From a prebiotic perspective, it is not only challenging but also worthwhile to investigate non-enzymatic oligomerization in water. Herein, preliminary results demonstrate that DAP, a plausible prebiotic reagent obtained from the reaction of inorganic phosphates and ammonia, serves as ammonia donor for the transition metal catalysed reductive amination employing  $\text{H}_2$  as a reductant in a plausible prebiotic environment. Additionally, DAP acts as a phosphorylating agent to enable the oligomerisation of amino acids under the same reaction conditions. Thus, in a single pot experiment, oligopeptides can be obtained from  $\alpha$ -keto acids in low to moderate yields. A further optimization of the reaction conditions is underway in order to increase oligopeptide chain length and yields.

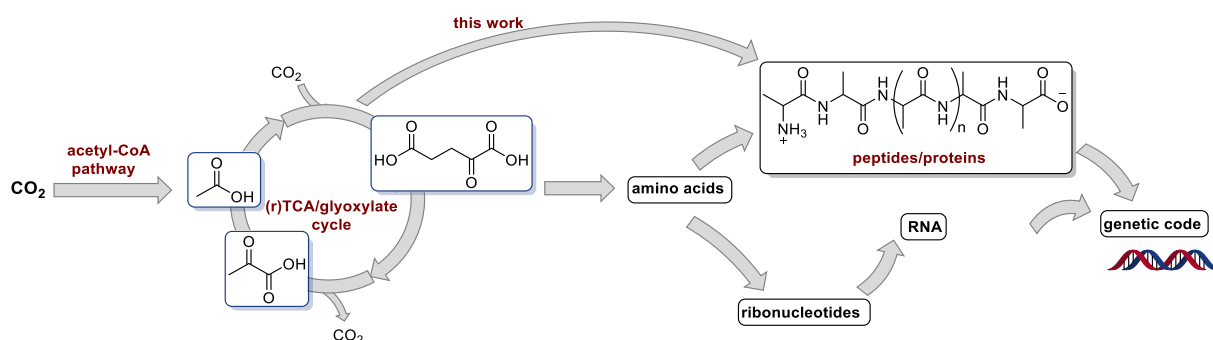


**Figure 43:** Map showing the path from  $\alpha$ -ketoacids to peptides.

## **Part III- Supporting Information**

## 13. Transaminations

### 13.1. Materials and methods

Sodium glyoxylate monohydrate ( $\geq 93\%$ ), glycine ( $\geq 99\%$ ), L-glutamic acid ( $\geq 99.5\%$ , BioUltra), L-alanine (BioUltra,  $\geq 99.5\%$ ), L-aspartic acid (BioUltra,  $\geq 99.5\%$ ), L-Serin (ReagentPlus®,  $\geq 99\%$ ),  $\alpha$ -ketoglutaric acid sodium salt ( $\geq 98\%$ ), sodium pyruvate (ReagentPlus®,  $\geq 99\%$ ), DL-glutamic acid monohydrate ( $\geq 98\%$ ), and DL-alanine ( $\geq 99\%$ ) were purchased from Sigma-Aldrich. The purity of sodium glyoxylate was determined before use by quantitative NMR spectroscopy (qNMR) using the methods outlined below to ensure correct concentrations. L-Glutamine ( $>99.0\%$ ) was purchased from TCI chemicals. D-Alanine (99%) and D-glutamic acid (99+%) were obtained from Alfa Aesar and Fmoc-Cl was obtained from Fluorochem.

The metal salts for the reaction screening were purchased from Sigma-Aldrich, Fluorochem, Merck Millipore, Fluka, Alfa Aesar or Strem chemicals and were generally of at least 95% purity.

The metal salts used for all mechanistic experiments were sodium metavanadate (Alfa Aesar, 96%), copper(II) chloride dihydrate (ACS reagent,  $\geq 99.0\%$ , Sigma-Aldrich), nickel(II) chloride hexahydrate (99.9% trace metals basis, Sigma-Aldrich) and cobalt(II) chloride hexahydrate (ACS reagent, 98%, Sigma-Aldrich).

Phosphate buffer (1 M) used as solvent was prepared from  $\text{KH}_2\text{PO}_4$  (ReagentPlus®, Sigma-Aldrich) and  $\text{KHPO}_4$  (ACS reagent,  $\geq 98\%$ , Sigma-Aldrich) following adjustment of the pH value by NaOH or HCl to pH = 7.00 as monitored by an AquaLytic AL10pH handheld pH meter calibrated before use.

Fully  $^{13}\text{C}$  labeled glyoxylic acid monohydrate (99%) was purchased from Cambridge Isotopes and 3- $^{13}\text{C}$ -pyruvate (sodium salt) from Sigma-Aldrich.

Chelex® 100 resin (50-100 mesh, sodium form) was obtained from Bio-Rad.

Water used for preparation of buffers or solutions was obtained from a Sartorius Arium purification system (18 M $\Omega$ cm).

### 13.2. Product analysis by NMR spectroscopy

NMR spectra were recorded on Bruker 400 or 500 MHz spectrometers equipped with Prodigy BBO cryoprobes at a sample temperature maintained at 23 °C. As solvent, a H<sub>2</sub>O:D<sub>2</sub>O mixture (11:1) was applied, using qNMR grade dimethyl sulfone (DMS, Sigma-Aldrich, TraceCERT) as internal standard (CH<sub>3</sub> group set to 3.00 ppm) or for some measurements sodium trimethylsilylpropanesulfonate (DSS, Sigma-Aldrich; Si(CH<sub>3</sub>)<sub>3</sub> group at 0.00 ppm).

Water suppression in <sup>1</sup>H NMR spectra was achieved using the Bruker *noesygprr1d* pulse program acquiring 8 scans for each sample. For quantitative NMR spectra (qNMR) the relaxation delay  $d_1$  was set to 20 s after having determined the  $T_1$  relaxation times of all relevant resonances with the inversion recovery method. Qualitative NMR spectra for some kinetic measurements were acquired in an analogous way using a relaxation delay of  $d_1 = 2$  s.

#### Adsorption Correction due to Chelex®

To quantify the adsorption of the analytes to the Chelex® resin used to remove metal ions, solutions of the amino acids (800 µL) in 1 M pH 7 phosphate buffer were added to Chelex® (400 ± 5 mg) and placed on a shaker for 10 or 60 minutes. Subsequently, 550 µL of the supernatant and 50 µL of a dimethyl sulfone (DMS) solution in D<sub>2</sub>O were added to a NMR tube and subjected to qNMR analysis.

We found that the amount of adsorbed analyte is independent of the incubation time. Moreover, within the investigated concentration range the relative amount of adsorbed analyte can be considered in good approximation as constant for most amino and keto acids. Tables S1-4 list the empirically determined correction factors  $f_x$  which described the ratio of the detected concentration, e.g. [Gly]<sub>NMR</sub> and the actual concentration of the analyte before treatment of the sample with the specific amount of Chelex®, e.g. [Gly]<sub>sample</sub>.



**Table S1.**  $^1\text{H}$  NMR integrals and concentrations for glycine (Gly) samples of different concentration after incubation over Chelex® (RM01-116).

Integral value						
Time over Chelex®	[Gly] <sub>sample</sub> (mM)	Gly (2 H)	DMS (6 H)	[DMS] <sub>stock</sub> (mM)	[Gly] <sub>NMR</sub> (mM)	$f_{\text{Gly}}$
10 min	46.89	6.2020	1.0000	20.88	35.32	0.753
60 min	46.89	6.2050	1.0000	20.88	35.33	0.754
10 min	15.63	2.0897	1.0000	20.88	11.90	0.761
60 min	15.63	2.0960	1.0000	20.88	11.94	0.764
10 min	4.69	0.6341	1.0000	20.88	3.61	0.770
60 min	4.69	0.6455	1.0000	20.88	3.68	0.784
<b>0.758 ± 0.012</b>						

**Table S2.**  $^1\text{H}$  NMR integrals and concentrations for  $\alpha$ -ketoglutarate ( $\alpha$ -KG) samples of different concentration after incubation over Chelex® (RM01-116).

Integral value						
Time over Chelex®	[ $\alpha$ -KG] <sub>sample</sub> (mM)	$\alpha$ -KG (2 H)	DMS (6 H)	[DMS] <sub>stock</sub> (mM)	[ $\alpha$ -KG] <sub>NMR</sub> (mM)	$f_{\alpha\text{-KG}}$
10 min	30.50	4.2460	1.0000	20.88	24.18	0.793
60 min	30.50	4.2280	1.0000	20.88	24.08	0.789
10 min	10.17	1.4348	1.0000	20.88	8.17	0.804
60 min	10.17	1.4247	1.0000	20.88	8.11	0.798
10 min	3.05	0.4274	1.0000	20.88	2.43	0.798
60 min	3.05	0.4373	1.0000	20.88	2.49	0.816
<b>0.796 ± 0.010</b>						

**Table S3.**  $^1\text{H}$  NMR integrals and concentrations for glutamic acid (Glu) samples of different concentration after incubation over Chelex® (RM01-116).

integral value						
Time over Chelex®	[Glu] <sub>sample</sub> (mM)	Glu (2 H)	DMS (6 H)	[DMS] <sub>stock</sub> (mM)	[Glu] <sub>NMR</sub> (mM)	$f_{\text{Glu}}$
10 min	23.92	3.276	1.0000	20.88	18.66	0.780
60 min	23.92	3.2910	1.0000	20.88	18.74	0.783
10 min	7.97	1.0991	1.0000	20.88	6.26	0.785
60 min	7.97	1.0893	1.0000	20.88	6.20	0.778
10 min	2.39	0.3347	1.0000	20.88	1.91	0.797
60 min	2.39	0.3354	1.0000	20.88	1.91	0.798
<b>0.781 ± 0.009</b>						

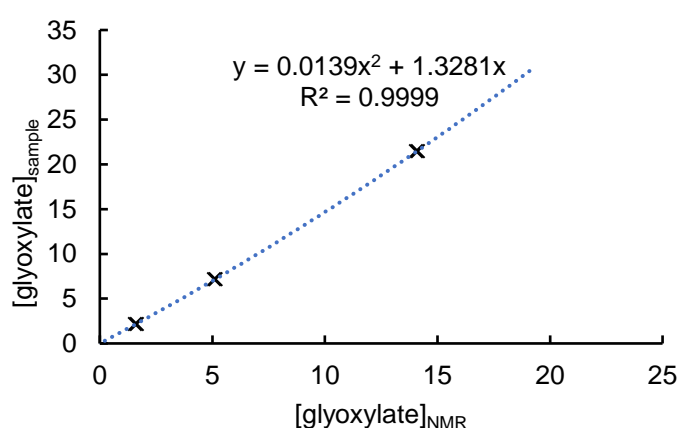
**Table S4.**  $^1\text{H}$  NMR integrals and concentrations for alanine (Ala) samples of different concentration after incubation over Chelex® (RM01-127).

Integral value						
	[Ala] <sub>sample</sub> (mM)	Ala (2 H)	DMS (6 H)	[DMS] <sub>stock</sub> (mM)	[Ala] <sub>NMR</sub> (mM)	$f_{\text{Ala}}$
10 min	45.0	9.1965	1.0000	19.76	33.04	0.734
10 min	30.0	6.1522	1.0000	19.76	22.10	0.737
10 min	15.0	3.0500	1.0000	19.76	10.96	0.731
<b>0.734 ± 0.003</b>						

**Table S5.**  $^1\text{H}$  NMR integrals and concentrations for glyoxylate (Glyox.) samples of different concentration after incubation over Chelex® (RM01-116).

Integral value						
Time over Chelex®	[Glyox.] <sub>sample</sub> (mM)	Glyox. (2 H)	DMS (6 H)	[DMS] <sub>stock</sub> (mM)	[Glyox.] <sub>NMR</sub> (mM)	$f_{\text{Glyox.}}$
10 min	21.47	1.234	1.0000	20.88	14.05	0.655
60 min	21.47	1.241	1.0000	20.88	14.13	0.658
10 min	7.16	0.4454	1.0000	20.88	5.07	0.709
60 min	7.16	0.4524	1.0000	20.88	5.15	0.720
10 min	2.15	0.1378	1.0000	20.88	1.57	0.731
60 min	2.15	0.1453	1.0000	20.88	1.65	0.771

For glyoxylate as analyte, the relative amounts of adsorbed substrate  $f_{\text{glyox.}}$  at different concentrations were found to be scattering more significant compared to the other analytes. Therefore, experimental data was corrected by the following polynomial relation:



### 13.3. Procedures and experimental data

#### 13.4. Reaction of glyoxylate (30 mM) and glutamic acid (1.5 equiv) in the presence of 20 mol% of different metals (pH = 7, 1 M phosphate buffer) – HK318, HK328

2 mL Eppendorf vials were charged with the metal salts (0.0060 mmol, 20 mol%; directly weighed), sodium glyoxylate monohydrate (0.0300 mmol) and L-glutamic acid (0.0450 mmol) from stock solutions in degassed phosphate buffer (pH 7, 1 M) in a total of 1 mL solvent (resulting concentrations: 30 mM in glyoxylate and 45 mM in glutamic acid). After purging the reaction mixture for 10 s with argon, the vials were sealed and placed for 24 h on a shaker maintained at 23 °C. 800  $\mu$ L of the reaction mixture were withdrawn onto an Eppendorf tube charged with 400  $\pm$  10 mg Chelex® and shaken thoroughly for 15-30 minutes to remove any metal salts. 550  $\mu$ L of the clear supernatant and 50  $\mu$ L of a solution of dimethyl sulfone in D<sub>2</sub>O of known concentration were transferred into an NMR tube for qNMR analysis.

Concentrations of glycine (Gly),  $\alpha$ -ketoglutarate ( $\alpha$ -KG) and glutamate (Glu) were determined based on the integral ratios relative to the resonance of the methyl protons of dimethyl sulfone (DMS) ("Concentration in NMR sample"). Two representative NMR spectra are depicted in Figures S1 and S2.

Finally, the concentrations of the specific analytes in the NMR samples were corrected for adsorption of the analytes to the Chelex® resin with the correction factors  $f_{\text{analyte}}$  determined as described above ("Concentration corrected for adsorption at Chelex®"). Concentrations of analytes determined in this way are estimated to have an error of less than 10%.

Experiments using Cu<sup>2+</sup>, Ni<sup>2+</sup>, Co<sup>2+</sup>, Fe<sup>3+</sup>, and V<sup>5+</sup> as catalysts as well as the controls were repeated multiple times independently and the error is reported as the standard deviation.

**Table S6.** <sup>1</sup>H NMR integrals and concentrations for the reactions of glyoxylate with glutamic acid in the presence of different metal salts.

Experiment	Salt	Integral (relative to dimethyl sulfone/DMS which was set to 1.0000)			DMS stock (mM)	Concentration in NMR sample (mM)			Concentration corrected for adsorption at Chelex® (mM)			Yield (%)
		Gly	a-KG	Glu		Gly	a-KG	Glu	Gly	a-KG	Glu	
		(2 H)	(2 H)	(2 H)								
HK318-1	AlCl <sub>3</sub>	0.3325	0.2870	5.7026	20.86	1.89	1.63	32.44	2.50	2.05	41.54	8.32
HK318-2	KAl(SO <sub>4</sub> ) <sub>2</sub> · 12 H <sub>2</sub> O	0.2674	0.2491	5.7745	20.86	1.52	1.42	32.85	2.01	1.78	42.06	6.69
HK318-3	ZnCl <sub>2</sub>	0.2859	0.2959	5.6729	20.86	1.63	1.68	32.27	2.15	2.11	41.32	7.15
HK318-4	FeCl <sub>3</sub> · 6 H <sub>2</sub> O	0.9894	1.1973	5.4232	19.76	5.33	6.45	29.23	7.03	8.11	37.42	23.45
HK328-A	FeCl <sub>3</sub> · 6 H <sub>2</sub> O	1.1260	1.3219	4.9048	20.39	6.26	7.35	27.28	8.26	9.23	34.92	27.54
average	FeCl <sub>3</sub> · 6 H <sub>2</sub> O											25.5 ± 2.9
HK318-5	PdCl <sub>2</sub>	0.2302	0.3616	5.2228	20.86	1.31	2.06	29.71	1.73	2.58	38.04	5.76
HK318-6	CaCl <sub>2</sub>	0.0135	0.0065	6.6444	19.76	0.07	0.04	35.81	0.10	0.04	45.85	0.32
HK318-7A	CoCl <sub>2</sub>	2.1242	1.6621	5.0532	20.86	12.08	9.46	28.75	15.94	11.88	36.81	53.14
HK328-CA	CoCl <sub>2</sub>	2.5874	1.9407	3.7778	20.39	14.39	10.79	21.01	18.98	13.56	26.90	63.27
HK328-CB	CoCl <sub>2</sub>	2.7148	2.0181	3.5936	20.39	15.10	11.22	19.98	19.92	14.10	25.59	66.39
average	CoCl <sub>2</sub>											60.9 ± 6.9
HK318-8	CrCl <sub>2</sub>	0.0260	0.0188	6.2868	20.86	0.15	0.11	35.77	0.20	0.13	45.80	0.65
HK318-9	FeCl <sub>2</sub> · 4 H <sub>2</sub> O	0.8091	0.9906	5.1231	20.86	4.60	5.64	29.15	6.07	7.08	37.32	20.24
HK318-10	HgCl <sub>2</sub>	0.2232	0.4879	5.3880	20.86	1.27	2.78	30.65	1.68	3.49	39.25	5.58
HK318-11	WCl <sub>6</sub>	0.0207	0.0136	5.8990	20.86	0.12	0.08	33.56	0.16	0.10	42.97	0.52
HK318-12	MoCl <sub>3</sub>	0.0141	0.0082	5.9247	20.86	0.08	0.05	33.71	0.11	0.06	43.16	0.35
HK318-13	CeCl <sub>3</sub> · 7 H <sub>2</sub> O	0.0132	0.0080	5.9731	20.86	0.08	0.05	33.98	0.10	0.06	43.51	0.33

HK318-14	MnCl <sub>2</sub> · 4 H <sub>2</sub> O	0.0137	0.0160	6.8523	20.86	0.08	0.09	38.98	0.10	0.11	49.91	0.34
HK318-16	NiCl <sub>2</sub> · 6 H <sub>2</sub> O	3.5698	3.0593	2.4049	20.86	20.31	17.40	13.68	26.79	21.87	17.52	89.31
HK318-16A	NiCl <sub>2</sub> · 6 H <sub>2</sub> O	3.6664	3.1196	2.4574	20.86	20.86	17.75	13.98	27.52	22.30	17.90	91.73
HK318-16B	NiCl <sub>2</sub> · 6 H <sub>2</sub> O	3.6158	3.0740	2.4777	20.86	20.57	17.49	14.10	27.14	21.97	18.05	90.46
average	NiCl <sub>2</sub> · 6 H <sub>2</sub> O											90.5 ± 1.2
HK318-17	CuCl <sub>2</sub> · 2 H <sub>2</sub> O	3.6918	3.5714	2.6360	19.76	19.90	19.25	14.21	26.25	24.18	18.19	87.49
HK318-17A	CuCl <sub>2</sub> · 2 H <sub>2</sub> O	3.5908	3.6124	2.5915	19.76	19.35	19.47	13.97	25.53	24.46	17.88	85.10
HK328-BA	CuCl <sub>2</sub> · 2 H <sub>2</sub> O	3.5606	3.4043	2.4398	20.39	19.80	18.93	13.57	26.12	23.78	17.37	87.07
average	CuCl <sub>2</sub> · 2 H <sub>2</sub> O											86.6 ± 1.3
HK318-18	NaVO <sub>3</sub>	1.7832	1.9333	4.5678	19.76	9.61	10.42	24.62	12.68	13.09	31.52	42.26
HK318-18A	NaVO <sub>3</sub>	2.0962	2.2854	3.5987	20.86	11.93	13.00	20.47	15.73	16.33	26.21	52.44
HK318-18A	NaVO <sub>3</sub>	2.1492	2.3580	3.9496	19.76	11.58	12.71	21.28	15.28	15.96	27.25	50.93
HK318-18B	NaVO <sub>3</sub>	2.0297	2.2287	3.4696	20.86	11.55	12.68	19.74	15.23	15.93	25.27	50.78
HK318-18B	NaVO <sub>3</sub>	2.0400	2.2301	4.1340	19.76	10.99	12.02	22.28	14.50	15.10	28.53	48.35
average	NaVO <sub>3</sub>											49.0 ± 4.0
HK318-19	VOSO <sub>4</sub>	0.0491	0.0484	6.2383	20.86	0.28	0.28	35.49	0.37	0.35	45.44	1.23
HK318-20	CrCl <sub>3</sub> · 6 H <sub>2</sub> O	0.0112	0.0097	6.1083	20.86	0.06	0.06	34.75	0.08	0.07	44.50	0.28
HK318-21	MgCl <sub>2</sub>	0.0188	0.0140	5.8802	20.86	0.11	0.08	33.45	0.14	0.10	42.83	0.47
HK318-22	none	0.0153	0.0094	5.9987	20.86	0.09	0.05	34.13	0.11	0.07	43.70	0.38
HK318-22A	none	0.0145	0.0074	5.8627	20.86	0.08	0.04	33.35	0.11	0.05	42.71	0.36
HK318-22B	none	0.0142	0.0090	5.9883	20.86	0.08	0.05	34.07	0.11	0.06	43.62	0.36
average	none											0.37 ± 0.01

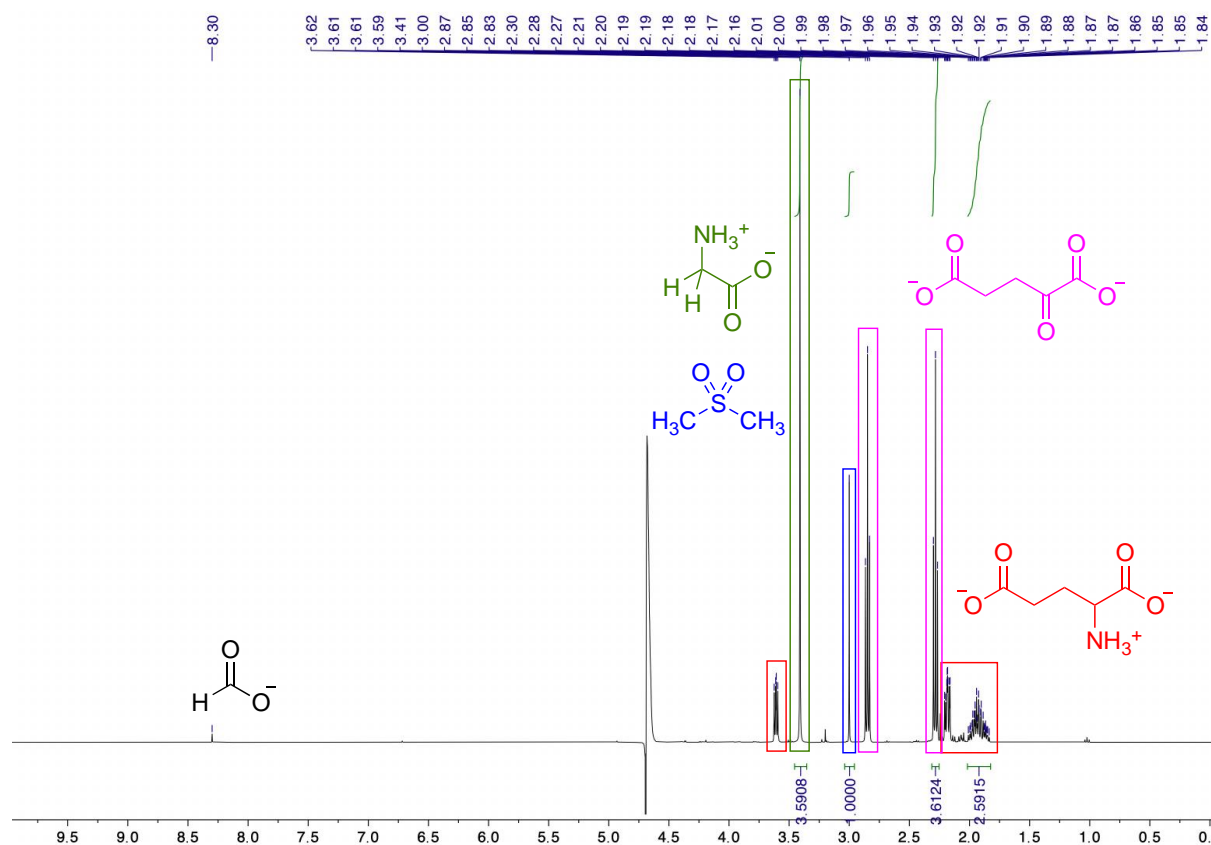


**Figure S1.**  $^1\text{H}$  NMR (noesygppr1d, 400 MHz, ns = 8, d<sub>1</sub> = 20 s) of the reaction HK318-17A indicating the different species and integrals used for quantification.

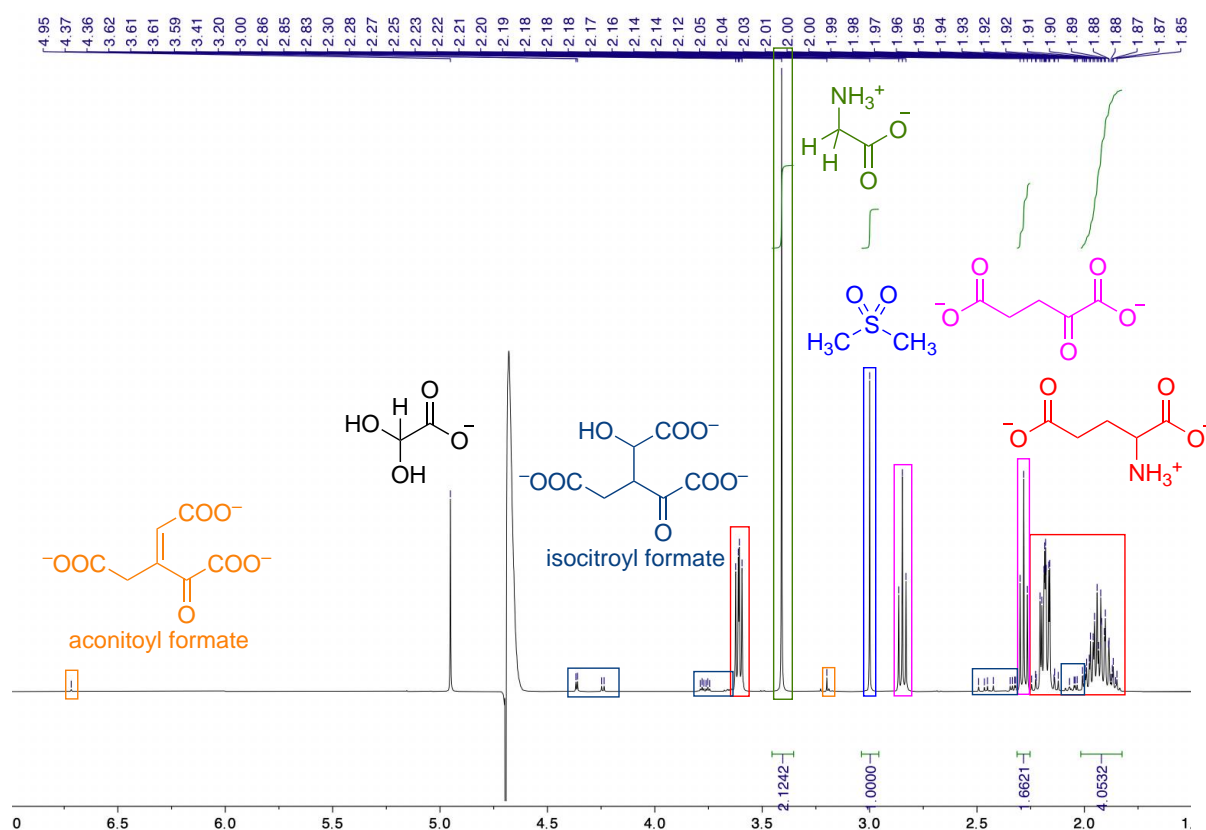


**Figure S2.** <sup>1</sup>H NMR (noesygppr1d, 400 MHz, ns = 8, d1 = 20 s) of the reaction HK318-7A indicating the different species and integrals used for quantification.

In some of the reactions that showed a slower rate of transamination, isocitroyl formate formed as side product due to the aldol reaction of α-ketoglutarate with glyoxylate. Additionally, traces of the corresponding dehydration product – aconitoyl formate – were detected based on the singlets at 3.20 and 6.72 ppm (assignment based on the NMR data reported in reference 144).

### **13.5. Transamination reaction of pyruvate (30 mM) with glutamic acid (45 mM) at 23 °C and 50 °C (1 M phosphate buffer, pH = 7, 24 h)**

2 mL Eppendorf vials were charged with the metal salts (20/50/100 mol%; directly weighed), sodium pyruvate (0.0300 mmol) and glutamic acid (0.0450 mmol) from stock solutions in degassed phosphate buffer (pH 7, 1 M, total volume: 1 mL). After purging the reaction mixture for 10 s with argon, the vials were sealed and placed for 24 h or 72 h on a shaker maintained at 23 or 50 °C (temperature inside the vial). 800  $\mu$ L of the reaction mixture were withdrawn onto an Eppendorf tube charged with 400  $\pm$  10 mg Chelex® and shaken thoroughly for 15-30 minutes to remove any metal salts. 550  $\mu$ L of the clear supernatant and 50  $\mu$ L of a solution of dimethyl sulfone in D<sub>2</sub>O of known concentration were transferred into an NMR tube for qNMR analysis.

Concentrations of alanine (Ala),  $\alpha$ -ketoglutarate ( $\alpha$ -KG) and glutamate (Glu) were determined based on the integral ratios relative to the resonance of dimethyl sulfone (DMS) ("Concentration in NMR sample"). Due to overlap of the two resonances of alanine with other resonances, the right half of the doublet assigned to the CH<sub>3</sub> group was integrated as illustrates in Figure S3. Additionally, due to overlap of one of the resonances of the symmetric AB system (3.18 – 3.00 ppm) of the central CH<sub>2</sub> group of the pyruvate dimer present in small amounts in the reaction mixture with the singlet of dimethyl sulfone, the integral value of the resonance at 3.18 ppm was subtracted from the one of dimethyl sulfone.

Finally, the concentrations of the NMR samples were correct for adsorption of the analytes to the Chelex® resin with the correction factors determined as described above ("Concentration corrected for adsorption at Chelex®").



**Table S7.**  $^1\text{H}$  NMR integrals and concentrations for the reactions of pyruvate with glutamic acid in the presence of different metal salts.

Experiment	Salt	Mol%	Tempera- ture (°C)	Integrals				DMS stock (mM)	Concentration in NMR sample (mM)			Concentration corrected for adsorption at Chelex® (mM)			Yield (%)
				Ala	α-KG	Glu	DMS		Ala	α-KG	Glu	Ala	α-KG	Glu	
				(1.5 H)	(2 H)	(2 H)	(6 H)								
Time = 24 h															
HK317-1	CoCl <sub>2</sub>	20	23	0.0000	0.0000	5.2750	1.0000	20.86	0.00	0.00	30.01	0.00	0.00	38.43	0.00
HK317-13	CoCl <sub>2</sub>	20	50	0.0000	0.0000	6.6598	1.0000	20.86	0.00	0.00	37.89	0.00	0.00	48.51	0.00
HK317-2	CoCl <sub>2</sub>	50	23	0.0000	0.0000	5.3501	1.0000	20.86	0.00	0.00	30.44	0.00	0.00	38.97	0.00
HK317-14	CoCl <sub>2</sub>	50	50	0.0109	0.0040	5.7620	1.0000	20.86	0.08	0.02	32.78	0.11	0.03	41.97	0.38
HK317-3	CoCl <sub>2</sub>	100	23	0.0000	0.0000	5.4380	1.0000	20.86	0.00	0.00	30.94	0.00	0.00	39.61	0.00
HK317-15	CoCl <sub>2</sub>	100	50	0.0215	0.0010	5.9287	1.0000	20.86	0.16	0.01	33.73	0.22	0.01	43.19	0.74
HK317-4	NiCl <sub>2</sub> · 6 H <sub>2</sub> O	20	23	0.0000	0.0000	5.4939	1.0000	20.86	0.00	0.00	31.26	0.00	0.00	40.02	0.00
HK317-16	NiCl <sub>2</sub> · 6 H <sub>2</sub> O	20	50	0.0808	0.0789	5.6791	1.0000	20.86	0.61	0.45	32.31	0.84	0.56	41.37	2.78
HK317-5	NiCl <sub>2</sub> · 6 H <sub>2</sub> O	50	23	0.0081	0.0035	5.4538	1.0000	20.86	0.06	0.02	31.03	0.08	0.03	39.73	0.28
HK317-17	NiCl <sub>2</sub> · 6 H <sub>2</sub> O	50	50	0.1178	0.1233	5.5728	1.0000	20.86	0.89	0.70	31.70	1.22	0.88	40.59	4.06
HK317-6	NiCl <sub>2</sub> · 6 H <sub>2</sub> O	100	23	0.0206	0.0105	5.1787	1.0000	20.86	0.16	0.06	29.46	0.21	0.08	37.72	0.71
HK317-18	NiCl <sub>2</sub> · 6 H <sub>2</sub> O	100	50	0.1378	0.1427	5.3986	1.0000	20.86	1.05	0.81	30.71	1.42	1.02	39.33	4.75
HK317-7	CuCl <sub>2</sub> · 2 H <sub>2</sub> O	20	23	0.0569	0.0561	6.4662	1.0000	20.86	0.43	0.32	36.79	0.59	0.40	47.10	1.96
HK317-19	CuCl <sub>2</sub> · 2 H <sub>2</sub> O	20	50	0.7984	1.0778	4.6416	1.0000	20.86	6.06	6.13	26.41	8.25	7.70	33.81	27.50
HK317-8	CuCl <sub>2</sub> · 2 H <sub>2</sub> O	50	23	0.1429	0.1875	4.9670	1.0000	20.86	1.08	1.07	28.26	1.48	1.34	36.18	4.92
HK317-20	CuCl <sub>2</sub> · 2 H <sub>2</sub> O	50	50	0.7375	1.0093	2.0453	1.0000	20.86	5.59	5.74	11.64	7.62	7.21	14.90	25.41
HK317-9	CuCl <sub>2</sub> · 2 H <sub>2</sub> O	100	23	0.2732	0.3983	4.8599	1.0000	20.86	2.07	2.27	27.65	2.82	2.85	35.40	9.41

HK317-21	CuCl <sub>2</sub> · 2 H <sub>2</sub> O	100	50	1.4376	2.1238	3.3319	1.0000	20.86	10.90	12.08	18.96	14.86	15.18	24.27	49.52
HK317-10	NaVO <sub>3</sub>	20	23	0.0249	0.0186	5.2684	1.0000	20.86	0.19	0.11	29.97	0.26	0.13	38.38	0.86
HK317-22	NaVO <sub>3</sub>	20	50	0.2481	0.3012	5.5399	1.0000	20.86	1.88	1.71	31.52	2.56	2.15	40.35	8.55
HK317-11	NaVO <sub>3</sub>	50	23	0.0389	0.0325	5.4352	1.0000	20.86	0.30	0.18	30.92	0.40	0.23	39.59	1.34
HK317-23	NaVO <sub>3</sub>	50	50	0.4813	0.6274	5.6940	1.0000	20.86	3.65	3.57	32.39	4.97	4.48	41.48	16.58
HK317-12	NaVO <sub>3</sub>	100	23	0.0557	0.0598	5.5169	1.0000	20.86	0.42	0.34	31.39	0.58	0.43	40.19	1.92
HK317-24	NaVO <sub>3</sub>	100	50	0.6350	0.8180	5.0926	1.0000	20.86	4.82	4.65	28.97	6.56	5.85	37.10	21.87
ControlA	none	0	23	0.0000	0.0000	5.5420	1.0000	20.86	0.00	0.00	31.53	0.00	0.00	40.37	0.00
ControlB	none	0	50	0.0000	0.0000	5.9831	1.0000	20.86	0.00	0.00	34.04	0.00	0.00	43.58	0.00
Time = 72 h															
HK319-1	CoCl <sub>2</sub>	20	23	0.0000	0.0082	5.8545	0.9663	20.86	0.00	0.05	33.31	0.00	0.06	42.65	0.00
HK319-13	CoCl <sub>2</sub>	20	50	0.0136	0.0000	6.2824	0.9711	20.86	0.11	0.00	35.74	0.14	0.00	45.76	0.48
HK319-2	CoCl <sub>2</sub>	50	23	0.0000	0.0000	5.5921	0.9351	20.86	0.00	0.00	31.81	0.00	0.00	40.73	0.00
HK319-14	CoCl <sub>2</sub>	50	50	0.0570	0.0173	6.1054	0.9643	20.86	0.45	0.10	34.73	0.61	0.12	44.47	2.04
HK319-3	CoCl <sub>2</sub>	100	23	0.0000	0.0094	6.0189	0.9450	20.86	0.00	0.05	34.24	0.00	0.07	43.84	0.00
HK319-15	CoCl <sub>2</sub>	100	50	0.0244	0.0634	6.2073	0.9566	20.86	0.19	0.36	35.31	0.26	0.45	45.22	0.88
HK319-4	NiCl <sub>2</sub> · 6 H <sub>2</sub> O	20	23	0.0128	0.0501	6.2625	0.9729	20.86	0.10	0.29	35.63	0.14	0.36	45.62	0.45
HK328-16	NiCl <sub>2</sub> · 6 H <sub>2</sub> O	20	50	0.2208	0.2402	6.3288	0.9566	20.39	1.71	1.34	35.19	2.33	1.68	45.06	7.77
HK319-5	NiCl <sub>2</sub> · 6 H <sub>2</sub> O	50	23	0.0201	0.0444	5.5648	0.9377	20.86	0.16	0.25	31.66	0.22	0.32	40.54	0.74
HK328-16A	NiCl <sub>2</sub> · 6 H <sub>2</sub> O	50	50	0.3214	0.3757	6.0833	0.9631	20.39	2.47	2.09	33.83	3.37	2.62	43.31	11.24
HK319-6	NiCl <sub>2</sub> · 6 H <sub>2</sub> O	100	23	0.0467	0.0256	5.4989	0.8994	20.86	0.39	0.15	31.28	0.54	0.18	40.06	1.79
HK328-16B	NiCl <sub>2</sub> · 6 H <sub>2</sub> O	100	50	0.4145	0.5111	6.0468	0.9692	20.39	3.17	2.84	33.63	4.32	3.57	43.05	14.40
HK319-17	CuCl <sub>2</sub> · 2 H <sub>2</sub> O	20	23	0.1873	0.2021	5.6723	0.9780	20.86	1.45	1.15	32.27	1.98	1.44	41.32	6.60
HK319-19	CuCl <sub>2</sub> · 2 H <sub>2</sub> O	20	50	1.3616	1.7384	4.2899	0.9789	20.86	10.55	9.89	24.41	14.37	12.42	31.25	47.92

HK319-8	$\text{CuCl}_2 \cdot 2 \text{H}_2\text{O}$	50	23	0.5043	0.6521	4.7549	0.9208	20.86	4.15	3.71	27.05	5.66	4.66	34.64	18.87
HK319-20	$\text{CuCl}_2 \cdot 2 \text{H}_2\text{O}$	50	50	1.9074	2.5175	3.8852	0.9875	20.86	14.65	14.32	22.10	19.96	17.99	28.30	66.54
HK319-9	$\text{CuCl}_2 \cdot 2 \text{H}_2\text{O}$	100	23	0.5743	0.7937	4.4167	0.9239	20.86	4.72	4.52	25.13	6.42	5.67	32.17	21.41
HK319-21	$\text{CuCl}_2 \cdot 2 \text{H}_2\text{O}$	100	50	1.5832	2.2021	3.4498	0.9893	20.86	12.14	12.53	19.63	16.54	15.74	25.13	55.13
HK319-10	$\text{NaVO}_3$	20	23	0.085	0.0654	7.3876	0.9819	20.86	0.66	0.37	42.03	0.89	0.47	53.81	2.98
HK319-22	$\text{NaVO}_3$	20	50	0.439	0.5737	5.2914	0.9842	20.86	3.38	3.26	30.10	4.61	4.10	38.54	15.37
HK319-11	$\text{NaVO}_3$	50	23	0.1154	0.1202	6.205	0.9574	20.86	0.91	0.68	35.30	1.25	0.86	45.20	4.15
HK319-23	$\text{NaVO}_3$	50	50	0.8609	1.1138	4.8277	0.9804	20.86	6.66	6.34	27.47	9.07	7.96	35.17	30.25
HK319-12	$\text{NaVO}_3$	100	23	0.1331	0.1526	5.5111	0.9407	20.86	1.07	0.87	31.35	1.46	1.09	40.14	4.87
HK319-24	$\text{NaVO}_3$	100	50	1.0986	1.3971	4.3938	0.9818	20.86	8.49	7.95	25.00	11.56	9.99	32.01	38.55

---

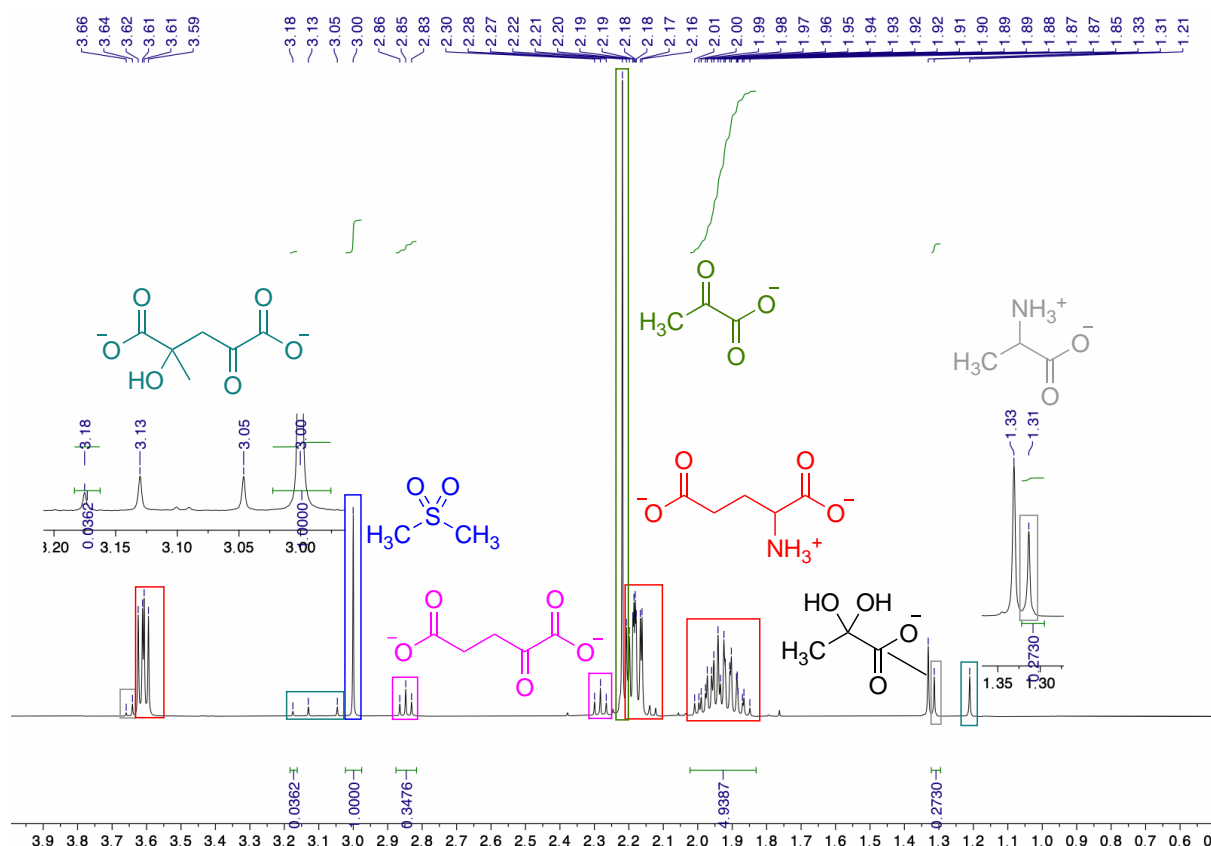


**Figure S3.**  $^1\text{H}$  NMR (noesygppr1d, 400 MHz, ns = 8, d<sub>1</sub> = 20 s) of the reaction HK319-17 indicating the different species and integrals used for quantification. Due to overlap of one of the resonances of the symmetric AB system (3.18 – 3.00 ppm) of the central CH<sub>2</sub> group of the pyruvate dimer with the singlet of dimethyl sulfone, the integral value of the resonance at 3.18 ppm is subtracted from the one of dimethyl sulfone.

### 13.6. Transamination reaction of different ketoacids (30 mM) with amino acids (45 mM) at 50 °C catalyzed by 20 mol% Cu<sup>2+</sup> (1 M phosphate buffer, pH = 7, 24 h)

2 mL Eppendorf vials were charged with CuCl<sub>2</sub> · 2 H<sub>2</sub>O (0.0060 mmol; directly weighed), the respective keto acid (0.0300 mmol) and the amino acid (0.0450 mmol) from stock solutions in 1 mL degassed phosphate buffer (pH 7, 1 M, total volume: 1 mL). After purging the reaction mixture for 10 s with argon, the vials were sealed and placed for 72 h on a shaker maintained at 50 °C (temperature measured inside the vial). 800 µL of the reaction mixture were withdrawn onto an Eppendorf tube charged with 400 ± 10 mg Chelex® and shaken thoroughly for 15-30 minutes to remove any metal salts. 550 µL of the clear supernatant and 50 µL of a solution of dimethyl sulfone in D<sub>2</sub>O of known concentration were transferred into an NMR tube for qNMR analysis.

Concentrations of the formed amino acids (glycine, alanine or glutamic acid) were determined based on the integral ratios relative to the resonance of dimethyl sulfone as depicted in the NMR spectra below ("Concentration in NMR sample"). Finally, the concentrations of the amino acids in the NMR samples were correct for adsorption of the analytes to the Chelex® resin with the correction factors determined as described above.

All NMR spectra of the individual reaction mixtures (with the respective reaction numbers) are depicted below with an assignment of the main species. The assignments were based on comparison with authentic samples or in the case of  $\alpha$ -ketoglutaramic acid with the in-situ synthesized  $\alpha$ -ketoglutaramic acid (see the NMR spectrum and experimental description below).

**Table S8.**  $^1\text{H}$  NMR integrals and concentrations for the reactions of glyoxylate with different amino acids in the presence of 20 mol%  $\text{CuCl}_2 \cdot 2\text{H}_2\text{O}$ .

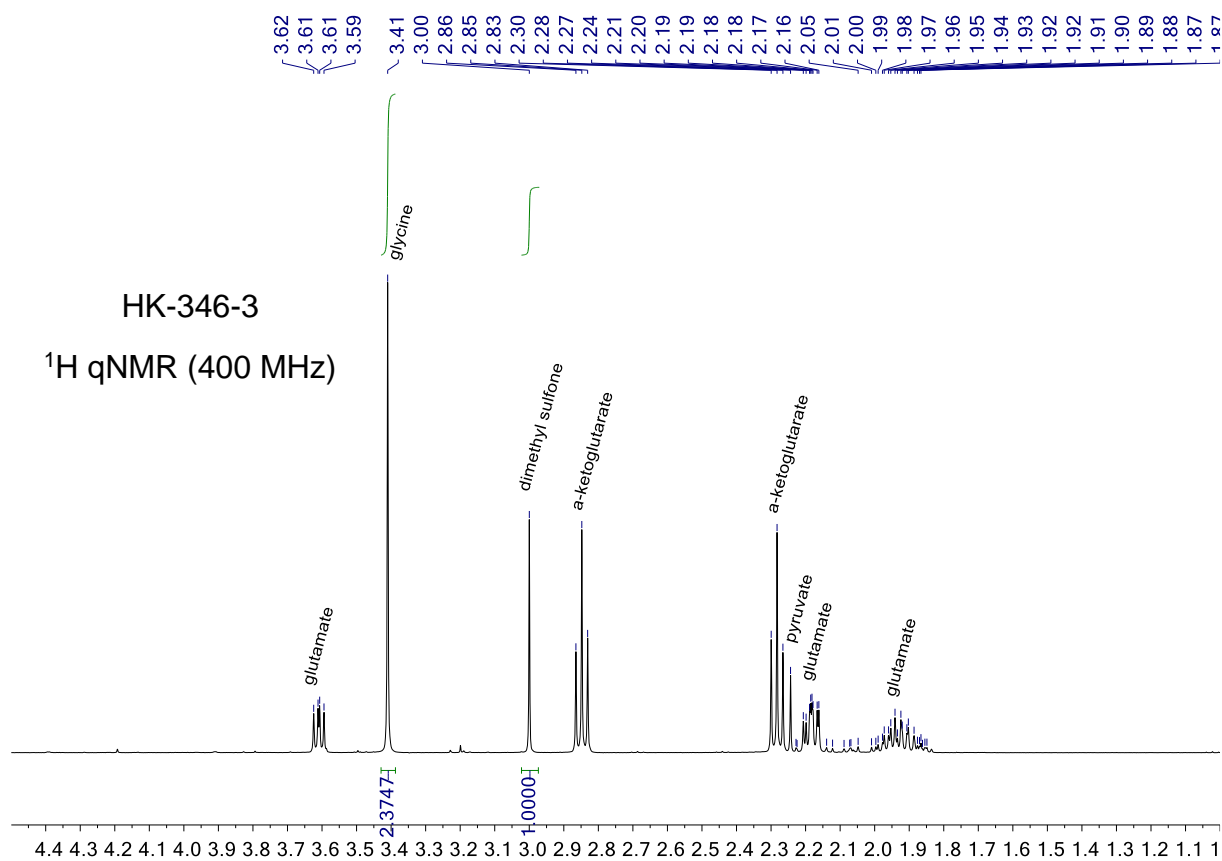
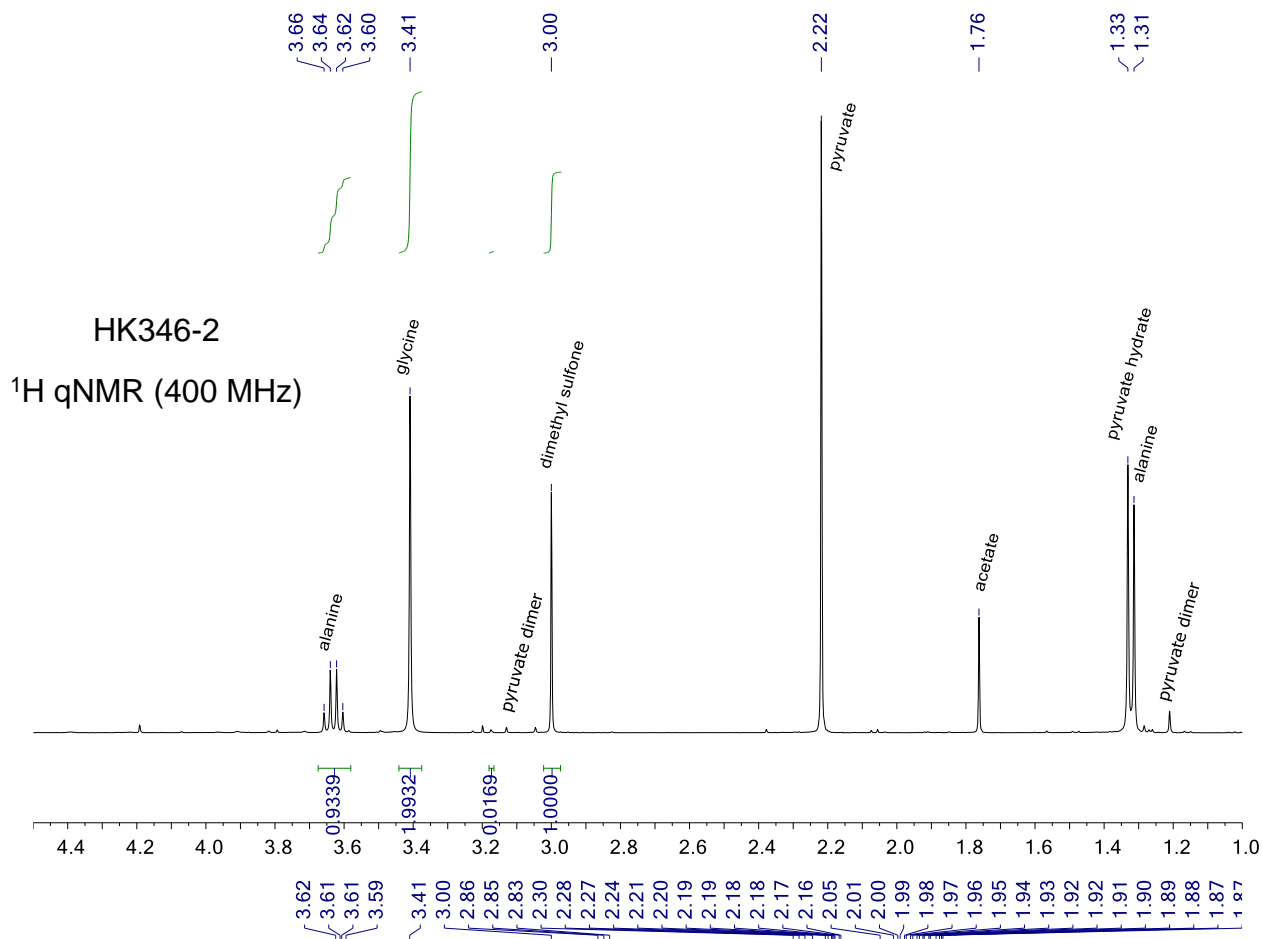
Experiment	Keto Acid	Amino Acid	Integrals			DMS stock (mM)	Concentration in NMR sample (mM)		Concentration corrected for adsorption at Chelex® (mM)	
			Gly	a-KG	DMS		Gly	Ala	Gly	Ala
			(2 H)	(2 H)	(6 H)				( $f_{\text{gly}} = 0.758$ )	( $f_{\text{ala}} = 0.734$ )
HK-346-2	Glyoxylate	L-Alanine	1.9932	0.9339	0.9831	30.66	16.67	15.62	21.99	21.28
HK-346-3	Glyoxylate	L-Glutamic acid	2.3747		1.0000	30.66	19.86		26.20	
HK-346-4	Glyoxylate	L-Glutamine	2.2417		1.0000	30.66	18.74		24.73	
HK-346-5	Glyoxylate	L-Aspartic acid	1.7814	0.6666	1.0000	30.66	14.90	11.15	19.65	15.19
HK-346-6	Glyoxylate	L-Serine	0.8377		1.0000	30.66	7.00		9.24	

**Table S9.**  $^1\text{H}$  NMR integrals and concentrations for the reactions of pyruvate with different amino acids in the presence of 20 mol%  $\text{CuCl}_2 \cdot 2\text{H}_2\text{O}$ .

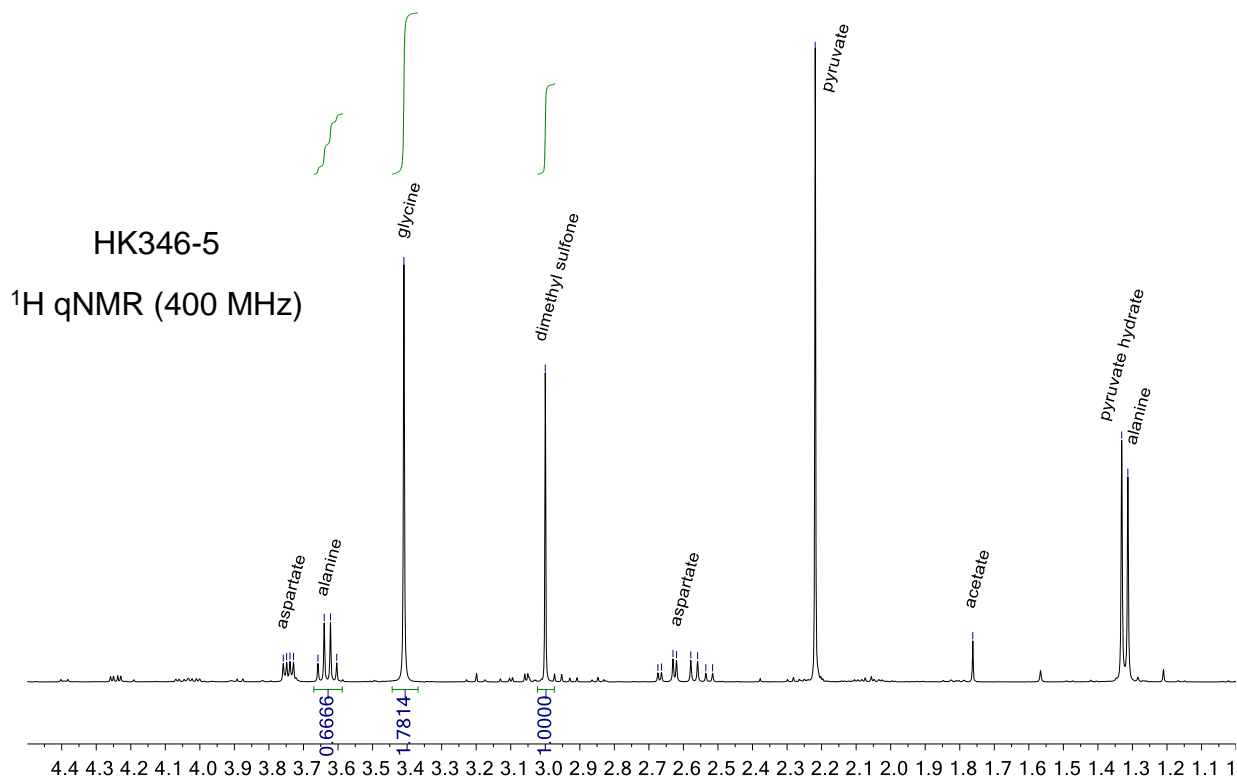
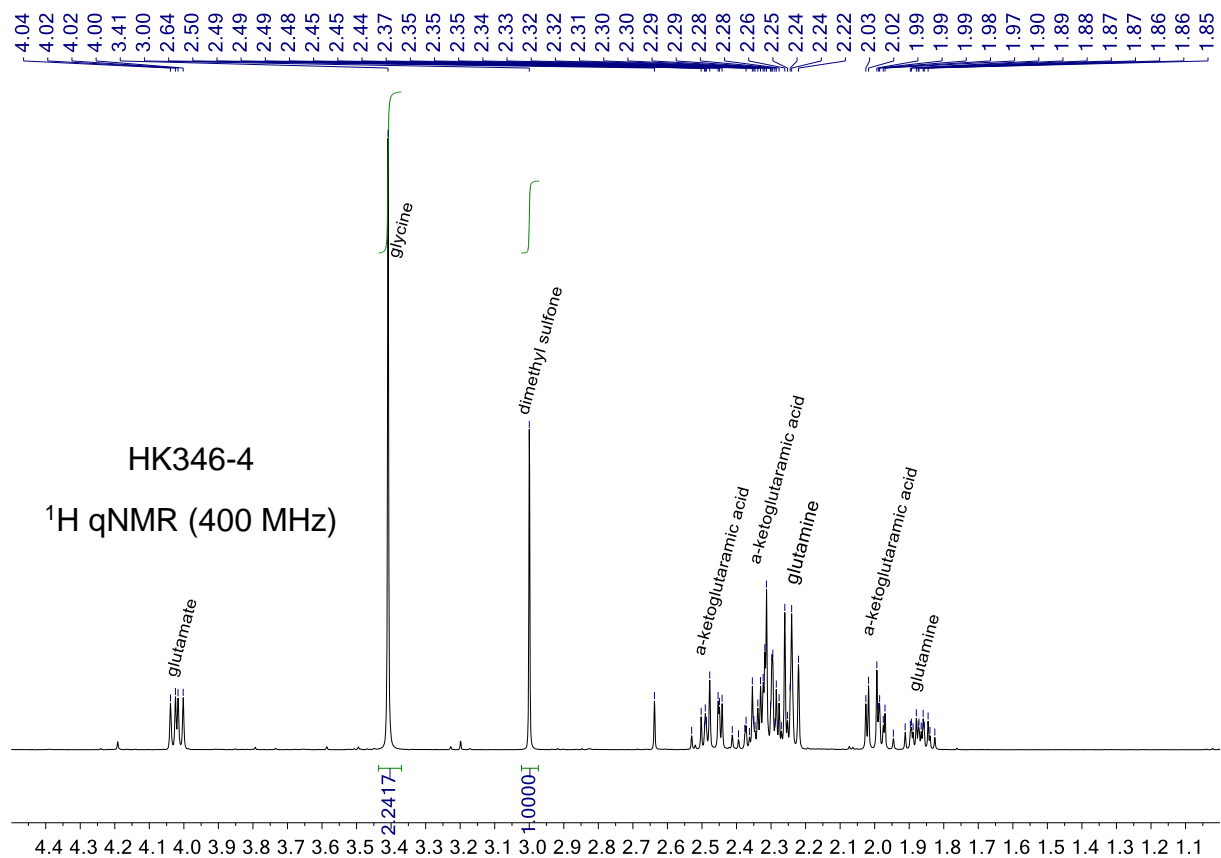
Experiment	Keto Acid	Amino Acid	Integrals		DMS stock (mM)	Concentration in NMR sample (mM)	Concentration corrected for adsorption at Chelex® (mM)
			Ala	DMS			
				(6 H)			( $f_{\text{ala}} = 0.734$ )
HK346-7	Pyruvate	Glycine	0.2480 (1H)	0.9813	30.66	4.15	5.65
HK346-9	Pyruvate	L-Glutamic acid	1.0170 (1.5 H)	0.9788	30.66	11.34	15.45
HK346-10	Pyruvate	L-Glutamine	0.2454 (1 H)	0.9717	30.66	4.10	5.59
HK346-11	Pyruvate	L-Aspartic acid	1.3084 (1 H)	0.9738	30.66	21.88	29.81
HK346-12	Pyruvate	L-Serine	0.0675 (1.5 H)	0.9762	30.66	0.75	1.03

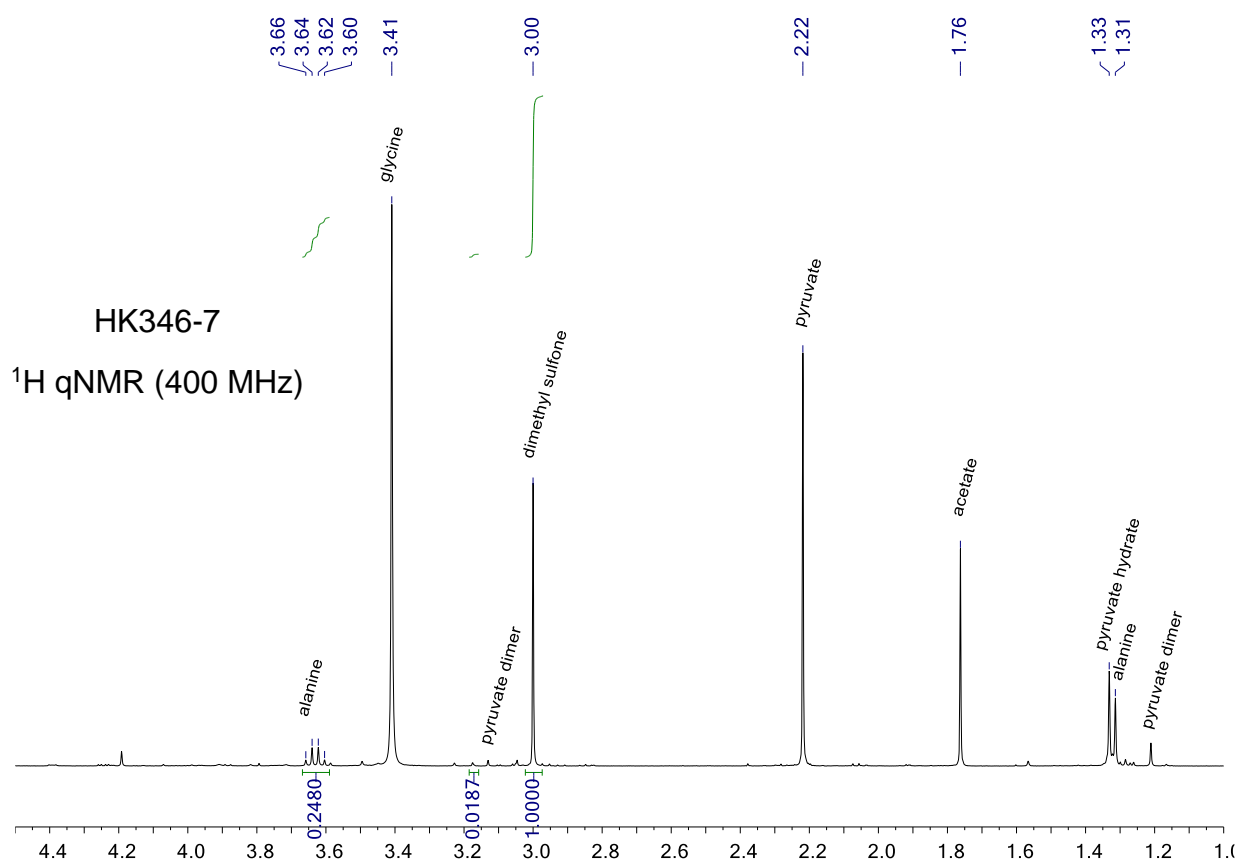
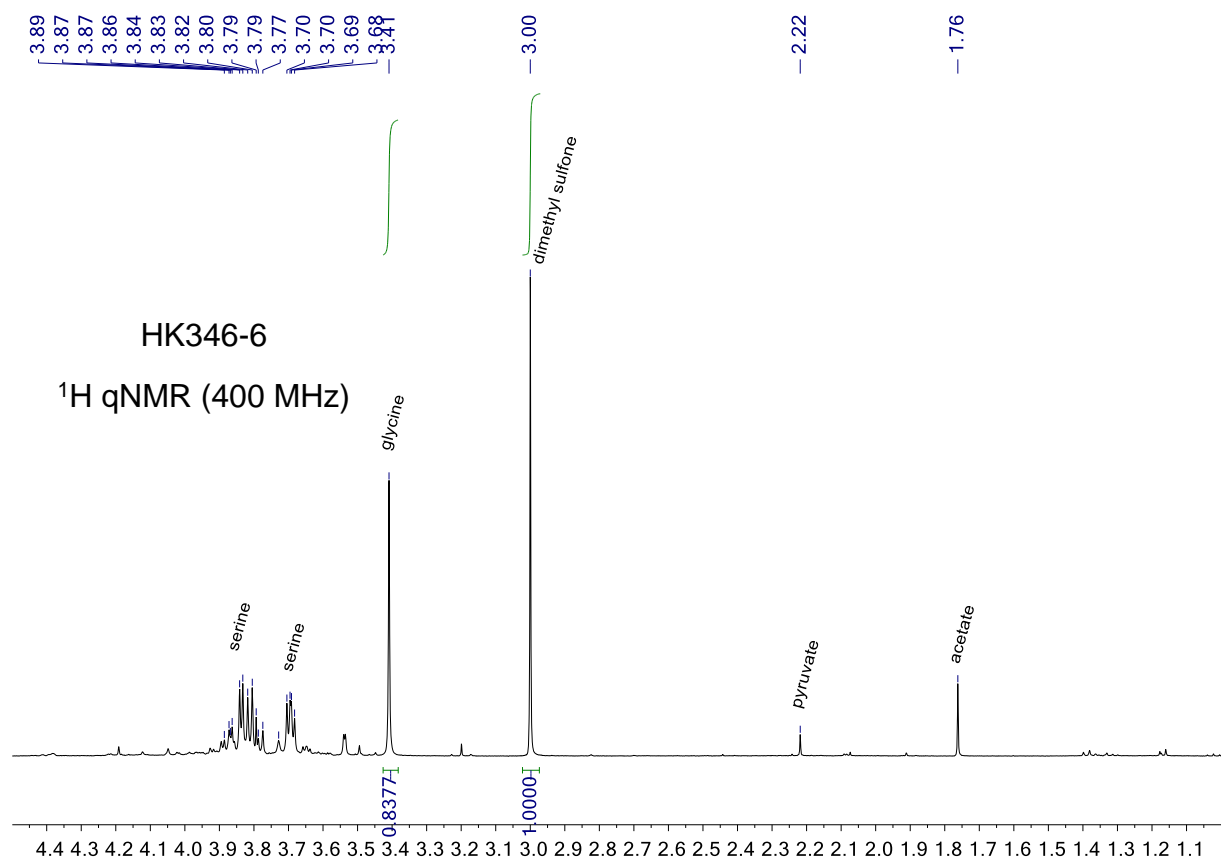
**Table S10.**  $^1\text{H}$  NMR integrals and concentrations for the reactions of  $\alpha$ -ketoglutarate with different amino acids in the presence of 20 mol%  $\text{CuCl}_2 \cdot 2\text{H}_2\text{O}$ .

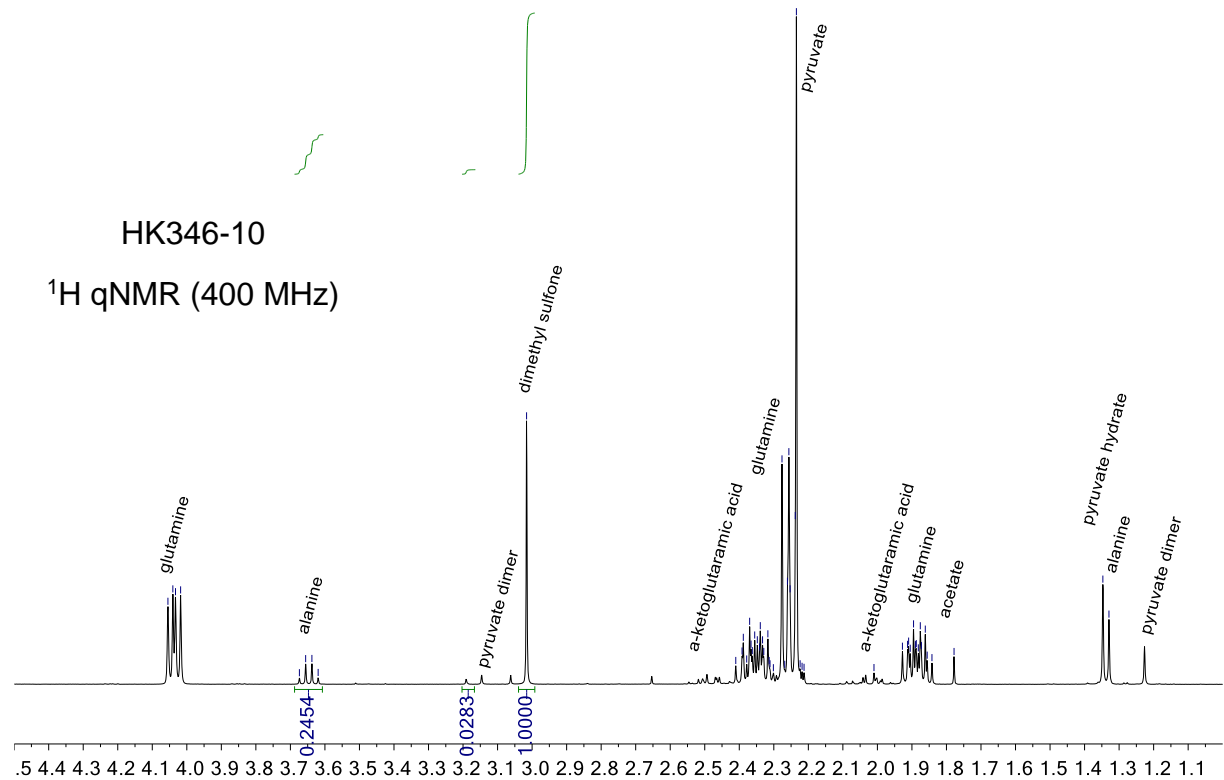
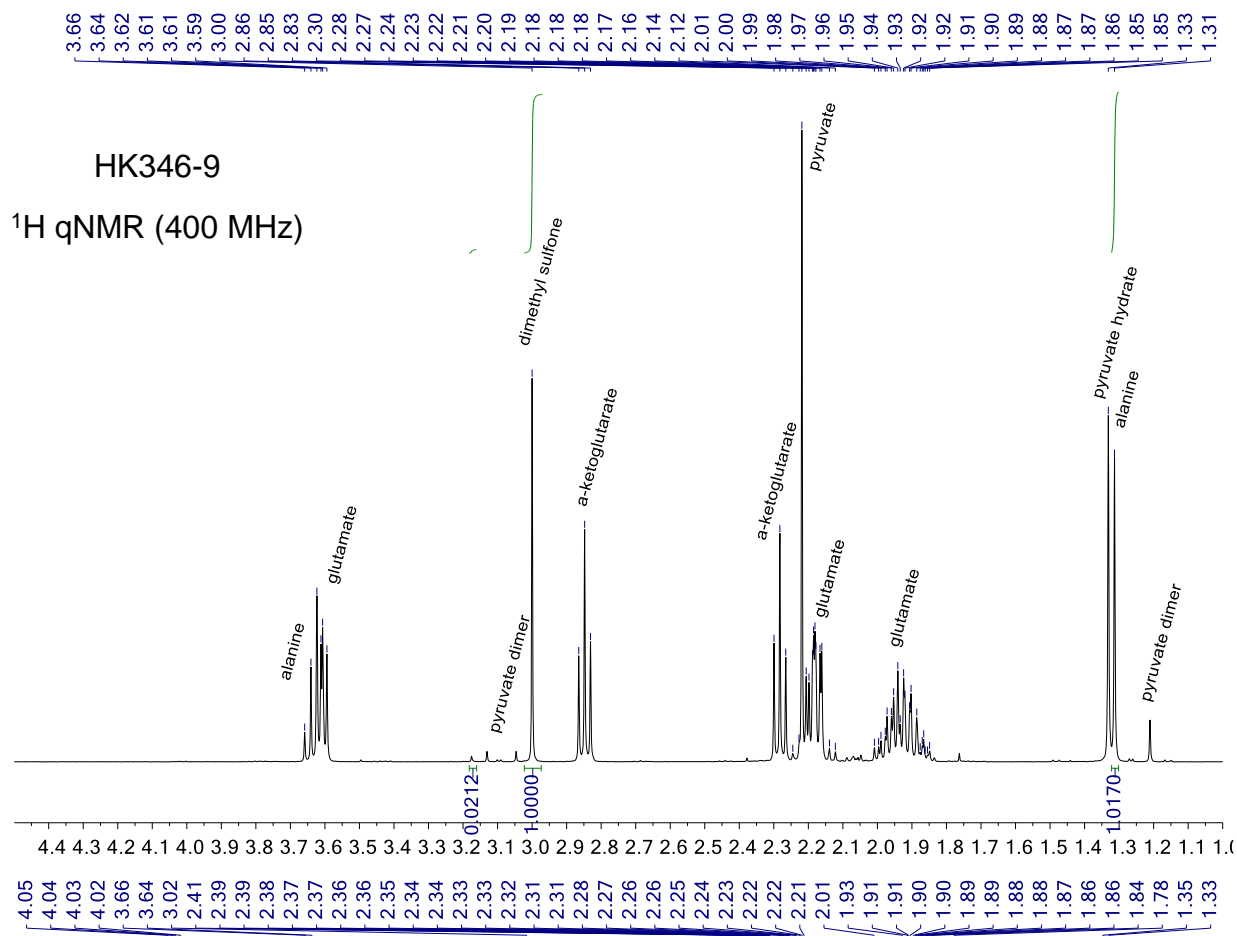
Experiment	Keto Acid	Amino Acid	Integrals			DMS stock (mM)	Concentration in NMR sample (mM)		Concentration corrected for adsorption at Chelex® (mM)	
			Glu (2 H)	Ala (1.5 H)	DMS (6 H)		Glu	Ala	Glu ( $f_{\text{glu}} = 0.781$ )	Ala ( $f_{\text{ala}} = 0.734$ )
HK346-13	a-KG	Glycine	0.4848		1.0000	30.66	4.05		5.19	
HK346-14	a-KG	L-Alanine	1.4462	2.1698	1.0000	30.66	12.09	24.19	15.48	32.96
HK346-16	a-KG	L-Glutamine	0.1263 (1H)		1.0000	30.66	2.11		2.70	
HK346-17	a-KG	L-Aspartic acid	0.8419	0.3776	1.0000	30.66	7.04	4.21	9.01	5.74
HK346-18	a-KG	L-Serine	0.0425		1.0000	30.66	0.71		0.91	

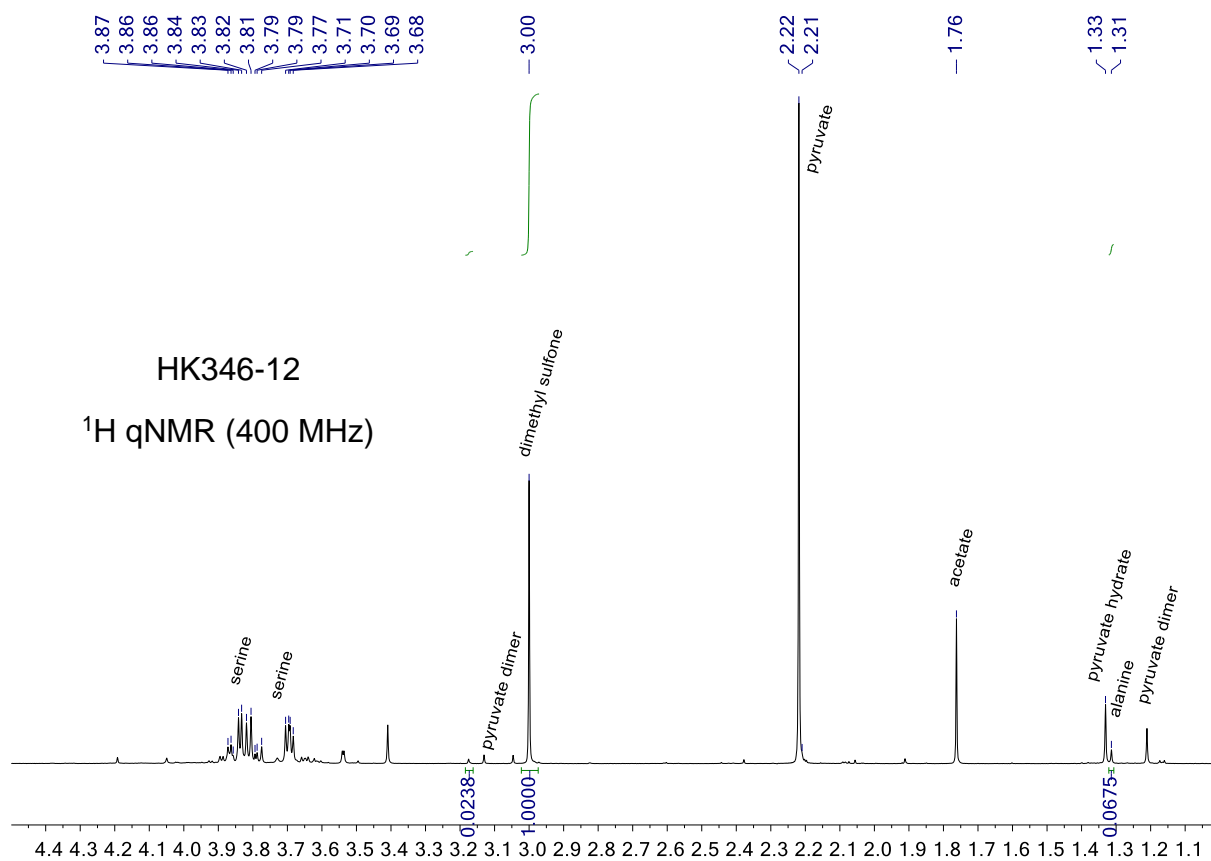
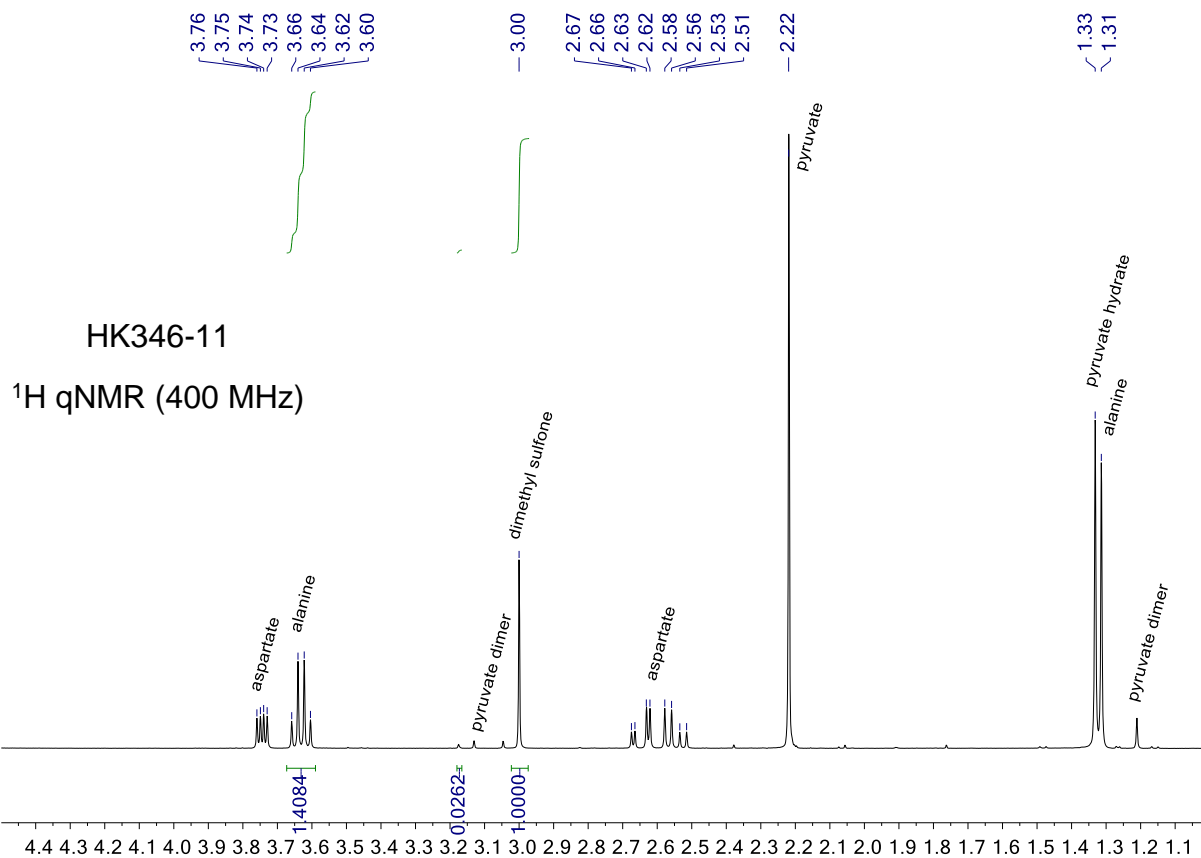


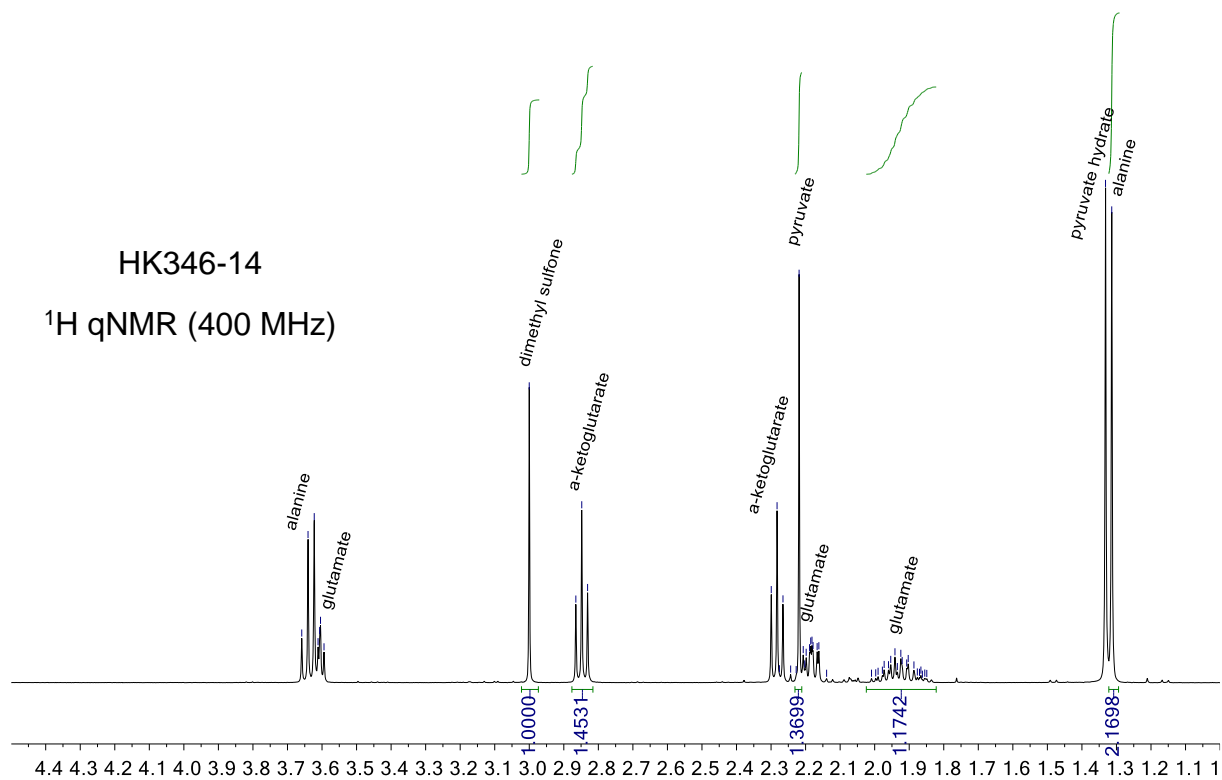
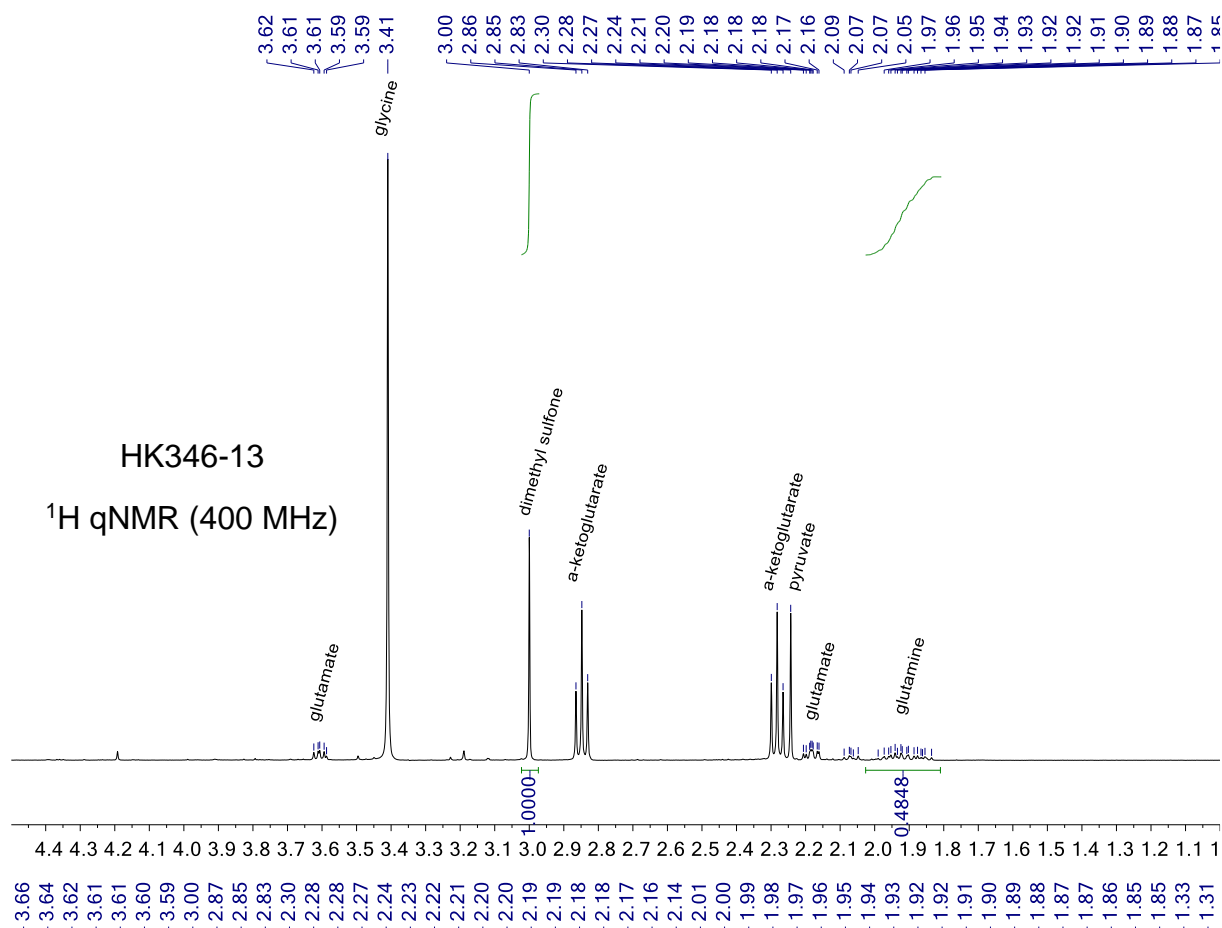


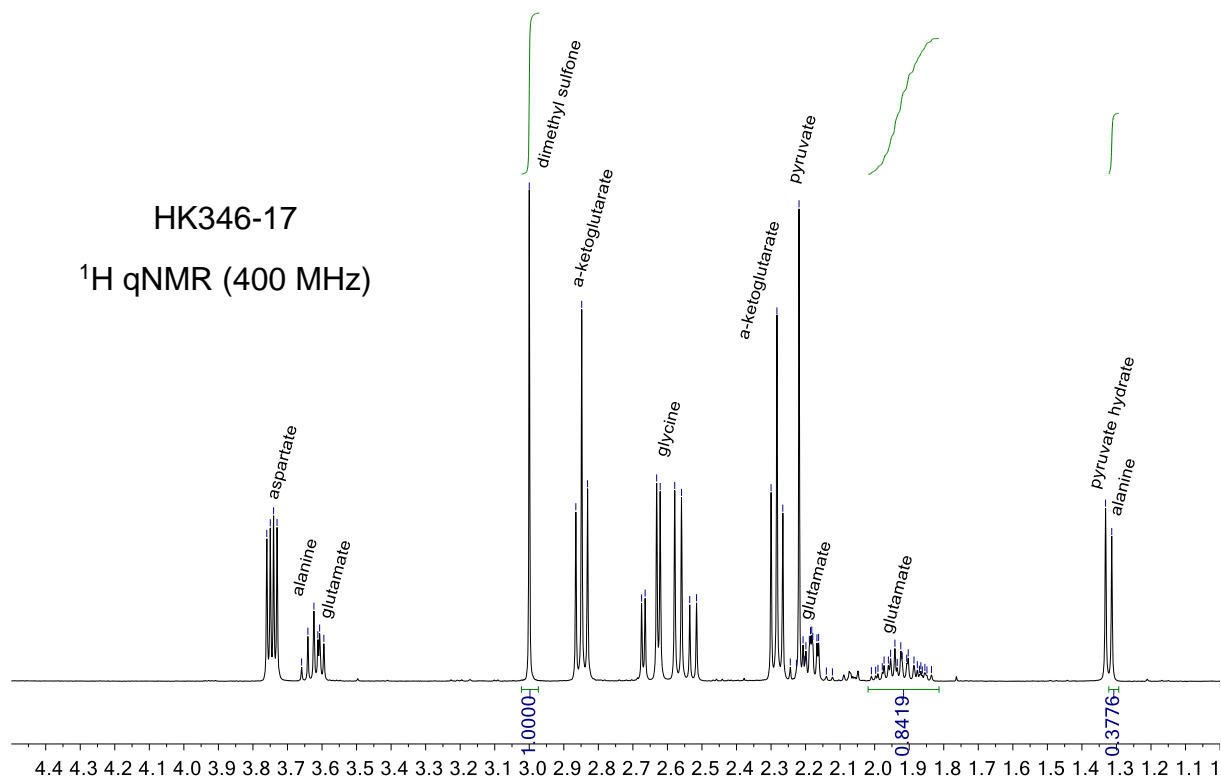
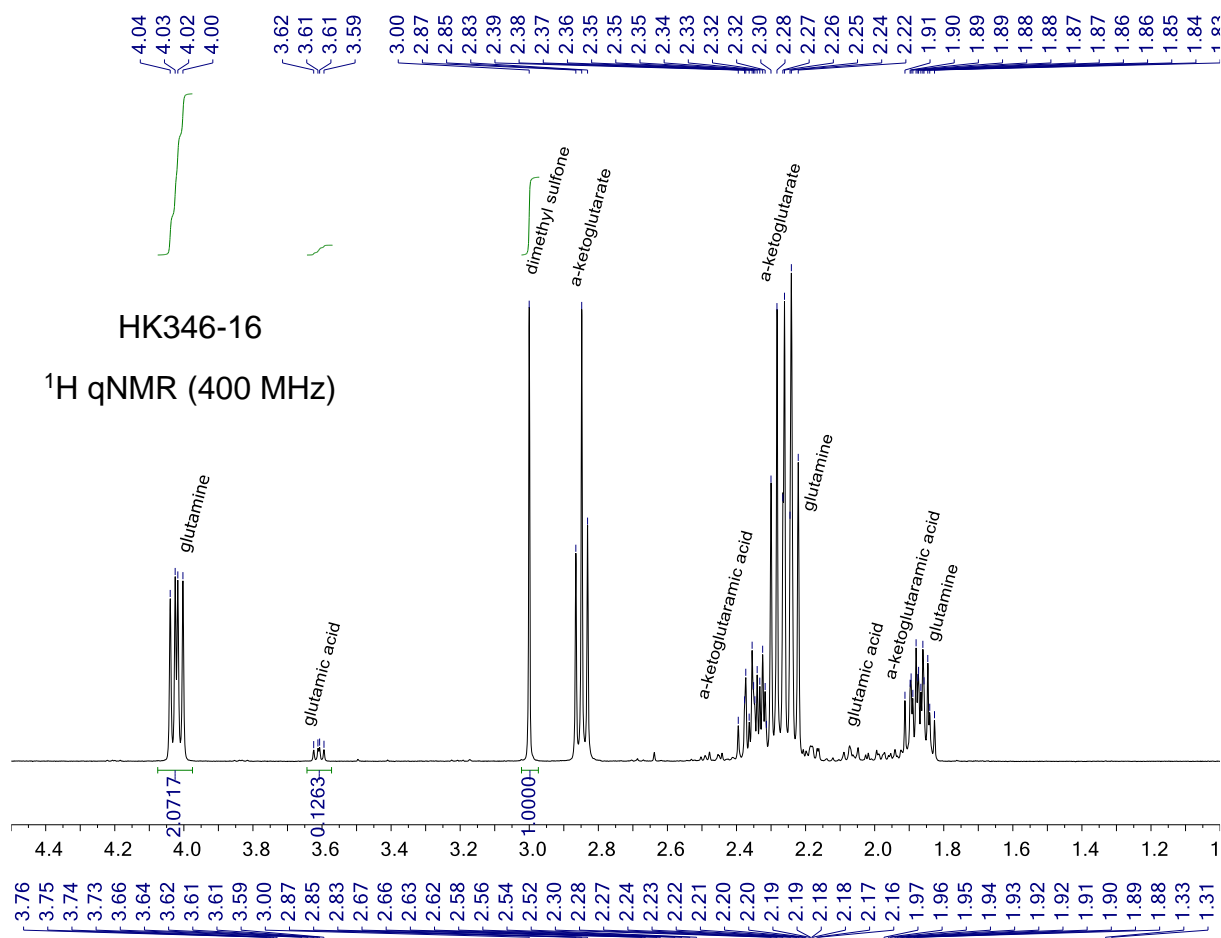


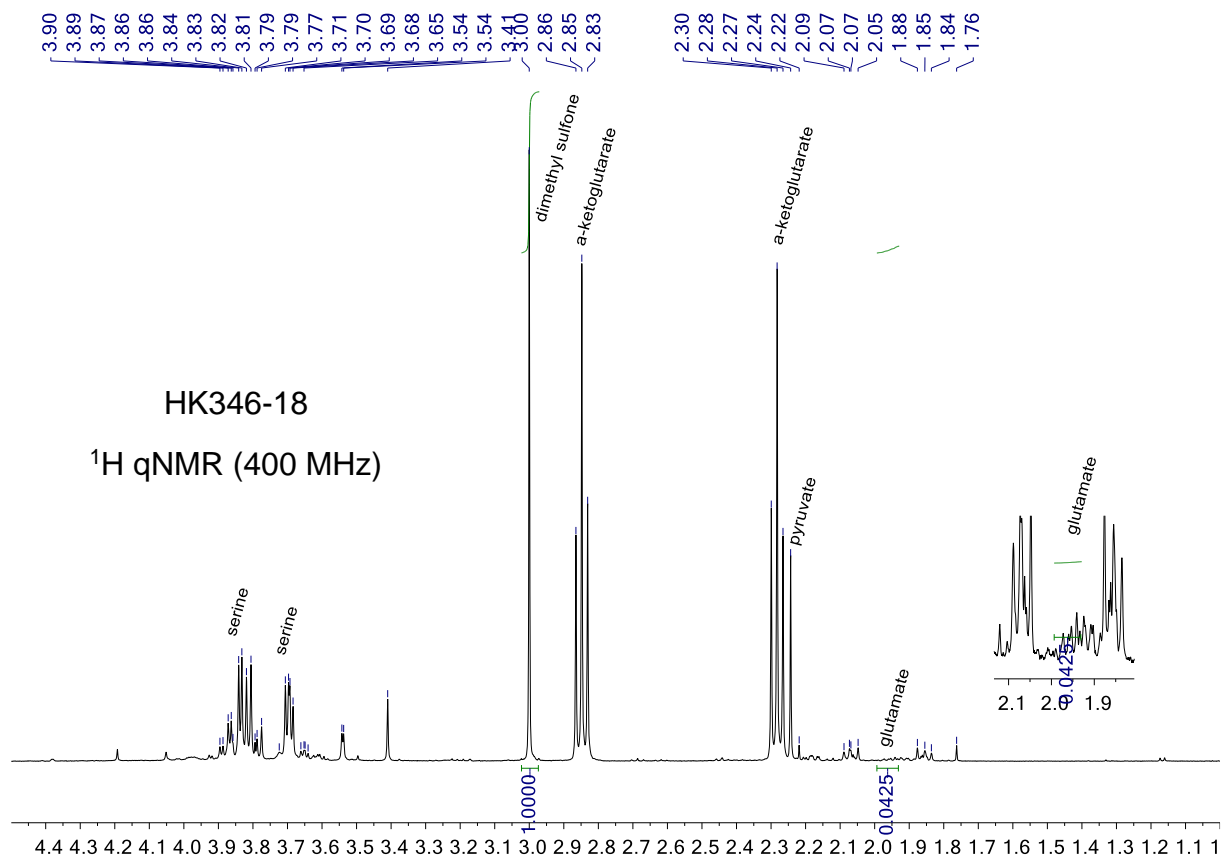












### 13.7. Kinetics of the reaction of glutamic acid with glyoxylate catalyzed by Ni, Co, Cu and V salts

A 25 mL round bottom flask was charged with L-glutamic acid (35.3 mg, 0.240 mmol), the metal salts (for concentrations, see the individual experiments 127) and degassed phosphate buffer (pH 7, 1 M, 7 mL). Sodium glyoxylate monohydrate (0.240 mmol) was dissolved in 1 mL phosphate buffer (pH 7, 1 M), added to the reaction flask (maintained under an atmosphere of argon) and a timer was started.

After specific intervals, aliquots of the reaction (800 µL) were withdrawn and added on Chelex® (400 ± 5 mg), mixed and placed on a shaker for 30 minutes. NMR tubes were charged with 550 µL of the supernatant reaction solution and 50 µL of a solution of dimethyl sulfone in D<sub>2</sub>O (integration standard). Vanadium catalyzed and uncatalyzed reactions were directly performed in NMR tube.

Concentrations were determined based on the integral ratios relative to the resonance of the methyl protons of dimethyl sulfone. Finally, the concentrations were corrected for adsorption to the Chelex® resin (in case of Ni, Co and Cu) with the correction factors  $f_{\text{analyte}}$  determined as described above. For further details please see supporting information of reference 127.

**For further experimental thermochemistry, mechanistic studies and DFT of transamination reactions (by Dr. Mayer) please see supporting information of reference 127.**



## 14. Reductive amination and oxaloacetate/glyoxylate networks

### 14.1. Materials and methods

Unless otherwise stated, all reagents were purchased from commercial suppliers and used without further purification.

**$\alpha$ -ketoacids:** glyoxylic acid solution (50 wt.% in H<sub>2</sub>O, Sigma-Aldrich), sodium pyruvate (ReagentPlus®, ≥99%, Sigma-Aldrich), oxaloacetic acid (≥97% (HPLC), Sigma-Aldrich),  $\alpha$ -ketoglutaric acid disodium salt dihydrate (≥98.0%, Sigma-Aldrich), sodium 3-methyl-2-oxobutyrates (2-oxoisovalerate, 95 %, Sigma-Aldrich), 4-methyl-2-oxovaleric acid (≥98.0%, Sigma-Aldrich), 3-methyl-2-oxopentanoic acid sodium salt (≥98.0%, Sigma-Aldrich). The purity of oxaloacetic acid was determined before use by quantitative <sup>1</sup>H NMR spectroscopy (qNMR).

**Amino acids:** glycine (ReagentPlus®, ≥99%), L-glutamic acid (≥99.5%, BioUltra), L-alanine (BioUltra, ≥99.5%), L-aspartic acid (BioUltra, ≥99.5%), *N*-carbamyl-DL-aspartic acid (>98.0%, TCI chemicals).

**Palladium** metal salts and palladium on different supports for the reaction screening were purchased or synthesized in the lab. Palladium (II) oxide (98%, Sigma-Aldrich), Pd/C (10 wt.% loading (dry basis), matrix carbon powder, wet support, Sigma-Aldrich), palladium 10 wt.% on carbon (wetted with ca. 55% water, TCI chemicals), palladium 5% on  $\gamma$ -alumina powder, reduced, Thermo Fisher Scientific). Pd/C and PdO/C were also synthesized in the lab.

**Other reagents:** ammonium formate (≥99.995%, Sigma-Aldrich), sodium formate (ACS reagent, ≥99.0%, Sigma-Aldrich), sodium bicarbonate (ACS reagent, ≥99.7%, Sigma-Aldrich), ammonium chloride (ACS reagent, ≥99.5%, Sigma-Aldrich), ammonium bicarbonate (BioUltra, ≥99.5%, Sigma-Aldrich), lithium carbamoyl phosphate dibasic hydrate (≥80%, Sigma-Aldrich). Palladium (II) nitrate dihydrate (Pd(NO<sub>3</sub>)<sub>2</sub>·2H<sub>2</sub>O) was purchased from Sigma-Aldrich. Nitric acid (HNO<sub>3</sub>, 65%) was purchased from J.T. Baker. Activated carbon was obtained from Riedel-de Haën. Water used as solvent was obtained from a Milli-Q purification system (18 M $\Omega$ cm). All reactions were carried out in 2 mL BRAND® microcentrifuge tubes with lid, glass GC vials or 4 mL glass vials. All stir bars were pre-washed with aqua regia and sand followed by distilled water and acetone, and oven dried to prevent any cross-contamination by metal salts. Control experiments without the use of any metals were carried out with new stir bars. The reactions under H<sub>2</sub> (5 bar) were carried out in stainless-steel Parr pressure reactors in 1.5 mL vials with pierced PTFE-lined caps or in 4 mL glass vials without caps. The pH value was measured using VWR Dosatest® pH test strips (pH 0-14).

## 14.2. Product identification by NMR and GC-MS

**<sup>1</sup>H NMR** (qNMR) spectra were recorded on a Bruker 400 spectrometer at ambient temperature in a H<sub>2</sub>O:D<sub>2</sub>O mixture (10:1) as solvent, with dimethyl sulfone (DMS, Sigma-Aldrich, trace CERT) as the internal standard (2CH<sub>3</sub> singlet at 3 ppm). Water suppression was achieved using the Bruker *noesygppr1d* pulse program acquiring 8 scans for each sample. For quantitative NMR spectra (qNMR) the relaxation delay d1 was set to 30 s after having determined the T1 relaxation times of all relevant resonances with the inversion recovery method. Integration was performed using *MestReNova v14.3.0* software.

**GC-MS:** reaction mixture (For reactions shown in Figure 32 of results and discussion section) was first derivatized to -COOH esters and brought into CHCl<sub>3</sub> organic phase in order to inject it on GC-MS for qualitative analysis.

*Derivatization procedure:* in a small glass tube 200 µL of sample + 150 µL of 1M NaOH + 150 µL EtOH (HPLC grade) + 30 µL of pyridine + 30 µL of ethyl chloroformate were added and vortexed for 30 sec. Then another 30 µL of ethyl chloroformate were added and vortexed again. Then 200 µL of CHCl<sub>3</sub> (GC grade) were added and vortexed for 30 sec to bring the derivatized products into organic phase. After neutralizing the solution with saturated sodium bicarbonate, the organic layer at the bottom of the tube were taken out with a pipette into an Eppendorf tube and a scoop of sodium sulfate was added in order to remove trace amounts of water over present. Then 50 µL of reaction sample was transferred to a GC vial with insert containing 150 µL of ethyl acetate (GC grade). After, the sample was injected to the GC using an Agilent High Resolution Gas Chromatography Column (PN 19091S – 433UI, HP – 5MS UI, 28 m×0.250 mm, 0.25 Micron, SN USD 489634H) was used. Hydrogen (99.999 % purity) was the carrier gas, supplied at a constant flow rate of 1.5 mL min<sup>-1</sup>. Samples were prepared in ethyl acetate (200 µL sample volume). The analysis was carried out on a 1 µL injection volume (splitless mode). The injection port temperature was 250 °C, and the column oven temperature program was: 60 °C for 1 min, then increased to 310 °C with a 30 °C min<sup>-1</sup> ramp, followed by a 3-min hold (total running time 12.33 min). The mass spectrometer was turned on after a 2-min delay and was operated at the electron ionization mode with quadrupole temperature of 150 °C. Data was acquired in the full-scan mode (50-500). Data analysis was performed using Agilent MassHunter Workstation v.B.06.00 software. Reaction products derivatized to ethyl esters were identified by comparing the mass spectra and retention times to those of analogously derivatized authentic samples.

### 14.3. Reductive aminations under hydrogen gas with ammonium bicarbonate ( $\text{H}_2/\text{NH}_4\text{HCO}_3$ )

**General procedure.** Stock solutions of ammonium bicarbonate at pH 8 (0.3 M) and the  $\alpha$ -ketoacid of interest (0.06 M, from glyoxylic acid, sodium pyruvate, oxaloacetic acid of 97% purity,  $\alpha$ -ketoglutarate disodium salt, 2-oxoisovaleric acid, 4-methyl-2-oxovaleric acid and 3-methyl-2-oxopentanoic acid sodium salt) were freshly prepared at pH 7 by adjusting with 1 M NaOH.

To a 1.5 mL glass vial with stir bar containing 10 wt.% Pd/C (1 mol%, 0.32 mg) were added the stock solutions of ammonium bicarbonate (5 equiv, 500  $\mu\text{L}$ , 0.15 mmol, final concentration = 0.15 M) and  $\alpha$ -ketoacid of interest (1 equiv, 500  $\mu\text{L}$ , 0.03 mmol, final concentration = 0.03 M). The pH was measured (pH 8) and the sample vials were closed with punctured caps and placed in a pressure reactor. The reactor was purged two times and placed under 5 bar of  $\text{H}_2$ . After 72 h stirring at 22  $^\circ\text{C}$  (500 rpm), the pressure was released, and the sample pH was measured again at the end of the reaction (pH  $\approx$  8). The contents were transferred into a 1.5 mL Eppendorf tube and centrifuged to separate the metal catalyst from the reaction solution. The samples were then analyzed by qNMR on a 400 MHz spectrometer after preparing an NMR tube containing 500  $\mu\text{L}$  of the reaction mixture and 50  $\mu\text{L}$  of a dimethyl sulfone internal standard solution in  $\text{D}_2\text{O}$  (concentration specified in the relevant tables). Control experiments were also carried out using the same procedure in the absence of Pd/C. Obtained product yields and  $^1\text{H}$  NMR spectra are shown in Table S11, S12 and Figures S4-S10.

### 14.4. Reductive amination with ammonium formate

**General procedure.** Stock solutions of ammonium formate at pH 7 (0.3 M) and  $\alpha$ -ketoacid of interest (0.06 M, from glyoxylic acid, sodium pyruvate, oxaloacetic acid of 97% purity,  $\alpha$ -ketoglutarate disodium salt, 2-oxoisovaleric acid, 4-methyl-2-oxovaleric acid and

3-methyl-2-oxopentanoic acid sodium salt) were freshly prepared at pH 7 by adjusting with 1 M NaOH.

To a 1.5 mL glass vial with stir bar containing 10 wt.% Pd/C (1 mol%, 0.32 mg) were added the stock solutions of ammonium formate (5 equiv, 500  $\mu$ L, 0.15 mmol, final concentration = 0.15 M) and the  $\alpha$ -ketoacid of interest (1 equiv, 500  $\mu$ L, 0.03 mmol, final concentration = 0.03 M). The pH was measured (pH 7) and the reaction was stirred for 72 h (500 rpm) at 22  $^{\circ}$ C. The sample pH was measured again at the end of the reaction (pH  $\approx$  8). The contents were transferred into a 1.5 mL Eppendorf tube and centrifuged to separate the metal catalyst from the reaction solution. The samples were then analyzed by qNMR on a 400 MHz spectrometer after preparing an NMR tube containing 500  $\mu$ L of the reaction mixture and 50  $\mu$ L of a dimethyl sulfone internal standard solution in D<sub>2</sub>O (concentration specified in the relevant tables). Control experiments were also carried out using the same procedure in the absence of Pd/C. Obtained product yields and <sup>1</sup>H NMR spectra are shown in Tables S13, S14.

#### **14.5. Reductive amination under H<sub>2</sub> (5 bar) without CO<sub>2</sub> source with ammonium chloride (NH<sub>4</sub>Cl)**

**General procedure.** Stock solutions of ammonium chloride (0.3 M) and the  $\alpha$ -ketoacid of interest (0.06 M, from glyoxylic acid, sodium pyruvate, oxaloacetic acid of 97% purity or  $\alpha$ -ketoglutarate disodium salt) were freshly prepared at pH 7 by adjusting with 1 M NaOH.

To a 1.5 mL glass vial with stir bar containing 10 wt.% Pd/C (1 mol%, 0.32 mg) were added the stock solutions of ammonium chloride (5 equiv, 500  $\mu$ L, 0.15 mmol, final concentration = 0.15 M) and  $\alpha$ -ketoacid of interest (1 equiv, 500  $\mu$ L, 0.03 mmol, final

concentration = 0.03 M). The pH was measured (pH 7) and the sample vials were closed with punctured caps and placed in a pressure reactor. The reactor was purged two times with H<sub>2</sub> and placed under 5 bar of H<sub>2</sub>. After 72 h stirring at 22 °C (500 rpm), the pressure was released, and the sample pH was measured again at the end of the reaction (pH ≈ 8). The contents were transferred into a 1.5 mL Eppendorf tube and centrifuged to separate the metal catalyst from the reaction solution. The samples were then analyzed by qNMR on a 400 MHz spectrometer after preparing an NMR tube containing 500 μL of the reaction mixture and 50 μL of a dimethyl sulfone internal standard solution in D<sub>2</sub>O (concentration specified in the relevant tables). Obtained product yields and <sup>1</sup>H NMR spectra are shown in Table S15.

#### **14.6. Reductive amination with Pd/C at 5 °C using ammonium formate (NH<sub>4</sub>OOCCH<sub>3</sub>).**

**General procedure.** To a 4 mL glass vial with stir bar containing 10 wt.% Pd/C (1 mol%, 0.32 mg) were added ammonium formate (5 equiv, 0.15 mmol, 9.46 mg, final concentration = 0.15 M) or ammonium bicarbonate (5 equiv, 0.15 mmol, 11.86 mg, final concentration = 0.15 M) and sodium pyruvate (0.03 mmol, 3.30 mg, final concentration = 0.03 M). The pH was measured (pH 7 in reaction containing ammonium formate, pH 8 in reaction containing ammonium bicarbonate). The reaction with ammonium bicarbonate was placed under H<sub>2</sub> balloon and both reactions were then stirred for 72 h (500 rpm) at 5 °C in a cryogenic refrigerator. The sample pH was measured again at the end of the reaction (pH ≈ 8). The contents were transferred into a 1.5 mL Eppendorf tube and centrifuged to separate the metal catalyst from the reaction solution. The samples were then analyzed by qNMR on a 400 MHz spectrometer after preparing an NMR tube containing 500 μL of the reaction mixture and 50 μL of a dimethyl sulfone internal standard solution in D<sub>2</sub>O (concentration specified in the relevant tables). Obtained product yields and <sup>1</sup>H NMR spectra are shown in Tables S16.

#### **14.7. Reductive amination with various concentrations of ammonium chloride in the presence of sodium formate as hydrogen source.**

**General procedure.** Stock solution  $\alpha$ -ketoacid, pyruvate (30 mM) were freshly prepared at pH 7.

To each 1.5 mL glass vial with stir bar containing 10 wt.% Pd/C (1 mol%, 0.32 mg) were added ammonium chloride 0.006 mmol; 0.03 mmol; 0.09 mmol; 0.15 mmol and 0.3 mmol by weighing in each vial of interest. Then, 5 equivalents of sodium formate were also added in each vial by weighing. Afterwards 1 mL from the stock solution of pyruvate (30 mM) were also added. The pH was measured (pH 7) and the sample vials were closed with caps and stirred at 22 °C (500 rpm) for 72 h. After 72 h the reactions were stopped and sample pH was measured again (pH  $\approx$  8). The contents were transferred into a 1.5 mL Eppendorf tube and centrifuged to separate the metal catalyst from the reaction solution. The samples were then analyzed by qNMR on a 400 MHz spectrometer after preparing an NMR tube containing 500  $\mu$ L of the reaction mixture and 50  $\mu$ L of a dimethyl sulfone internal standard solution in D<sub>2</sub>O (concentration specified in the relevant tables). Obtained product yields and <sup>1</sup>H NMR spectra are shown in Table S17.

#### **14.8. General procedure for oxaloacetate/glyoxylate networks in the presence of formate**

Stock solutions of ammonium formate or sodium formate (2.4 M), oxaloacetate (0.24 M, from oxaloacetic acid of 97% purity) and glyoxylate (0.48 M, from glyoxylic acid) were freshly prepared and the pH was adjusted to 7 with 1 M NaOH.

To a 4 mL glass vial with stir bar containing 10 wt.% Pd/C (1 mol%, 0.64 mg) were added the stock solutions of ammonium formate (10 equiv, 250  $\mu$ L, 0.6 mmol, final concentration = 0.6 M) or sodium formate (10 equiv, 250  $\mu$ L, 0.6 mmol, final concentration = 0.6 M), oxaloacetate (1 equiv, 250  $\mu$ L, 0.06 mmol, final concentration = 0.06 M) and glyoxylate (2

equiv, 250  $\mu$ L, 0.12 mmol, final concentration = 0.12 M). The final volume of the reaction mixture was brought to 1 mL by the addition of 250  $\mu$ L of water. The pH was measured (pH 7) and the reaction was stirred for 72 h (500 rpm) at 22  $^{\circ}$ C. The sample pH was measured again at the end of the reaction (pH  $\approx$  8). The contents were transferred into a 1.5 mL Eppendorf tube and centrifuged to separate the metal catalyst from the reaction solution. The supernatant was then analyzed by qNMR on a 400 MHz spectrometer after preparing an NMR tube containing 500  $\mu$ L of the reaction mixture and 50  $\mu$ L of a dimethyl sulfone internal standard solution in D<sub>2</sub>O (concentration specified in the relevant tables). Obtained product yields and <sup>1</sup>H NMR spectra are shown in Tables S18, S19 and Figures S11, S12.

#### **14.9. General procedure for oxaloacetate/glyoxylate networks in the presence of bicarbonate and H<sub>2</sub> (H<sub>2</sub>/HCO<sub>3</sub><sup>-</sup>)**

Stock solutions of ammonium bicarbonate or sodium bicarbonate (2.4 M) at pH 8, oxaloacetate (0.24 M, from oxaloacetic acid of 97% purity) and glyoxylate (0.48 M, from glyoxylic acid) were freshly prepared at pH 7 by adjusting with 1 M NaOH.

To a 4 mL glass vial with stir bar containing 10 wt.% Pd/C (1 mol%, 0.64 mg) were added the stock solutions of ammonium bicarbonate (10 equiv, 250  $\mu$ L, 0.6 mmol, final concentration = 0.6 M) or sodium bicarbonate (10 equiv, 250  $\mu$ L, 0.6 mmol, final concentration = 0.6 M), oxaloacetate (1 equiv, 250  $\mu$ L, 0.06 mmol, final concentration = 0.06 M) and glyoxylate (2 equiv, 250  $\mu$ L, 0.12 mmol, final concentration = 0.12 M). The final volume of the reaction mixture was brought to 1 mL by the addition of 250  $\mu$ L of water. The pH was measured (pH 8) and the samples were placed in a pressure reactor. The reactor was purged two times with H<sub>2</sub> and placed under H<sub>2</sub> (5 bar). After stirring for 72 h at 22  $^{\circ}$ C (500 rpm), the pressure was released, and the sample pH was measured again (pH  $\approx$  8). The contents were transferred into a 1.5 mL Eppendorf tube and centrifuged to separate the metal catalyst from the reaction solution. The supernatant was

then analyzed by qNMR on a 400 MHz spectrometer after preparing an NMR tube containing 500  $\mu$ L of the reaction mixture and 50  $\mu$ L of a dimethyl sulfone internal standard solution in D<sub>2</sub>O (concentration specified in the relevant tables). Obtained product yields and <sup>1</sup>H NMR spectra are shown in Table S20, S21 and Figure S13, S14.

#### **14.10. General procedure for network control experiments in the absence of catalyst Pd/C**

Control experiments starting from oxaloacetate/glyoxylate: Stock solutions of ammonium formate at pH 7 or ammonium bicarbonate at pH 8 (2.4 M), oxaloacetate (0.24 M, from oxaloacetic acid of 97% purity) and glyoxylate (0.48 M, from glyoxylic acid) were freshly prepared at pH 7 by adjusting with 1 M NaOH.

To a 4 mL glass vial with stir bar were added the stock solutions of ammonium formate or ammonium bicarbonate (10 equiv, 250  $\mu$ L, 0.6 mmol, final concentration = 0.6 M), oxaloacetate (1 equiv, 250  $\mu$ L, 0.06 mmol, final concentration = 0.06 M) and glyoxylate (2 equiv, 250  $\mu$ L, 0.12 mmol, final concentration = 0.12 M). The final volume of the reaction mixture was brought to 1 mL by the addition of 250  $\mu$ L of water and the pH was measured (pH 7 in reaction containing ammonium formate, pH 8 in reaction containing ammonium bicarbonate). The reaction with ammonium formate was carried out outside the reactor without H<sub>2</sub>, while the reaction with ammonium bicarbonate was placed in the pressure reactor under 5 bar H<sub>2</sub>; both were stirred for 72 h (500 rpm) at 22 °C. The sample pH was measured again at the end of the reactions (pH  $\approx$  8) and analyzed by qNMR on a 400 MHz spectrometer after preparing an NMR tube containing 500  $\mu$ L of the reaction mixture and 50  $\mu$ L of a dimethyl sulfone internal standard solution in D<sub>2</sub>O (concentration specified in the relevant tables). Obtained product yields and <sup>1</sup>H NMR spectra are shown in Tables S22, S23 and Figures S15, S16.



Control experiments starting from  $\alpha$ -ketoglutarate: Stock solutions of ammonium formate at pH 7 or ammonium bicarbonate at pH 8 (2.4 M),  $\alpha$ -ketoglutarate (0.24 M) and glyoxylate (0.24 M, from glyoxylic acid) were freshly prepared at pH 7 by adjusting with 1 M NaOH.

To a 4 mL glass vial with stir bar were added the stock solutions of ammonium formate or ammonium bicarbonate (10 equiv, 250  $\mu$ L, 0.6 mmol, final concentration = 0.6 M),  $\alpha$ -ketoglutarate (1 equiv, 250  $\mu$ L, 0.06 mmol, final concentration = 0.06 M) and glyoxylate (1 equiv, 250  $\mu$ L, 0.06 mmol, final concentration = 0.06 M). The final volume of the reaction mixture was brought to 1 mL by the addition of 250  $\mu$ L of water and the pH was measured (pH 7 in reaction containing ammonium formate and pH 8 in reaction containing ammonium bicarbonate). The reaction with ammonium formate was carried out outside the reactor without H<sub>2</sub>, while the reaction with ammonium bicarbonate was placed in the pressure reactor under 5 bar H<sub>2</sub>; both were stirred for 72 h (500 rpm) at 22 °C. The sample pH was measured again at the end of the reaction (pH  $\approx$  8) and analyzed by qNMR on a 400 MHz spectrometer after preparing an NMR tube containing 500  $\mu$ L of the reaction mixture and 50  $\mu$ L of a dimethyl sulfone internal standard solution in D<sub>2</sub>O (concentration specified in the relevant tables). Obtained product yields and <sup>1</sup>H NMR spectra are shown in Tables S24, S25 and Figures S17, S18.

#### **14.11. Reductive amination with different palladium catalysts on different supports and with a meteorite**

Reductive amination was studied using different commercial and freshly synthesized palladium catalysts with different oxidation states, on different supports, or in the absence of support to better understand the reactivity. The analyses shown in Fig. S19, S20 indicate that commercial Pd/C was nearly fully Pd<sup>II</sup>O. Therefore, catalysts with Pd<sup>0</sup> and Pd<sup>II</sup> oxidation state were synthesized as described above and tested in the reductive amination of pyruvate.

Stock solutions of ammonium formate (0.3 M) and pyruvate (0.06 M, from sodium pyruvate) were freshly prepared at pH 7.

**General procedure.** To a 1.5 mL glass vial with stir bar containing 10 wt.% Pd/C (1 mol%, 0.32 mg) were added the stock solutions of ammonium formate (5 equiv, 500  $\mu$ L, 0.15 mmol, final concentration = 0.15 M) and pyruvate (1 equiv, 500  $\mu$ L, 0.03 mmol, final concentration = 0.03 M). The pH was measured (pH 7) and the reaction was stirred for 72 h (500 rpm) at 22  $^{\circ}$ C. The sample pH was measured again at the end of the reaction (pH  $\approx$  8). The contents were transferred into a 1.5 mL Eppendorf tube and centrifuged to separate the metal catalyst from the reaction solution. The samples were then analyzed by qNMR on a 400 MHz spectrometer after preparing an NMR tube containing 500  $\mu$ L of the reaction mixture and 50  $\mu$ L of a dimethyl sulfone internal standard solution in D<sub>2</sub>O (concentration specified in the relevant tables). Obtained product yields and <sup>1</sup>H NMR spectra are shown in Table S26.

As reported, palladium catalysts (1 mol%) either Pd<sup>0</sup> and Pd<sup>II</sup>O supported on carbon both showed reactivity. However, it cannot be excluded that, under H<sub>2</sub> or in the presence of formate, Pd<sup>II</sup> can be reduced to Pd<sup>0</sup>. Bulk PdO without support showed reactivity at higher catalyst loadings. Commercial Pd/C from different suppliers (Sigma and TCI) or Pd catalysts on different supports (Pd/C, Pd/Al<sub>2</sub>O<sub>3</sub>) showed roughly similar reactivity. Generally, and perhaps unsurprisingly, the most active catalysts were those with the smallest particle sizes.

#### **14.12. Preparation of the catalysts (by Dr. Harun Tüysüz and Dr. Youngdong Song)**

##### **Pd/C**

Pd(NO<sub>3</sub>)<sub>2</sub>·2H<sub>2</sub>O (250 mg) was dissolved in 40 mL of diluted HNO<sub>3</sub> solution (6.7 M). Activated carbon (900 mg) was added to the solution and stirred for 30 min at room temperature, followed by heating at 120  $^{\circ}$ C overnight with continuous stirring. The dried powder was reduced in a horizontal tube furnace with 10% hydrogen flow in Ar (100 mL/min) at 100  $^{\circ}$ C for 1 h at a ramp of 10  $^{\circ}$ C/min. After 1 h of reduction, the furnace was cooled down naturally to room temperature. Then passivation was performed with 2% air in Ar (100 mL/min) for 30 min.

## **PdO/C**

$\text{Pd}(\text{NO}_3)_2 \cdot 2\text{H}_2\text{O}$  (250 mg) was dissolved in 40 mL of diluted  $\text{HNO}_3$  solution (6.7 M). Activated carbon (900 mg) was added to the solution and stirred for 30 min at room temperature, followed by heating at 120 °C overnight. The dried powder was treated in a muffle furnace at 250 °C for 1 h with a ramp of 5 °C/min.

### **14.13. Characterization of the catalysts (by Dr. Harun Tüysüz and Dr. Youngdong Song)**

Powder X-ray diffraction (PXRD) patterns were collected on a STOE theta/theta diffractometer in Bragg-Brentano geometry.  $\text{Cu K}\alpha_{1,2}$  radiation ( $\lambda = 1.5406 \text{ \AA}$ ) was used as X-ray source (40 kV and 40 mA). Each sample was analyzed with a step of  $0.01^\circ$  of  $2\theta$ , and data was recorded for 4.0 seconds in each step. Matching was performed on WinXPOW software with a choice of elements. Transmission electron microscopy (TEM) and high-resolution TEM images were analyzed on a HF-2000, Hitachi (200 kV). Samples were prepared by depositing dry powder on a Cu grid. (Figures S19 and S20).

### **14.14. Experimental data**

**Table S11.** Reductive amination of  $\alpha$ -ketoacids with Pd/C under H<sub>2</sub> 5 bar and NH<sub>4</sub>HCO<sub>3</sub>.

Entry	Substrate (30 mM)	Solvent	pH	DMS stock (mM)	Product quantification ( <sup>1</sup> H qNMR)				
					Integrals relative to DMS (6H)		Concentration (mM)	Yield (%)	
1	glyoxylate	water	8	44.24	amino acid	glycine (2H)	6.49	14.36	47.87
					hydroxy acid	glycolate (2H)	0.62	1.37	4.57
					starting material	glyoxylate (1H)	0.94	4.16	13.87
					total		19.89	66.31	
					rest: unknown product, amino acid carbamate and decarboxylation/degradation of SM to formate, CO <sub>2</sub>				
2	pyruvate	water	8	44.24	amino acid	alanine (3H) <sup>a</sup>	13.64	20.13	67.1
					hydroxy acid	lactate (3H)	1.44	2.12	7.07
					starting material	pyruvate (3H)	1.65	2.43	8.10
					total		24.68	82.27	
					rest: alanine carbamate, traces of pyruvate hydrate, pyruvate dimer and decarboxylation of SM to acetate, formate, and CO <sub>2</sub>				
3	oxaloacetate	water	8	14.46	amino acid	aspartate (2H) <sup>a</sup>	27.34	19.77	65.9
					hydroxy acid	malate (1H)	0.18	0.26	0.87
					starting material	oxaloacetate (2H)	-	-	-
					total		20.03	66.77	
					rest: decarboxylation of oxaloacetate to pyruvate, alanine, lactate, pyruvate dimer, acetate, amino acid carbamate, formate and CO <sub>2</sub>				
4	α-ketoglutarate	water	8	20.54	amino acid	glutamate (1H)	7.20	14.79	49.3
					hydroxy acid	hydroxyketoglutarate (1H)	0.70	1.44	4.8
					starting material	α-ketoglutarate (2H)	12.68	13.02	43.4
					total		29.25	97.5	
					rest: amino acid carbamate and SM decarboxylation product succinate.				
5	2-oxoisovalerate	water	8	44.24	amino acid	valine (1H)	4.04	17.87	59.57
					hydroxy acid	2-hydroxyisovalerate (1H)	0.90	3.98	13.27
					starting material	2-oxoisovalerate (1H)	0.96	4.25	14.17
total		26.10	87.01						

rest: amino acid carbamate					
6	4-methyl-2-oxopentanoate	water	8	14.86	amino acid leucine (3H) 31.22 15.46 51.53
					hydroxy acid 2-hydroxy isocaproate (1H) 0.76 1.13 3.77
					starting material 4-methyl-2-oxopentanoate (2H) 20.47 15.21 50.70
					total 31.80 106
					rest: amino acid carbamate
7	3-methyl-2-oxopentanoate	water	8	44.24	amino acid isoleucine/allo-isoleucine (1H) 2.77 / 2.14 12.25 / 9.47 40.83 / 31.57
					hydroxy acid 2-hydroxy-3-methylpentanoate (1H) (mixture of two diastereoisomers) 0.68 3.01 10.03
					starting material 3-methyl-2-oxopentanoate (1H) 0.79 3.49 11.63
					total 28.22 94.06
					rest: traces of amino acid carbamate

<sup>a</sup>Due to overlapping peaks, a consistent portion of the aspartate CH<sub>2</sub> and alanine CH<sub>3</sub> signals was integrated, and the resulting concentration was calculated accordingly.

**Table S12:** Reductive amination control experiments without Pd/C under 5 bars of H<sub>2</sub> and NH<sub>4</sub>HCO<sub>3</sub>.

Entry	Substrate (30 mM)	solvent	pH	DMS stock(mM)	Product quantification ( <sup>1</sup> H qNMR)				
						Integrals relative to DMS (6H)	Concentration (mM)	Yield (%)	
1	glyoxylate	water	8	44.24	amino acid	glycine (2H)	-	-	-
					hydroxy acid	glycolate (2H)	-	-	-
					starting material	glyoxylate (1H)	3.18	14.07	46.9
					total			<b>14.07</b>	<b>46.9</b>
					<i>rest: decarboxylation/degradation of SM to formate, CO<sub>2</sub></i>				
2	pyruvate	water	8	14.86	amino acid	alanine (3H)	-	-	-
					hydroxy acid	lactate (3H)	-	-	-
					starting material	pyruvate (3H)	54.54	27.02	90.07
					total			<b>27.02</b>	<b>90.07</b>
					<i>rest: pyruvate hydrate, pyruvate dimer and decarboxylation/degradation of SM to acetate, formate, CO<sub>2</sub></i>				

3	oxaloacetate	water	8	14.86	amino acid	aspartate (2H)	-	-	-
					hydroxy acid	malate (1H)	-	-	-
					starting material	oxaloacetate (2H)	-	-	-
					total			-	-
					<i>rest: dimerization to citroyl formate, decarboxylation to pyruvate 82%, pyruvate hydrate, pyruvate dimer, acetate, formate and CO<sub>2</sub></i>				
4	a-ketoglutarate	water	8	14.86	amino acid	glutamate (1H)	-	-	-
					hydroxy acid	hydroxyketoglutarate (1H)	-	-	-
					starting material	a-ketoglutarate	41.91	31.14	103.8
					total			31.14	103.8
					<i>rest: decarboxylation to succinate</i>				
5	2-oxoisovalerate	water	8	11.80	amino acid	valine (1H)	-	-	-
					hydroxy acid	2-hydroxyisovalerate (1H)	-	-	-
					starting material	2-oxoisovalerate (1H)	21.77	25.69	85.63
					total			25.69	85.63
					<i>rest: none</i>				
6	4-methyl-2-oxopentanoate	water	8	14.86	amino acid	leucine (3H)	-	-	-
					hydroxy acid	2-hydroxyisocaproate (1H)	-	-	-
					starting material	4-methyl-2-oxopentanoate (2H)	37.03	27.51	91.7
					total			27.51	91.7
					<i>rest: none</i>				
7	3-methyl-2-oxopentanoate	water	8	11.80	amino acid	isoleucine/allo-isoleucine (1H)	-	-	-
					hydroxy acid	2-hydroxy-3-methylpentanoate (mixture of two diastereoisomers) (1H)	-	-	-
					starting material	3-methyl-2-oxopentanoate(1H)	25.17	29.70	99
					total			29.70	99
					<i>rest: none</i>				

**Table S13:** Reductive amination of  $\alpha$ -ketoacids with Pd/C and  $\text{NH}_4\text{OOCH}$ .

Entry	Substrate (30 mM)	Solvent	pH	DMS stock (mM)	Product quantification ( $^1\text{H}$ qNMR)			
						Integrals relative to DMS (6H)	Concentration (mM)	Yield (%)
1	pyruvate	water	7 - 8	29	amino acid	alanine (3H) <sup>a</sup>	24.02	77.43
					hydroxy acid	lactate (3H)	0.91	2.90
					starting material	pyruvate (3H)	1.52	4.93
					total		<b>25.58</b>	<b>85.26</b>
					<i>rest: amino acid carbamate, pyruvate hydrate, pyruvate dimer and decarboxylation/degradation of SM to acetate</i>			
2	oxaloacetic acid	water	7-8	29	amino acid	aspartate (2H) <sup>a</sup>	4.54	21.93
					hydroxy acid	malate (1H)	0.01	0.10
					starting material	oxaloacetate (2H)	-	-
					total		<b>6.61</b>	<b>22.03</b>
					<i>rest: citrolyl formate and SM decarboxylated to pyruvate, alanine, lactate, pyruvate hydrate, pyruvate dimer and acetate</i>			
3	$\alpha$ -ketoglutarate	water	7-8	29	amino acid	glutamate (1H)	7.11	68.73
					hydroxy acid	2-hydroxypenanedioate (1H)	0.39	3.77
					starting material	$\alpha$ -ketoglutarate (2H)	6.57	31.8
					total		<b>31.28</b>	<b>104.3</b>
					<i>rest: succinate, amino acid carbamate</i>			



4	2-oxoisovaleric acid	water	7-8	29	amino acid	valine (1H)	7.28	21.11	70.37
					hydroxy acid	2-hydroxyisovalerate (1H)	0.41	1.19	3.97
					starting material	2-oxoisovaleric acid (1H)	1.76	5.10	17
					total			<b>27.4</b>	<b>91.34</b>
					<i>rest: carbamate</i>				
5	4-methyl-2-oxopentanoate	water	7-8	29	amino acid	leucine (3H)	16.77	16.21	54.03
					hydroxy acid	2-hydroxyisocaproate (1H)	0.10	0.29	0.97
					starting material	4-methyl-2-oxopentanoic acid (2H)	5.33	7.73	25.8
					total			<b>24.23</b>	<b>80.8</b>
					<i>rest: amino acid carbamate</i>				
6	3-methyl-2-oxopentanoate	water	7-8	29	amino acid	isoleucine/allo-isoleucine (1H)	4.61/3.49	13.37/10.12	44.57/33.73
					hydroxy acid	2-hydroxy-3-methylpentanoate (mixture of two diastereoisomers) (1H)	0.77	2.23	7.43
					starting material	3-methyl-2-oxopentanoate (1H)	0.24	0.70	2.33
					total			<b>26.42</b>	<b>88.06</b>
					<i>rest: traces carbamate</i>				

<sup>a</sup>Due to overlapping peaks, a portion of the relevant signal was integrated and the resulting concentration was calculated accordingly.

**Table S14:** Reductive amination control experiments without Pd/C in the presence of NH<sub>4</sub>OOCH

Entry	Substrate (30 mM)	Solvent	pH	DMS stock (mM)	Product quantification ( <sup>1</sup> H qNMR)			
						Integrals relative to DMS (6H)	Concentration (mM)	Yield (%)
1	pyruvate	water	7 - 8	29	amino acid	alanine (3H)	-	-
					hydroxy acid	lactate (2H)	-	-
					starting material	pyruvate (3H)	29.17	28.20
					total		<b>28.20</b>	<b>94.0</b>
					<i>rest: pyruvate hydrate, pyruvate dimer and decarboxylation/degradation of SM to acetate</i>			
2	oxaloacetate	water	7-8	23	amino acid	aspartate (2H)	-	-
					hydroxy acid	malate (1H)	-	-
					starting material	oxaloacetate (2H)	-	-
					total		-	-
					<i>rest: citryl formate and almost all SM decarboxylated to pyruvate, traces of pyruvate hydrate, pyruvate dimer and acetate.</i>			
3	α-ketoglutarate	water	7-8	29	amino acid	glutamate (1H)	-	-
					hydroxy acid	2-hydroxypentanedioate (1H)	-	-
					starting material	α-ketoglutarate (2H)	17.98	26.1
					total		<b>26.1</b>	<b>87</b>
					<i>rest: traces succinate</i>			

4	2-oxoisovalerate	water	7-8	29	amino acid	valine (1H)	-	-	-
					hydroxy acid	2-hydroxyisovalerate (1H)	-	-	-
					starting material	2-oxoisovaleric acid (1H)	10.05	29.15	97.17
					total			<b>29.15</b>	<b>97.17</b>
					<i>rest: none</i>				
5	4-methyl-2-oxopentanoate	water	7-8	29	amino acid	leucine (3H)	-	-	-
					hydroxy acid	2-hydroxyisocaproate (1H)	-	-	-
					starting material	4-methyl-2-oxopentanoic acid (2H)	17.48	25.35	84.5
					total			<b>25.35</b>	<b>84.5</b>
					<i>rest: none</i>				
6	3-methyl-2-oxopentanoate	water	7-8	29	amino acid	isoleucine/allo-isoleucine (1H)	-	-	-
					hydroxy acid	2-hydroxy-3-methylpentanoate (1H) (mixture of two diastereoisomers)	-	-	-
					starting material	3-methyl-2-oxopentanoate (1H)	10.28	29.81	99.37
					total			<b>29.81</b>	<b>99.37</b>
					<i>rest: none</i>				

**Table S15:** Reductive aminations with Pd/C under H<sub>2</sub> and NH<sub>4</sub>Cl

Entry	Substrate (30 mM)	Solvent	pH	DMS stock (mM)	Product quantification ( <sup>1</sup> H qNMR)				
							Integrals relative to DMS (6H)	Concentration (mM)	Yield (%)
1	glyoxylate	water	7-8	10.46	amino acid	glycine (2H)	10.35	5.41	18.03
					hydroxy acid	glycolate (2H)	11.94	6.24	20.8
					starting material	glyoxylate (1H)	18.94	19.81	66.03
					total			31.46	104.86
					rest: decarboxylation to formate and CO <sub>2</sub>				
2	pyruvate	water	7-8	10.46	amino acid	alanine (3H) <sup>a</sup>	1.92	0.67	2.23
					hydroxy acid	lactate (3H)	9.22	3.21	10.70
					starting material	pyruvate (3H)	64.14	22.36	74.53
					total			26.24	87.46
					rest: pyruvate hydrate, pyruvate dimer and decarboxylation/degradation of SM to acetate, formate and CO <sub>2</sub>				
3	oxaloacetate	water	7-8	10.46	amino acid	aspartate (2H) <sup>a</sup>	11.14	5.83	19.43
					hydroxy acid	malate (1H)	1.21	1.27	4.23
					starting material	oxaloacetate (2H)	-	-	-
					total			7.1	23.66
					rest: citryl formate and SM decarboxylated to pyruvate, pyruvate hydrate, pyruvate dimer, acetate, formate and pyruvate reductive amination and reduction products alanine and lactate respectively				
4	α-ketoglutarate	water	7-8	10.46	amino acid	glutamate (1H)	0.34	0.36	1.2
					hydroxy acid	2-hydroxypenanedioate (1H)	6.38	6.67	22.23
					starting material	α-ketoglutarate (2H)	34.45	18.02	60.07
					total			25.05	83.5
					rest: α-ketoglutarate decarboxylation to succinate				

<sup>a</sup>Due to overlapping peaks, a portion of the relevant signal was integrated, and the resulting concentration was calculated accordingly.

**Table S16.** Reductive amination at 5 °C using pyruvate as a model substrate.<sup>a</sup>

Entry	Ammonia and hydride source	Solvent	pH	DMS stock (mM)	Product quantification ( <sup>1</sup> H qNMR)				
							Integrals relative to DMS (6H)	Concentration (mM)	Yield (%)
1	NH <sub>4</sub> OOCH (ammonium formate)	water	7-8	14.86	alanine (3H)		10.82	5.36	17.87
					lactate (3H)		0.47	0.23	0.77
					starting material (3H)		20.38	10.09	33.63
					acetate (3H)		28.82	14.28	47.6
					total			29.96	99.87
2	NH <sub>4</sub> HCO <sub>3</sub> + H <sub>2</sub> (ammonium bicarbonate)	water	7-8	14.86	alanine (3H)		33.22	16.45	54.83
					lactate (3H)		3.10	1.54	5.13
					starting material (3H)		2.46	1.22	4.07
					acetate (3H)		12.34	6.11	20.37
					total			25.32	84.4

<sup>a</sup>Due to overlapping peaks, only half of the signal corresponding to the CH<sub>3</sub> group of alanine was integrated and the resulting concentration was calculated accordingly.

**Table S17.** Reductive amination with different NH<sub>4</sub>Cl concentration and pyruvate (30 Mm) under Pd/C (1 mol%) catalysis.<sup>a</sup>

Entry	Catalyst mol % (mg)	Solvent	pH	DMS stock (mM)	Product quantification ( <sup>1</sup> H qNMR)		
					Integrals relative to DMS (6H)	Concentration (mM)	Yield (%)
1	Pd/C 1mol% 0.32 mg (HK525-6)	water	7-8	21	alanine (3H)	0.64	2.99
					lactate (3H)	1.58	5.27
					starting material (3H)	29.53	98.42
					<b>total</b>	<b>32.01</b>	<b>106.7</b>
2	Pd/C 1mol% 0.32 mg (HK390-3)	water	7-8	17.28	alanine (3H)	5.48	18.27
					lactate (3H)	0.83	2.77
					starting material (3H)	17.19	57.3
					<b>total</b>	<b>23.5</b>	<b>78.33</b>
3	Pd/C 1mol% 0.32 mg (HK390-8)	water	7-8	17.28	alanine (3H)	8.45	28.16
					lactate (3H)	0.64	2.13
					starting material (3H)	14.01	46.7
					<b>total</b>	<b>23.1</b>	<b>77</b>
4	Pd/C 1mol% 0.32 mg (HK337-4)	water	7-8	24	alanine (3H)	15.05	50.17
					lactate (3H)	0.32	1.07
					starting material (3H)	12.50	41.67
					<b>total</b>	<b>27.87</b>	<b>92.9</b>
5	Pd/C 1mol% 0.32 mg (HK390-19)	water	7-8	17.28	alanine (3H)	14.34	47.8
					lactate (3H)	0.43	1.43
					starting material (3H)	6.91	23.03
					<b>total</b>	<b>21.68</b>	<b>72.26</b>

**Table S18.** Oxaloacetate/glyoxylate reaction network with Pd/C and sodium formate.<sup>a</sup>

Product quantification ( <sup>1</sup> H qNMR)					
Entry	Compound	Signal integrated	Integrals relative to DMS (6H) concentration (20.54 mM)	Concentration (mM)	Yield (%)
1	glyoxylate, <b>2</b>	1H (4.93 ppm)	13.07	26.85	22.38
2	glycine, <b>2a</b>	2H	-	-	-
3	glycolate, <b>2b</b>	2H (3.80 ppm)	0.66	0.68	0.57
4	oxaloacetate, <b>3</b>	2H	-	-	-
5	aspartate, <b>3a</b>	2H	-	-	-
6	malate, <b>3b</b>	2H (2.19-2.26 ppm, 1H) <sup>b</sup>	1.06	1.09	1.82
7	pyruvate, <b>4</b>	3H (2.22 ppm)	1.65	1.13	1.88
8	alanine, <b>4a</b>	3H	-	-	-
9	lactate, <b>4b</b>	3H (1.17-1.19 ppm)	0.23	0.08	0.13
10	maloyl formate, <b>5</b>	2H (3.06-3.11 ppm, 1H) <sup>b</sup>	46.46	47.71	79.52
11	fumaroyl formate, <b>6</b>	2H (6.62 -6.74 ppm)	0.12	0.12	0.20
12	α-ketoglutarate, <b>7</b>	2H (2.84-2.88 ppm)	0.69	0.72	1.20
13	glutamate, <b>7a</b>	2H	-	-	-
15	hydroxyketoglutarate, <b>7b</b>	1H	-	-	-
16	succinate	4H	-	-	-
17	isocitroyl formate, <b>8</b> diastereoisomer (erythro)	1H (4.38-4.39 ppm)	0.07	0.14	0.23
18	aconitoyl formate, <b>9</b>	2H (3.21 ppm)	0.05	0.05	0.08
19	citroyl formate, <b>10</b>	4H	-	-	-
20	di-DHKG <sup>1</sup>	1H (6.80 ppm)	0.29	0.60	1.00
21	acetate	3H (1.77 ppm)	3	2.11	3.52
Total	excluding SM. and glycolate			<b>53.75</b>	<b>89.58</b>
Total	including glycolate			<b>54.43</b>	<b>90.15</b>

<sup>a</sup>Additional products are visible by NMR but their identities could not be elucidated. Yields are calculated relative to initial oxaloacetate concentration (60 mM), except glyoxylate, glycine and glycolate, where yields are given relative to the initial glyoxylate concentration (120 mM).

<sup>b</sup>Due to overlapping peaks, only the specified portion of the signal could be integrated, and the resulting concentration was calculated accordingly.

**Table S20.** Oxaloacetate/glyoxylate reaction network with Pd/C and sodium bicarbonate under H<sub>2</sub> (5 bar).<sup>a</sup>

Product quantification ( <sup>1</sup> H qNMR)					
Entry	Compound	Signal integrated	Integrals relative to DMS (6H) concentration (14.86 mM)	Concentration (mM)	Yield (%)
1	glyoxylate, <b>2</b>	1H	-	-	-
2	glycine, <b>2a</b>	2H	-	-	-
3	glycolate, <b>2b</b>	2H (3.80 ppm)	7.53	5.60	4.67
4	oxaloacetate, <b>3</b>	2H	-	-	-
5	aspartate, <b>3a</b>	2H	-	-	-
6	malate, <b>3b</b>	2H (2.19 ppm: 1/8 of 2H) <sup>b</sup>	1.28	0.95	1.58
7	pyruvate, <b>4</b>	3H (2.22 ppm)	1.66	0.82	1.37
8	alanine, <b>4a</b>	3H	-	-	-
9	lactate, <b>4b</b>	3H (1.17-1.19 ppm)	0.39	0.19	0.32
10	maloyl formate, <b>5</b>	2H (3.06-3.11 ppm, 1H) <sup>b</sup>	53.98	40.11	66.85
11	fumaroyl formate, <b>6</b>	2H (6.66 ppm, 1/4 of 2H) <sup>b</sup>	0.08	0.06	0.10
12	α-ketoglutarate, <b>7</b>	2H (2.84-2.87 ppm)	2.50	1.86	3.1
13	glutamate, <b>7a</b>	2H	-	-	-
15	hydroxyketoglutarate, <b>7b</b>	1H	-	-	-
16	succinate	4H	-	-	-
17	isocitroyl formate, <b>8</b> diastereoisomer (erythro)	1H (4.37-4.38 ppm)	0.87	1.29	2.15
18	aconitoyl formate, <b>9</b>	2H (3.21 ppm)	0.12	0.09	0.15
19	citroyl formate, <b>10</b>	4H	-	-	-
20	di-DHKG <sup>1</sup>	1H (6.80 ppm)	0.07	0.10	0.17
21	acetate	3H (1.77 ppm)	4.57	2.26	3.77
Total	excluding SM and glycolate			<b>47.73</b>	<b>79.56</b>
Total	including glycolate			<b>53.33</b>	<b>82.23</b>

<sup>a</sup>Additional products are visible by NMR but their identities could not be elucidated. Yields are calculated relative to initial oxaloacetate concentration (60 mM), except glyoxylate, glycine and glycolate, where yields are given relative to the initial glyoxylate concentration (120 mM).

<sup>b</sup>Due to overlapping peaks, only the specified portion of the signal could be integrated, and the resulting concentration was calculated accordingly.



**Table S19.** Oxaloacetate/glyoxylate reaction network with Pd/C and ammonium formate.<sup>a</sup>

Product quantification ( <sup>1</sup> H qNMR)					
Entry	Compound	Signal integrated	Integrals relative to DMS (6H) concentration (20.34 mM)	Concentration (mM)	Yield (%)
1	glyoxylate, <b>2</b>	1H (4.94 ppm)	0.16	0.33	0.28
2	glycine, <b>2a</b>	2H (3.41 ppm)	0.53	0.54	0.45
3	glycolate, <b>2b</b>	2H (3.80 ppm)	0.63	0.64	0.53
4	oxaloacetate, <b>3</b>	2H	-	-	-
5	aspartate, <b>3a</b>	2H (2.63-2.68 ppm, 1H) <sup>b</sup>	2.92	2.97	4.95
6	malate, <b>3b</b>	2H (2.19 ppm 1/8 of 2H) <sup>b</sup>	1.44	1.46	2.43
7	pyruvate, <b>4</b>	3H (2.22 ppm)	1.08	0.73	1.22
8	alanine, <b>4a</b>	3H	-	-	-
9	lactate, <b>4b</b>	3H (1.17-1.19 ppm)	0.23	0.16	0.27
10	maloyl formate, <b>5</b>	2H (3.06-3.11 ppm, 1H) <sup>b</sup>	16.8	17.09	28.48
11	fumaroyl formate, <b>6</b>	2H (6.62-6.75 ppm)	0.04	0.04	0.07
12	α-ketoglutarate, <b>7</b>	2H (2.84-2.87 ppm)	2.20	2.24	3.73
13	glutamate, <b>7a</b>	2H	-	-	-
15	hydroxyketoglutarate, <b>7b</b>	1H	-	-	-
16	succinate	4H	-	-	-
17	isocitroyl formate, <b>8</b> diastereoisomer (erythro)	1H (4.39-4.40 ppm)	0.25	0.51	0.85
18	aconitoyl formate, <b>9</b>	2H (3.20 ppm)	0.26	0.26	0.43
19	citroyl formate, <b>10</b>	4H (2.60 ppm 1H) <sup>b</sup>	0.16	0.08	0.13
20	di-DHKG <sup>1</sup>	1H (6.80 ppm)	0.10	0.20	0.33
21	acetate	3H (1.77 ppm)	3.01	2.04	3.40
Total	excluding SM and glycine, glycolate			<b>27.78</b>	<b>46.29</b>
Total	including glycine and glycolate			<b>29.29</b>	<b>47.55</b>

<sup>a</sup>Additional products are visible by NMR but their identities could not be elucidated. Yields are calculated relative to initial oxaloacetate concentration (60 mM), except glyoxylate, glycine and glycolate, where yields are given relative to the initial glyoxylate concentration (120 mM).

<sup>b</sup>Due to overlapping peaks, only the specified portion of the signal could be integrated, and the resulting concentration was calculated accordingly.

**Table S21.** Oxaloacetate/glyoxylate reaction network with Pd/C and ammonium bicarbonate under H<sub>2</sub> (5 bar).<sup>a</sup>

Product quantification ( <sup>1</sup> H qNMR)					
Entry	Compound	Signal integrated	Integrals relative to DMS (6H) concentration (14.86 mM)	Concentration (mM)	Yield (%)
1	glyoxylate, <b>2</b>	1H	-	-	-
2	glycine, <b>2a</b>	2H (3.39 ppm)	7.44	5.53	4.61
3	glycolate, <b>2b</b>	2H (3.80 ppm)	2.81	2.10	1.75
4	oxaloacetate, <b>3</b>	2H	-	-	-
5	aspartate, <b>3a</b>	2H (2.67 ppm 1/8 of 2H) <sup>b</sup>	1.2	0.89	1.48
6	malate, <b>3b</b>	2H (2.19 ppm 1/8 of 2H) <sup>b</sup>	7.84	5.83	9.72
7	pyruvate, <b>4</b>	3H (2.22 ppm)	5.34	2.65	4.42
8	alanine, <b>4a</b>	3H	-	-	-
9	lactate, <b>4b</b>	3H (1.17-1.19 ppm)	0.47	0.23	0.38
10	maloyl formate, <b>5</b>	2H (2.91-2.97 ppm, 1H) <sup>b</sup>	32.9	24.44	40.73
11	fumaroyl formate, <b>6</b>	2H	-	-	-
12	α-ketoglutarate, <b>7</b>	2H (2.84-2.87 ppm)	9.40	6.98	11.63
13	glutamate, <b>7a</b>	2H	-	-	-
15	hydroxyketoglutarate, <b>7b</b>	1H	-	-	-
16	succinate	4H	-	-	-
17	isocitroyl formate, <b>8</b> diastereoisomer (erythro)	1H (4.37-4.38 ppm)	0.24	0.36	0.60
18	aconitoyl formate, <b>9</b>	2H (3.21 ppm)	0.34	0.25	0.42
19	citroyl formate, <b>10</b>	4H (2.59 ppm 1H) <sup>b</sup>	0.84	0.31	0.52
20	di-DHKG <sup>1</sup>	1H (6.80 ppm)	-	-	-
21	acetate	3H (1.77 ppm)	6.27	3.11	5.18
Total	excluding SM and glycine, glycolate			<b>45.05</b>	<b>75.08</b>
Total	including glycine and glycolate			<b>52.68</b>	<b>81.44</b>

<sup>a</sup>Additional products are visible by NMR but their identities could not be elucidated. Yields are calculated relative to initial oxaloacetate concentration (60 mM), except glyoxylate, glycine and glycolate, where yields are given relative to the initial glyoxylate concentration (120 mM).

<sup>b</sup>Due to overlapping peaks, only the specified portion of the signal could be integrated, and the resulting concentration was calculated accordingly.

**Table S22.** Oxaloacetate/glyoxylate reaction network with ammonium formate without Pd/C.<sup>a</sup>

Product quantification ( <sup>1</sup> H qNMR)					
Entry	Compound	Signal integrated	Integrals relative to DMS (6H) concentration (14.86 mM)	Concentration (mM)	Yield (%)
1	glyoxylate, <b>2</b>	1H (4.93 ppm)	23.73	35.26	29.38
2	glycine, <b>2a</b>	2H	-	-	-
3	glycolate, <b>2b</b>	2H (3.80 ppm)	0.88	0.65	0.54
4	pyruvate, <b>4</b>	3H (2.22 ppm)	4.01	1.99	3.32
5	maloyl formate, <b>5</b>	2H (3.06-3.11 ppm, 1H) <sup>b</sup>	75.78	56.30	93.83
6	fumaroyl formate, <b>6</b>	2H (6.62-6.74 ppm)	1.58	1.17	1.95
7	α-ketoglutarate, <b>7</b>	2H	-	-	-
8	di-DHKG <sup>1</sup>	1H (6.80 ppm)	0.19	0.28	0.47
9	acetate	3H (1.77 ppm)	4.21	2.09	3.48
Total	excluding SM glyoxylate			<b>62.48</b>	<b>103.05</b>
Total	excluding SM, glycine, glycolate.			<b>61.83</b>	<b>103.59</b>

<sup>a</sup>Yields are calculated relative to initial oxaloacetate concentration (60 mM), except glyoxylate, glycine and glycolate, where yields are given relative to the initial glyoxylate concentration (120 mM).<sup>b</sup>Only one portion of the signal corresponding to maloyl formate was integrated and resulting value adjusted accordingly.

**Table S23.** Oxaloacetate/glyoxylate reaction network with ammonium bicarbonate without Pd/C under H<sub>2</sub> (5 bar).<sup>a</sup>

Product quantification ( <sup>1</sup> H qNMR)					
Entry	Compound	Signal integrated	Integrals relative to DMS (6H) concentration (20.68 mM)	Concentration (mM)	Yield (%)
1	glyoxylate, <b>2</b>	1H	-	-	-
2	glycine, <b>2a</b>	2H (3.40 ppm)	0.42	0.43	0.36
3	glycolate, <b>2b</b>	2H (3.80 ppm)	1.82	1.88	1.57
4	pyruvate, <b>4</b>	3H (2.22 ppm)	2.62	1.81	3.02
5	maloyl formate, <b>5</b>	2H (3.10 ppm, 1/6 of 2H) <sup>b</sup>	13.26	13.71	22.85
6	fumaroyl formate, <b>6</b>	2H	-	-	-
7	α-ketoglutarate, <b>7</b>	2H	-	-	-
8	di-DHKG <sup>1</sup>	1H	-	-	-
9	acetate	3H (1.77 ppm)	2.55	1.76	2.93
Total	excluding SM glyoxylate			<b>19.59</b>	<b>30.73</b>
Total	excluding SM, glycine, glycolate			<b>17.28</b>	<b>28.80</b>

<sup>a</sup>Yields are calculated relative to initial oxaloacetate concentration (60 mM), except glyoxylate, glycine and glycolate, where yields are given relative to the initial glyoxylate concentration (120 mM).

<sup>b</sup>Only a 1/6 portion of the signal corresponding to maloyl formate could be integrated and the resulting concentration was calculated accordingly.

**Table S24.**  $\alpha$ -KG and glyoxylate reaction in the presence of ammonium formate without Pd/C.<sup>a</sup>

Product quantification ( <sup>1</sup> H qNMR)					
Entry	Compound	Signal integrated	Integrals relative to DMS (6H) concentration (29.00 mM)	Concentration (mM)	Yield (%)
1	glyoxylate, <b>2</b>	1H (4.93 ppm)	5.75	16.68	27.8
2	glycine, <b>2a</b>	2H (3.41 ppm)	0.18	0.26	0.43
3	glycolate, <b>2b</b>	2H (3.80 ppm)	0.35	0.51	0.85
4	$\alpha$ -ketoglutarate, <b>7</b>	2H (2.84-2.87 ppm)	22.97	33.31	55.52
5	succinate	4H (2.27 ppm)	0.35	0.25	0.42
6	isocitroyl formate, <b>8</b> diastereoisomer (erythro)	1H (4.38-4.38 ppm)	1.70	4.93	8.22
7	isocitroyl formate, <b>8</b> diastereoisomer (threo)	1H (4.25-4.26 ppm)	0.59	1.71	2.85
8	aconitoyl formate, <b>9</b>	2H (3.21 ppm)	0.52	0.75	1.25
Total	excluding SM			<b>8.41</b>	<b>14.02</b>
Total	excluding SM and glycine, glycolate			<b>7.64</b>	<b>12.74</b>

<sup>a</sup>Yields are calculated relative to initial  $\alpha$ -ketoglutarate/glyoxylate concentration (60 mM).

**Table S25.**  $\alpha$ -KG and glyoxylate reaction in the presence of ammonium bicarbonate without Pd/C under H<sub>2</sub> (5 bar).<sup>a</sup>

Product quantification ( <sup>1</sup> H qNMR)					
Entry	Compound	Signal integrated	Integrals relative to DMS (6H) concentration (20.68 mM)	Concentration (mM)	Yield (%)
1	glyoxylate, <b>2</b>	1H	-	-	-
2	glycine, <b>2a</b>	2H (3.41 ppm)	0.03	0.03	0.07
3	glycolate, <b>2b</b>	2H (3.80 ppm)	1.20	1.24	2.07
4	$\alpha$ -ketoglutarate, <b>7</b>	2H (2.84-2.87 ppm)	10.20	10.55	17.58
5	succinate	4H (2.27 ppm)	0.11	0.06	0.10
6	isocitroyl formate, <b>8</b> diastereoisomer (erythro)	1H (4.38-4.38 ppm)	3.07	6.35	10.58
7	isocitroyl formate, <b>8</b> diastereoisomer (threo)	1H (4.24-4.25 ppm)	1.40	2.90	4.83
8	aconitoyl formate, <b>9</b>	2H (3.20 ppm)	0.16	0.16	0.25
Total	excluding SM			<b>10.74</b>	<b>17.9</b>
Total	excluding SM and glycine, glycolate			<b>9.47</b>	<b>15.76</b>

<sup>a</sup>Yields are calculated relative to initial  $\alpha$ -ketoglutarate/glyoxylate concentration (60 mM).

**Table S26.** Reductive amination with different Pd catalysts using pyruvate as a model substrate.<sup>a</sup>

Entry	Catalyst mol % (mg)	Solvent	pH	DMS stock (mM)	Product quantification ( <sup>1</sup> H qNMR)		
					Integrals relative to DMS (6H)	Concentration (mM)	Yield (%)
1	<b>Pd/Al<sub>2</sub>O<sub>3</sub> 5 wt% (Sigma)</b>  <b>1 mol % (0.64 mg)</b>	water	7-8	10.46	alanine (3H)	39.18	45.53
					lactate (3H)	8.54	9.93
					starting material (3H)	17.09	19.87
					<b>total</b>	<b>22.6</b>	<b>75.33</b>
2	<b>Pd/C 10 wt% (synthesized)</b>  <b>1 mol% (0.32 mg)</b>	water	7-8	10.46	alanine (3H)	15.3	17.77
					lactate (3H)	3.29	3.83
					starting material (3H)	31.30	36.37
					<b>total</b>	<b>17.39</b>	<b>57.97</b>
3	<b>PdO/C 10 wt% (synthesized)</b>  <b>1 mol% (0.37 mg)</b>	water	7-8	10.46	alanine (3H)	18.82	21.87
					lactate (3H)	1.66	1.93
					starting material (3H)	32.72	38.03
					<b>total</b>	<b>18.55</b>	<b>61.83</b>

4	<b>PdO (Sigma)</b>  <b>1 mol%, (0.036 mg)</b>	water	7-8	34	alanine (3H)	-	-	-
					lactate (3H)	-	-	-
					starting material (3H)	24.68	27.97	93.23
					<b>total</b>		<b>27.97</b>	<b>93.23</b>
5	<b>PdO (Sigma)</b>  <b>20 mol%, (0.73 mg)</b>	water	7-8	29	alanine (3H)	8.88	8.58	28.6
					lactate (3H)	1.12	1.08	3.60
					starting material (3H)	12.11	11.71	39.03
					<b>total</b>		<b>21.37</b>	<b>71.23</b>
6	<b>Pd/C 10 wt% (TCI) 1 mol%</b>	water	7-8	28	alanine (3H)	7.47	20.92	69.72
					lactate (3H)	0.65	1.82	6.07
					starting material (3H)	1.74	4.87	16.24
					<b>total</b>		<b>27.61</b>	<b>92.03</b>
7	<b>Pd/C 10 wt% (Sigma) 1 mol%</b>	water	7-8	28	alanine (3H)	24.02	23.23	77.43
					lactate (3H)	0.91	0.87	2.90
					starting material (3H)	1.52	1.48	4.93
					<b>total</b>		<b>25.58</b>	<b>85.27</b>
8	<b>Meteorite (Gibeon)<sup>b</sup> 5 mg</b>	water	7-8	21	alanine (3H)	0.65	<b>0.07</b>	<b>3.03</b>
					lactate (3H)	0.07	<b>0.05</b>	<b>0.16</b>
					starting material (3H)	39.78	<b>27.85</b>	<b>92.82</b>
					<b>total</b>		<b>27.97</b>	<b>92.95</b>

<sup>a</sup>Yields are calculated relative to initial  $\alpha$ -ketoglutarate/glyoxylate concentration (60 mM).

<sup>b</sup> Gibeon from Namibia (year 1836) containing Ni and Co (7.93% and 0.41 %) and iridium and rhodium in 2 ppm levels. The meteorite consist mainly of iron. It should be noted that the composition between pieces of the same meteorite and in a meteorite piece itself is not homogeneously distributed. For ore details see reference 195

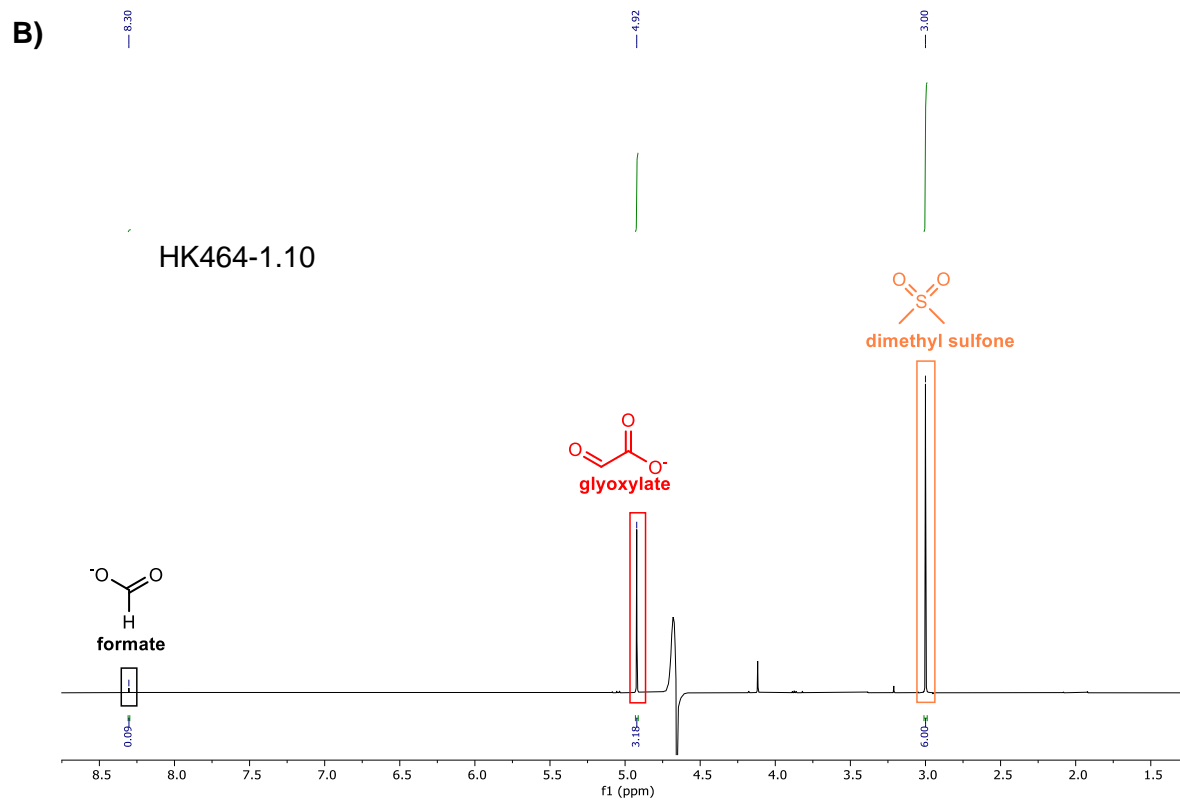
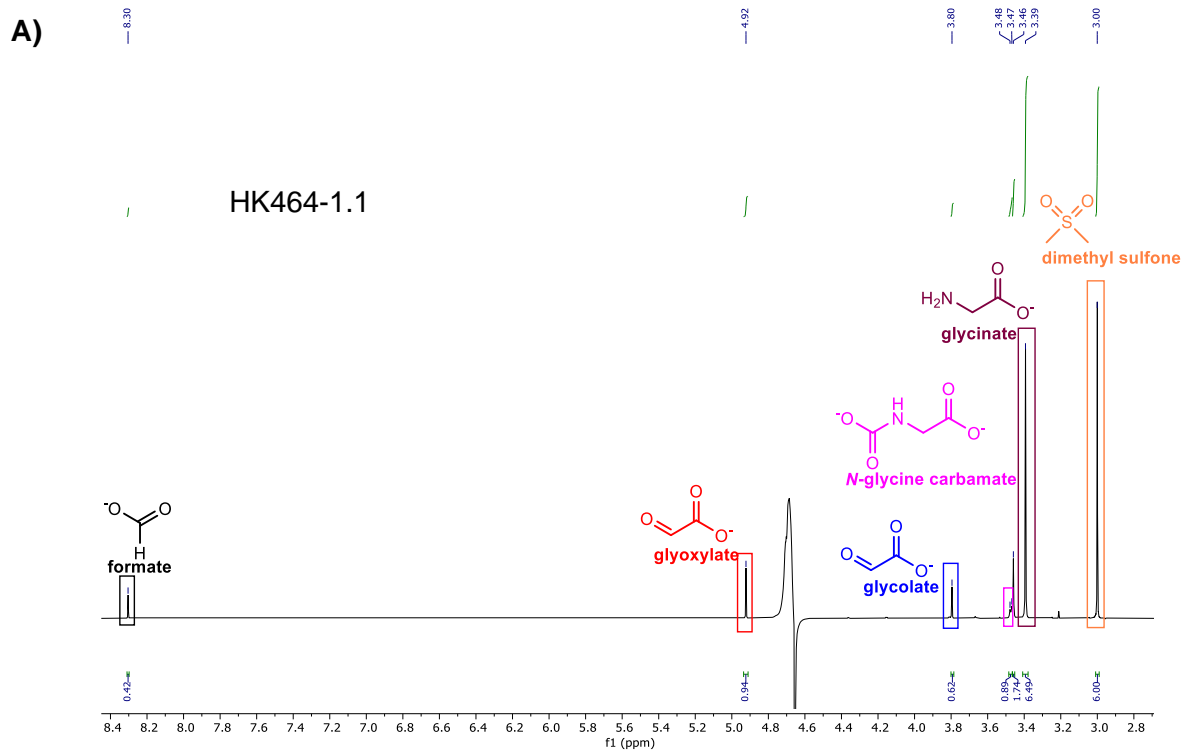


**Figure S4.**  $^1\text{H}$  NMR of reductive amination of glyoxylate under  $\text{H}_2/\text{NH}_4\text{HCO}_3$   
**A)** with Pd/C; **B)** control without Pd/C.

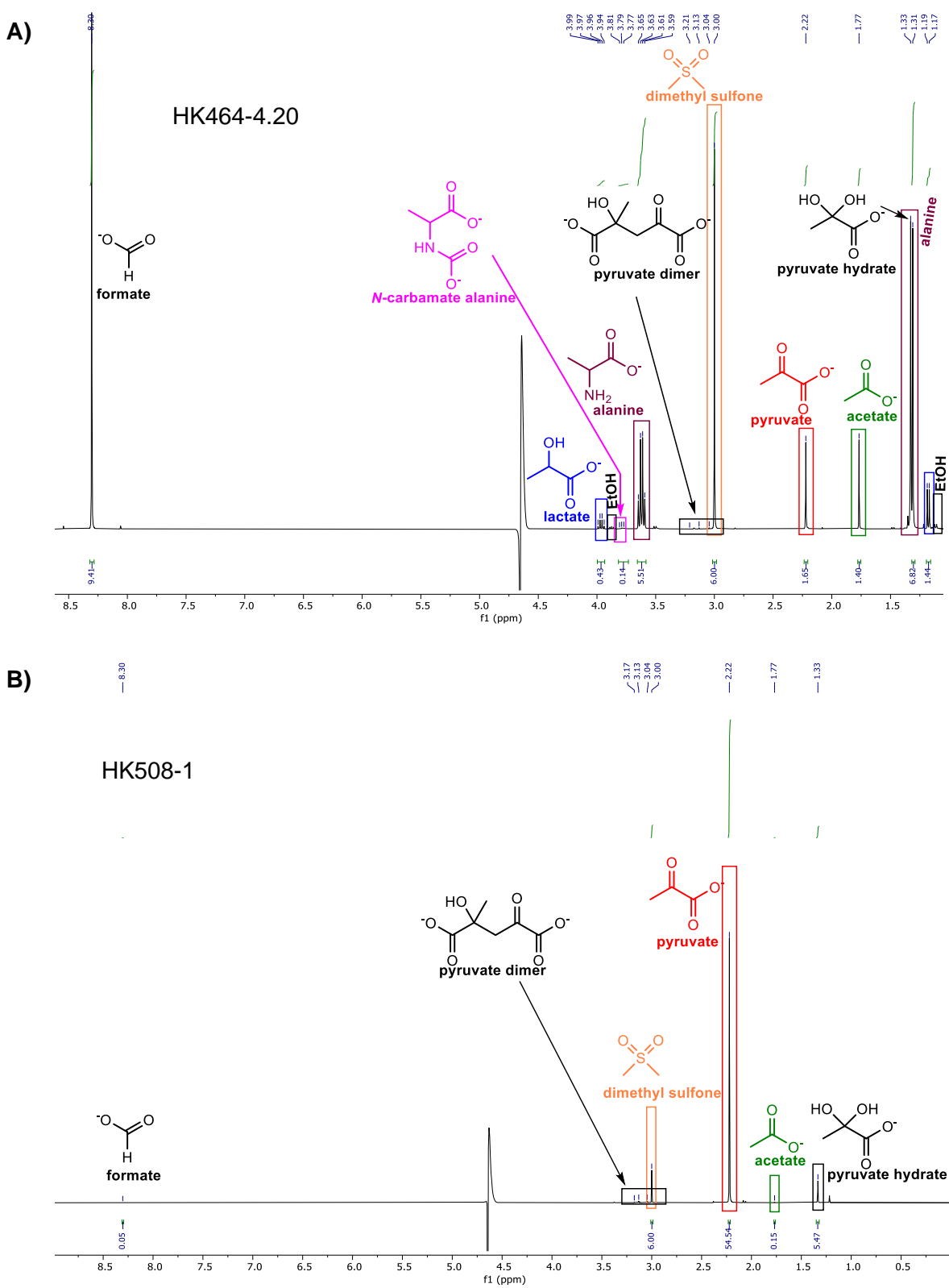


**Figure S5.**  $^1\text{H}$  NMR of reductive amination of pyruvate under  $\text{H}_2/\text{NH}_4\text{HCO}_3$   
**A)** with Pd/C; **B)** control without Pd/C.



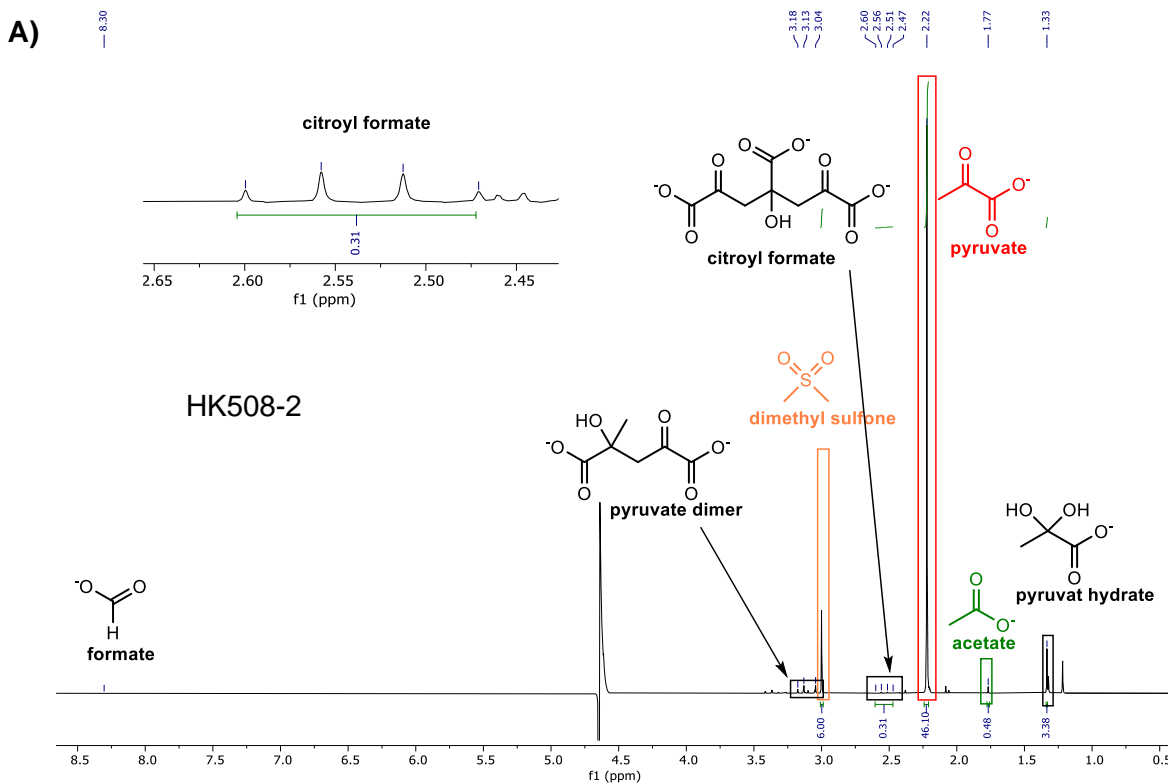
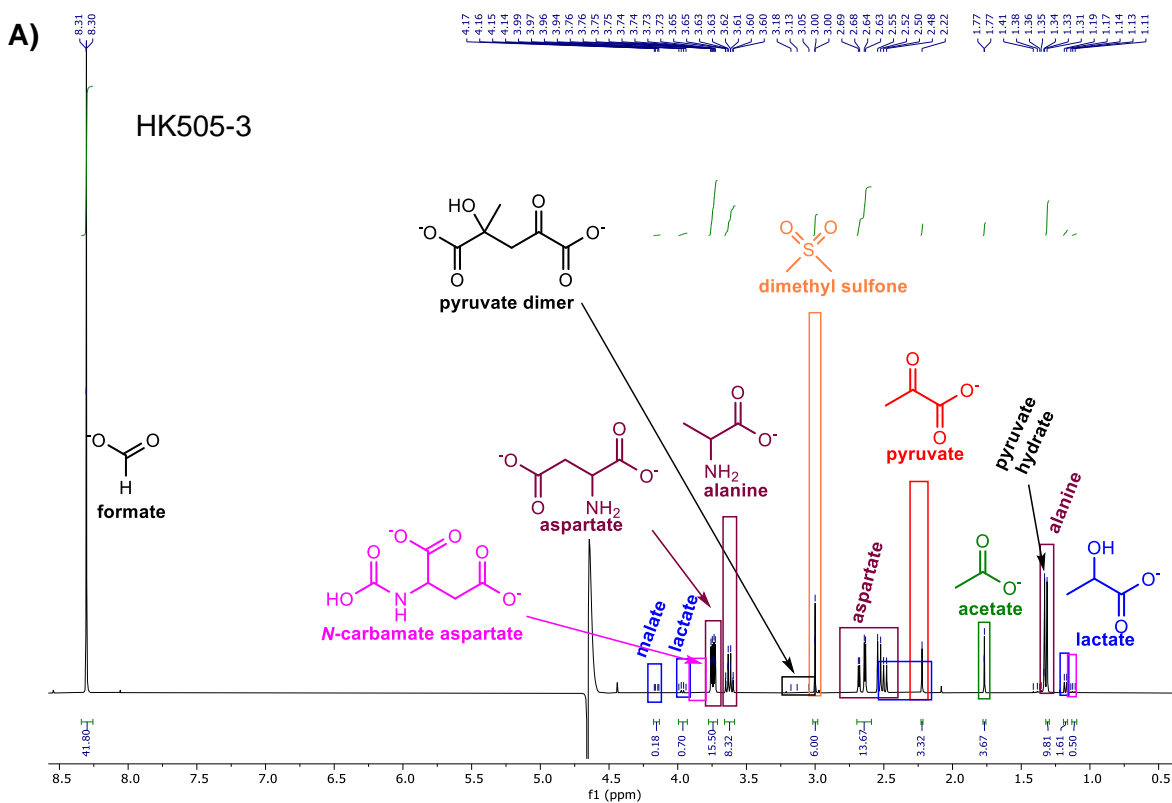


**Figure S6.**  $^1\text{H}$  NMR of reductive amination of oxaloacetate under  $\text{H}_2/\text{NH}_4\text{HCO}_3$   
**A)** with Pd/C; **B)** control without Pd/C.

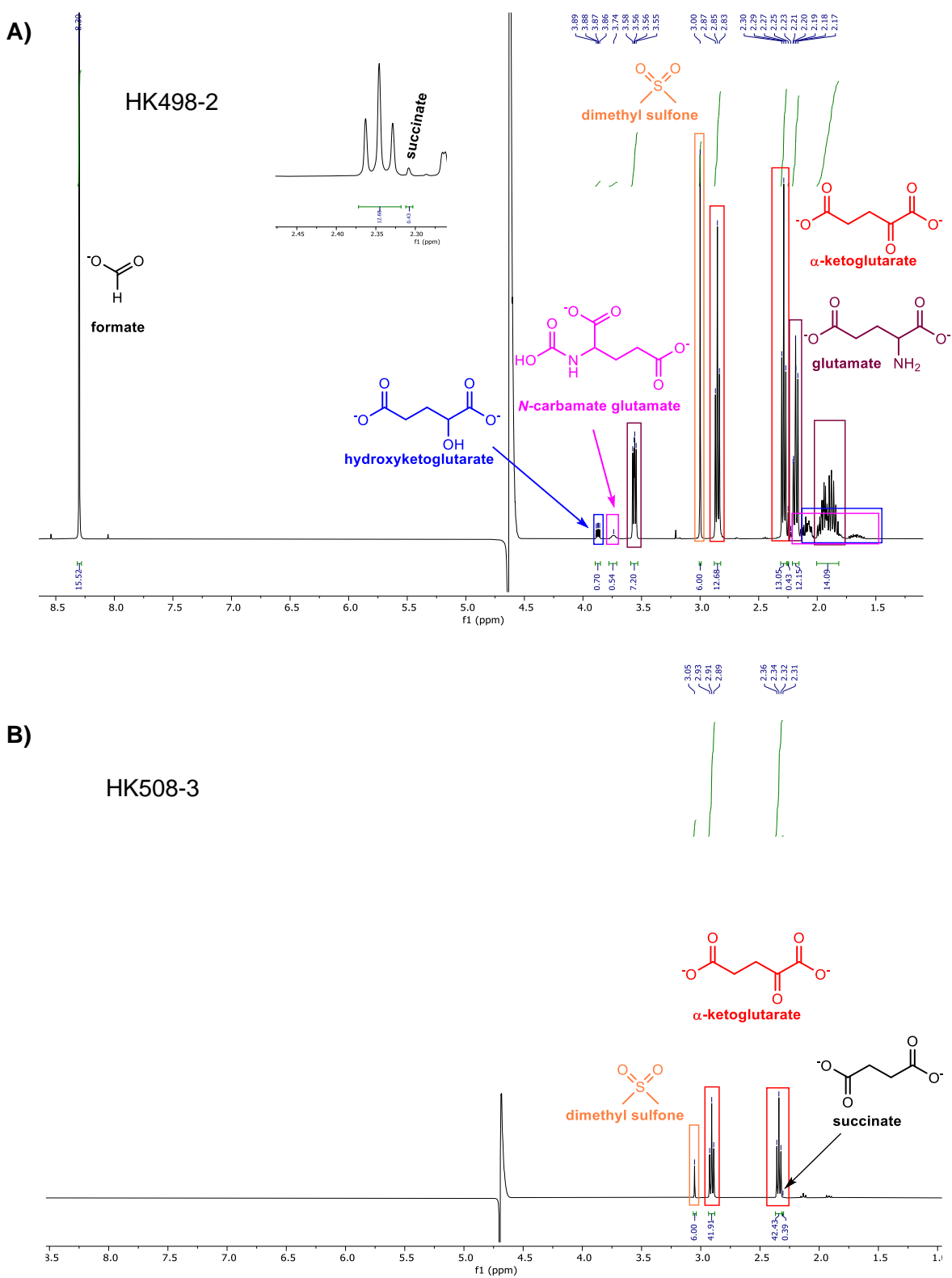


**Figure S7.**  $^1\text{H}$  NMR of reductive amination of  $\alpha$ -ketoglutarate under  $\text{H}_2/\text{NH}_4\text{HCO}_3$  **A)** with Pd/C; **b)** control without Pd/C.

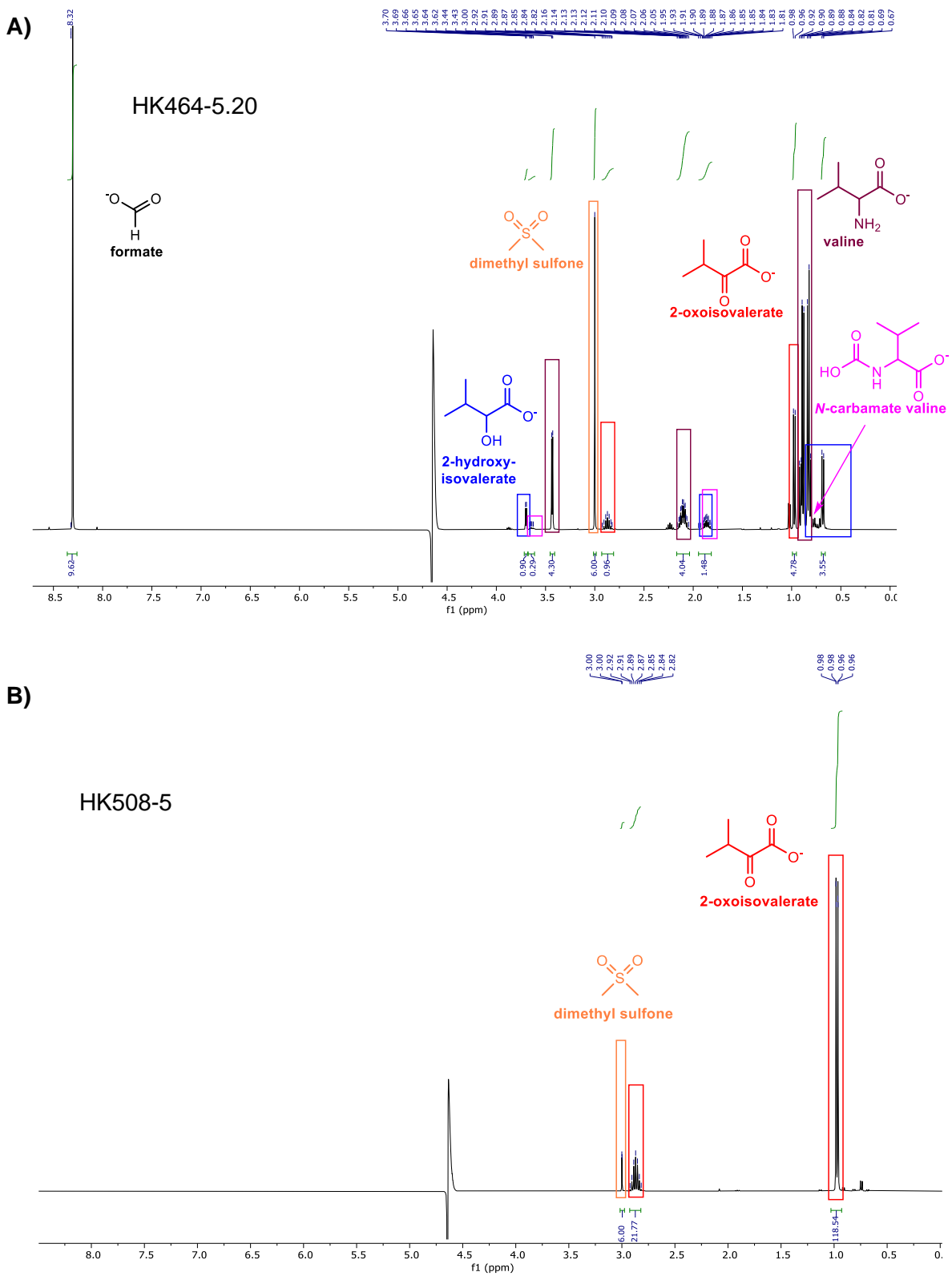


**Figure S8.**  $^1\text{H}$  NMR of reductive amination of 2-oxoisovalerate under  $\text{H}_2/\text{NH}_4\text{HCO}_3$   
**A)** with  $\text{Pd/C}$ ; **B)** control without  $\text{Pd/C}$ .

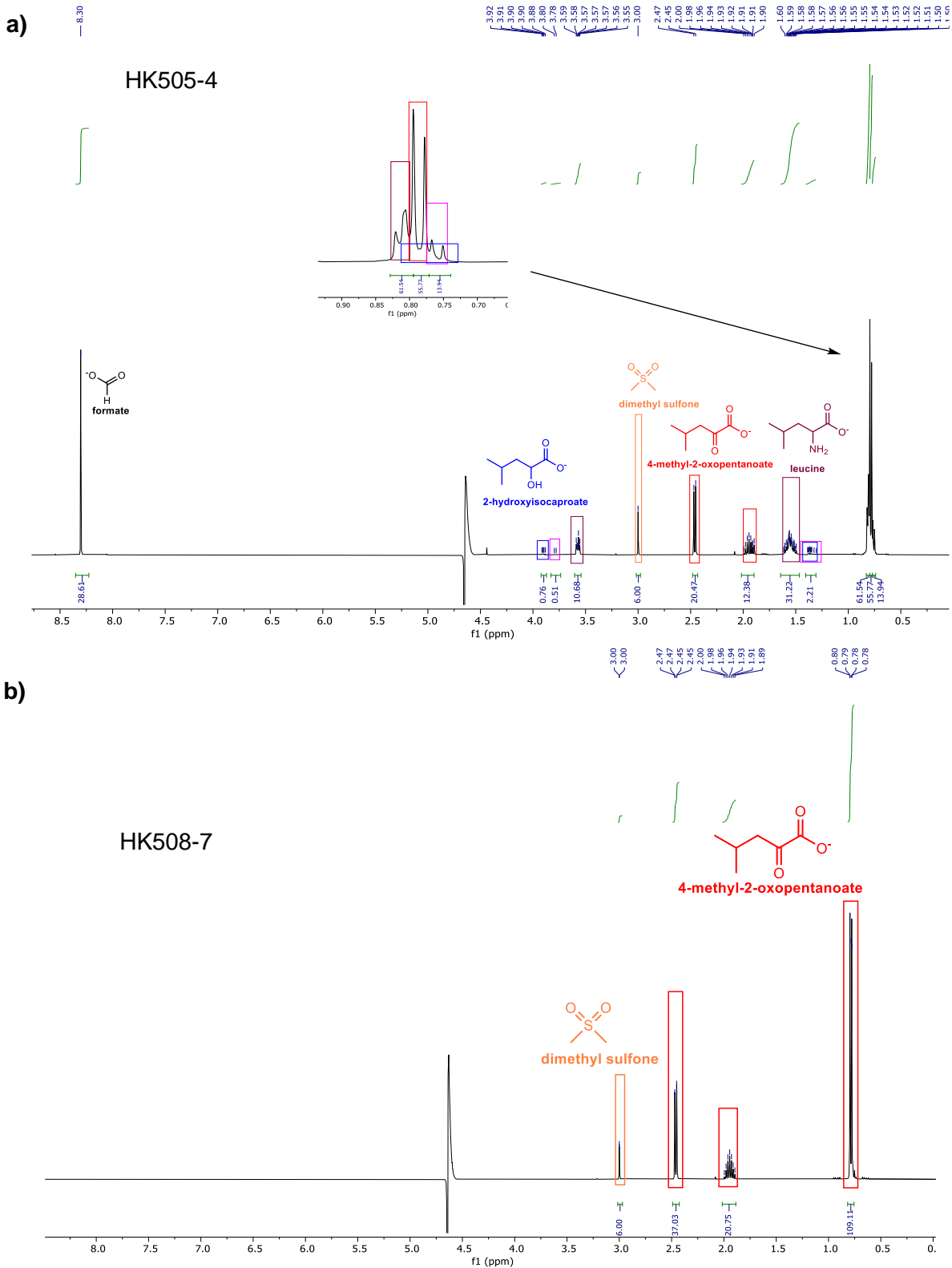


**Figure S9.**  $^1\text{H}$  NMR of reductive amination of 4-methyl-2-oxopentanoate under  $\text{H}_2/\text{NH}_4\text{HCO}_3$  **A)** with Pd/C; **B)** control without Pd/C.

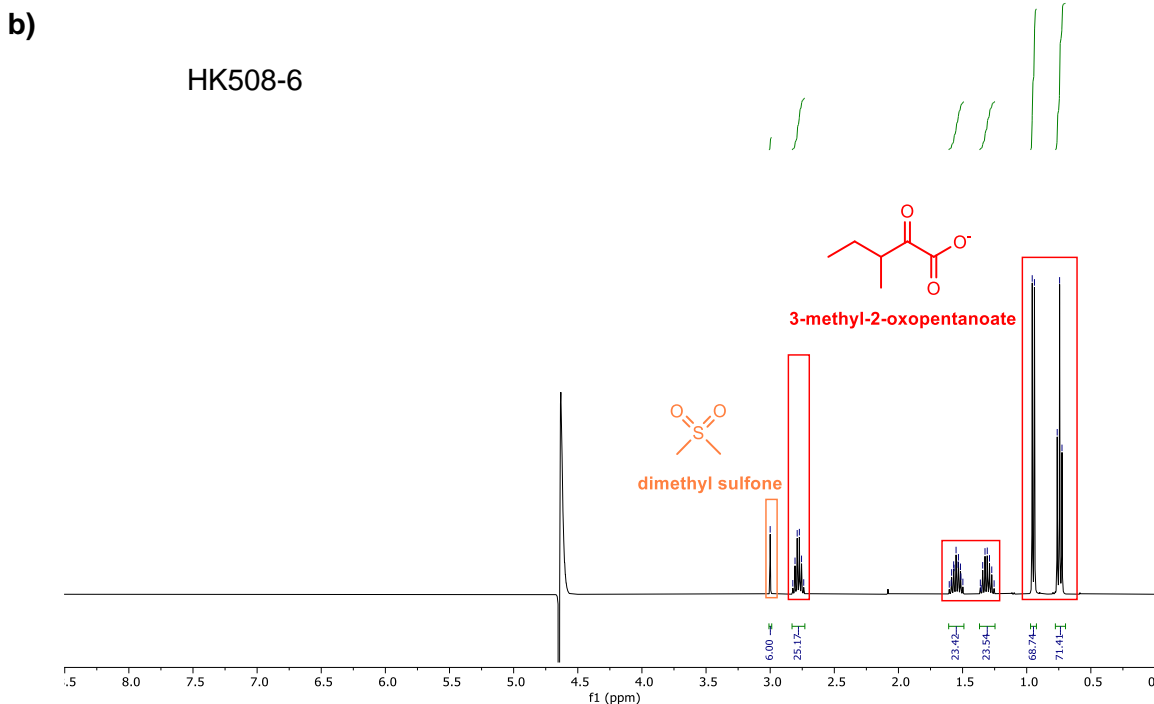
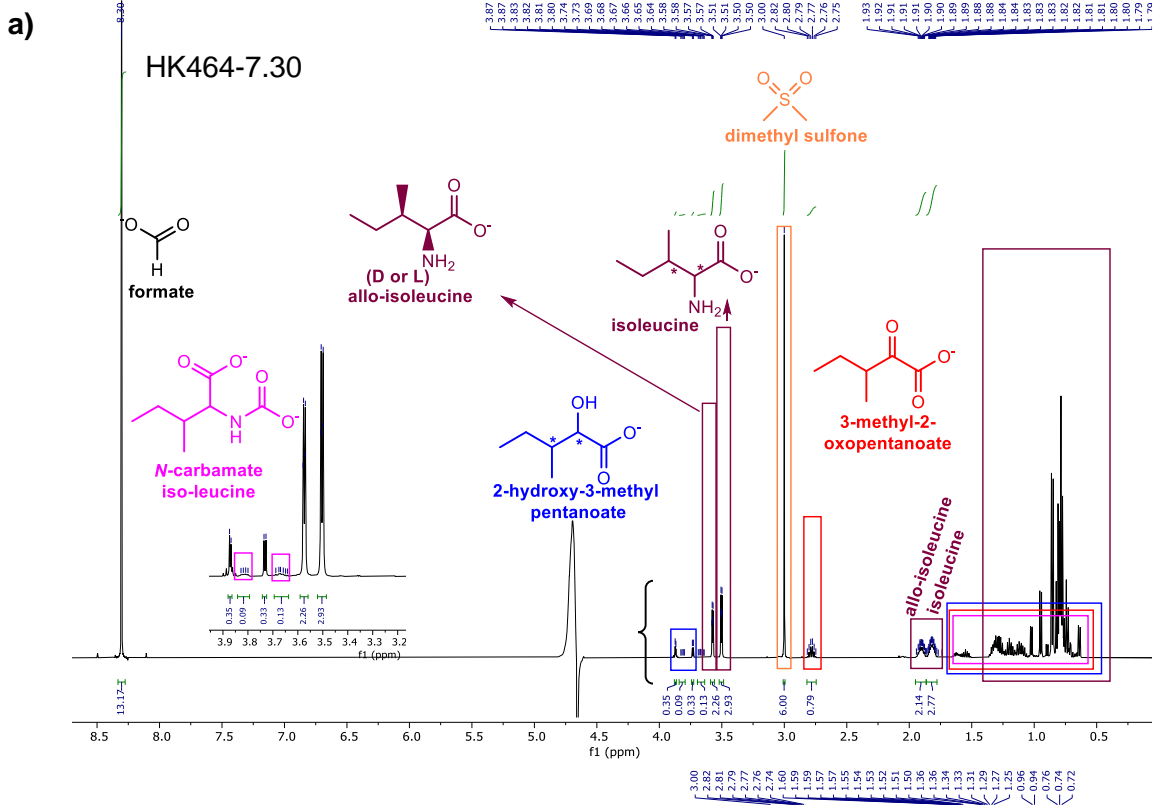


**Figure S10.**  $^1\text{H}$  NMR of reductive amination of 3-methyl-2-oxopentanoate under  $\text{H}_2/\text{NH}_4\text{HCO}_3$  a) with Pd/C; b) control without Pd/C

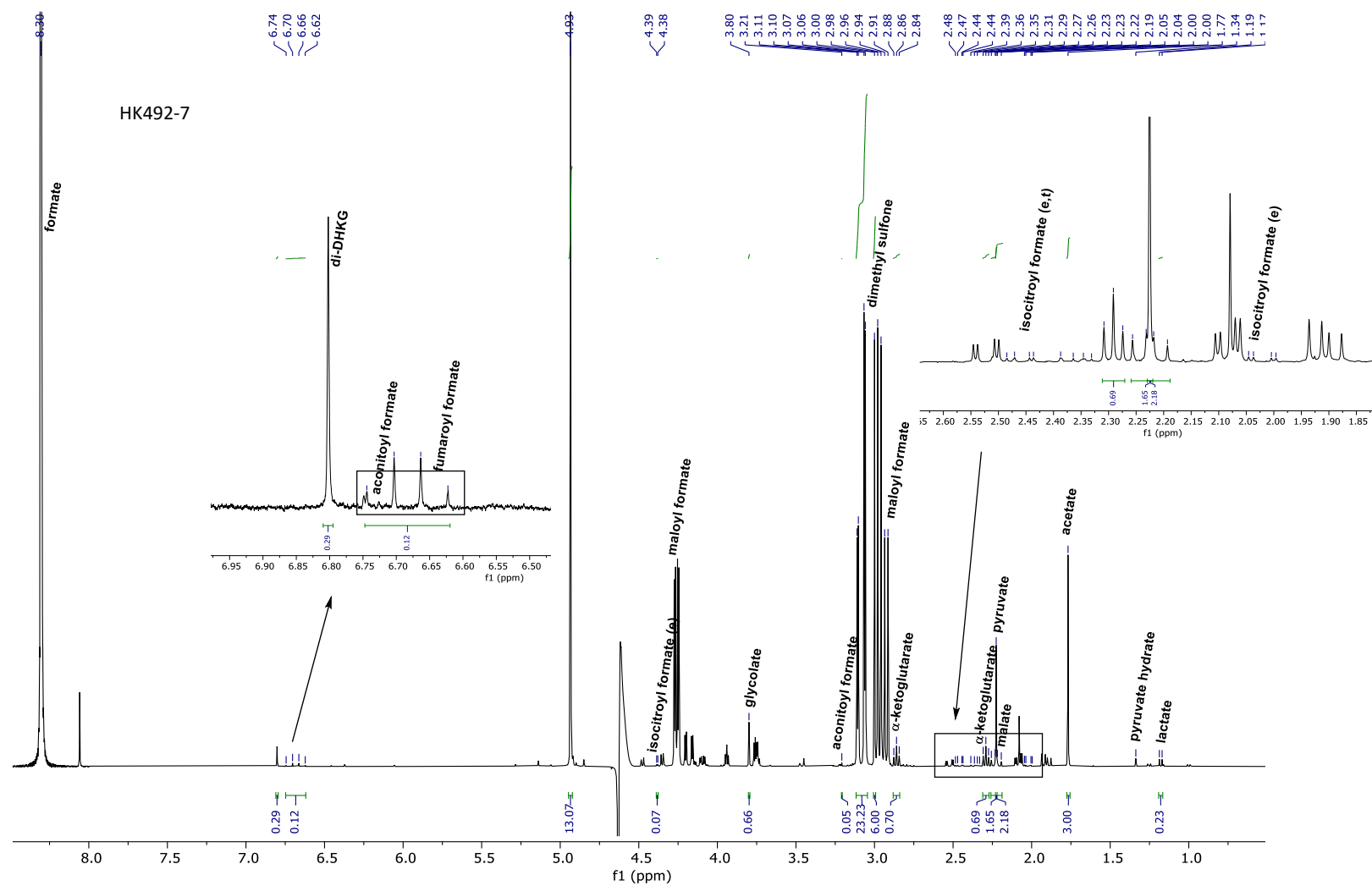


**Figure S11.**  $^1\text{H}$  NMR of reaction network with Pd/C and sodium formate.

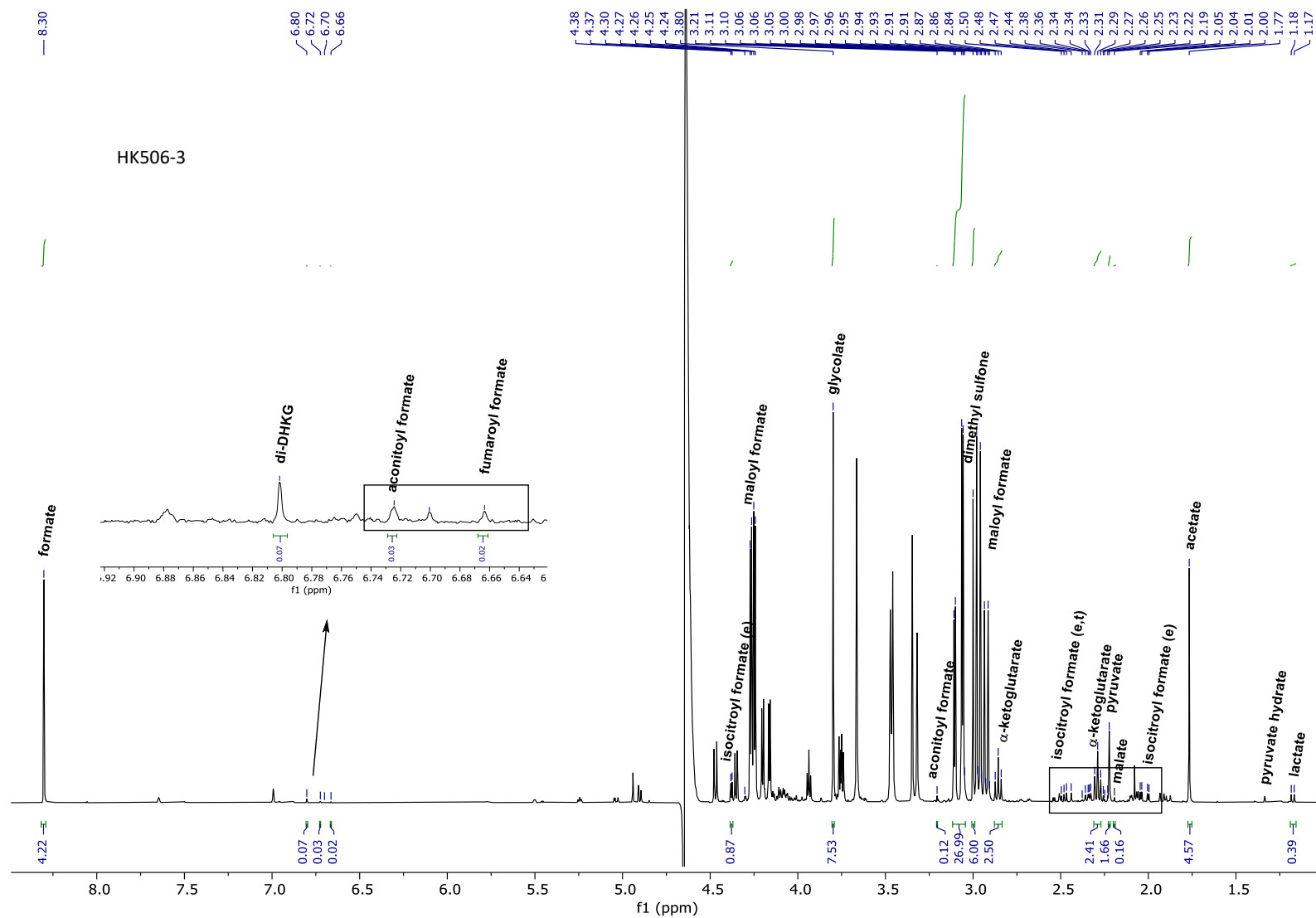


**Figure S13.**  $^1\text{H}$  NMR of reaction network with Pd/C and sodium bicarbonate under  $\text{H}_2$  (5 bar).

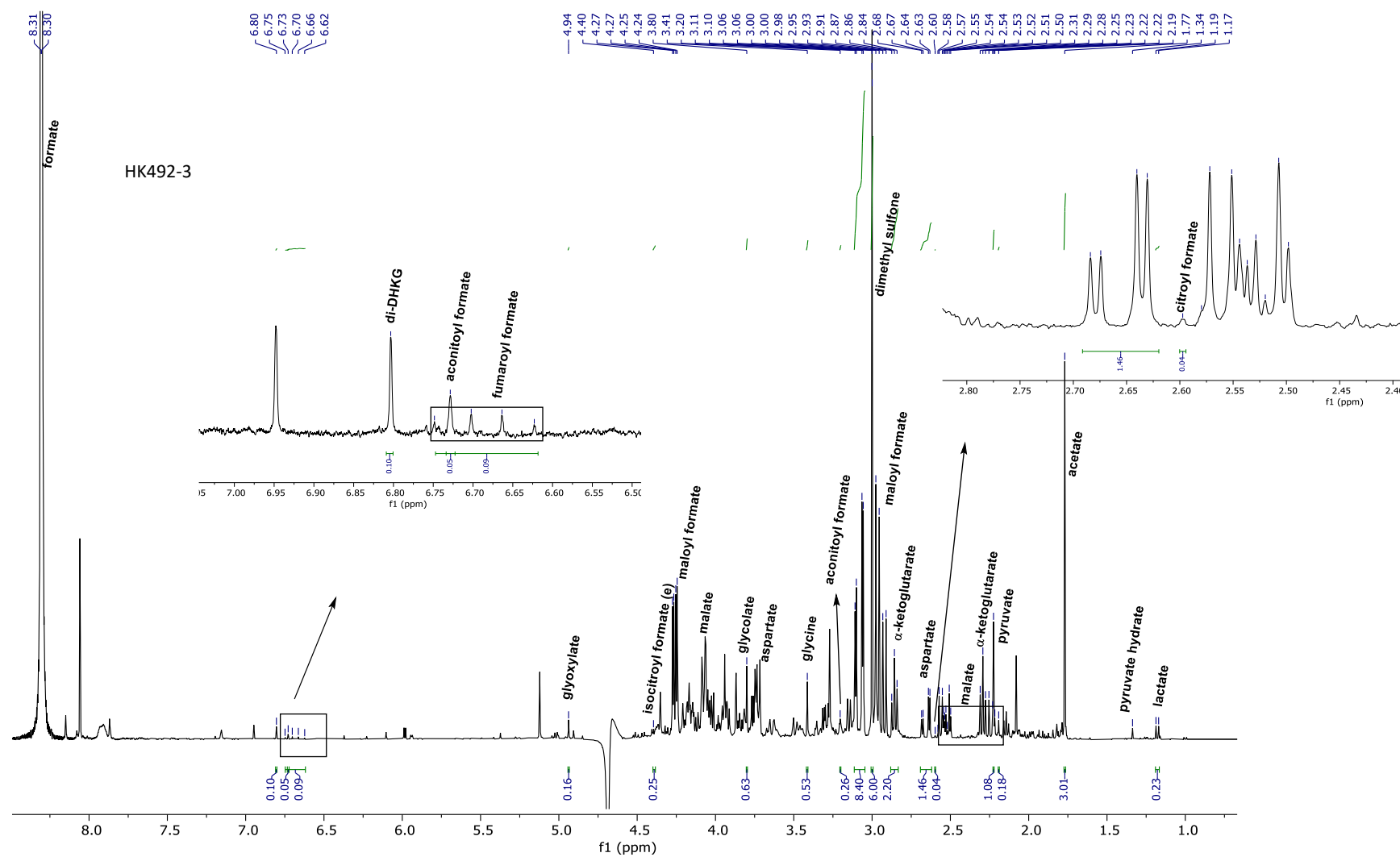


**Figure S12.** <sup>1</sup>H NMR of reaction network with Pd/C and ammonium formate. GC-MS spectra is shown in results and discussion section (Figure 32-IA).



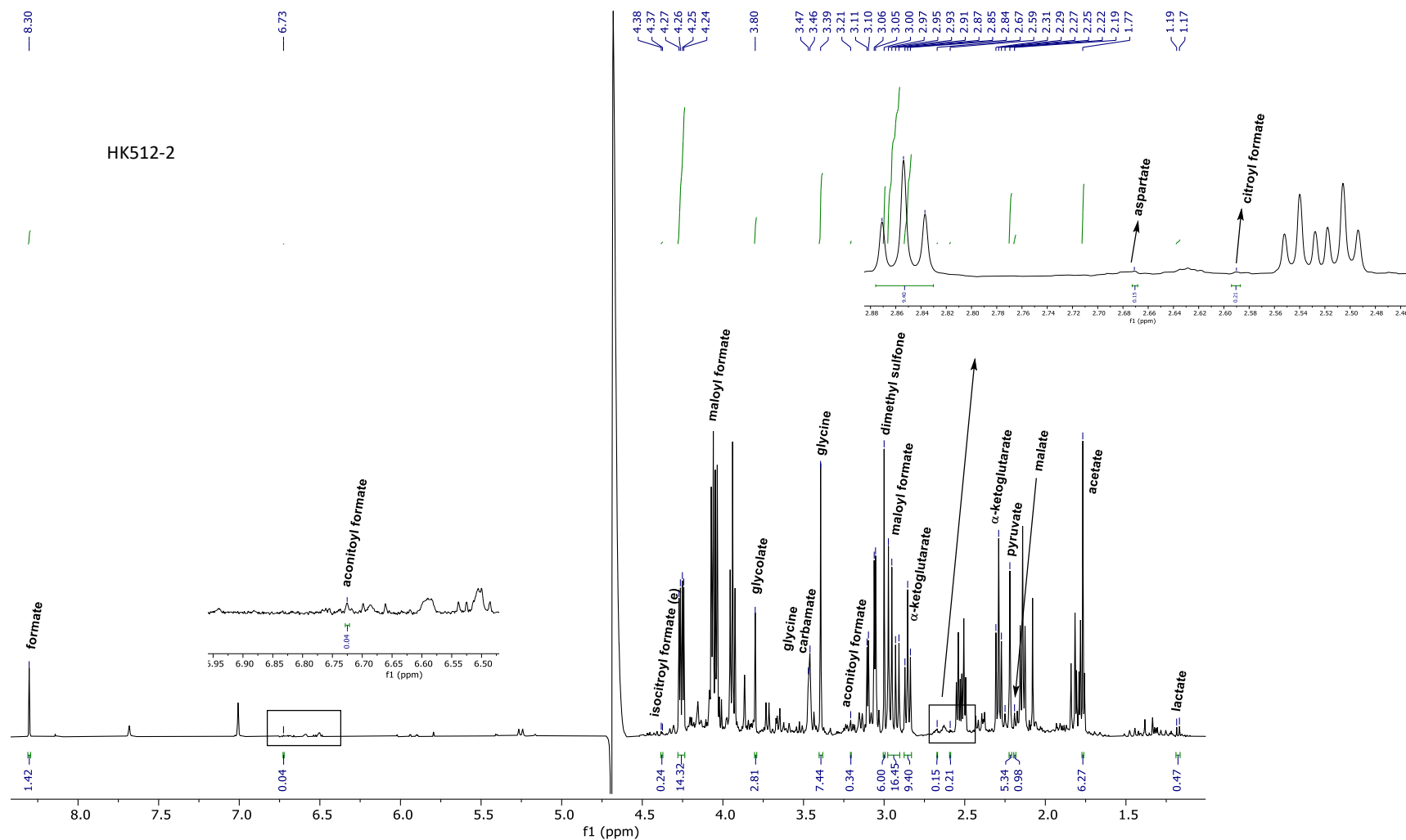


**Figure S14.**  $^1\text{H}$  NMR of reaction network with Pd/C and ammonium bicarbonate under  $\text{H}_2$  (5 bar). GC-MS spectra is shown in results and discussion section (Figure 32-IB).

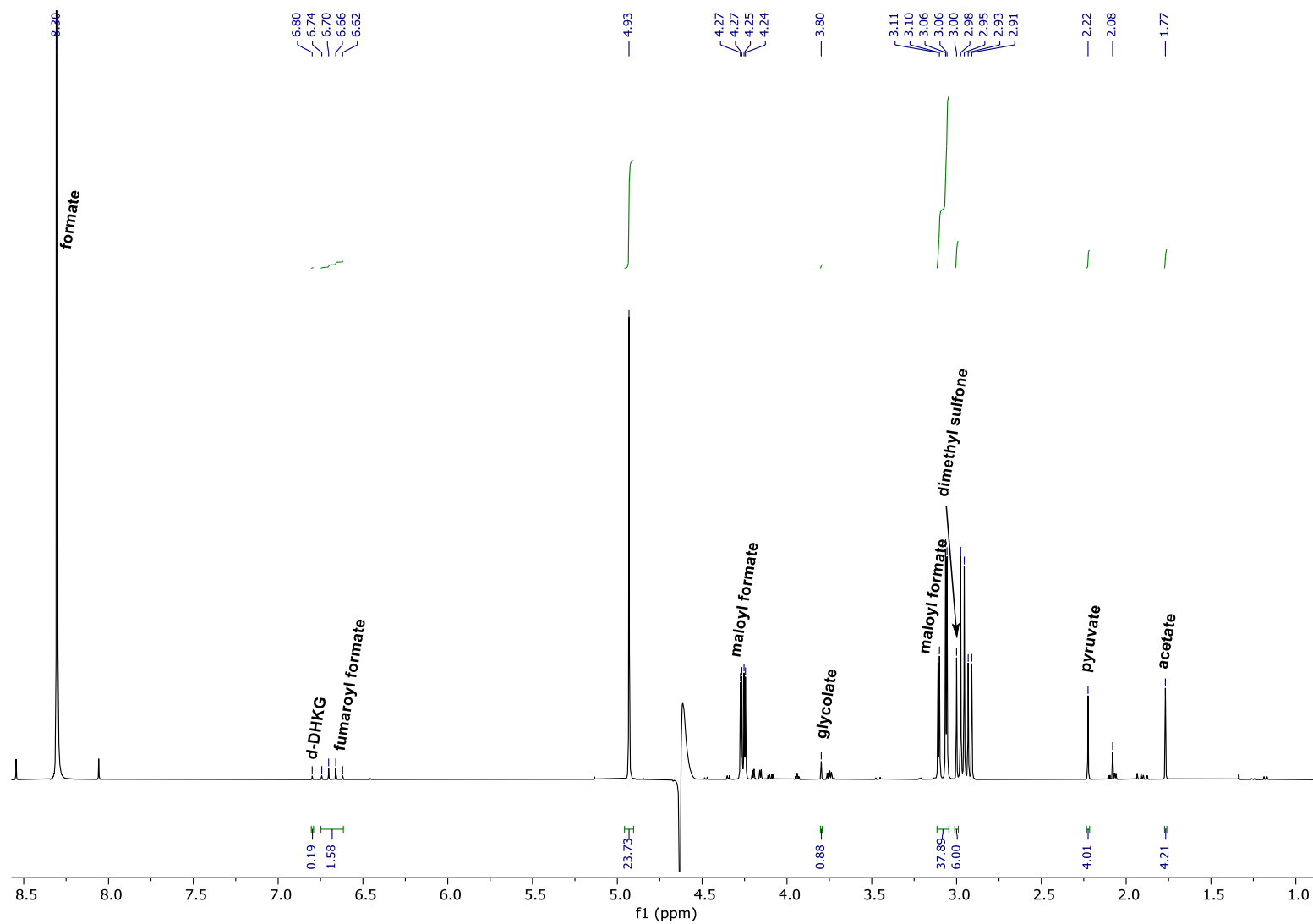


**Figure S15.**  $^1\text{H}$  NMR of reaction network with ammonium formate without Pd/C.

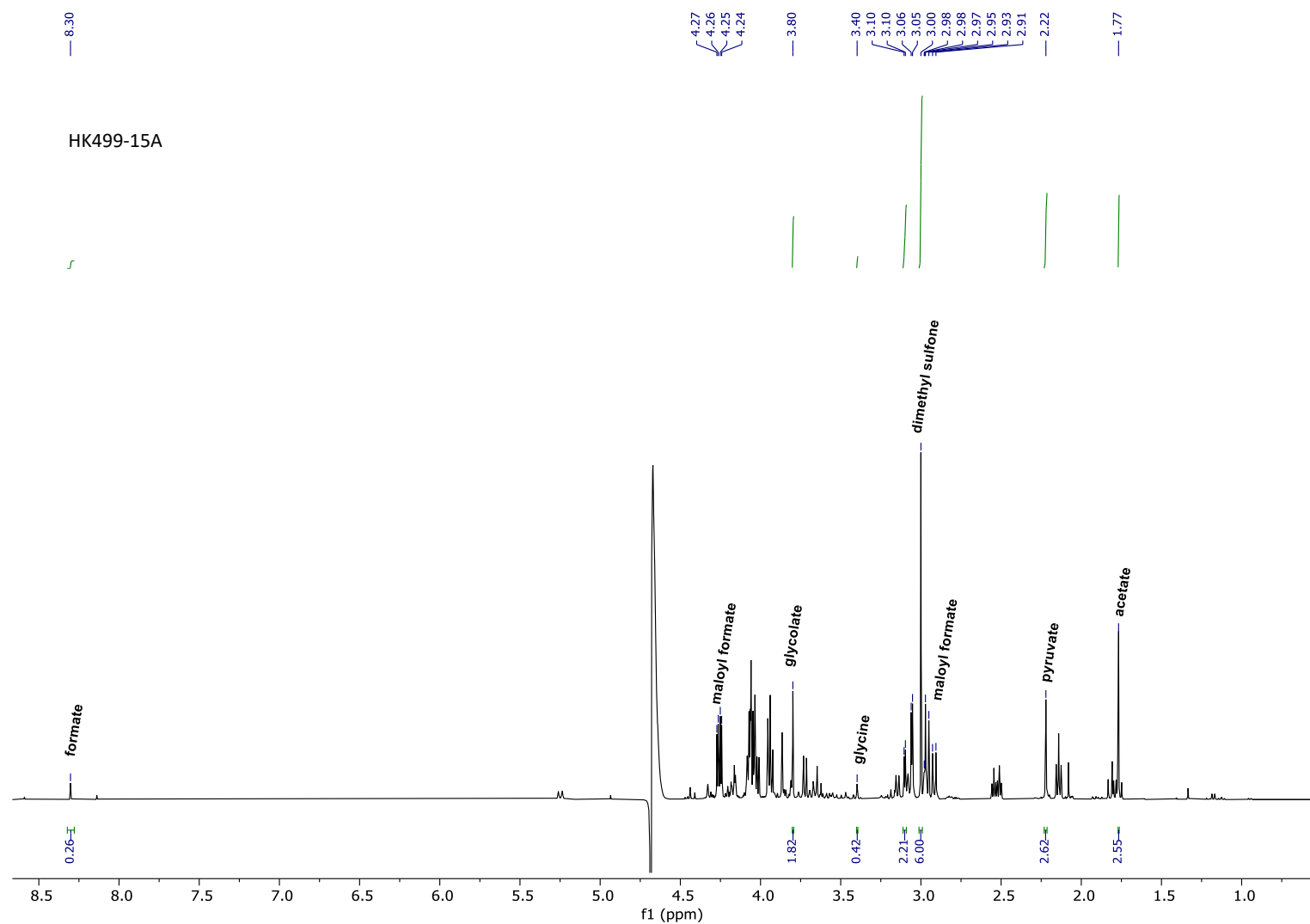


**Figure S16.**  $^1\text{H}$  NMR of reaction network with ammonium bicarbonate under  $\text{H}_2$  (5 bar) without Pd/C.

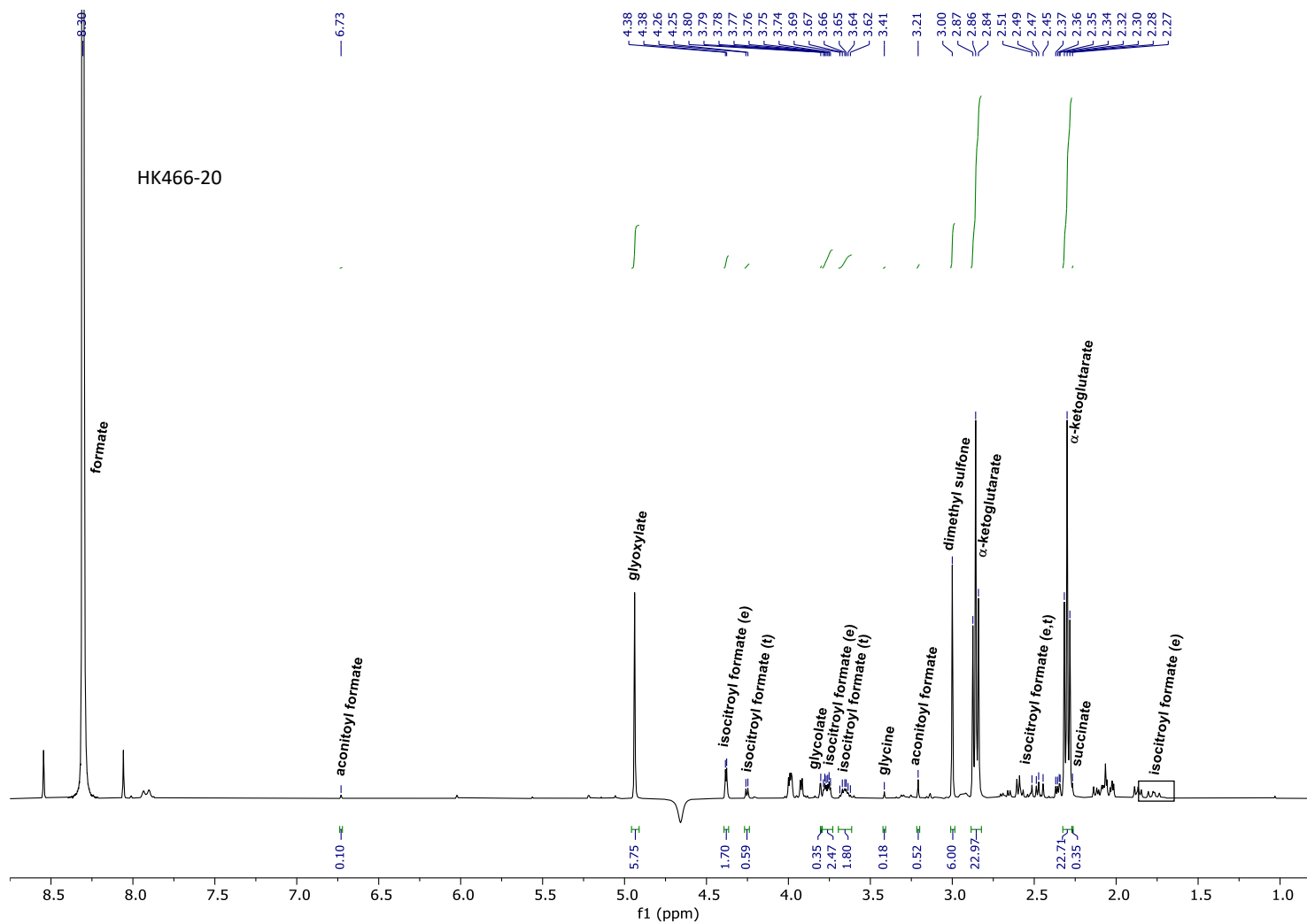


**Figure S17.**  $^1\text{H}$  NMR of reaction between  $\alpha$ -KG and glyoxylate in the presence of ammonium formate without  $\text{Pd/C}$ .

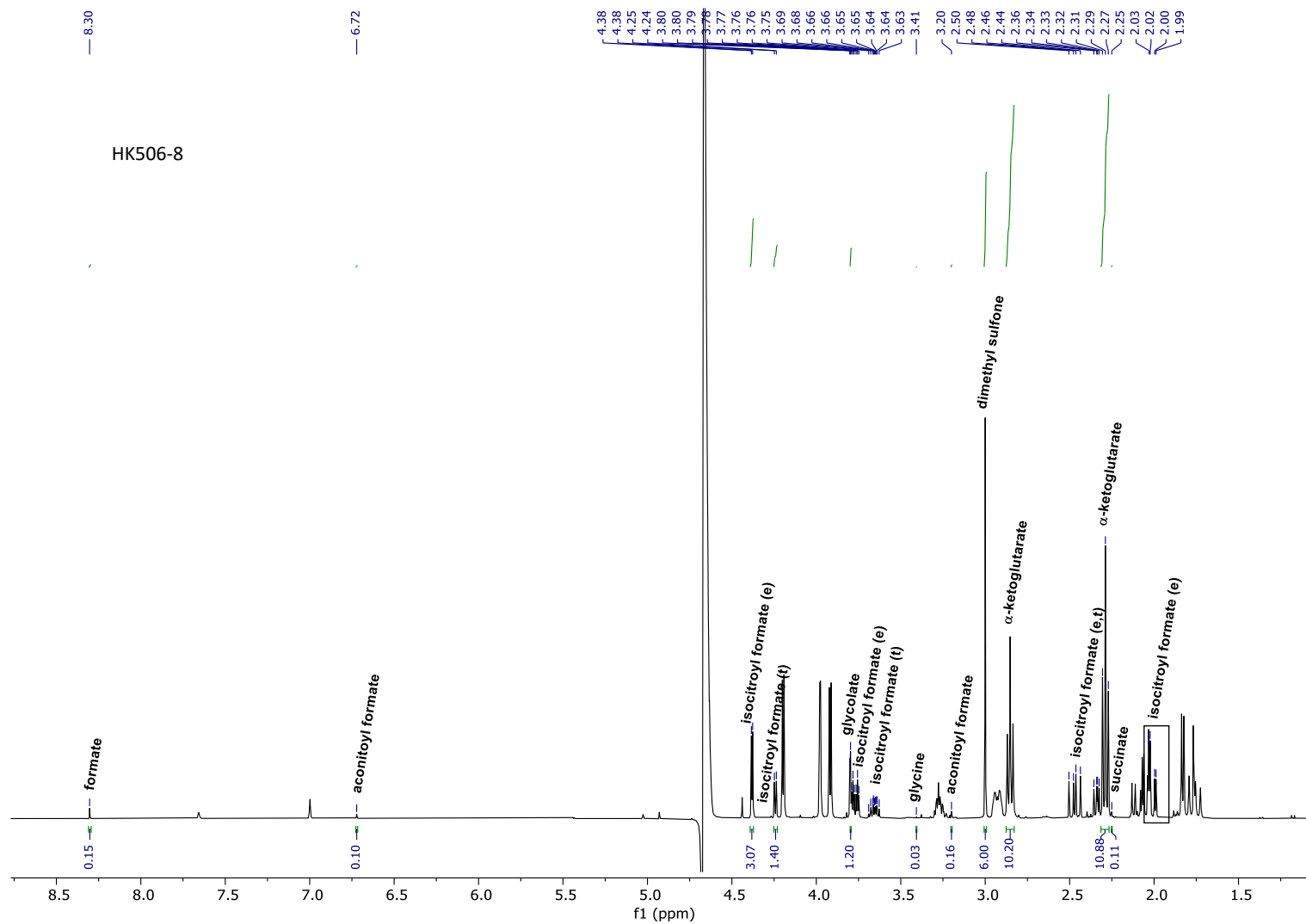


**Figure S18.**  $^1\text{H}$  NMR of reaction between  $\alpha$ -KG and glyoxylate in the presence of ammonium bicarbonate under  $\text{H}_2$  (5 bar) without Pd/C.

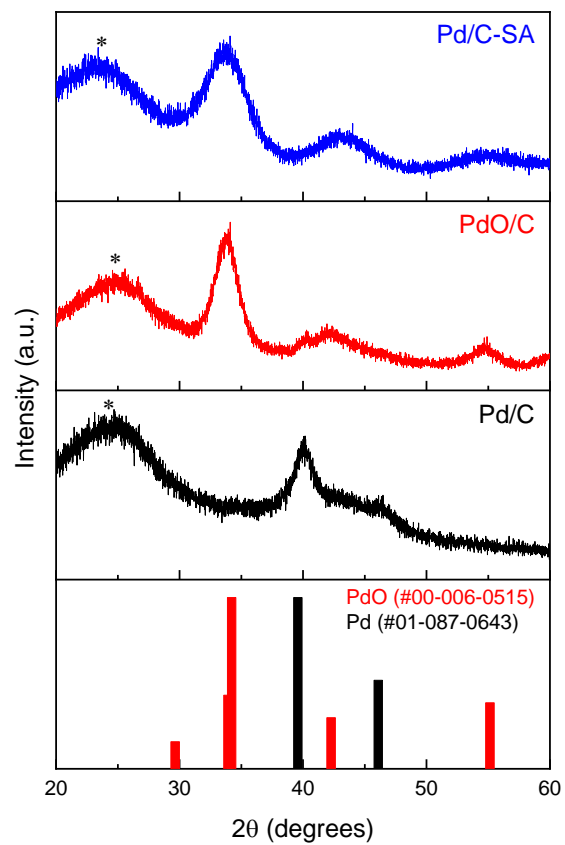


**Figure S19.** PXRD patterns of Pd/C (synthesized), PdO/C (synthesized) and Pd/C-SA (Sigma Aldrich). \*: amorphous carbon from activated carbon support.

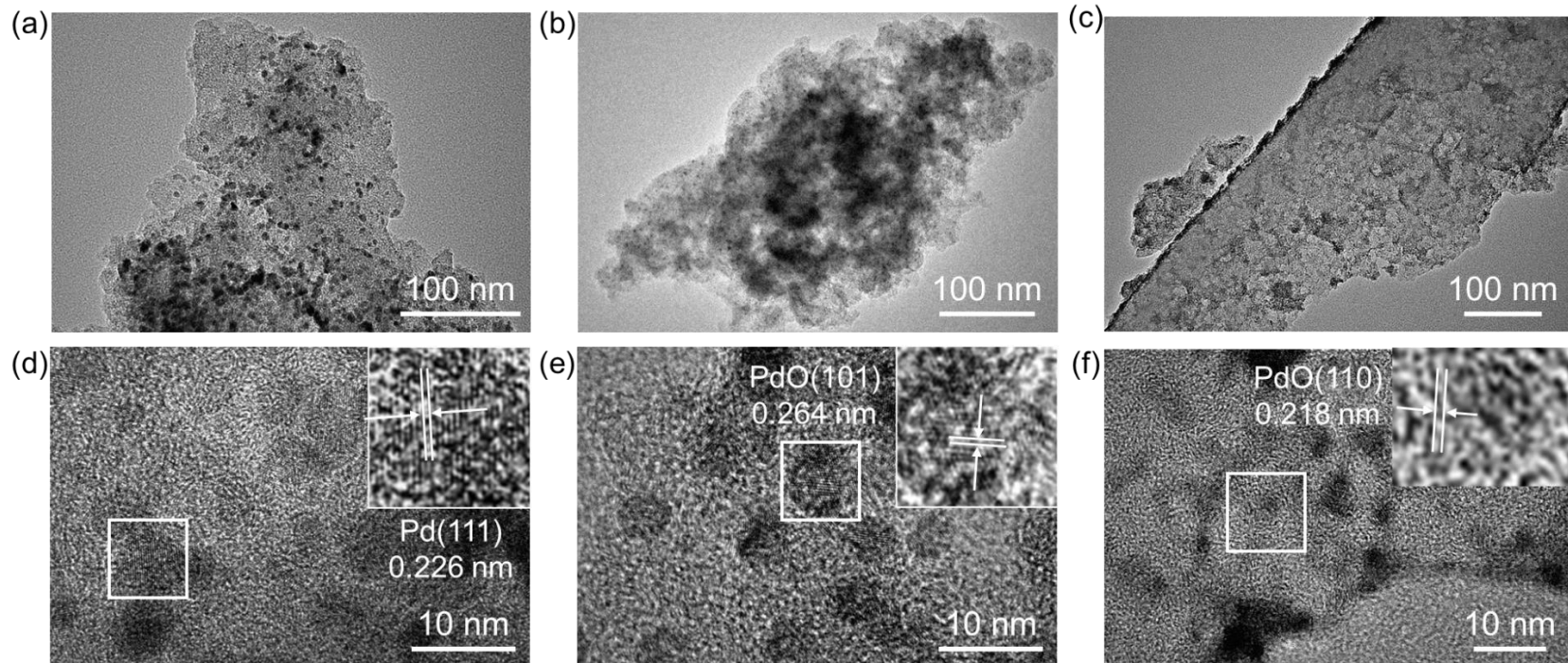


**Figure S20.** TEM images of Pd/C (a), PdO/C (b), and Pd/C-SA (c). HRTEM images of Pd/C (d), PdO/C (e), and Pd/C-SA (f). Particle size of Pd in Pd/C, PdO in PdO/C, and PdO in Pd/C-SA are 5 nm, 6 nm, 3 nm, respectively.

## 15. DAP as a potential source of amino acids synthesis and their oligomerization

### 15.1. Product analysis

Glyoxylic acid solution (50 wt.% in H<sub>2</sub>O, Sigma-Aldrich), sodium pyruvate (ReagentPlus®, ≥99%, Sigma-Aldrich), oxaloacetic acid (Sigma-Aldrich), α-ketoglutaric acid disodium salt dihydrate (≥98.0%, Sigma-Aldrich). Glycine (ReagentPlus®, ≥99%), L-glutamic acid (≥99.5%, BioUltra), L-alanine (BioUltra, ≥99.5%) and L-aspartic acid (BioUltra, ≥99.5%). Ala-Ala; Ala-Ala-Ala; Gly-Gly; Gly-Gly-Gly; Glu-Glu were purchased from Sigma-Aldrich with purity ≥ 98 %. Ala-Ala-Ala-Ala; Asp-Asp; Asp-Asp-Asp and Glu-Glu-Glu were purchased from Bachem with purity ≥ 98 %. Phthalaldehyde (≥99.0% (HPLC) and 2-mercaptoethanol (≥99.0% (GC) were purchased from Sigma-Aldrich.

The metal salts for the reaction screening were purchased from Sigma-Aldrich, Fluorochem, Merck Millipore, Fluka, Alfa Aesar or Strem chemicals and were generally of at least 95% purity. Diamidophosphate starting material phenyl phosphorodiamidate was bought from Alfa Aesar, 97 %) (ref 168.)

Borate buffer (0.1 M) used in amino acid and peptide derivatization method was prepared from Boric acid (ACS reagent, ≥99.5%, Sigma-Aldrich) following adjustment of the pH value by NaOH to pH = 9.2 as monitored by an AquaLyctic AL10pH handheld pH meter calibrated before use. Chelex® 100 resin (50-100 mesh, sodium form) was obtained from Bio-Rad. Water used for reactions was obtained from a Sartorius Arium purification system (18 MΩcm).

### 15.2. Product analysis

#### 15.2.1. NMR Spectroscopy

NMR spectra were recorded on Bruker 400 MHz spectrometer equipped with Prodigy BBO cryoprobes at a sample temperature maintained at 23 °C. As solvent, a H<sub>2</sub>O: D<sub>2</sub>O mixture (10:1) was applied, using qNMR grade dimethyl sulfone (DMS, Sigma-Aldrich, TraceCERT) as internal standard (CH<sub>3</sub> group set to 3.00 ppm).

Water suppression in <sup>1</sup>H NMR spectra was achieved using the Bruker *noesygppr1d* pulse program acquiring 8 scans for each sample. For quantitative NMR spectra



(qNMR) the relaxation delay  $d_1$  was set to 10 s or 30 s. For authentic samples  $d_1$  was set to 10s.

### 15.2.2. U-HPLC-QTOF-MS

**U-HPLC-QTOF-MS** analysis was performed on an Agilent 1290 Infinity II liquid chromatography (LC) system hyphenated with QTOF 6546 Accurate-Mass QTOF LC/MS system, equipped with a Dual Agilent Jet Stream spray source (ESI) and connected to an N<sub>2</sub> generator (Nitrocrafft® NCP-032-R). All chromatographic separations were performed on ZORBAX Eclipse Plus C18 column (2 x 150 mm, 1.8  $\mu$ m), with a flow of 0.8 mL/min.

<b>Eluent A</b>	50 mM Ammonium acetate pH 6		
<b>Eluent B</b>	Methanol:ACN:H <sub>2</sub> O (45:45:10)		
<b>Gradient</b>	Time (min)	%A	%B
	0.00	90	10
	1.50	90	10
	5.00	50	50
	8.00	0	100
	10.00	0	100
<b>Sample loop</b>	20 $\mu$ l		
<b>Injection volume</b>	17.5 $\mu$ l		
<b>Column temperature</b>	23 °C		
<b>Run time</b>	10.0 min		
<b>Sample preparation</b>	automated derivatization by autosampler		

**Automated derivatization:** 2.5  $\mu$ L of sample + 10  $\mu$ L of OPA (phthalaldehyde) reagent = mixed in air for 50 seconds. Then dilution with 5  $\mu$ L of water and injection.

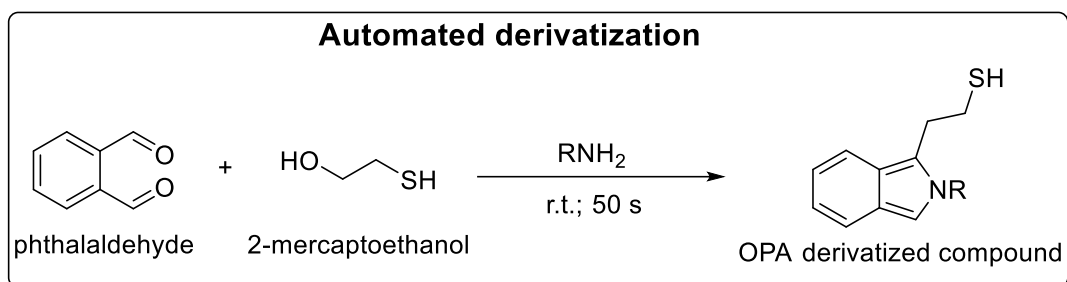
The OPA derivatized sample was then detected by UV at 338 nm.

ESI-QTOF-MS analysis was performed in a 2 GHz extended dynamic range, negative ionization mode, with fragmentor energy of 100 V, drying gas temp: 300°C, drying gas flow: 5 L/min, sheath gas temp: 350 °C, sheath gas flow: 11 L/min; nebulizer pressure: 50 psi, capillary V (+): 3 500 V, and skimmer: 65 V. The acquisition parameters were as follows: auto MS/MS mode; mass range 20–750 m/z for MS and 20–750 m/z for MS/MS experiment; and 1 spectra/s acquisition. The collision-induced dissociation (CID) energy was optimized to 7 V. The identification of the compounds present in the samples was performed by comparison with authentic samples. Data analysis was performed using Agilent MassHunter Workstation Quantitative Analysis for Q-TOF v.B.10.1 software.

### 15.2.3. OPA derivatization method

**Derivatization method:** 25 mg of phthalaldehyde was dissolved in 3 mL of methanol+ 2 mL 0.1 M borate buffer (37 mM). Then 25  $\mu$ L of mercaptoethanol was added to the solution. This freshly prepared reagent was used within 24 h at room temperature.

The reaction sample at 50 mM used for derivatization was diluted to 12.5 mM using water and borate buffer in 50: 50 ratios.



### 15.3. Diamidophosphate synthesis (DAP) procedure

DAP was synthesized according to a previously reported protocol.<sup>168</sup> A reaction mixture of phenyl phosphorodiamidate (5 g, 29.0 mmol, 1.0 equiv.), NaOH (2.3998 g, 60 mmol, 2.1 equiv.) and H<sub>2</sub>O (50 mL) was stirred at 110 °C for 20 min. The brown solution was concentrated to 10-15 mL and 70 mL of ethanol was added dropwise at 0 °C under vigorous stirring. The grey precipitate was filtered and dissolved in 50 mL of cold water. The resulting solution was washed consecutively with dichloromethane twice (30 mL  $\times$  2) and ethyl acetate three times (30 mL  $\times$  3) until no phenol or phenoxide was present in the organic phase (checked by <sup>1</sup>H NMR). The slightly yellowish aqueous phase was concentrated to 10-15 mL and was added dropwise to 50 mL of cold ethanol under vigorous stirring to afford a white precipitate. The precipitate was filtered, washed with cold ethanol two times (20 mL  $\times$  2) and dried at rotavapor to afford 85%) of DAP as a white powder. <sup>1</sup>H and <sup>31</sup>P NMR of DAP are shown in Figure S21.

**15.4. Procedure for the reductive amination reaction of pyruvate, (100 mM) and diamidophosphate (DAP 5 equiv) in the presence of 20 mol% of different metals (pH = 7- 9, HK515)**

1.5 mL GC glass vials were charged with the metal salts (0.01 mmol, 20 mol%; directly weighed), sodium pyruvate (0.05 mmol) and DAP (0.25 mmol) from stock solutions in water (pH 7) in a total of 0.5 mL solvent (resulting concentrations: 100 mM in pyruvate and 500 mM in DAP). After putting the stirrer bars, the vials were sealed, punctured with a syringe needle and placed in a pressure reactor. The reactor was purged two times and placed under 10 bar of H<sub>2</sub>. After 24 h stirring at 50 °C (600 rpm), the reactor was cooled down to room temperature and the pressure was released. The reactions were taken out from the reactor. 500  $\mu$ L of water was added to bring the volume to 1 mL (resulting concentration: 50 mM pyruvate and 2500 mM in DAP). The reaction pH was ~ 9. The reaction mixture was withdrawn onto an Eppendorf tube, charged with 300  $\pm$  10 mg Chelex® and shaken thoroughly for 15-30 minutes to remove any metal salts. 500  $\mu$ L of the clear supernatant and 50  $\mu$ L of a solution of dimethyl sulfone in D<sub>2</sub>O of known concentration were transferred into an NMR tube for qNMR analysis. Concentrations of resulting products: alanine, dipeptide and others shown in Table 1 were determined based on the integral ratios relative to the resonance of the methyl protons of dimethyl sulfone (DMS) ("Concentration in NMR sample"). Two representative NMR spectra (<sup>1</sup>H NMR and <sup>31</sup>P non decoupled) are depicted in Figures S21.

Concentrations of analytes determined in this way are estimated to have an error, as the chelex resin can adsorb some amino acid and peptide product.

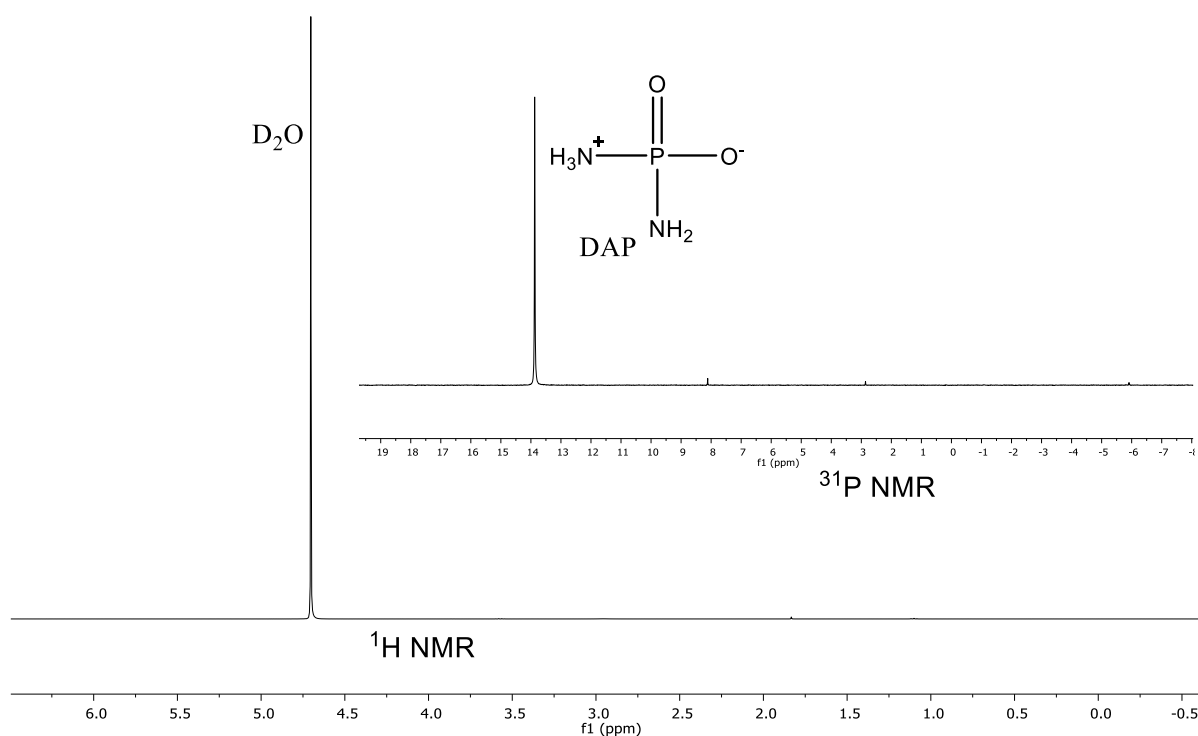


**Figure S21.**  $^1\text{H}$  NMR (ns = 8,  $d_1$  = 10 s) and  $^{31}\text{P}$  NMR of synthesized DAP.

**15.5. General procedure for the reductive amination reaction of glyoxylate, pyruvate, oxaloacetate and  $\alpha$ -ketoglutarate (100 mM) with diamidophosphate (DAP 5 equiv.) in the presence of 20 mol% of Ni-Al alloy (pH = 7- 9, HK522)**

1.5 mL GC glass vials were charged with Ni-Al alloy catalyst (0.01 mmol, 20 mol%; directly weighed), the ketoacid of interest (0.05 mmol) and DAP (0.25 mmol) from stock solutions in water (pH 7, adjusted with 1M NaOH where needed) in a total of 0.5 mL solvent (resulting concentrations: 100 mM in ketoacid and 500 mM in DAP). After adding the stir bars, the vials were sealed, punctured with a syringe needle and placed in a pressure reactor. The reactor was purged two times and placed under 10 bar of  $\text{H}_2$ . After 24 h stirring at 50  $^\circ\text{C}$  (600 rpm), the reactor was cooled down to room temperature and the pressure was released. The reactions were taken out from the reactor. 500  $\mu\text{L}$  of water was added to bring the volume to 1 mL (resulting concentration: 50 mM ketoacid and 2500 mM in DAP). The reaction pH was increased

to ~ 9, due to DAP hydrolysis. The reaction mixture was withdrawn onto an Eppendorf tube and centrifuged without using chelex. 500  $\mu$ L of the clear supernatant and 50  $\mu$ L of a solution of dimethyl sulfone in D<sub>2</sub>O of known concentration were transferred into an NMR tube for qNMR analysis. Concentrations of resulting products are shown in Table S27-S31, were determined based on the integral ratios relative to the resonance of the methyl protons of dimethyl sulfone (DMS) ("Concentration in NMR sample"). Representative NMRs and UV-MS analysis are shown in Figures S22-S41.

**15.6. General procedure for the oligomerization reaction of glycine, alanine, aspartate and glutamate (100 mM) with and without diamidophosphate (DAP 5 equiv; pH = 7- 9, HK521).**

1.5 mL GC glass vials were charged with stirrer bars, amino acid of interest (0.05 mmol) and DAP (0.25 mmol) from stock solutions in water (pH 7, adjusted with 1M NaOH where needed) in a total of 0.5 mL solvent (resulting concentrations: 100 mM in ketoacid and 500 mM in DAP). The vials were sealed, punctured with a syringe needle and placed in a pressure reactor. The reactor was purged two times and placed under 10 bar of H<sub>2</sub>. After 72 h stirring at 50 °C (600 rpm), the reactor was cooled down to room temperature and the pressure was released. The reactions were taken out from the reactor. 500  $\mu$ L of water was added to bring the volume to 1 mL (resulting concentration: 50 mM ketoacid and 2500 mM in DAP). The reaction pH was increased to ~ 9, due to DAP hydrolysis. The reaction mixture was withdrawn onto an Eppendorf tube and centrifuged without using chelex. 500  $\mu$ L of the clear supernatant and 50  $\mu$ L of a solution of dimethyl sulfone in D<sub>2</sub>O of known concentration were transferred into an NMR tube for qNMR analysis. Concentrations of resulting products are shown in Table S27-S31, were determined based on the integral ratios relative to the resonance of the methyl protons of dimethyl sulfone (DMS) ("Concentration in NMR sample"). Control experiments were also performed in the same way, except adding DAP to them. Table S27-S31.

Representative NMRs and UV-MS analysis is shown in Figures S22-S41.

## 15.7. Experimental data

**Table S27.** <sup>1</sup>H NMR integrals and concentrations for the reactions of pyruvate with DAP in the presence of different metals.<sup>a</sup>

Experiment	Metal (20 mol%)	Integral (relative to dimethyl sulfone/DMS which was set to 6)			DMS stock (mM)	Concentration in NMR sample (mM)			Yield (%)		
		Ala (0.5 of 1 H)	Ala-Ala (1 H and 0.5 of 1 H)	Lactate (1 H)		Ala	Ala-Ala	Lactate	Ala	Ala-Ala	Lactate
HK515-1	Fe	0	0	0	20.42	0	0	0	0	0	0
HK515-2	FeS	0	0	0	20.42	0	0	0	0	0	0
HK515-3	FeO	0	0	0	20.42	0	0	0	0	0	0
HK515-4	FeCl <sub>2</sub> * 4 H <sub>2</sub> O	0	0	0	20.42	0	0	0	0	0	0
HK515-5	Fe <sub>3</sub> O <sub>4</sub>	0	0	0	20.42	0	0	0	0	0	0
HK515-6	Ni	2.22	0.24	0.42	20.42	9.06	0.49	0.86	18.12	0.98	1.71
HK515-7	NiCl <sub>2</sub> * 2 H <sub>2</sub> O	0	0	0	20.42	0	0	0	0	0	0
HK515-8	Ni-Al alloy	4.83	2.50	2.08	20.42	19.71	5.10	4.25	39.43	10.21	8.49
HK515-9	Ni-Fe alloy	3.93	1.28	1.41	20.42	16.04	2.61	2.88	32.08	5.22	5.76
HK515-10	Co	1.28	0.34	0.80	20.42	5.22	0.69	1.63	10.45	1.39	3.27
HK515-11	Co <sub>2</sub> Al <sub>2</sub> O <sub>5</sub> (39 – 41%)	0.04	0	0	20.42	0.16	0	0	0.33	0	0
HK515-12	CuCl <sub>2</sub> * 2 H <sub>2</sub> O	0	0	0	20.42	0	0	0	0	0	0
HK515-13	Zn	0.15	0.04	3.44	20.42	0.61	0.08	7.02	1.22	0.16	14.04
HK515-15	Mg	0	0	0.31	20.42	0	0	0.63	0	0	1.26
HK515-16	MgCl <sub>2</sub>	0	0	0	20.42	0	0	0	0	0	0
HK515-17	Mn	0	0	0.19	20.42	0	0	0.39	0	0	0.78
HK515-18	MnCl <sub>2</sub>	0	0	0	20.42	0	0	0	0	0	0
HK515-19	CoCl <sub>2</sub>	0	0	0	20.42	0	0	0	0	0	0
HK515-20	Cu	0	0	0	20.42	0	0	0	0	0	0

HK515-21	FeCl <sub>3</sub>	0	0	0	20.42	0	0	0	0	0	0
HK515-22	CeCl <sub>3</sub> * 7 H <sub>2</sub> O	0	0	0	20.42	0	0	0	0	0	0
HK515-23	CrCl <sub>2</sub>	0	0	0	20.42	0	0	0	0	0	0
HK515-34	AlCl <sub>3</sub> * 6 H <sub>2</sub> O	0	0	0	20.42	0	0	0	0	0	0
HK515-35	No metal	0	0	0	20.42	0	0	0	0	0	0

<sup>a</sup>Rest: in all reactions starting material pyruvate almost degraded to acetate and CO<sub>2</sub>.

**Table S28.** <sup>1</sup>H NMR integrals and concentrations for the reactions of glyoxylate or glycine with or without DAP.

Experiment	Metal (20 mol%)	DAP (5 equiv.)	Integral (relative to dimethyl sulfone/DMS which was set to 6)			DMS stock (mM)	Concentration in NMR sample (mM)			Yield (%)		
			gly (2 H)	gly-gly (2 H)	glycolate (2 H)		gly	gly-gly	glycolate	gly	gly-gly	glycolate
HK522-10	Ni-Al alloy	5 equiv.	2.43	2.04	0.9	21	2.55	2.14	0.95	5.10	4.28	1.90
HK521-2	-	5 equiv.	16.97	16.63	0	21	17.82	17.46	0	35.64	34.92	0
HK515-3	-	-	51.26	0	0	21	48.82	0	0	102.52	0	0

**Table S29.** <sup>1</sup>H NMR integrals and concentrations for the reactions of pyruvate or alanine with or without DAP.

Experiment	Metal (20 mol%)	DAP (5 equiv.)	Integral (relative to dimethyl sulfone/DMS which was set to 6)			DMS stock (mM)	Concentration in NMR sample (mM)			Yield (%)		
			ala (0.5 of 1 H)	ala-ala (0.5 of both 1 H)	lactate (1 H)		ala	ala-ala	lactate	ala	ala-ala	lactate
HK522-9	Ni-Al alloy	5 equiv.	4.71	1.86	3.59	21	19.78	3.91	7.54	39.56	7.81	15.08
HK521-1	-	5 equiv.	10.76	4.26	0	21	45.19	8.95	0	90.38	17.90	0
HK521-5	-	-	12.19	0	0	21	51.20	0	0	102.40	0	0



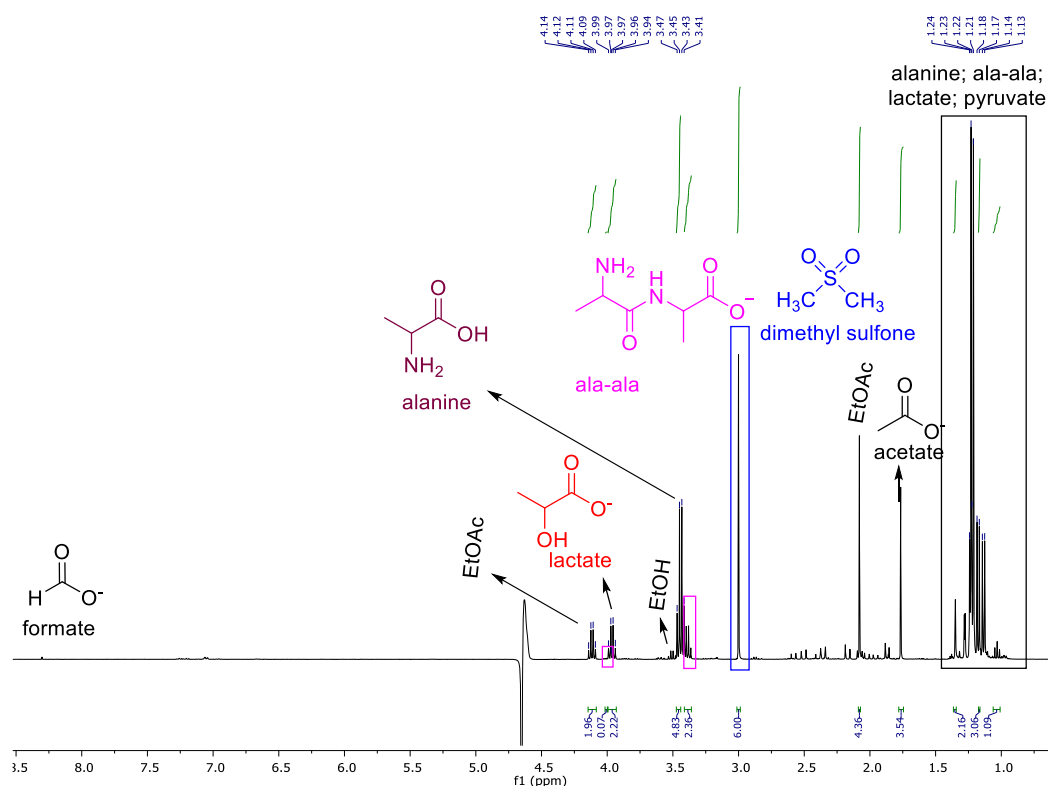
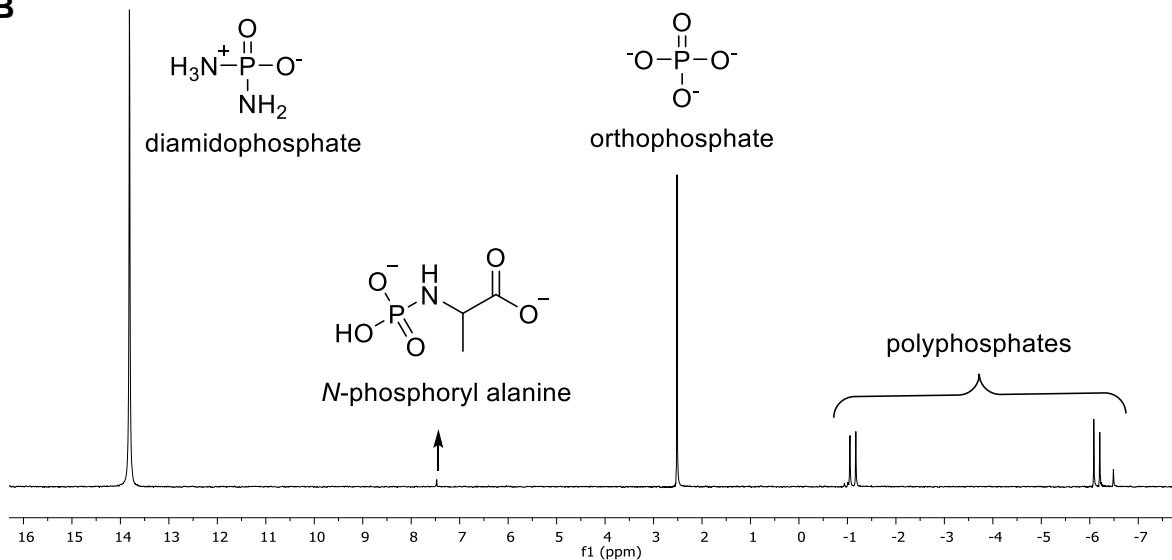
**Table S30.** <sup>1</sup>H NMR integrals and concentrations for the reactions of α-ketoglutarate or glutamate with or without DAP.<sup>a,b</sup>

Experiment	Metal (20 mol%)	DAP (5 equiv.)	Integral (relative to dimethyl sulfone/DMS which was set to 6)			DMS stock (mM)	Concentration in NMR sample (mM)			Yield (%)		
			glu (1 H)	glu-glu (1 H)	hydroxy acid (1 H)		glu	glu-glu	hydroxy acid	glu	glu-glu	hydroxy acid
HK522-12	Ni-Al alloy	5 equiv.	5.68	-	3.36	21	11.93	-	7.06	23.86	-	14.11
HK521-4	-	5 equiv.	18.95	0.47	0	21	39.80	0.99	0	79.59	1.97	0
HK521-8	-	-	23.45	0	0	21	49.25	0	0	98.49	0	0

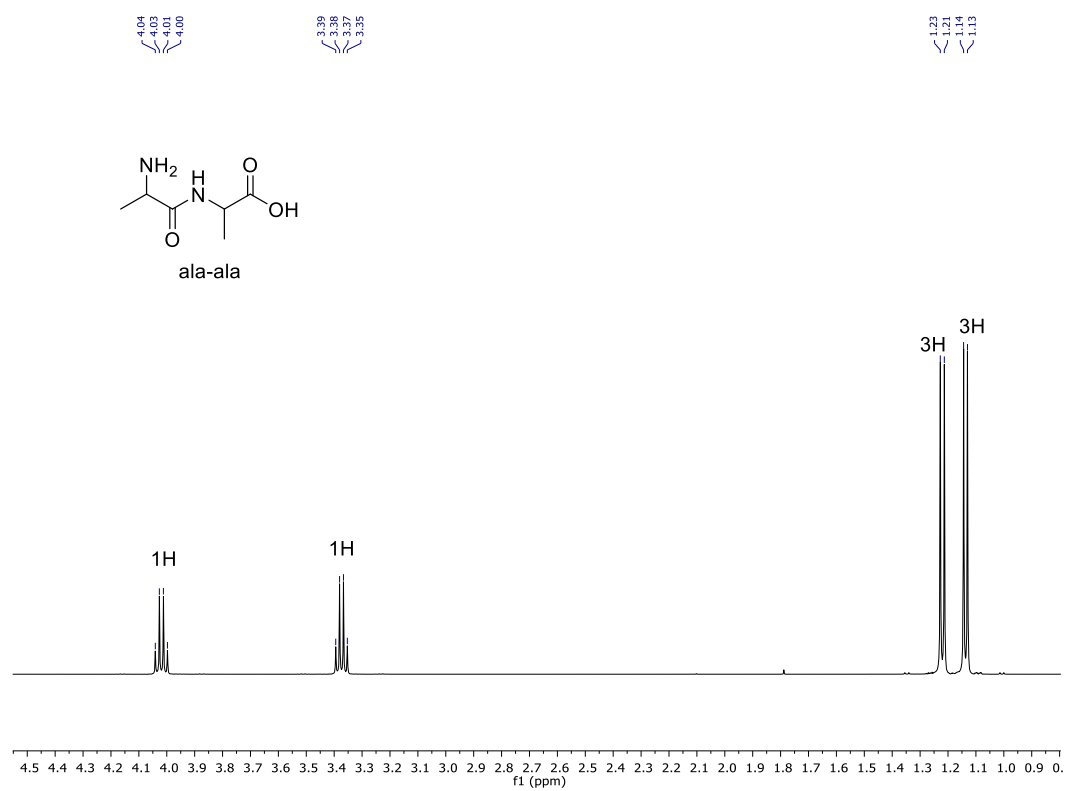
<sup>a</sup> other products observed: pyroglutamate and glutamine. <sup>b</sup> integration calculated in HK522-10: glutamate = integration area – glutamine integration (due to overlap of the integrated glutamate/glutamine peaks).

**Table S31.** <sup>1</sup>H NMR integrals and concentrations for the reactions of aspartate with or without DAP.

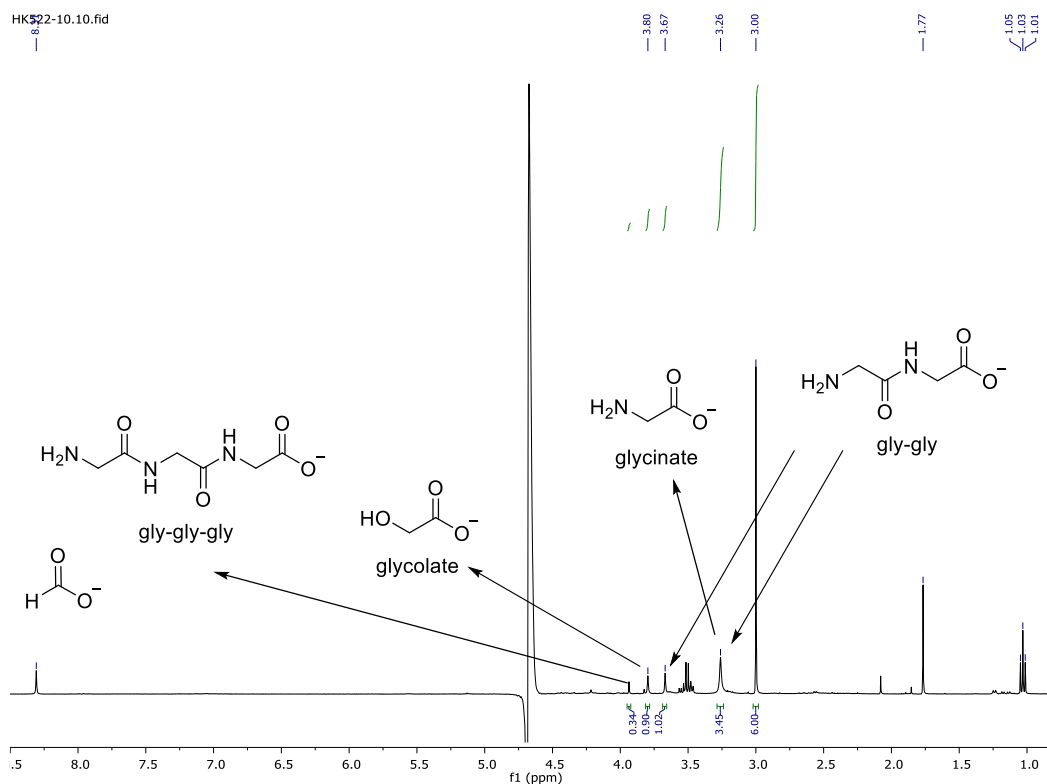
Experiment	Metal (20 mol%)	DAP (5 equiv.)	Integral (relative to dimethyl sulfone/DMS which was set to 6)			DMS stock (mM)	Concentration in NMR sample (mM)			Yield (%)		
			asp (1 H)	asp-asp (1 H)	asp-asp-asp (1 H)		asp	asp-asp	asp-asp-asp	asp	asp-asp	asp-asp-asp
HK521-3	-	5 equiv.	21.75	3.03	-	21	45.68	6.36	-	91.35	12.73	traces by UV
HK521-7	-	-	21.75	0	0	21	45.68	0	0	91.35	0	0

**A****B**

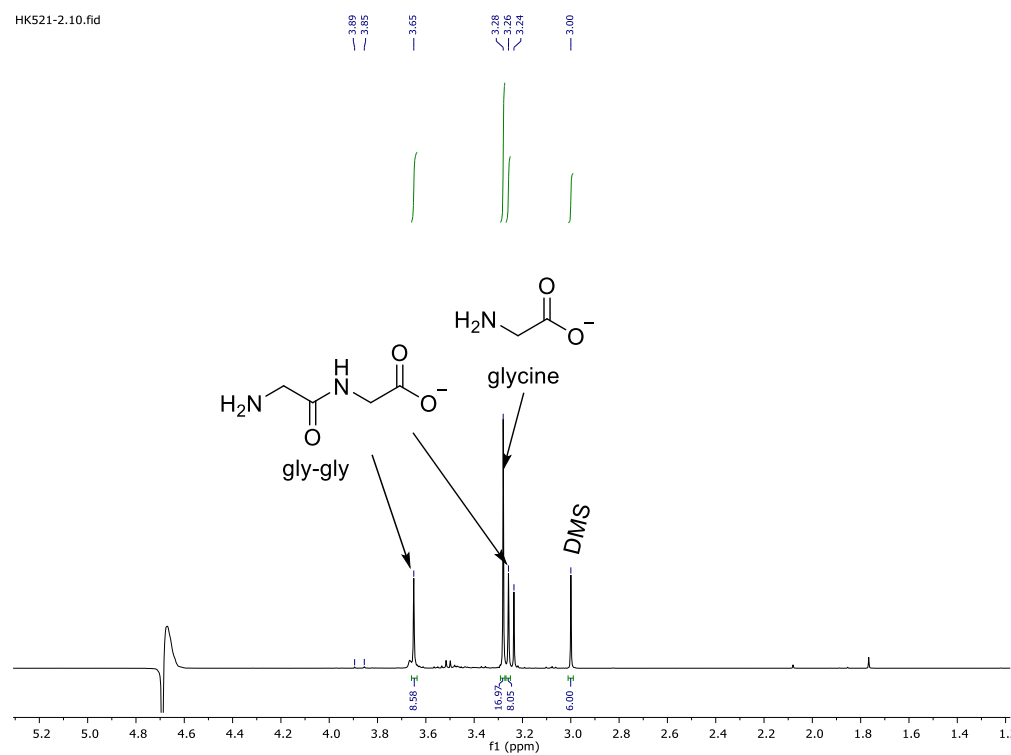
**Figure S22. (A)** <sup>1</sup>H NMR (ns = 8, d<sub>1</sub> = 10 s) of the reaction HK515-8 (pH ~ 9) indicating the different species and integrals used for quantification (EtOAc and EtOH are coming from DAP as the last batch synthesized contained some solvent traces) **(B)** <sup>31</sup>P NMR (400 MHz, ns = 8, d<sub>1</sub> = 10 s) of the same reaction indicating different species containing phosphates.



**Figure S23.**  $^1\text{H}$  NMR ( $n_s = 8$ ,  $d_1 = 10$  s) of the authentic sample of ala-ala, pH 8.

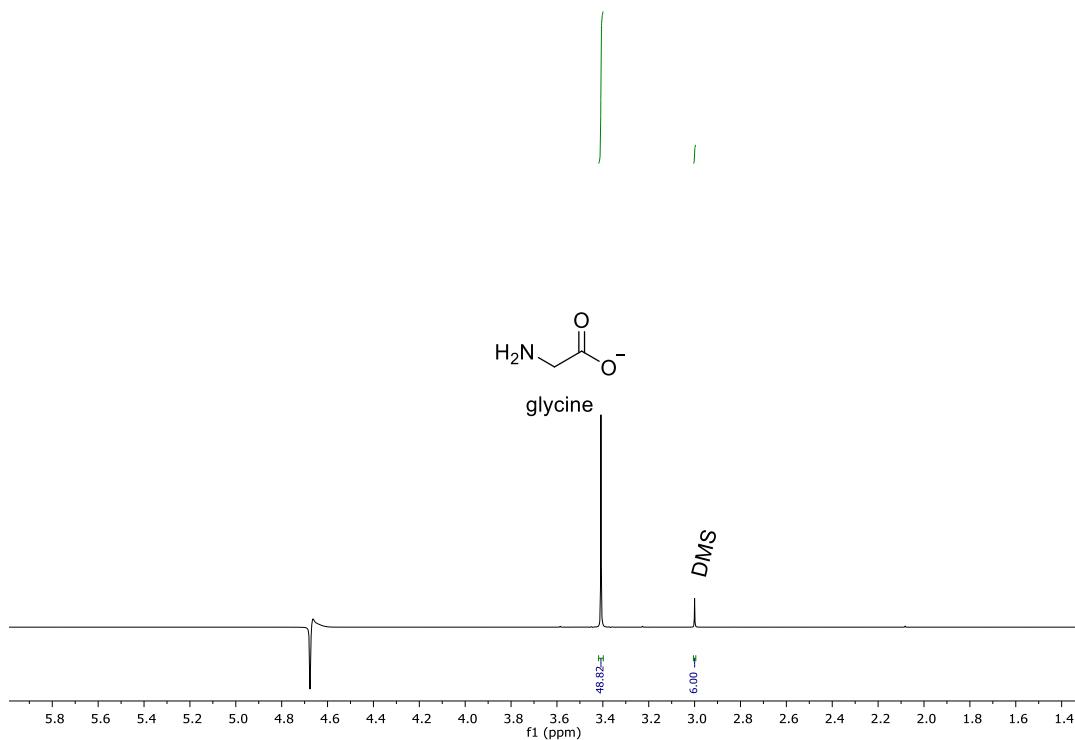


**Figure S24.**  $^1\text{H}$  NMR (ns = 8,  $d_1$  = 30 s) of glyoxylate reaction with DAP under  $\text{H}_2$  using Ni-Al catalyst (HK522-10, pH 9).

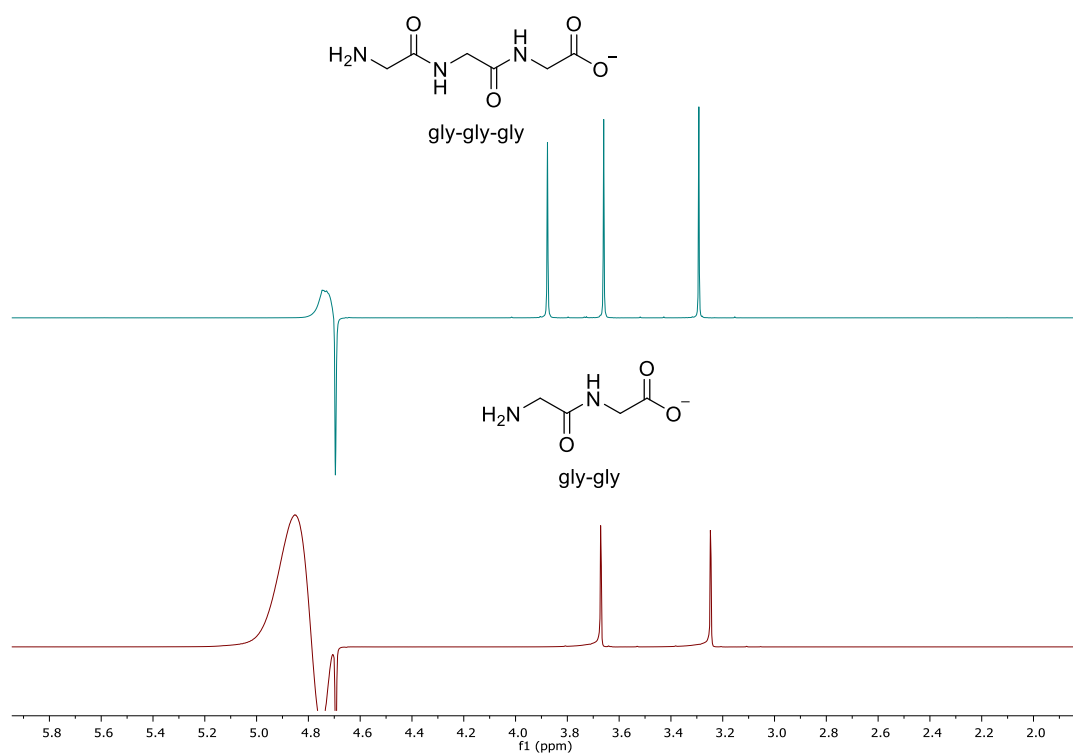


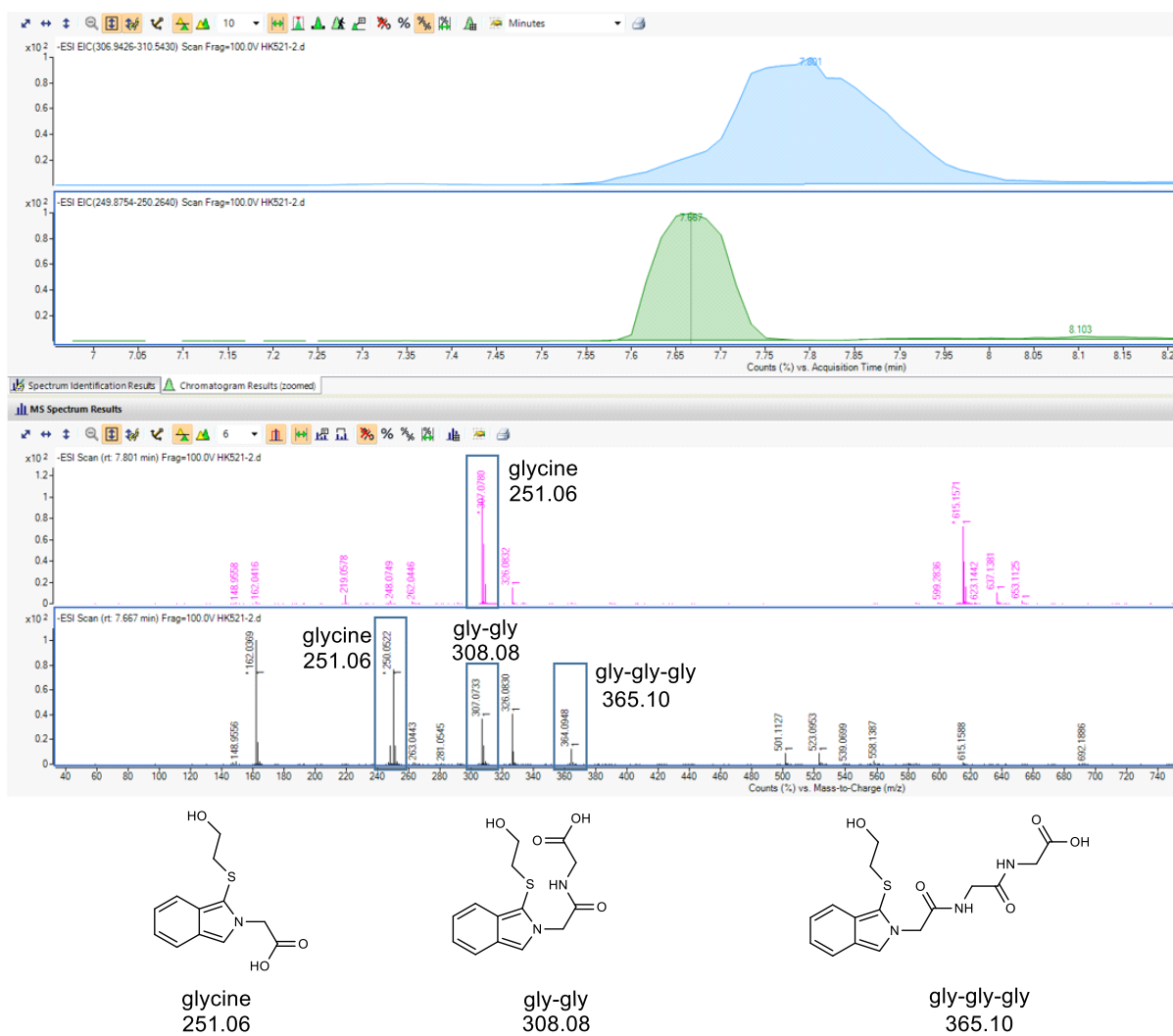
**Figure S25.**  $^1\text{H}$  NMR ( $n_s = 8$ ,  $d_1 = 30$  s) of glycine reaction with DAP under  $\text{H}_2$  without Ni-Al catalyst (HK521-2, pH 9).

HK521-6.10.fid

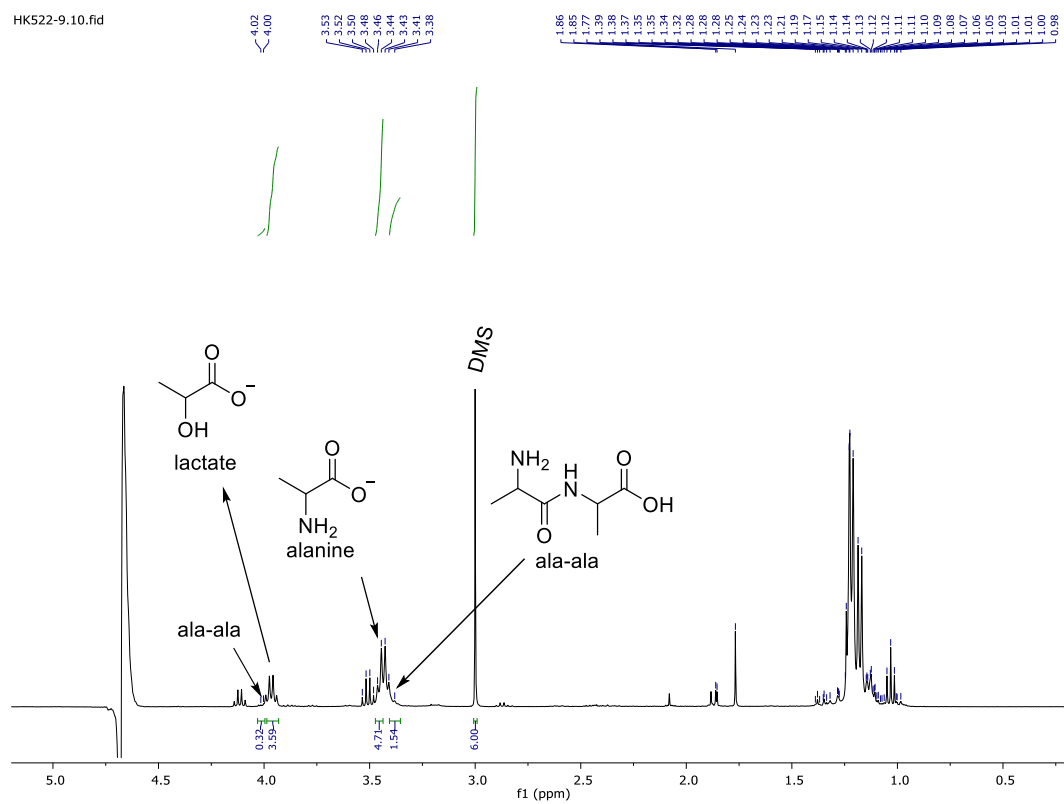


**Figure 26.**  $^1\text{H}$  NMR ( $n_s = 8$ ,  $d_1 = 30$  s) of glycine reaction in the absence of catalyst and DAP (HK521-6, pH 8).



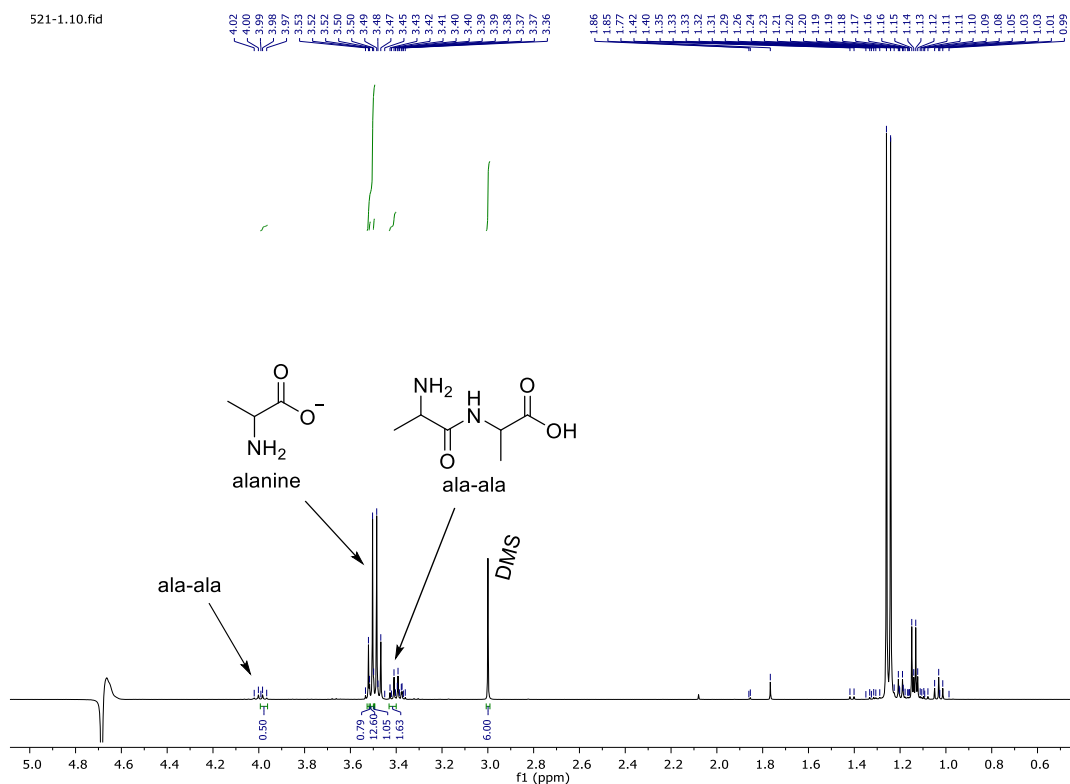
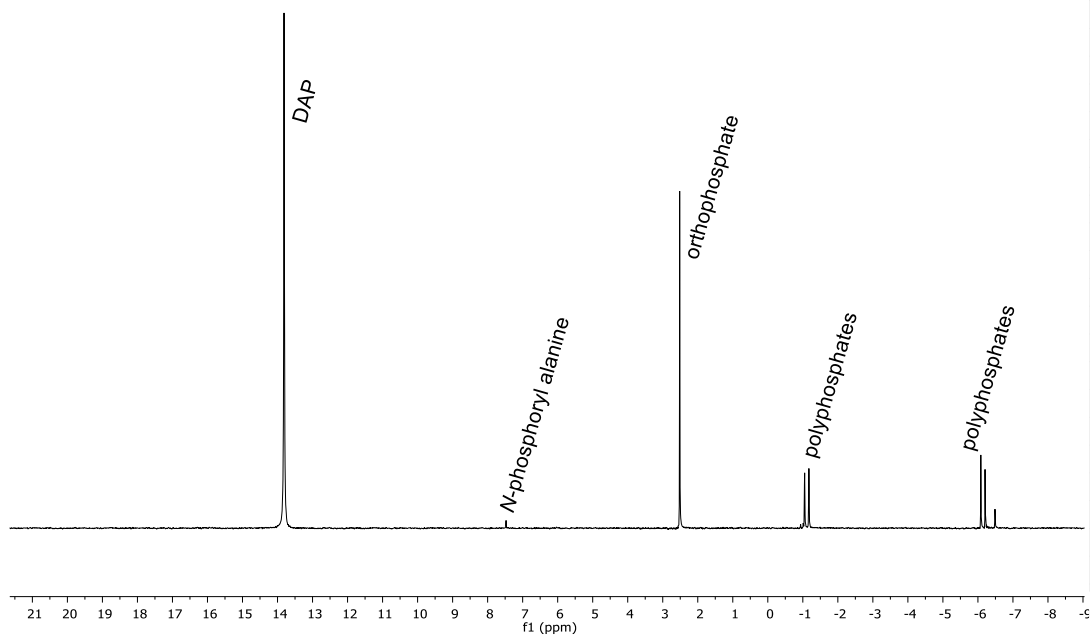


**Figure S28.** ESI-QTOF-MS analysis of glycine reaction with DAP (HK521-2).



**Figure S29.**  $^1\text{H}$  NMR ( $n_s = 8$ ,  $d_1 = 10$  s) of pyruvate reaction with DAP under  $\text{H}_2$  using Ni-Al catalyst (HK522-10, pH 9).



**a****b**

**Figure S30. a)**  $^1\text{H}$  NMR (ns = 8, d<sub>1</sub> = 10 s) of alanine reaction with DAP under  $\text{H}_2$  without Ni-Al catalyst (HK521-1, pH 9). **b)**  $^{31}\text{P}$  NMR (400 MHz, ns = 8, d<sub>1</sub> = 10 s) of the same reaction indicating different species containing phosphates.

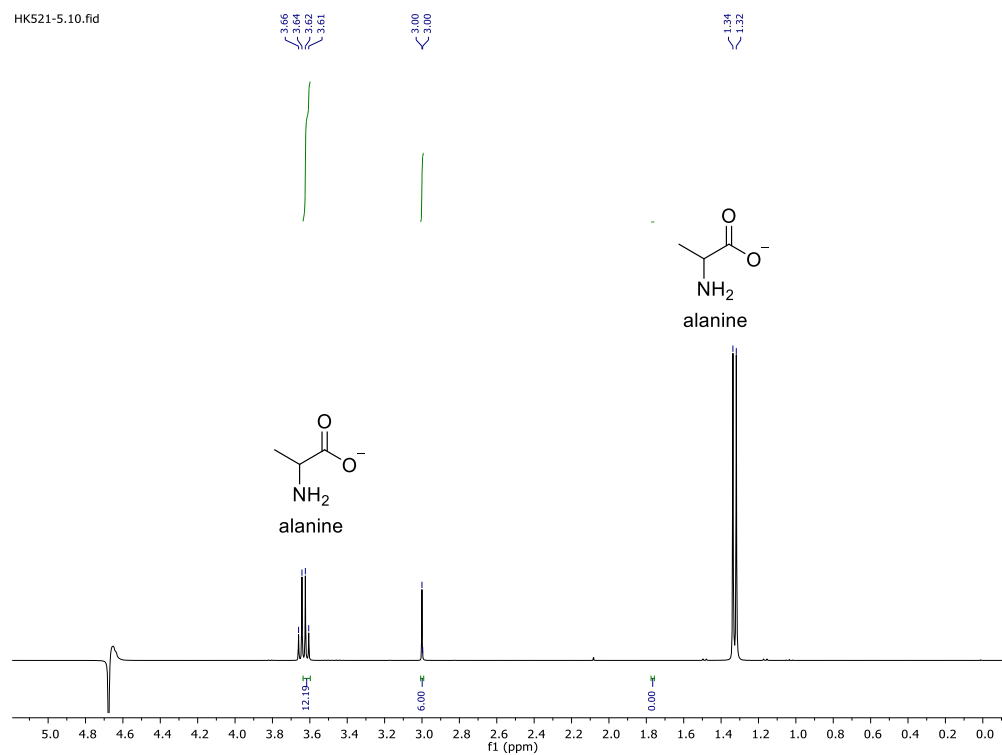


**Figure S31.**  $^1\text{H}$  NMR ( $n_s = 8$ ,  $d_1 = 30$  s) of the alanine reaction in the absence of catalyst and DAP (HK521-5, pH 8).

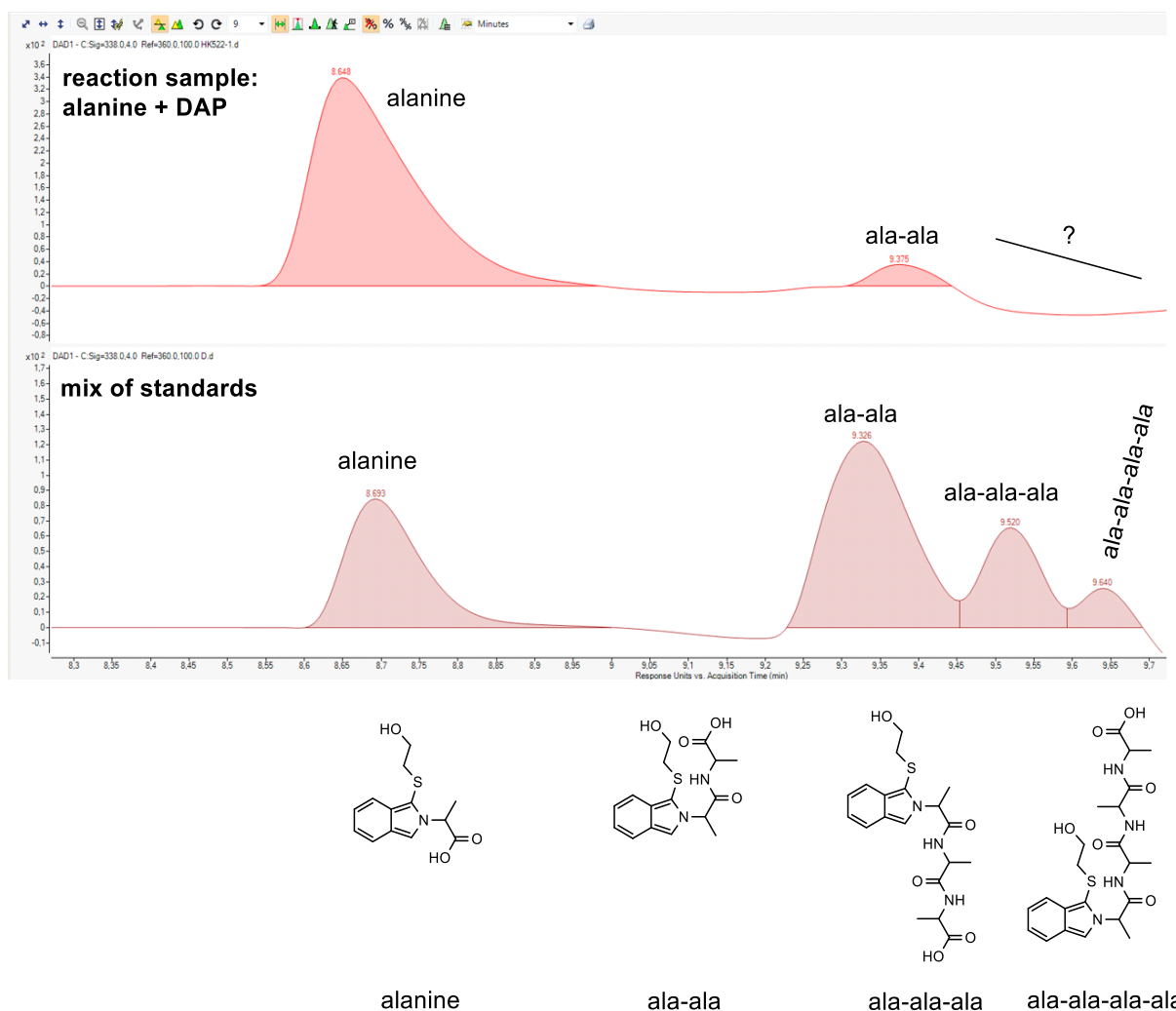


**Figure S32.** UV analysis of alanine reaction with DAP (HK521-1).

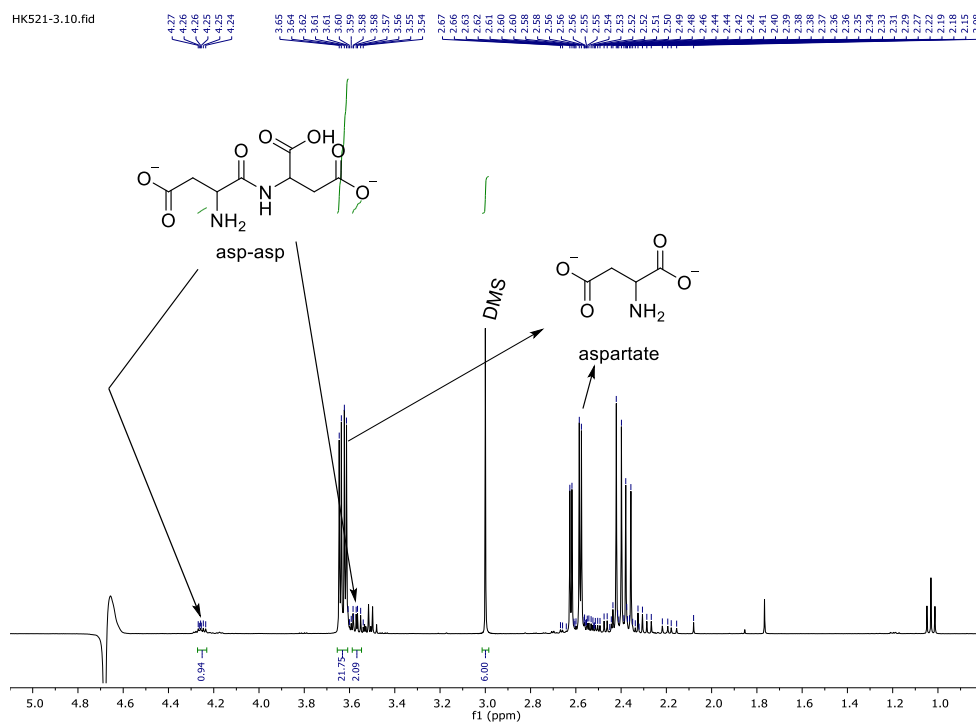


**Figure S33.**  $^1\text{H}$  NMR ( $n_s = 8$ ,  $d_1 = 30$  s) of aspartate reaction with DAP under  $\text{H}_2$  without Ni-Al catalyst (HK521-3, pH 9).

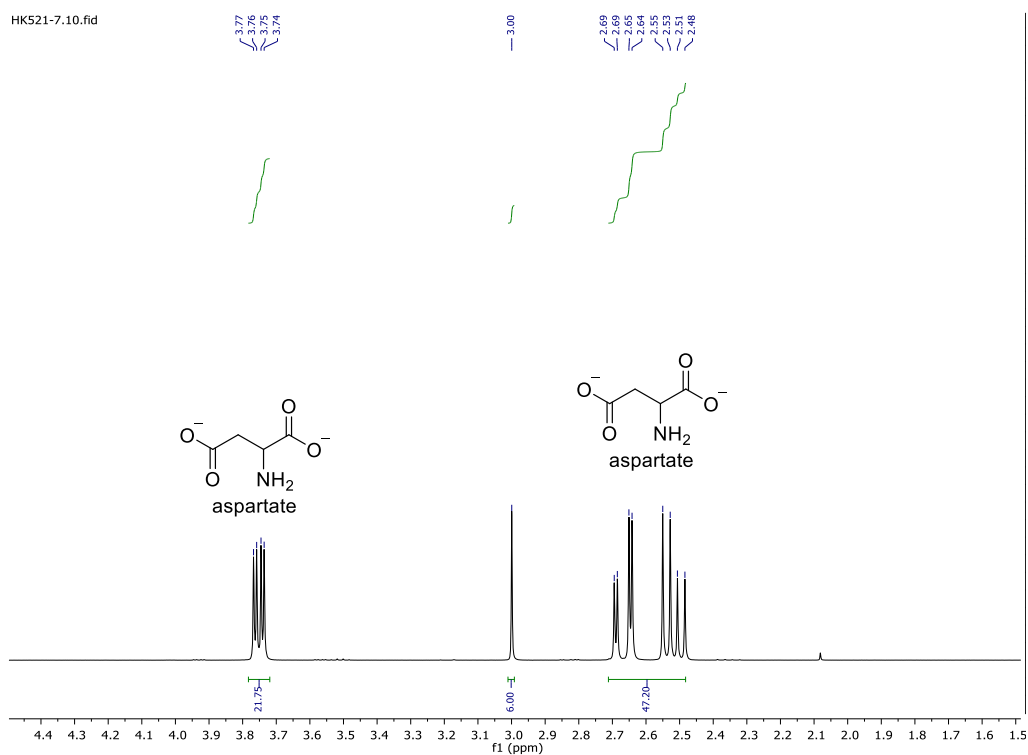


**Figure S34.**  $^1\text{H}$  NMR ( $n_s = 8$ ,  $d_1 = 30$  s) of aspartate reaction under  $\text{H}_2$  without Ni-Al catalyst and DAP (HK521-7, pH 8).

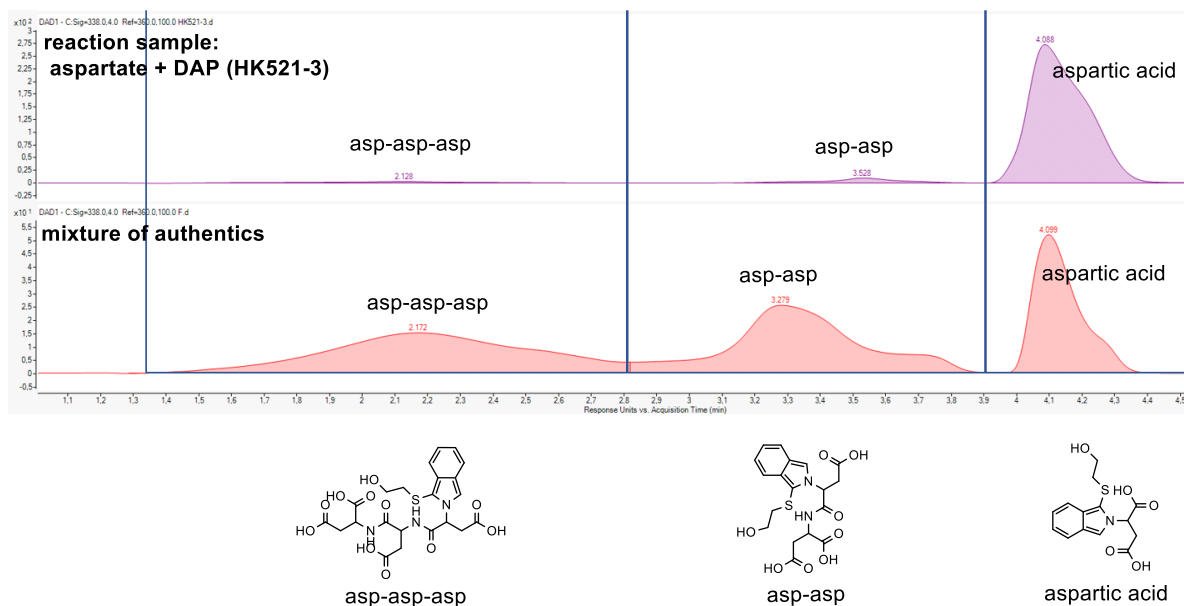


**Figure S35.** UV analysis of aspartate reaction with DAP (HK521-3).

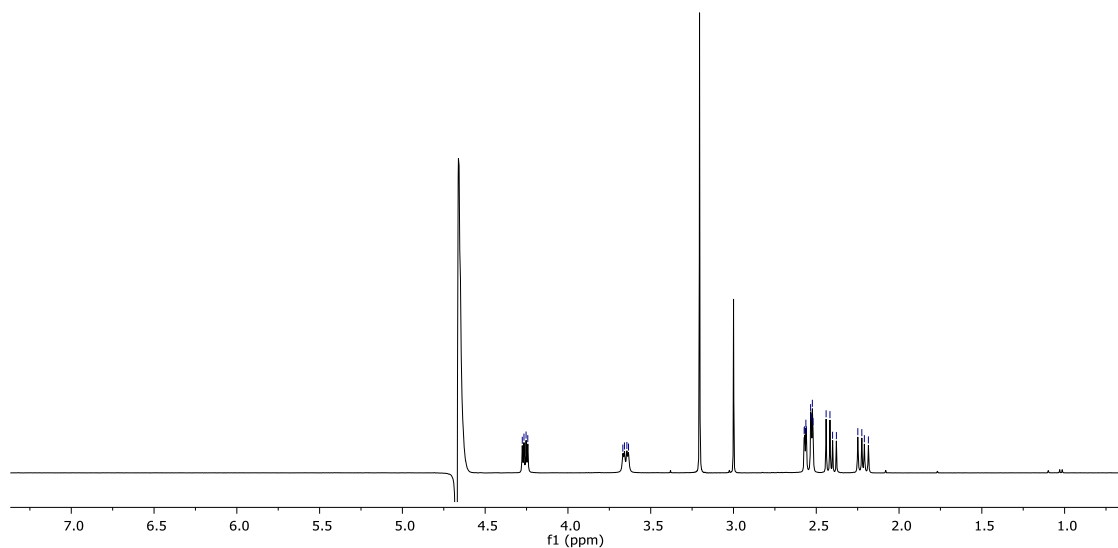


**Figure S36.** Authentic sample of dipeptide asp-asp.

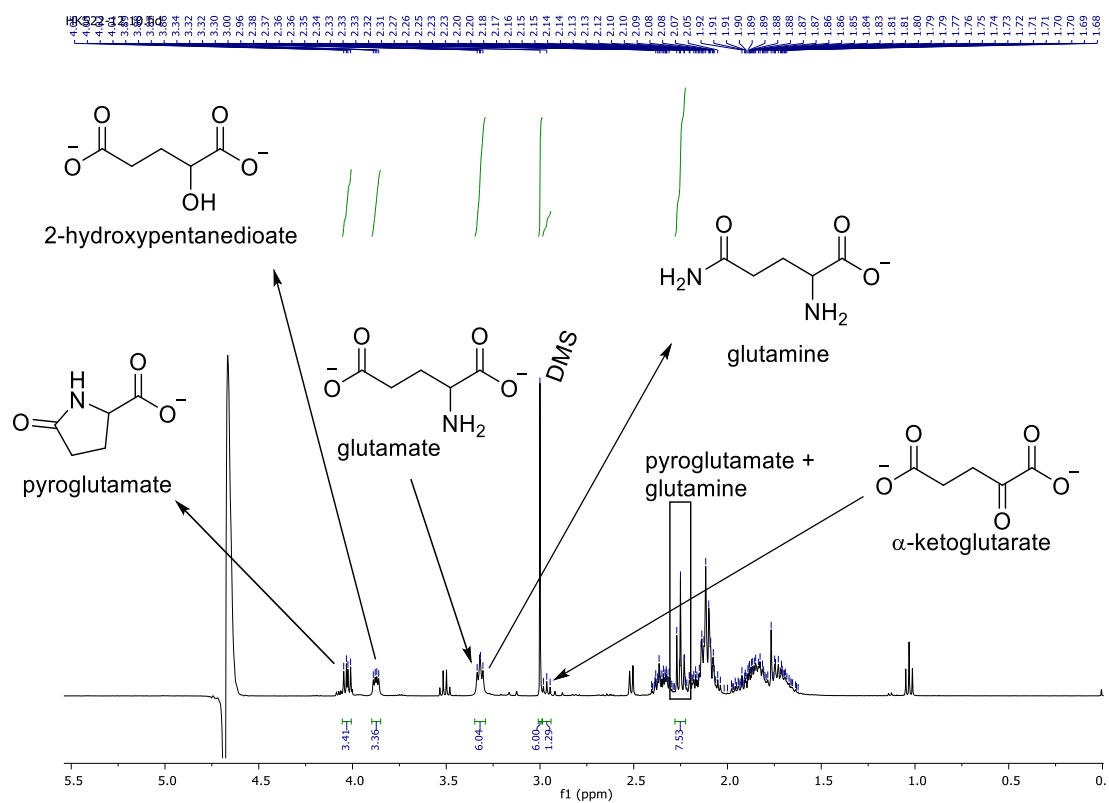


**Figure S37.**  $^1\text{H}$  NMR (ns = 8, d<sub>1</sub> = 30 s) of  $\alpha$ -ketoglutarate reaction under  $\text{H}_2$  with Ni-Al catalyst and DAP (HK522-12, pH 9).

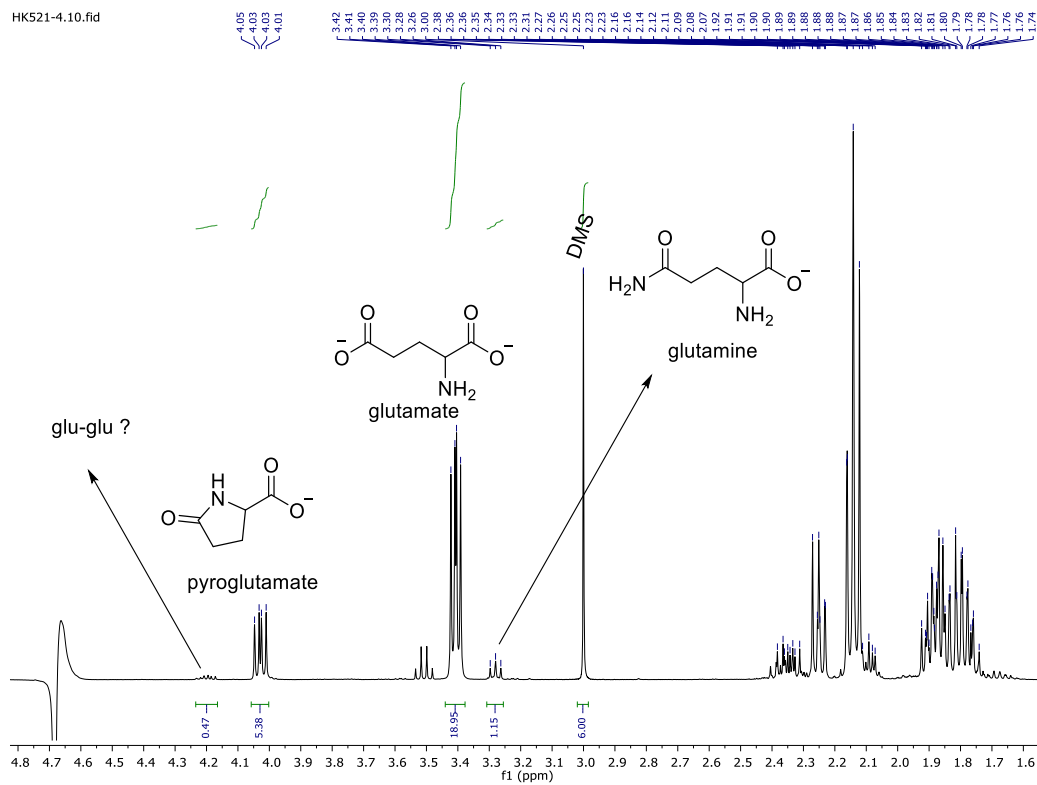


**Figure S38.**  $^1\text{H}$  NMR (noesygppr1d, 400 MHz, ns = 8, d<sub>1</sub> = 10 s) of glutamate reaction with DAP under H<sub>2</sub> without Ni-Al catalyst (HK521-4, pH 9).

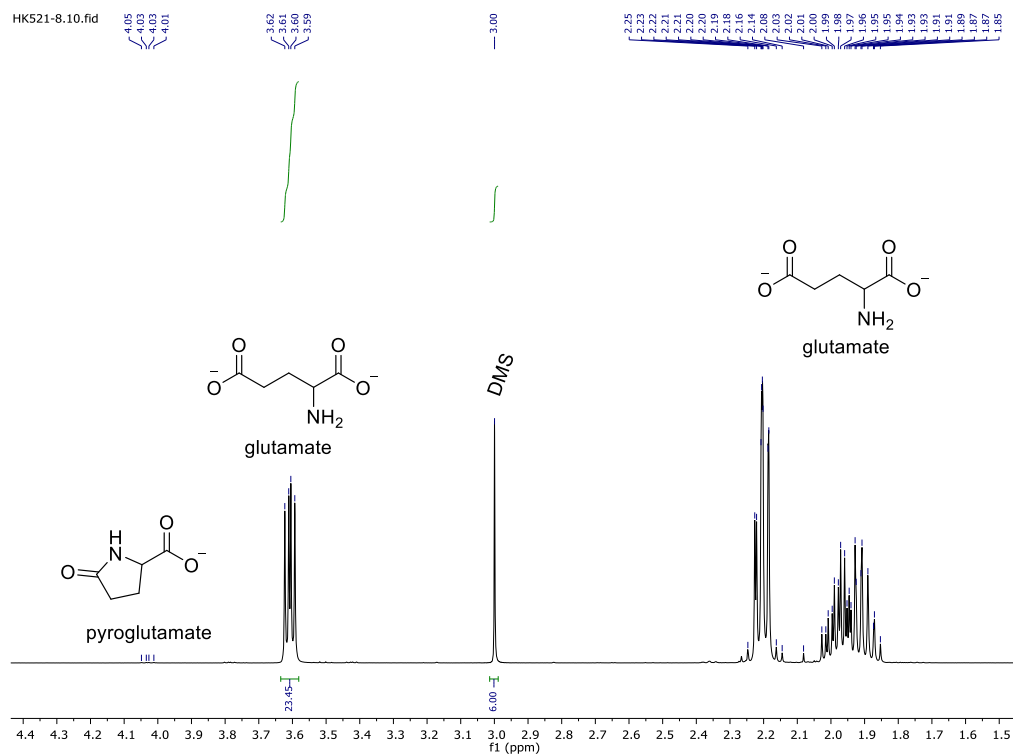


**Figure S39.**  $^1\text{H}$  NMR (ns = 8,  $d_1$  = 30 s) of glutamate reaction under  $\text{H}_2$  without Ni-Al catalyst and DAP (HK521-8, pH 8).

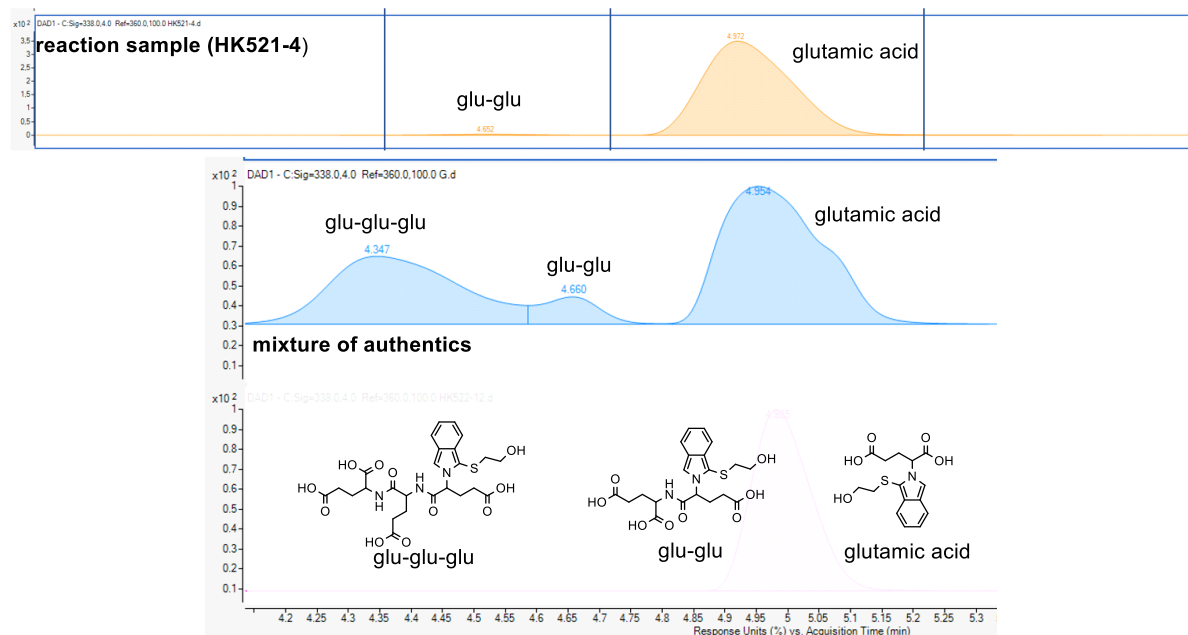


**Figure S40.** UV analysis of glutamate reaction with DAP (HK521-4).



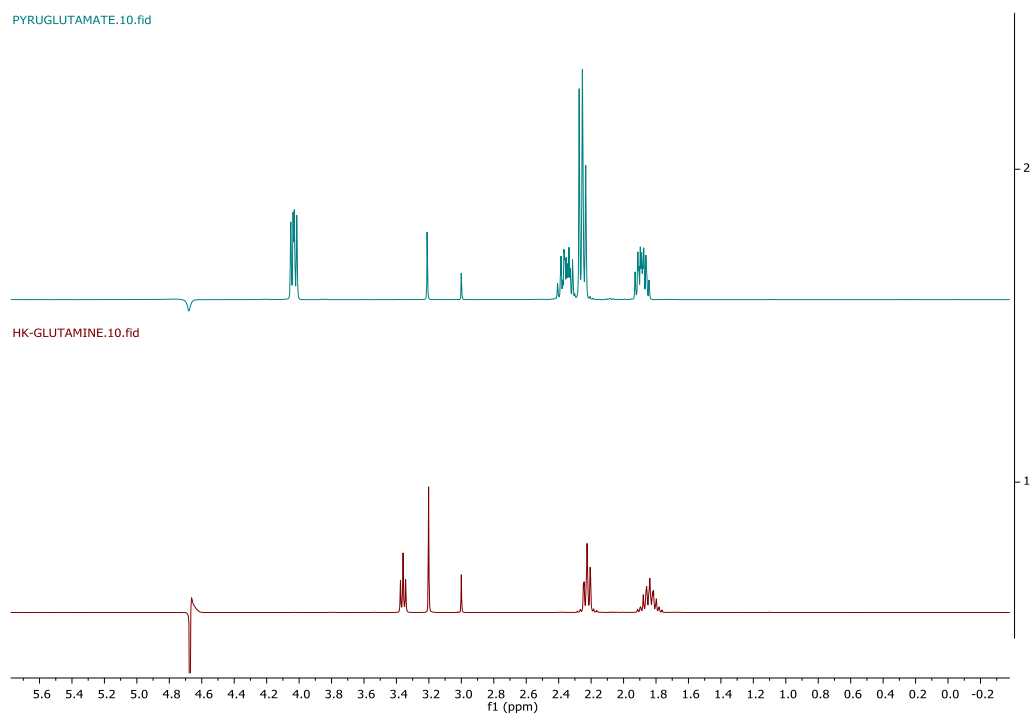


**Figure S41.** Authentic samples of pyroglutamate and glutamine.

## **General conclusions**

Throughout my dissertation work, we explored that under metal catalysis, life-like chemistry is possible if certain conditions or mechanisms are met. We successfully uncovered amino acids synthesis, their oligomerization and H<sub>2</sub> driven self-organised reaction network connecting rTCA cycle to amino acids in one-pot conditions, strengthening the link between prebiotic chemistry and biochemistry.

To understand self-organizing, interconnected dynamic systems on which life is based on, it is essential to broaden our mind sets by incorporating various geochemical possibilities and using biochemistry as a guide.

## References

1. Morowitz, H. J. (1999). A hypothesis of biochemical organization, metabolic pathways, and evolution. *Complexity*, 4(6), 39–53.
2. Safronov, V. S. (1972). *Evolution of the protoplanetary cloud and formation of the earth and the planets*. Jerusalem, Israel Program for Scientific Translations.
3. Betts, H. C., Puttick, M. N., Clark, J. W., Williams, T. A., Donoghue, P. C., & Pisani, D. (2018). Integrated genomic and fossil evidence illuminates life's early evolution and eukaryote origin. *Nature Ecology & Evolution*, 2(10), 1556–1562.
4. Mariscal, C., Barahona, A., Aubert-Kato, N., Aydinoglu, A. U., Bartlett, S., Cárdenas, M. L., Chandru, K., Cleland, C., Cocanougher, B. T., Comfort, N., Cornish-Bowden, A., Deacon, T., Froese, T., Giovannelli, D., Hernlund, J., Hut, P., Kimura, J., Maurel, M.-C., Merino, N., & Moreno, A. (2019). Hidden Concepts in the History and Philosophy of Origins-of-Life Studies: a Workshop Report. *Origins of Life and Evolution of Biospheres*, 49(3), 111–145.
5. Croswell, K. (2020). Inner Workings: Was Jupiter born beyond the current orbits of Neptune and Pluto? *Proceedings of the National Academy of Sciences*, 117(29), 16716–16719.
6. Von Hegner, I. (2020). A *limbus mundi* elucidation of habitability: the Goldilocks Edge. *International Journal of Astrobiology*, 19(4), 320–329.
7. Meadows, V. S., & Barnes, R. K. (2018). Factors Affecting Exoplanet Habitability. *Handbook of Exoplanets*, 2771–2794.
8. Canup, R. M., & Asphaug, E. (2001). Origin of the Moon in a giant impact near the end of the Earth's formation. *Nature*, 412(6848), 708–712.
9. Zahnle, K., & Sleep, N. H. (n.d.). Impacts and the Early Evolution of Life. *Comets and the Origin and Evolution of Life*, 207–251.
10. Bottke, W. F., & Norman, M. D. (2017). The Late Heavy Bombardment. *Annual Review of Earth and Planetary Sciences*, 45(1), 619–647.

11. Goldschmidt, V. M. (1937). The principles of distribution of chemical elements in minerals and rocks. The seventh Hugo Müller Lecture, delivered before the Chemical Society on March 17th, 1937. *Journal of the Chemical Society*, 0(0), 655–673.
12. Rubin, A. E., & Ma, C. (2017). Meteoritic minerals and their origins. *Geochemistry*, 77(3), 325–385.
13. Walker, R. J. (2014). Siderophile element constraints on the origin of the Moon. *Philosophical Transactions of the Royal Society A: Mathematical, Physical and Engineering Sciences*, 372(2024), 20130258.
14. Wilde, S. A., Valley, J. W., Peck, W. H., & Graham, C. M. (2001). Evidence from detrital zircons for the existence of continental crust and oceans on the Earth 4.4 Gyr ago. *Nature*, 409(6817), 175–178.
15. Izuka, T., Horie, K., Komiya, T., Maruyama, S., Hirata, T., Hidaka, H., & Windley, B. F. (2006). 4.2 Ga zircon xenocryst in an Acasta gneiss from northwestern Canada: Evidence for early continental crust. *Geology*, 34(4), 245.
16. Mulder, J. A., Nebel, O., Gardiner, N. J., Cawood, P. A., Wainwright, A. N., & Ivanic, T. J. (2021). Crustal rejuvenation stabilised Earth's first cratons. *Nature Communications*, 12(1).
17. Lepot, K. (2020). Signatures of early microbial life from the Archean (4 to 2.5 Ga) eon. *Earth-Science Reviews*, 209, 103296.
18. Fossil evidence of Archaean life | Philosophical Transactions of the Royal Society B: Biological Sciences. (2021). Retrieved August 22, 2022, from Philosophical Transactions of the Royal Society B: Biological.
19. Tian, F. (2005). A Hydrogen-Rich Early Earth Atmosphere. *Science*, 308(5724), 1014–1017.
20. Zahnle, K., Schaefer, L., & Fegley, B. (2010). Earth's Earliest Atmospheres. *Cold Spring Harbor Perspectives in Biology*, 2(10), a004895–a004895.
21. Charnay, B., Wolf, E. T., Marty, B., & Forget, F. (2020). Is the Faint Young Sun Problem for Earth Solved? *Space Science Reviews*, 216(5).

22. Yang, J., Turner, M. S., Schramm, D. N., Steigman, G., & Olive, K. A. (1984). Primordial nucleosynthesis - A critical comparison of hypothesis and observation. *The Astrophysical Journal*, 281, 493.
23. Catling, D. C., & Kasting, J. F. (2017). *Atmospheric evolution on inhabited and lifeless worlds*. Cambridge: Cambridge University Press.
24. Hagemann, R., Nief, G., & Roth, E. (1970). Absolute isotopic scale for deuterium analysis of natural waters. Absolute D/H ratio for SMOW. *Tellus*, 22(6), 712–715.
25. Daly, R. T., & Schultz, P. H. (2018). The delivery of water by impacts from planetary accretion to present. *Science Advances*, 4(4).
26. Hallis, L. J., Huss, G. R., Nagashima, K., Taylor, G. J., Halldórsson, S. A., Hilton, D. R., Meech, K. J. (2015). Evidence for primordial water in Earth's deep mantle. *Science*, 350(6262), 795–797.
27. Genda, H. (2016). Origin of Earth's oceans: An assessment of the total amount, history and supply of water. *Geochemical Journal*, 50(1), 27–42.
28. Peslier, A. H., Schönbächler, M., Busemann, H., & Karato, S.-I. (2017). Water in the Earth's Interior: Distribution and Origin. *Space Science Reviews*, 212(1-2), 743–810.
29. Halevy, I., & Bachan, A. (2017). The geologic history of seawater pH. *Science*, 355(6329), 1069–1071.
30. Stephens, G. L., Slingo, J. M., Rignot, E., Reager, J. T., Hakuba, M. Z., Durack, P. J., Rocca, R. (2020). Earth's water reservoirs in a changing climate. *Proceedings of the Royal Society A: Mathematical, Physical and Engineering Sciences*, 476(2236), 20190458.
31. Liquid ammonia - Thermal Properties at saturation pressure. (n.d.). Retrieved from [www.engineeringtoolbox.com](https://www.engineeringtoolbox.com/ammonia-liquid-thermal-properties-d_1765.html) website:  
[https://www.engineeringtoolbox.com/ammonia-liquid-thermal-properties-d\\_1765.html](https://www.engineeringtoolbox.com/ammonia-liquid-thermal-properties-d_1765.html)
32. Natural gas (methane) and propane as fuel gases. (2017). Retrieved October 20, 2022, from Chem 13 News Magazine website: <https://uwaterloo.ca/chem13-news->

[magazine/december-2014-january-2015/chemistry/natural-gas-methane-and-propane-fuel-gases](#)

33. Water - Gas, Liquid, and Solid Water. (2018). Retrieved September 1, 2022, from Biology LibreTexts website:  
[https://bio.libretexts.org/Bookshelves/Introductory and General Biology/Book%3A General Biology \(Boundless\)/02%3A The Chemical Foundation of Life/2.12%3A Water - Gas Liquid and Solid Water](https://bio.libretexts.org/Bookshelves/Introductory_and_General_Biology/Book%3A_General_Biology_(Boundless)/02%3A_The_Chemical_Foundation_of_Life/2.12%3A_Water_-_Gas_Liquid_and_Solid_Water)
34. Westall, F., & Brack, A. (2018). The Importance of Water for Life. *Space Science Reviews*, 214(2).
35. ATP: Adenosine Triphosphate. (2015, November 2). Retrieved from Biology LibreTexts website:  
[https://bio.libretexts.org/Bookshelves/Introductory and General Biology/Book%3A General Biology \(OpenStax\)/2%3A The Cell/06%3A Metabolism/6.4%3A ATP%3A Adenosine Triphosphate](https://bio.libretexts.org/Bookshelves/Introductory_and_General_Biology/Book%3A_General_Biology_(OpenStax)/2%3A_The_Cell/06%3A_Metabolism/6.4%3A_ATP%3A_Adenosine_Triphosphate)
36. Aversa, R., Petrescu, V., Apicella, A., & Petrescu, I. T. (2016). The Basic Elements of Life's. *American Journal of Engineering and Applied Sciences*, 9(4), 1189–1197.
37. Zahnle, K., Schaefer, L., & Fegley, B. (2010). Earth's Earliest Atmospheres. *Cold Spring Harbor Perspectives in Biology*, 2(10), a004895–a004895.
38. Kasting, J. F. (1993). Earth's early atmosphere. *Science*, 259(5097), 920–926.
39. McClintock, P. V. E. (2016). The origin and nature of life on earth: the emergence of the fourth geosphere, by Eric Smith and Harold J. Morowitz. *Contemporary Physics*, 58(1), 115–116.
40. Fox, G. E., Stackebrandt, E., Hespell, R. B., Gibson, J., Maniloff, J., Dyer, T. A., Woese, C. R. (1980). The Phylogeny of Prokaryotes. *Science*, 209(4455), 457–463.
41. Kitadai, N., Kameya, M., & Fujishima, K. (2017). Origin of the Reductive Tricarboxylic Acid (rTCA) Cycle-Type CO<sub>2</sub> Fixation: A Perspective. *Life*, 7(4), 39.

42. Fuchs, G. (2011). Alternative Pathways of Carbon Dioxide Fixation: Insights into the Early Evolution of Life? *Annual Review of Microbiology*, 65(1), 631–658.
43. Martin, W. F. (2020). Older Than Genes: The Acetyl CoA Pathway and Origins. *Frontiers in Microbiology*, 11.
44. Lemaire, O. N., Jespersen, M., & Wagner, T. (2020). CO<sub>2</sub>-Fixation Strategies in Energy Extremophiles: What Can We Learn from Acetogens? *Frontiers in Microbiology*, 11.
45. Nitschke, W., & Russell, M. J. (2013). Beating the acetyl coenzyme A-pathway to the origin of life. *Philosophical Transactions of the Royal Society B: Biological Sciences*, 368(1622), 20120258.
46. Fuchs, G. (1989). Alternative pathways of autotrophic CO<sub>2</sub> fixation. Autotrophic bacteria (eds H. G. Schlegel & B. Bowien), pp. 365–382. Madison, WI: Science Tech Publishers.
47. Fuchs, G. & Stupperich, E. (1985). Evolution of autotrophic CO<sub>2</sub> fixation. In Evolution of prokaryotes (eds K. H. Schleifer & E. Stackebrandt) FEMS Symposium No. 29, pp. 235–251. London, UK: Academic Press.
48. Russell, M. J., & Martin, W. (2004). The rocky roots of the acetyl-CoA pathway. *Trends in Biochemical Sciences*, 29(7), 358–363.
49. Evans, M. C., Buchanan, B. B., & Arnon, D. I. (1966). A new ferredoxin-dependent carbon reduction cycle in a photosynthetic bacterium. *Proceedings of the National Academy of Sciences*, 55(4), 928–934.
50. Baross, J. A., & Hoffman, S. E. (1985). Submarine hydrothermal vents and associated gradient environments as sites for the origin and evolution of life. *Origins of Life and Evolution of the Biosphere*, 15(4), 327–345.
51. Blackmond, Donna G. (2009). An Examination of the Role of Autocatalytic Cycles in the Chemistry of Proposed Primordial Reactions. *Angewandte Chemie International Edition*, 48(2), 386–390.

52. Orgel, L. E. (2008). The Implausibility of Metabolic Cycles on the Prebiotic Earth. *PLoS Biology*, 6(1), e18.
53. Smith, E., & Morowitz, H. J. (2004). Universality in intermediary metabolism. *Proceedings of the National Academy of Sciences of the United States of America*, 101(36), 13168–13173.
54. Krebs, H. A., & Johnson, W. A. (1937). Metabolism of ketonic acids in animal tissues. *Biochemical Journal*, 31(4), 645–660.
55. Ralser, M. (2018). An appeal to magic? The discovery of a non-enzymatic metabolism and its role in the origins of life. *Biochemical Journal*, 475(16), 2577–2592.
56. Martin, W., & Russell, M. J. (2006). On the origin of biochemistry at an alkaline hydrothermal vent. *Philosophical Transactions of the Royal Society B: Biological Sciences*, 362(1486), 1887–1926.
57. Duve, C. (2003). *Origins of Life and Evolution of the Biosphere*, 33(6), 559–574.
58. Lane, N., Allen, J. F., & Martin, W. (2010). How did LUCA make a living? Chemiosmosis in the origin of life. *BioEssays*, 32(4), 271–280.
59. Weiss, M. C., Sousa, F. L., Mrnjavac, N., Neukirchen, S., Roettger, M., Nelson-Sathi, S., & Martin, W. F. (2016). The physiology and habitat of the last universal common ancestor. *Nature Microbiology*, 1(9).
60. Theobald, D. L. (2010). A formal test of the hypothesis of universal common ancestry. *Nature*, 465(7295), 219–222.
61. Weiss, M. C., Sousa, F. L., Mrnjavac, N., Neukirchen, S., Roettger, M., Nelson-Sathi, S., & Martin, W. F. (2016). The physiology and habitat of the last universal common ancestor. *Nature Microbiology*, 1(9).
62. *Creatures Born of Mud and Slime*. (2017). Johns Hopkins University Press.



63. Bardell, D. (1985). Francesco Redi's Description of the Spontaneous Generation of Gall Flies. *The American Biology Teacher*, 47(4), 237–238.
64. Hugh Tristram Engelhardt, & Caplan, A. L. (1987). *Scientific controversies: case studies in the resolution and closure of disputes in science and technology*. Cambridge; New York: Cambridge University Press.
65. Wöhler, F. (1828). Ueber künstliche Bildung des Harnstoffs. *Annalen Der Physik Und Chemie*, 88(2), 253–256.
66. Peretó, J., Bada, J. L., & Lazcano, A. (2009). Charles Darwin and the Origin of Life. *Origins of Life and Evolution of Biospheres*, 39(5), 395–406.
67. Fox, S. W. (2022). Aleksandr Oparin. Encyclopedia Britannica. <https://www.britannica.com/biography/Aleksandr-Oparin>
68. Miller, S. L. (1953). A Production of Amino Acids Under Possible Primitive Earth Conditions. *Science*, 117(3046), 528–529.
69. Fox, S. W., & Harada, K. (1958). Thermal Copolymerization of Amino Acids to a Product Resembling Protein. *Science*, 128(3333), 1214–1214.
70. Cronin, J. R., & Moore, C. B. (1971). Amino Acid Analyses of the Murchison, Murray, and Allende Carbonaceous Chondrites. *Science*, 172(3990), 1327–1329.
71. Furukawa, Y., Chikaraishi, Y., Ohkouchi, N., Ogawa, N. O., Glavin, D. P., Dworkin, J. P., Nakamura, T. (2019). Extraterrestrial ribose and other sugars in primitive meteorites. *Proceedings of the National Academy of Sciences of the United States of America*, 116(49), 24440–24445.
72. Wagner, A. (2014). Arrival of the fittest: solving evolution's greatest puzzle. Penguin.
73. Watson, J. D., & Crick, F. H. C. (1953). Molecular Structure of Nucleic Acids: A Structure for Deoxyribose Nucleic Acid. *Nature*, 171(4356), 737–738.
74. Oró, J. (1960). Synthesis of adenine from ammonium cyanide. *Biochemical and Biophysical Research Communications*, 2(6), 407–412.

75. Fox, S. W., & Matsuno, K. (1983). Genetic takeover and the mineral origins of life. *Trends in Biochemical Sciences*, 8(9), 341–342.
76. Orgel, L. E. (1968). Evolution of the genetic apparatus. *Journal of Molecular Biology*, 38(3), 381–393.
77. Gilbert, W. (1986). Origin of life: The RNA world. *Nature*, 319(6055), 618–618.
78. Ferris, J. P., Huang, C.-H., & Hagan, W. J. (1988). Montmorillonite: A multifunctional mineral catalyst for the prebiological formation of phosphate esters. *Origins of Life and Evolution of the Biosphere*, 18(1-2), 121–133.
79. Eschenmoser, A., & Dobler, M. (1992). Warum Pentose- und nicht Hexose-Nucleinsäuren?? Teil I. Einleitung und Problemstellung, Konformationsanalyse für Oligonucleotid-Ketten aus 2',3'-Dideoxyglucopyranosyl-Bausteinen (?Homo-DNS?) sowie Betrachtungen zur Konformation von A- und B-DNS. *Helvetica Chimica Acta*, 75(1), 218–259.
80. Nielsen, P. E., Egholm, M., Berg, R. H., & Buchardt, O. (1991). Sequence-selective recognition of DNA by strand displacement with a thymine-substituted polyamide. *Science*, 254(5037), 1497–1500.
81. Haase, R. (1972). P. Glansdorff und I. Prigogine: Thermodynamic Hypothesis of Structure, Stability and Fluctuations, Wiley-Interscience, London 1971, 306 S. *Berichte Der Bunsengesellschaft Für Physikalische Chemie*, 76(5), 466–466.
82. Woese, C. R., & Fox, G. E. (1977). Phylogenetic structure of the prokaryotic domain: The primary kingdoms. *Proceedings of the National Academy of Sciences*, 74(11), 5088–5090.
83. Baross, J. A., & Hoffman, S. E. (1985). Submarine hydrothermal vents and associated gradient environments as sites for the origin and evolution of life. *Origins of Life and Evolution of the Biosphere*, 15(4), 327–345.
84. Corliss, J. B., Dymond, J., Gordon, L. I., Edmond, J. M., von Herzen, R. P., Ballard, R. D., Van Andel, T. H. (1979). Submarine Thermal Springs on the Galápagos Rift. *Science*, 203(4385), 1073–1083.

- <sup>85</sup>. Spiess, F. N., Macdonald, K. C., Atwater, T., Ballard, R., Carranza, A., Cordoba, D., Normark, W. (1980). East Pacific Rise: Hot Springs and Geophysical Experiments. *Science*, 207(4438), 1421–1433.
- <sup>86</sup>. Duve, C. D. (1998). Clues from present-day biology: the thioester world. *The Molecular Origins of Life*, 219–236.
- <sup>87</sup>. Wächtershäuser, G. (1988). Before enzymes and templates: hypothesis of surface metabolism. *Microbiological Reviews*, 52(4), 452–484.
- <sup>88</sup>. Martin, W., Baross, J., Kelley, D., & Russell, M. J. (2008). Hydrothermal vents and the origin of life. *Nature Reviews Microbiology*, 6(11), 805–814.
- <sup>89</sup>. Muchowska, K. B., Chevallot-Beroux, E., & Moran, J. (2019). Recreating ancient metabolic pathways before enzymes. *Bioorganic & Medicinal Chemistry*, 27(12), 2292–2297.
- <sup>90</sup>. Cleaves, H. (2013). Prebiotic Chemistry: Geochemical Context and Reaction Screening. *Life*, 3(2), 331–345.
- <sup>91</sup>. Powner, M. W., Gerland, B., & Sutherland, J. D. (2009). Synthesis of activated pyrimidine ribonucleotides in prebiotically plausible conditions. *Nature*, 459(7244), 239–242.
- <sup>92</sup>. Horowitz, N. H. (1945). On the Evolution of Biochemical Syntheses. *Proceedings of the National Academy of Sciences*, 31(6), 153–157.
- <sup>93</sup>. Braakman, R. (2013). Mapping metabolism onto the prebiotic organic chemistry of hydrothermal vents. *Proceedings of the National Academy of Sciences*, 110(33), 13236–13237.
- <sup>94</sup>. Novikov, Y., & Copley, S. D. (2013). Reactivity landscape of pyruvate under simulated hydrothermal vent conditions. *Proceedings of the National Academy of Sciences*, 110(33), 13283–13288.
- <sup>95</sup>. Ralser, M. (2014). The RNA world and the origin of metabolic enzymes. *Biochemical Society Transactions*, 42(4), 985–988.

96. Keller, M. A., Piedrafita, G., & Ralser, M. (2015). The widespread role of non-enzymatic reactions in cellular metabolism. *Current Opinion in Biotechnology*, 34, 153–161.
97. Muchowska, K. B., Varma, S. J., & Moran, J. (2020). Nonenzymatic Metabolic Reactions and Life's Origins. *Chemical Reviews*, 120(15), 7708–7744.
98. Patel, B. H., Percivalle, C., Ritson, D. J., Duffy, C. D., & Sutherland, J. D. (2015). Common origins of RNA, protein and lipid precursors in a cyanosulfidic protometabolism. *Nature Chemistry*, 7(4), 301–307.
99. Martin, W., & Russell, M. J. (2006). On the origin of biochemistry at an alkaline hydrothermal vent. *Philosophical Transactions of the Royal Society B: Biological Sciences*, 362(1486), 1887–1926.
100. Metzler, D. E., & Metzler, C. M. Biochemistry: the chemical reactions of living cells. Volume 2. San Diego, Calif.: Academic Press.
101. Muchowska, K. B., Varma, S. J., & Moran, J. (2020). Nonenzymatic Metabolic Reactions and Life's Origins. *Chemical Reviews*, 120(15), 7708–7744.
102. Pross, A., & Pascal, R. (2017). How and why kinetics, thermodynamics, and chemistry induce the logic of biological evolution. *Beilstein Journal of Organic Chemistry*, 13, 665–674.
103. Peretó, J. (2012). Out of fuzzy chemistry: from prebiotic chemistry to metabolic networks. *Chemical Society Reviews*, 41(16), 5394.
104. Smith, E., & Morowitz, H. J. (2004). Universality in intermediary metabolism. *Proceedings of the National Academy of Sciences of the United States of America*, 101(36), 13168–13173.
105. Sousa, F. L., & Martin, W. F. (2014). Biochemical fossils of the ancient transition from geoeconomics to bioenergetics in prokaryotic one carbon compound metabolism. *Biochimica et Biophysica Acta (BBA) - Bioenergetics*, 1837(7), 964–981.
106. Kitadai, N., Kameya, M., & Fujishima, K. (2017). Origin of the Reductive Tricarboxylic Acid (rTCA) Cycle-Type CO<sub>2</sub> Fixation: A Perspective. *Life*, 7(4), 39.

- <sup>107</sup>. Wachtershauser, G. (1990). Evolution of the first metabolic cycles. *Proceedings of the National Academy of Sciences*, 87(1), 200–204.
- <sup>108</sup>. Morowitz, H. J., Kostelnik, J. D., Yang, J., & Cody, G. D. (2000). The origin of intermediary metabolism. *Proceedings of the National Academy of Sciences*, 97(14), 7704–7708.
- <sup>109</sup>. Goldford, J. E., & Segrè, D. (2018). Modern views of ancient metabolic networks. *Current Opinion in Systems Biology*, 8, 117–124.
- <sup>110</sup>. Goldford, J. E., Hartman, H., Smith, T. F., & Segrè, D. (2017). Remnants of an Ancient Metabolism without Phosphate. *Cell*, 168(6), 1126–1134.
- <sup>111</sup>. Varma, S. J., Muchowska, K. B., Chatelain, P., & Moran, J. (2018). Native iron reduces CO<sub>2</sub> to intermediates and end-products of the acetyl CoA pathway. *Nature Ecology & Evolution*, 2(6), 1019–1024.
- <sup>112</sup>. Eggins, B. R., Brown, E. M., McNeill, E. A., & Grimshaw, J. (1988). Carbon dioxide fixation by electrochemical reduction in water to oxalate and glyoxylate. *Tetrahedron Letters*, 29(8), 945–948.
- <sup>113</sup>. Roldan, A., Hollingsworth, N., Roffey, A., Islam, H.-U., Goodall, J. B. M., Catlow, C. R. A., Leeuw, N. H. de. (2015). Bio-inspired CO<sub>2</sub> conversion by iron sulfide catalysts under sustainable conditions. *Chemical Communications*, 51(35), 7501–7504.
- <sup>114</sup>. Tze-Fei Wong, J. (1981). Coevolution of genetic code and amino acid biosynthesis. *Trends in Biochemical Sciences*, 6, 33–36.
- <sup>115</sup>. Meléndez-Hevia, E., Waddell, T. G., & Cascante, M. (1996). The puzzle of the Krebs citric acid cycle: Assembling the pieces of chemically feasible reactions, and opportunism in the design of metabolic pathways during evolution. *Journal of Molecular Evolution*, 43(3), 293–303.
- <sup>116</sup>. Lehninger, A. L., Nelson, D. L., & Cox, M. M. (2005). *Lehninger principles of biochemistry*. New York: W.H. Freeman.
- <sup>117</sup>. Shapiro, B. M., & Stadtman, E. R. (1970). The Regulation of Glutamine Synthesis in Microorganisms. *Annual Review of Microbiology*, 24(1), 501–524.

118. Mcmurry, J., & Begley, T. P. (2016). The organic chemistry of biological pathways. Greenwood Village, Colorado: Roberts and Company Pub.
119. The translation (polypeptide synthesis) cycle. (2016). Retrieved from Biology LibreTexts website: [https://bio.libretexts.org/Bookshelves/Cell and Molecular Biology/Book%3A Bio fundamentals \(Klymkowsky and Cooper\)/08%3A Pe](https://bio.libretexts.org/Bookshelves/Cell_and_Molecular_Biology/Book%3A_Bio_fundamentals_(Klymkowsky_and_Cooper)/08%3A_Pe)
120. Erhees, C. H., Kengen, S. W. M., Tuininga, J. E., Schut, G. J., Adams, M. W. W., de Vos, W. M., & Oost, J. van der. (2003). The unique features of glycolytic pathways in Archaea. *Biochemical Journal*, 375(2), 231–246.
121. Keller, M. A., Turchyn, A. V., & Ralser, M. (2014). Non-enzymatic glycolysis and pentose phosphate pathway-like reactions in a plausible Archean Ocean. *Molecular Systems Biology*, 10(4), 725.
122. Keller, M. A., Zylstra, A., Castro, C., Turchyn, A. V., Griffin, J. L., & Ralser, M. (2016). Conditional iron and pH-dependent activity of a non-enzymatic glycolysis and pentose phosphate pathway. *Science Advances*, 2(1), e1501235
123. Jia, T. Z., Chandru, K., Hongo, Y., Afrin, R., Usui, T., Myojo, K., & Cleaves, H. J. (2019). Membraneless polyester microdroplets as primordial compartments at the origins of life. *Proceedings of the National Academy of Sciences*, 116(32), 15830–15835.
124. Vieregg, J. R., & Tang, T-Y. D. (2016). Polynucleotides in cellular mimics: Coacervates and lipid vesicles. *Current Opinion in Colloid & Interface Science*, 26, 50–57.
125. Yi, J., Kaur, H., Kazöne, W., Rauscher, S. A., Gravillier, L., Muchowska, K. B., & Moran, J. (2022). A Nonenzymatic Analog of Pyrimidine Nucleobase Biosynthesis. *Angewandte Chemie International Edition*, 61(23).
126. Elodie, C. (2022). Non-enzymatic metabolic processes to understand the origin of life. Doctoral dissertation, University of Strasbourg, France). Retrieved from website: <https://www.theses.fr/257825304>
127. Mayer, R. J., Kaur, H., Rauscher, S. A., & Moran, J. (2021). Mechanistic Insight into Metal Ion-Catalyzed Transamination. *Journal of the American Chemical Society*, 143(45), 19099–19111.

- <sup>128</sup>. Cronin, J. R., & Pizzarello, S. (1983). Amino acids in meteorites. *Advances in Space Research*, 3(9), 5–18.
- <sup>129</sup>. Kvenvolden, K., Lawless, J., Pering, K., Peterson, E., Flores, J., Ponnamperna, C., Moore, C. (1970). Evidence for Extraterrestrial Amino-acids and Hydrocarbons in the Murchison Meteorite. *Nature*, 228(5275), 923–926.
- <sup>130</sup>. Ehrenfreund, P., & Charnley, S. B. (2000). Organic Molecules in the Interstellar Medium, Comets, and Meteorites: A Voyage from Dark Clouds to the Early Earth. *Annual Review of Astronomy and Astrophysics*, 38(1), 427–483.
- <sup>131</sup>. Ruiz-Bermejo, M., Osuna-Esteban, S., & Zorzano, M.-P. (2013). Role of Ferrocyanides in the Prebiotic Synthesis of  $\alpha$ -Amino Acids. *Origins of Life and Evolution of Biospheres*, 43(3), 191–206.
- <sup>132</sup>. Taillades, J., Beuzelin, I., Garrel, L., Tabacik, V., Bied, C., & Commeyras, A. (1998). *Origins of Life and Evolution of the Biosphere*, 28(1), 61–77.
- <sup>133</sup>. Pulletikurti, S., Yadav, M., Springsteen, G., & Krishnamurthy, R. (2022). Prebiotic synthesis of  $\alpha$ -amino acids and orotate from  $\alpha$ -ketoacids potentiates transition to extant metabolic pathways. *Nature Chemistry*, 1–9.
- <sup>134</sup>. Johnson, D. C., Dean, D. R., Smith, A. D., & Johnson, M. K. (2005). Structure, function, and formation of biological iron-sulfur clusters. *Annual Review of Biochemistry*, 74, 247–281.
- <sup>135</sup>. Kitadai, N., Nakamura, R., Yamamoto, M., Takai, K., Yoshida, N., & Oono, Y. (2019). Metals likely promoted protometabolism in early ocean alkaline hydrothermal systems. *Science Advances*, 5(6).
- <sup>136</sup>. Huber, C., & Wächtershäuser, G. (2003). Primordial reductive amination revisited. *Tetrahedron Letters*, 44(8), 1695–1697.
- <sup>137</sup>. Barge, L. M., Flores, E., Baum, M. M., VanderVelde, D. G., & Russell, M. J. (2019). Redox and pH gradients drive amino acid synthesis in iron oxyhydroxide mineral systems. *Proceedings of the National Academy of Sciences*, 116(11), 4828–4833.
- <sup>138</sup>. Muchowska, K. B., Varma, S. J., Chevallot-Beroux, E., Lethuillier-Karl, L., Li, G., & Moran, J. (2017). Metals promote sequences of the reverse Krebs cycle. *Nature Ecology & Evolution*, 1(11), 1716–1721.
- <sup>139</sup>. Muchowska, K. B., Varma, S. J., & Moran, J. (2019). Synthesis and breakdown of universal metabolic precursors promoted by iron. *Nature*, 569(7754), 104–107.

- <sup>140</sup>. Nakada, H. I., & Weinhouse, S. (1953). Non-enzymatic transamination with glyoxylic acid and various amino acids. *Journal of Biological Chemistry*, 204(2), 831–836.
- <sup>141</sup>. Mix, H. (1959). Nichtenzymatische Transaminierung zwischen  $\alpha$ -Aminosäuren und  $\alpha$ -Ketosäuren in Gegenwart von Metallionen. *Hoppe-Seyler's Zeitschrift Für Physiologische Chemie*, 315(Jahresband), 1–12.
- <sup>142</sup>. Doctor, V. M., & Oró, J. (1969). Mechanism of non-enzymic transamination reaction between histidine and  $\alpha$ -oxoglutaric acid. *Biochemical Journal*, 112(5), 691–697.
- <sup>143</sup>. Meisch, H.-U., Hoffmann, H., & Reinle, W. (1978). Vanadium Catalysis in the Nonenzymatic Transamination of  $\delta$ -Aminolevulinic Acid. *Zeitschrift Für Naturforschung C*, 33(9-10), 623–628.
- <sup>144</sup>. Stubbs, R. T., Yadav, M., Krishnamurthy, R., & Springsteen, G. (2020). A plausible metal-free ancestral analogue of the Krebs cycle composed entirely of  $\alpha$ -ketoacids. *Nature Chemistry*, 1–7.
- <sup>145</sup>. Muchowska, K. B., Varma, S. J., Chevallot-Beroux, E., Lethuillier-Karl, L., Li, G., & Moran, J. (2017). Metals promote sequences of the reverse Krebs cycle. *Nature Ecology & Evolution*, 1(11), 1716–1721.
- <sup>146</sup>. Muchowska, K. B., Varma, S. J., & Moran, J. (2019). Synthesis and breakdown of universal metabolic precursors promoted by iron. *Nature*, 569(7754), 104–107.
- <sup>147</sup>. Preiner, M., Igarashi, K., Muchowska, K. B., Yu, M., Varma, S. J., Kleinermanns, K., Martin, W. F. (2020). A hydrogen-dependent geochemical analogue of primordial carbon and energy metabolism. *Nature Ecology & Evolution*, 4(4), 534–542.
- <sup>148</sup>. Krebs, H. A. (1953). Equilibria in transamination systems. *Biochemical Journal*, 54(1), 82–86.



- <sup>149</sup>. Miller, S. L., & Smith-Magowan, D. (1990). The Thermodynamics of the Krebs Cycle and Related Compounds. *Journal of Physical and Chemical Reference Data*, 19(4), 1049–1073.
- <sup>150</sup>. Crugeiras, J., Rios, A., Riveiros, E., Amyes, T. L., & Richard, J. P. (2008). Glycine Enolates: The Effect of Formation of Iminium Ions to Simple Ketones on  $\alpha$ -Amino Carbon Acidity and a Comparison with Pyridoxal Iminium Ions. *Journal of the American Chemical Society*, 130(6), 2041–2050.
- <sup>151</sup>. Crugeiras, J., Rios, A., Riveiros, E., & Richard, J. P. (2011). Substituent Effects on Electrophilic Catalysis by the Carbonyl Group: Anatomy of the Rate Acceleration for PLP-Catalyzed Deprotonation of Glycine. *Journal of the American Chemical Society*, 133(9), 3173–3183.
- <sup>152</sup>. Keefte, J. R., & Kresge, A. J. (n.d.). Kinetics and mechanism of enolization and ketonization. *Enols* (1990), 399–480.
- <sup>153</sup>. Richard, J. P., Amyes, T. L., & Toteva, M. M. (2001). Formation and Stability of Carbocations and Carbanions in Water and Intrinsic Barriers to Their Reactions. *Accounts of Chemical Research*, 34(12), 981–988.
- <sup>154</sup>. Leussing, D. L., & Shultz, D. C. (1964). Metal Ion Catalysis in Transamination. II. Pyruvate-Glycinate Equilibrium Systems with Some Divalent Metal Ions. *Journal of the American Chemical Society*, 86(22), 4846–4850.
- <sup>155</sup>. Anderegg, G., Arnaud-Neu, F., Delgado, R., Felcman, J., & Popov, K. (2006). Critical Evaluation of Stability Constants of Metal Complexes of Complexones for Biomedical and Environmental Applications. *ChemInform*, 37(1).
- <sup>156</sup>. Rios, A., & Richard, J. P. (1997). Biological Enolates: Generation and Stability of the Enolate of N-Protonated Glycine Methyl Ester in Water. *Journal of the American Chemical Society*, 119(35), 8375–8376.
- <sup>157</sup>. Rios, A., Amyes, T. L., & Richard, J. P. (2000). Formation and Stability of Organic Zwitterions in Aqueous Solution: Enolates of the Amino Acid Glycine and Its Derivatives. *Journal of the American Chemical Society*, 122(39), 9373–9385.

- <sup>158</sup>. Zabinski, R. F., & Toney, M. D. (2000). Metal Ion Inhibition of Nonenzymatic Pyridoxal Phosphate Catalyzed Decarboxylation and Transamination. *Journal of the American Chemical Society*, 123(2), 193–198.
- <sup>159</sup>. Leussing, D. L. (1963). The Determination of the Stabilities of Schiff Base Complexes Involving Dissociated Schiff Bases. *Journal of the American Chemical Society*, 85(2), 231–232.
- <sup>160</sup>. Leussing, D., & Stanfield, C. K. (1964). A Nuclear Magnetic Resonance Study of Aqueous Pyruvate-Glycinate-Zinc(II) and Related Systems. *Journal of the American Chemical Society*, 86(14), 2805–2810.
- <sup>161</sup>. Nakahara, A., Yamamoto, H., & Matsumoto, H. (1964). The Stability of Fused Rings in Metal Chelates. II. Copper(II) Complexes of Schiff Bases Derived from Pyruvic Acid and Amino Acids or Diamines. *Bulletin of the Chemical Society of Japan*, 37(8), 1137–1142.
- <sup>162</sup>. Leussing, D. L. (1964). Schiff base complexes. A numerical study of the nickel(II)—pyruvate—glycinate system using a high-speed computer. *Talanta*, 11(2), 189–201.
- <sup>163</sup>. Xie, Y., Pan, H., Liu, M., Xiao, X., & Shi, Y. (2015). Progress in asymmetric biomimetic transamination of carbonyl compounds. *Chemical Society Reviews*, 44(7), 1740–1748.
- <sup>164</sup>. Kuzuhara, H., Komatsu, T., & Emoto, S. (1979). ChemInform Abstract: Synthesis of a chiral pyridoxamine analog and nonenzymatic stereoselective transamination. *Chemischer Informationsdienst*, 10(4).
- <sup>165</sup>. Tan, X., & Liu, C.-F. (2018). Investigating Glyoxylate-Mediated Transamination Using Dipeptide Arrays and Proteomic Peptide Mixtures. *Bioconjugate Chemistry*, 29(10), 3285–3292.
- <sup>166</sup>. Krebs, H. A. (1942). The effect of inorganic salts on the ketone decomposition of oxaloacetic acid. *Biochemical Journal*, 36(3-4), 303–305.

- <sup>167</sup>. Holleman, A. F., Wiberg, N., & Wiberg, E. (2007). *Lehrbuch der Anorganischen Chemie*.
- <sup>168</sup>. Dixon, J. E., & Bruice, T. C. (1973). Comparison of the rate constants for general base catalyzed prototropy and racemization of the aldimine species formed from 3-hydroxypyridine-4-carboxaldehyde and alanine. *Biochemistry*, 12(23), 4762–4766.
- <sup>169</sup>. Witkop, B., & Beiler, T. W. (1954). Studies on Schiff Bases in Connection with the Mechanism of Transamination. *Journal of the American Chemical Society*, 76(22), 5589–5597.
- <sup>170</sup>. Leussing, D. L., & Hanna, E. M. (1966). Metal Ion Catalysis in Transamination. IV. Nickel(II)-and Zinc(II)-Glyoxalate-Amino Acid Complexes<sup>1</sup>. *Journal of the American Chemical Society*, 88(4), 696–699.
- <sup>171</sup>. G. Schmidt and H. Palme, “Abundances of Os, Ir, Ru, Rh, Pt and Pd in the Earth’s crust,” in *The origin and fractionation of highly siderophile elements in the Earth’s mantle*, 1997.
- <sup>172</sup>. Kalugin, V., Gusev, V., Tolstykh, N., Lavrenchuk, A., & Nigmatulina, E. (2021). Origin of the Pd-Rich Pentlandite in the Massive Sulfide Ores of the Talnakh Deposit, Norilsk Region, Russia. *Minerals*, 11(11), 1258.
- <sup>173</sup>. Hazen, R. M., & Morrison, S. M. (2021). Mineralogical Environments of the Hadean Eon: Rare Elements Were Ubiquitous in Surface Sites of Rock-Forming Minerals. *Prebiotic Chemistry and the Origin of Life*, 43–61.
- <sup>174</sup>. Roy, D., & Uozumi, Y. (2017). Recent Advances in Palladium-Catalyzed Cross-Coupling Reactions at ppm to ppb Molar Catalyst Loadings. *Advanced Synthesis & Catalysis*, 360(4), 602–625.
- <sup>175</sup>. Braakman, R., & Smith, E. (2012). The compositional and evolutionary logic of metabolism. *Physical Biology*, 10(1), 011001.
- <sup>176</sup>. Roldan, A., Hollingsworth, N., Roffey, A., Islam, H.-U., Goodall, J. B. M., Catlow, C. R. A., Leeuw, N. H. de. (2015). Bio-inspired CO<sub>2</sub> conversion by iron sulfide

catalysts under sustainable conditions. *Chemical Communications*, 51(35), 7501–7504.

- <sup>177</sup>. Keller, M. A., Kampjut, D., Harrison, S. A., & Ralser, M. (2017). Sulfate radicals enable a non-enzymatic Krebs cycle precursor. *Nature Ecology & Evolution*, 1(4).
- <sup>178</sup>. Zhang, X. V., & Martin, S. T. (2006). Driving Parts of Krebs Cycle in Reverse through Mineral Photochemistry. *Journal of the American Chemical Society*, 128(50), 16032–16033.
- <sup>179</sup>. Crawford, C. J. et al. Defining the Qualities of High-Quality Palladium on Carbon Catalysts for Hydrogenolysis. *Org. Process Res. Dev.* 25, 1573–1578 (2021).
- <sup>180</sup>. Zubay, G. (2003). The glyoxylate cycle, a possible evolutionary precursor of the TCA cycle. *Chemtracts* 16, 783–788.
- <sup>181</sup>. Eschenmoser, A. (2007). The search for the chemistry of life's origin. *Tetrahedron*, 63(52), 12821–12844.
- <sup>182</sup>. Eggins, B. R., Brown, E. M., McNeill, E. A., & Grimshaw, J. (1988). Carbon dioxide fixation by electrochemical reduction in water to oxalate and glyoxylate. *Tetrahedron Letters*, 29(8), 945–948.
- <sup>183</sup>. Marín-Yaseli, M. R., González-Toril, E., Mompeán, C., & Ruiz-Bermejo, M. (2016). The Role of Aqueous Aerosols in the “Glyoxylate Scenario”: An Experimental Approach. *Chemistry - a European Journal*, 22(36), 12785–12799.
- <sup>184</sup>. Beyazay, T., Belthle, K., Farès, C., Vieira, A., Preiner, M., Moran, J., Martin, W. F., Tüysüz, H. (2022). Ambient temperature conversion of CO<sub>2</sub> and H<sub>2</sub> to pyruvate and citramalate over iron and nickel nanoparticles. *Submitted*.
- <sup>185</sup>. Sherwood Lollar, B., Heuer, V. B., McDermott, J., Tille, S., Warr, O., Moran, J. J., Hinrichs, K.-U. (2021). A window into the abiotic carbon cycle – Acetate and formate in fracture waters in 2.7-billion-year-old host rocks of the Canadian Shield. *Geochimica et Cosmochimica Acta*, 294, 295–314.

186. Patel, B. H., Percivalle, C., Ritson, D. J., Duffy, C. D., & Sutherland, J. D. (2015). Common origins of RNA, protein and lipid precursors in a cyanosulfidic protometabolism. *Nature Chemistry*, 7(4), 301–307.
187. Wu, X., & Xiao, J. (2013). Hydrogenation and Transfer Hydrogenation in Water. Metal-Catalyzed Reactions in Water, 173–242.
188. Preiner, M., Xavier, J., Sousa, F., Zimorski, V., Neubeck, A., Lang, S., Martin, W. (2018). Serpentinization: Connecting Geochemistry, Ancient Metabolism and Industrial Hydrogenation. *Life*, 8(4), 41.
189. Irrgang, T., & Kempe, R. (2020). Transition-Metal-Catalyzed Reductive Amination Employing Hydrogen. *Chemical Reviews*, 120(17), 9583–9674.
190. Knoop, F. & Oesterlin, H. Über die natürliche Synthese der Aminosäuren und ihre experimentelle Reproduktion. *Hoppe Seylers Z. Physiol. Chem.* 148, 294-315 (1925).
191. Stalder, C. J., Chao, S., Summers, D. P., & Wrighton, M. S. (1983). Supported palladium catalysts for the reduction of sodium bicarbonate to sodium formate in aqueous solution at room temperature and one atmosphere of hydrogen. *Journal of the American Chemical Society*, 105(20), 6318–6320.
192. Bada, J. L., & Miller, S. L. (1968). Ammonium Ion Concentration in the Primitive Ocean. *Science*, 159(3813), 423–425.
193. Mao, Z., Gu, H., & Lin, X. (2021). Recent Advances of Pd/C-Catalyzed Reactions. *Catalysts*, 11(9), 1078.
194. Saha, B. C., & Woodward, J. (Eds.). (1997). Fuels and Chemicals from Biomass. ACS Symposium Series.
195. Vagn Fabritius Buchwald. (1976). Handbook of iron meteorites: their history, distribution, composition and structure. Lyngby Inst. F. Metal.

- <sup>196</sup>. Longo, L. M., Despotović, D., Weil-Ktorza, O., Walker, M. J., Jabłońska, J., Fridmann-Sirkis, Y., Tawfik, D. S. (2020). Primordial emergence of a nucleic acid-binding protein via phase separation and statistical ornithine-to-arginine conversion. *Proceedings of the National Academy of Sciences*, 117(27), 15731–15739.
- <sup>197</sup>. Martin, R. B. (1998). Free energies and equilibria of peptide bond hydrolysis and formation. *Biopolymers*, 45(5), 351–353.
- <sup>198</sup>. Deamer, D., & Weber, A. L. (2010). Bioenergetics and Life's Origins. *Cold Spring Harbor Perspectives in Biology*, 2(2), a004929–a004929.
- <sup>199</sup>. Rodriguez-Garcia, M., Surman, A. J., Cooper, G. J. T., Suárez-Marina, I., Hosni, Z., Lee, M. P., & Cronin, L. (2015). Formation of oligopeptides in high yield under simple programmable conditions. *Nature Communications*, 6(1).
- <sup>200</sup>. Fox, S., Pleyer, H. L., & Strasdeit, H. (2018). An automated apparatus for the simulation of prebiotic wet–dry cycles under strictly anaerobic conditions. *International Journal of Astrobiology*, 18(1), 60–72.
- <sup>201</sup>. Pedreira-Segade, U., Hao, J., Montagnac, G., Cardon, H., & Daniel, I. (2019). Spontaneous Polymerization of Glycine under Hydrothermal Conditions. *ACS Earth and Space Chemistry*, 3(8), 1669–1677.
- <sup>202</sup>. Kitadai, N., Nishiuchi, K., & Takahagi, W. (2021). Thermodynamic Impact of Mineral Surfaces on Amino Acid Polymerization: Aspartate Dimerization on Two-Line Ferrihydrite, Anatase, and  $\gamma$ -Alumina. *Minerals*, 11(3), 234.
- <sup>203</sup>. Lambert, J.-F. (2008). Adsorption and Polymerization of Amino Acids on Mineral Surfaces: A Review. *Origins of Life and Evolution of Biospheres*, 38(3), 211–242.
- <sup>204</sup>. Sibilska, I., Chen, B., Li, L., & Yin, J. (2017). Effects of Trimetaphosphate on Abiotic Formation and Hydrolysis of Peptides. *Life*, 7(4), 50.
- <sup>205</sup>. Ferris, J. P., Hill, A. R., Liu, R., & Orgel, L. E. (1996). Synthesis of long prebiotic oligomers on mineral surfaces. *Nature*, 381(6577), 59–61.

206. Gibard, C., Bhowmik, S., Karki, M., Kim, E.-K., & Krishnamurthy, R. (2017). Phosphorylation, oligomerization and self-assembly in water under potential prebiotic conditions. *Nature Chemistry*, 10(2), 212–217.
207. Canavelli, P., Islam, S., & Powner, M. W. (2019). Peptide ligation by chemoselective aminonitrile coupling in water. *Nature*, 571(7766), 546–549.
208. Goldwhite, H. (1981). *Introduction to Phosphorous Chemistry*. Cambridge University Press.
209. Osumah, A., & Krishnamurthy, R. (2021). Diamidophosphate (DAP): A Plausible Prebiotic Phosphorylating Reagent with a Chem to BioChem Potential? *ChemBioChem*, 22(21), 3001–3009.
210. Pasek, M. A. (2008). Rethinking early Earth phosphorus geochemistry. *Proceedings of the National Academy of Sciences*, 105(3), 853–858.
211. Yamagata, Y., Watanabe, H., Saitoh, M., & Namba, T. (1991). Volcanic production of polyphosphates and its relevance to prebiotic evolution. *Nature*, 352(6335), 516–519.
212. Peacock, C. J., & Nickless, G. (1969). The Dissociation Constants of some Phosphorus(V) Acids. *Zeitschrift Für Naturforschung A*, 24(2), 245–247.